SIMULATION OF SINGLE CHAR PARTICLE GASIFICATION IN CONDITIONS OF A COAL GASIFIER

Ph.D. THESIS

by

VINOD KUMAR YADAV

DEPARTMENT OF CHEMICAL ENGINEERING
INDIAN INSTITUTE OF TECHNOLOGY ROORKEE
ROORKEE – 247 667 (INDIA)
DECEMBER, 2014

SIMULATION OF SINGLE CHAR PARTICLE GASIFICATION IN CONDITIONS OF A COAL GASIFIER

A THESIS

Submitted in partial fulfilment of the requirements for the award of the degree

of

DOCTOR OF PHILOSOPHY

in

CHEMICAL ENGINEERING

by

VINOD KUMAR YADAV

DEPARTMENT OF CHEMICAL ENGINEERING
INDIAN INSTITUTE OF TECHNOLOGY ROORKEE
ROORKEE - 247 667 (INDIA)
DECEMBER, 2014

INDIAN INSTITUTE OF TECHNOLOGY ROORKEE
ROORKEE

CANDIDATE'S DECLARATION

I hereby certify that the work which is being presented in this thesis entitled "**SIMULATION OF SINGLE CHAR PARTICLE GASIFICATION IN CONDITIONS OF A COAL GASIFIER"** in partial fulfilment of the requirements for the award of the Degree of Doctor of Philosophy and submitted in the Department of **Chemical Engineering** of the Indian Institute of Technology Roorkee is an authentic record of my own work carried out during a period from **July, 2012** to **December, 2014** under the supervision of **Dr. Vineet Kumar**, Associate Professor, Department of **Chemical Engineering**, Indian Institute of Technology Roorkee.

The matter presented in this thesis has not been submitted by me for the award of any other degree of this or any other Institute.

(VINOD KUMAR YADAV)

This is to certify that the above statement made by the candidate is correct to the best of my knowledge.

Date:

(Vineet Kumar)
Supervisor

ABSTRACT

Coals from different regions of the world have different characteristics regarding mineral content and coal matrix. In high ash coals, beneficiation process is difficult for removal of the mineral matter that leads to the lower efficiency and greater environmental pollution by coal combustion. The carbon dioxide emissions from the coal combustion leads to global warming which has led to the international agreement that sets the target for controlling CO_2 emissions. To achieve these goals, we require increasing energy efficiency by making changes in the combustion practices of the coal. Coal gasification has the potential to provide a solution to the increasing demand for energy through fuel synthesis. The compositions of H_2 and CO in the product gases mostly depend on the reactant gas used the coal type, operating condition, and gasification process. The char gasification with steam enhances the production of H_2 while with CO_2, gasification improves the CO formation in the product gas.

For the char gasification, a number of kinetic models have been proposed. The simplest of these models are homogeneous and shrinking-core model. In the homogeneous model, it is assumed that the particle size of char remains same but the density decreases during its gasification, whereas, in the shrinking-core model, the gaseous reactant are assumed to diffuse through the gas film and ash layer to reach the unreacted core surfaces. As reaction proceeds, the unreacted core of a char particle continues to shrinking. Based on the kinetic approach, many other researchers have also studied the modeling and simulation of coal gasification. The gasification of a single coal char particle is carried out by the active penetration of the reactant gases through the porous structure of the char particle leading to change in the porous structure which cause the changing in the effective diffusivity of the gaseous components and hence change in the reaction rates. Therefore, modeling of a single coal char particle is important for the analysis of the effects of different parameters on the coal char gasification which is useful for the design of a gasfier. The model for the gasification and combustion of a single coal char particle are developed by a few researchers.

The rate of char gasification is affected by many parameters such as concentration of gasifying agent, temperature, and the physic-chemical properties of the char particle like effective diffusivity, carbon content, ash content, and porosity.

Mathematical modeling and simulation of gasification of a single char particle for production of synthesis gas is challenging due to complex chemical reactions coupled with the changing physico-chemical properties of the char particle during gasification. In the present work we have developed a mathematical model for a single char particle. The resulting non-linear partial differential equation representing unsteady state diffusion controlled reaction of a gasification agent (steam and mixture of steam and CO_2) inside the non-catalytic porous solid (char particle) was solved numerically using staggered grid finite volume method with appropriate initial and boundary condition.

The rate of steam gasification of char particle was found to be proportional to the steam concentration. Increasing the steam concentration from 0.5 to 2 mol/m^3, the rate of steam gasification reaction increases rapidly which produces more hydrogen and carbon monoxide. The carbon monoxide is further reacted with steam through water gas shift reaction to form more hydrogen and carbon dioxide causing several fold increase of hydrogen fluxes at 2 mol/m^3 compared to that at 0.5 mol/m^3 steam concentration. At a lower reaction temperature (1100 K), less increments in the carbon monoxide flux is observed. Hence for obtaining high yield of hydrogen the steam concentration should be high.

The reaction temperature is expected to be one of the most promising variables that directly affect the performance of a gasifier during gasification because the main gasification reactions are strongly endothermic. On increasing the reaction temperature beyond 1100K; the rate of reaction increases which shifts the reaction mechanism from the progressive reaction model to the shrinking core model. When the gasification reaction rates are slow (for example, at temperature 1000K), sufficient amount of gasifying agent diffuses deep into the particle and reaction continues throughout the char particle similar to the progressive reaction model. At higher temperature (>1100 K), however, the rate of reactions become fast which leads to maximum conversion of char near the outer surface resembling the shrinking core model. Thus at higher temperatures an un-reacted core is formed that shrinks with time. This study reveals that the highest concentration of CO and H_2 in the synthesis gas is obtained

when the reaction temperature is greater than 1200 K which also minimizes the fraction of CO_2 in the product gas. Also, removal of the ash layer from the particle surface at time interval of 100 second for less ash content char (<1%) and 10 second for high ash content char (>25%) may give higher CO concentration. For obtaining high H_2 concentration, the steam partial pressure should be kept high.

Carbon concentration directly affects the rate of gasification of the char particle. Apparently, a higher carbon concentration should lead to higher conversion, however, the simulation results reveal that if the parameters like size, density, and porosity of the particle remain unchanged, the rate of percent conversion is high for low char concentration but low at high char concentration in the central core of the particle. Since the consumption near the particle surface is more for charcoal with higher carbon concentration. But in this case too, near the center, carbon consumption is high when its concentration is low. This is because of the fact that keeping density constant, reduction in carbon concentration ultimately leads to increase in the diffusivity of gasifying agent. Therefore availability of gasifying agent in the core region is more when carbon concentration is less.

The effects of particle sizes were analyzed using particle sizes 5, 7.5, and 10 mm at the reaction temperature of 1100 K. It was observed that the overall rate of conversion increases with a decrease in the particle size. In a smaller particle, the steam diffuses deep in the char particle and reactions continue throughout the particle following the progressive model. In the case of large particle, reactions take place at the outer surface of the particle and steam does not reach deep into the particle follow the shrinking core model. Hence the rate of the surface reaction of large char particle is high compared to the small particle.

The porosity of char particle affects the total conversion only in the initial phase of gasification, in the other words, the time required to reaches complete conversion is almost the same for all initial porosity values. The variation of initial porosity is more prominent towards the low porosity range. For higher initial porosity, curves between total conversion and time get closer to each other. Due to nearly same time requirement for complete conversion of char particle of different initial porosity, the flux ratios of H_2 to CO and CO to CO_2 remains the same for all initial porosity of char particle after a certain period of time (≈2500 s).

Since the reactivity data of coal char particle with high ash content is limited, the study on the effect of ash content in the coal char particle on the gasification is important for the design of a gasifier to use high ash content in the coal char. Because of this, in the modeling of a single char particle is also included the effect of ash content on the conversion rate and overall rate of generation of gaseous components from the outer surface of the coal char particle. The study reveals that although product yield decline but the overall carbon conversion of high ash content coal char particle is higher than lower one. The variation of carbon conversion near the surface of coal char particle for the fraction of different ash content in the char particle are nearly same whereas towards the centre of the char particle, because of the available specific surface area for the gasification reactions, conversion is significantly high.

In this work, unsteady state modeling and simulation for coal char gasification with varying gasifying agent composition of steam and CO_2 is also developed. This study revealed that the highest fraction of H_2 and CO with lower CO_2 concentration (dry basis) is obtained when the gasifying agent composition is 70 % steam and 30 % CO_2 in the gasifying medium. The synthesis gas obtained at this composition of reactant gases having higher heating value in comparison with the other cases.

The work done in this study is organized into **five chapters**. The introduction of the gasification process is presented in the **first chapter**, a literature review related to gasification of char particles in conditions of a coal gasifier follows in the **second chapter**.

Chapter 3 deals with the model development for single char particle gasification along with the porosity and diffusivity and kinetic model for gasification.

Results of the simulation of single char particle gasification are presented and discussed in **chapter 4**. The numerical model is validated by comparing the experimental data. Then the parametric analysis is done with the change in each parameter's value (keeping other parameters same).

Chapter 5 summarizes the conclusions and recommendations drawn from this study.

ACKNOWLEDGEMENT

I take this golden opportunity to express my heartfelt and deepest sense of gratitude to those who helped me to complete my dissertation.

This thesis would not have been possible without the support and meticulous guidance of my supervisor **Dr. Vineet Kumar**, Associate Professor, Department of Chemical Engineering, Indian Institute of Technology Roorkee. I take this opportunity to express my deepest sense of gratitude to such a sincere academician and generous guide who have been a source of inspiration and encouragement to me in completing this research work in its present form. I have a deep sense of admiration for his goodness and for his anytime availability during this research work.

I express my sincere gratitude to **Dr. V. K. Agarwal**, Head, Department of Chemical Engineering, **Dr. Bikas Mohanty**, Chairman DRC for their timely encouragement, for providing me the best facilities and for their kind help in departmental affairs.

I am also thankful to **Dr. I. M. Mishra** and **Dr. B. Prasad**, Professors, Department of Chemical Engineering, Indian Institute of Technology Roorkee who extended all possible help during all stages of this research work.

I would also like to express my heartfelt thanks to Ravikant Gupta, Richa Agarwal, Nirupama, Anil Varma, Soumitra maiti, Partha Kundu, Krunal Gangwane, Vijay Verma, Nilambar, Bhisham, Deepak Sahu, Ambrish Maurya, Nitin Pandhare, Satya Murthy whose friendship has always given me a mental support and whose communications, though from near and far places, have been great sources of inspiration. Also, my warmest thanks goes to all my friends, seniors and colleagues at IIT Roorkee, whose names would form a big list, for their unparalleled company and valuable and timely assistance. I would also like to thank the technical staff of Chemical Engineering Department especially Mr. Rajendra Bhatnagar who extended all possible helps during all stages of this research work.

Inspite of all my efforts, this was not at all possible without the endless care, unfailing love, support and understanding of my dear wife Neelu Yadav who faced every difficult moment with me during my doctoral program smilingly and always stood along with me.

I am deeply and thoroughly indebted to my parents for all the freedom they have given to my choice of career. I am also thankful to Arjun Yadav, Brijendra Kumar Yadav, Shailendra Kumar Yadav and other family members and relatives for their continuous love and moral support.

Last but not the least; I am always thankful to the omnipresent, **GOD**, for providing me an opportunity, strength and ambience to successfully accomplish this work.

DECEMBER, 2014 (**VINOD KUMAR YADAV**)

PUBLICATIONS FROM DISSERTATION

- **Under Review**

1. Vinod Kumar Yadav and Vineet Kumar, 2014, Staggered Grid Finite Volume Approach for Modeling Single Particle Char Gasification. International Journal of Chemical Reactor Engineering (Communicated).

2. Vinod Kumar Yadav and Vineet Kumar, 2014, Numerical Simulation for the Steam gasification of Single Char Particle. Fuel (Communicated).

3. Vinod Kumar Yadav and Vineet Kumar, 2014, Modelling and Simulation for Effect of Reactant Gas on Synthesis Gas Production from Coal Char Particle (manuscript under preparation).

- **In International and/or National Conferences**

1. Vinod Kumar Yadav and Vineet Kumar, 2014, Modelling Gasification of Single Coal Particle, 5th International and 41st National Conference on Fluid Mechanics and Fluid Power, FMFP14-F-293, Indian Institute of Technology Kanpur, December 12-14, 2014.

2. Vinod Kumar Yadav and Vineet Kumar, 2014, Modelling Synthesis Gas Production from Coal Particle, International conference on Environment and Energy, ICEE 2014, Jawaharlal Nehru Technological University Hyderabad, December 15-17, 2014.

3. Vinod Kumar Yadav, Gupta Ravikant, Vineet Kumar, Effect of Temperature and Pressure on the Conversion of Coal-Char Gasification with CO_2, Chemcon 2014, Abstract ID: PM/0009, Chandigarh Regional Centre Indian Institute of Chemical Engineers, December 27-30, 2014.

CONTENTS

LIST OF FIGURES

LIST OF TABLES

NOMENCLATURE

C_{As}	Concentration of reactant (CO_2) at surface of char particle, mol/m^3
C	Concentration of reactant (steam), mol/m^3
C_C	Concentration of carbon in coal char particle, mol/m^3
C_j	Concentration of j^{th} component, mol/m^3
C_{j0}	Initial concentration of j^{th} component, mol/m^3
C_{ji}	Concentration of j^{th} component in i^{th} volume element, mol/m^3
$C_{j(i-1)}$	Concentration of j^{th} component in $(i-1)^{th}$ volume element, mol/m^3
$C_{j(i+1)}$	Concentration of j^{th} component in $(i+1)^{th}$ volume element, mol/m^3
C_{H_2O}	Concentration of steam, mol/m^3
C_{H_2}	Concentration of hydrogen, mol/m^3
C_{CO}	Concentration of carbon monoxide, mol/m^3
C_{CO_2}	Concentration of carbon dioxide, mol/m^3
C_{CH_4}	Concentration of methane, mol/m^3
d_p	Diameter of coal char particle, m
d_{p0}	Initial diameter of coal char particle, m
d_m	Mean pore diameter, m
D_a	Effective diffusivity for macro-pores, m^2/s
D_e	Effective diffusivity for meso-pores, m^2/s
D_i	Effective diffusivity for micro-pores, m^2/s
D_{ej}	Effective diffusivity of j^{th} component, m^2/s
D_{ej}^0	Initial effective diffusivity, m^2/s
D_{eji}	Effective diffusivity of j^{th} component in ith volume element, m^2/s
$D_{ej(i-1)}$	Effective diffusivity of j^{th} component in $(i-1)^{th}$ volume element, m^2/s
$D_{ej(i+1)}$	Effective diffusivity of j^{th} component in $(i+1)^{th}$ volume element, m^2/s
D_{jK}	Knudsen diffusion coefficient, m^2/s
D_{jl}	Binary diffusion coefficient, m^2/s
D_N	Diffusion coefficient including molecular and Knudsen diffusion, m^2/s

f_c	Correction factor
F_C	Fraction of carbon in char
h_{steam}	Heat transfer coefficient of steam, W/m^{2}K
k_{char}	Thermal conductivity of coal char, W/m.K
k_1	Rate constant for reaction R1
k_2	Rate constant for reaction R2
k_3	Rate constant for reaction R3
k_4	Rate constant for reaction R4
k_5	Rate constant for reaction R5
L_0	Pore length, m
L_P	Characteristics length of the char particle, m
$m(t)$	Mass of coal char particle (carbon and ash) at time t, kg
m_0	Initial mass of coal char particle (carbon and ash), kg
M_C	Molecular weight of carbon, kg/kmol
MW_j	Molecular weight of j^{th} component, kg/kmol
MW_l	Molecular weight of species l, kg/kmol
P	Pressure, atm
r_i	Radius of coal char particle of i^{th} volume element, m
r_{i-1}	Radius of coal char particle of $(i-1)^{th}$ volume element, m
r_{i+1}	Radius of coal char particle of $(i+1)^{th}$ volume element, m
Δr_i	Thickness of i^{th} volume element, m
Δr_{i-1}	Thickness of $(i-1)^{th}$ volume element, m
Δr_{i+1}	Thickness of $(i+1)^{th}$ volume element, m
r_m	Radius of shrinking unreacted core, m
R	Gas constant, m^{3}Pa/mol K
R_C	Overall rate of consumption of carbon, mol/m^{3}s
R_g	Gas constant, m^{3}atm/kmol K
R_j	Overall volumetric rate of formation of any j^{th} component, mol/m^{3}s
S_0	Initial surface area per unit volume of the char particle, m^2/m^3
S	Surface area per unit volume of the char particle, m^2/m^3

S_μ	Pore surface area, m^2
$S_{\mu E}$	Pore surface area per unit volume of solid, m^2/m^3
t	Time, s
Δt	Time interval, s
T	Temperature, K
$V_{\mu E}$	Pore volume per unit volume of solid, m^3/m^3
x	Conversion ratio of the char
X	Fractional conversion of char particle
Subscripts	
A, B	Components
i	i^{th} volume element in the coal char particle
$i-1$	$(i-1)^{th}$ volume element in the coal char particle
$i+1$	$(i+1)^{th}$ volume element in the coal char particle
j	j^{th} component
0	Initial
Supercripts	
0	Initial
m, n	Reaction order
Greek letters	
α	Diameter variation factor
$\Phi/2$	Radius of coal char particle, m
ϕ_{C-H_2O}	Thiele modulus for C-H_2O reaction
ϕ_{CO_2}	Thiele modulus for C- CO_2 reaction
ϕ_M	Modified Thiele number
ψ	Initial pore structure
ε_0	Initial porosity of coal char particle
ε_a	Macro-porosity
ε_e	Meso-porosity
ε_i	Micro-porosity
ε_P	Porosity of coal char particle

$\varepsilon_{\mu 0}$	Initial microporosity of char particle
ε_{μ}	Microporosity of char particle
ρ_b	Bulk density, kg/m^3
ρ_C	Density of char particle, kg/m^3
ρ_s	Solid density, kg/m^3
σ_{jl}	Mean collision diameter for the j^{th} species and l^{th} species, m
Ω_D	Collision integral for diffusion
γ_1	Rate of reaction for reaction R1, mol/m^{3}s
γ_2	Rate of reaction for reaction R2, mol/m^{3}s
γ_3	Rate of reaction for reaction R3, mol/m^{3}s
γ_4	Rate of reaction for reaction R4, mol/m^{3}s
γ_5	Rate of reaction for reaction R5, mol/m^{3}s
ξ_m	Dimensionless shrinking unreacted core radius, m
η_{CO_2}	Effectiveness factor for C-CO_2 reaction
η_{C-H_2O}	Effectiveness factor for C-H_2O reaction

CHAPTER 1

INTRODUCTION

Since prehistoric period (prior to the Bronze Age), coal is being used as a source of energy and carbon. Even today most of the electricity and heat is being produced by burning coal. Other industrial applications of coal include - refining metals, production of syn-gas, liquid fuels, etc. Its excessive use makes it the main offender for the huge release of anthropogenic carbon dioxide into the atmosphere in the form of greenhouse gases. Emission of these greenhouse gases after coal combustion has lead to global warming which has obligated the international bodies to make an agreement that sets the target for controlling CO_2 emissions. Because of the rising problems due to emission of these gases, it becomes mandatory to control it. To achieve these goals, we require increasing energy efficiency and making changes in the combustion practices of coal such as producing gaseous fuel using gasifiers.

1.1 Types of Gasifiers

There are several types of gasifiers available which are classified broadly on the basis of the two factors: (a) the pattern of contacting materials in the gasifier, and (b) the path through which heat is supplied to the gasifier.

For the first approach, the gasifier can be further classified into three types: (1) fixed bed, (2) fluidized bed, and (3) entrained flow.

For the second approach, the gasifiers can be classified on the basis of the source of heating for the gasification reaction, which is autothermal or allothermal. In autothermal gasifier, the heat of reaction is provided by the partial oxidation of the carbonaceous solid fuel with air or pure O_2 in the gasifier. For increasing the H_2 content in the product gas, steam can be used as oxidant. In allothermal gasifier, the heat of reaction is provided by an external source like heat exchanger or by circulating the hot bed material into the gasifier.

In a fixed (or moving) bed gasifier, the gasification reaction occurs above the stationary grate. In such gasifiers, the gasifying agent can be fed either from above or from below the grate while the solid fuel is fed from the top of the gasifier. The product gas can be obtained either from the upper part of the gasifier or from the bottom of the gasifier. In the fixed bed gasifier, the gas flow velocity is very low and due to this reason the gas just

percolates through the bed of the solid particles. The solid bed of the particle remains stationary in fixed bed gasifier, because the intensity of momentum exchange is not enough to move the particles.

In a fluidized bed gasifier, the gasifying agent is supplied from the bottom of the gasifier and flows towards the top of the gasifier through the bed of solid fuel. Inert material and chars and product gas flows out from the top of the gasifier. In case of fluidized bed, the gas flow rate is higher than fixed bed gasifier.

1.1.1 Fixed (or moving) bed gasifier

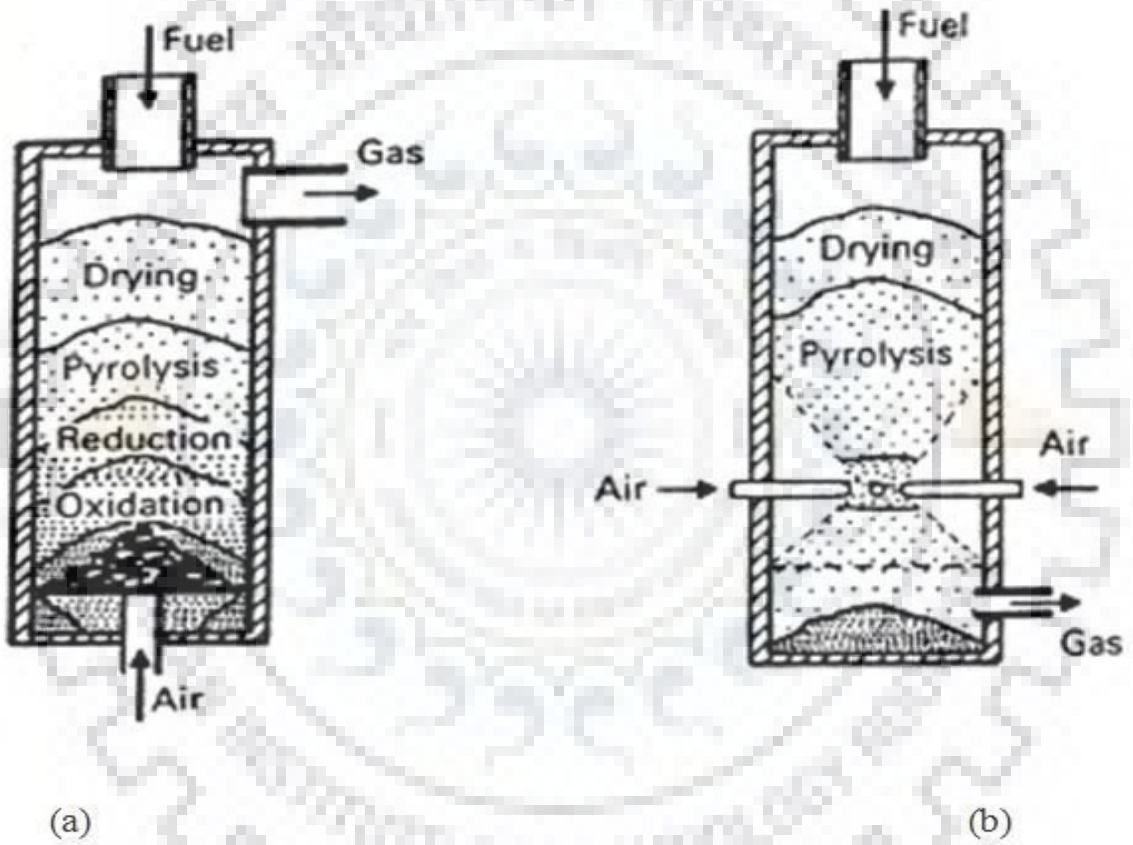

Figure 1.1: Schematic diagram of (a) updraft fixed bed gasifier and (b) downdraft fixed bed gasifier (Source: Warnecke, 2000)

The fixed bed gasifiers are based on the flow direction of gasifying agent and syn gas can be classified into two types: updraft which is shown in Figure 1.1 (a) and downdraft is shown in Figure 1.1 (b). In updraft gasifier, the solid fuel is fed from the top of gasifier the feed is dried, pyrolysis, burnt, and/or gasified sequentially as it moves down and residue leaves from the bottom of the gasifier. The syn gas leaves from the top of the gasifier. On the other hand, for the downdraft gasifier, the solid fuel is fed from the top of the gasifier undergoes sequential steps like updraft gasifier and syn gas leaves from the

bottom of the gasifier. The gasifying agent is fed above the stationary grate in to gasifier and residue leaves from the bottom of the gasifier.

The main advantage of updraft gasifier has high energy efficiency because the contact between feed solid fuel and hot syn gas provides the heats to feed solid fuel for the drying and pyrolysis. Due to this reason, the syn gas leaves the reactor at relatively low temperature compared to the downdraft gasifier. Therefore, the temperature distribution is non-uniform and gas solid contact is non-homogeneous. So, the fixed bed gasifiers are generally used for small-medium scale plants (1-10 MW). The downdraft gasifier has advantage of low tar content in the syn gas compared to the updraft gasifier.

1.1.2 Fluidized bed gasifier

The fluidized bed gasifiers can be further classified on the basis of the fluidization velocity into two types: bubbling fluidized and circulating fluidized bed which is shown in Figure 1.2 (a) and Figure 1.2 (b), respectively. A fluidized bed is operated between the flow regimes from the bubbling to circulating fluidized bed.

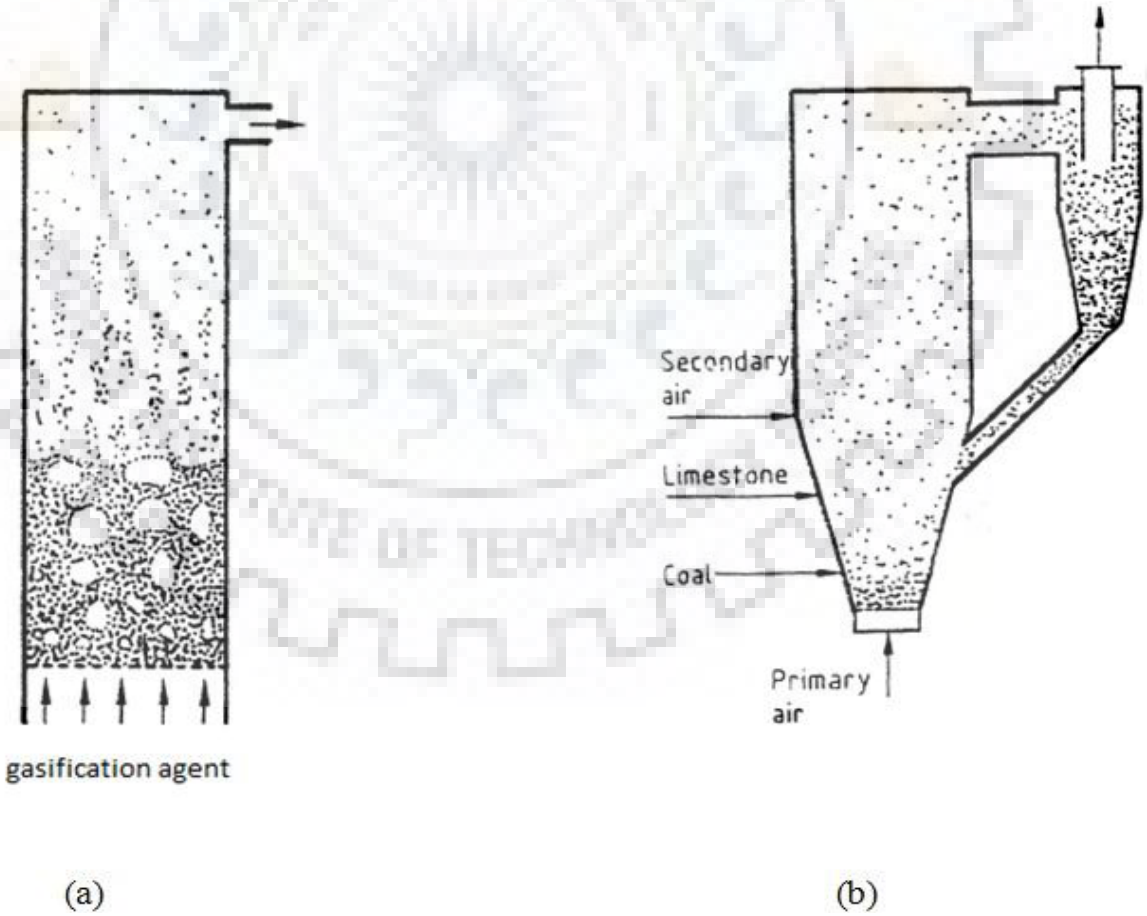

Figure 1.2: Schematic diagram of (a) Bubbling Fluidized Bed and (b) Circulating Fluidized Bed (Source: Warnecke, 2000)

In this gasifier, the gasifying agent is fed from the bottom of the gasifier through the distributor for uniform distribution of gasifying agent in the bed. Bubbling fluidized bed is operated between the minimum fluidization velocity and terminal velocity whereas in circulating fluidized bed (CFB), the gas velocity is above the terminal velocity. In the CBF, the fine particles and inert bed material being entrained and carried out with the syn gas from the gasifier and the particulate are separated from the syn gas in a cyclone where the particles are recycle to the gasifier and the ash is removed and syn gas leaves the cyclone from the top. Before operating the gasifier, the bed is first heated up to the desired temperature, and then the solid fuel is fed into the gasifier.

In fluidized bed gasifier, all process in the gasifier like drying, devolatilization, and gasification take place simultaneously over the whole bed volume of solid. Since in the fluidized bed gasifier, the solid particles are uniformly distributed in the bed, therefore the process can be regarded as isothermal. The uniform distribution of solid fuel in the bed enhances mass and heat transfer in the gasifier which makes the solid fuel gasification possible at relatively low operating temperature (700-900 ^{0}C) compared to fixed bed gasifier. The tar content in fluidized bed gasifier is lower than that in updraft gasifier and higher than that in tha downdraft fixed bed gasifier.

1.1.3 Entrained flow gasifier

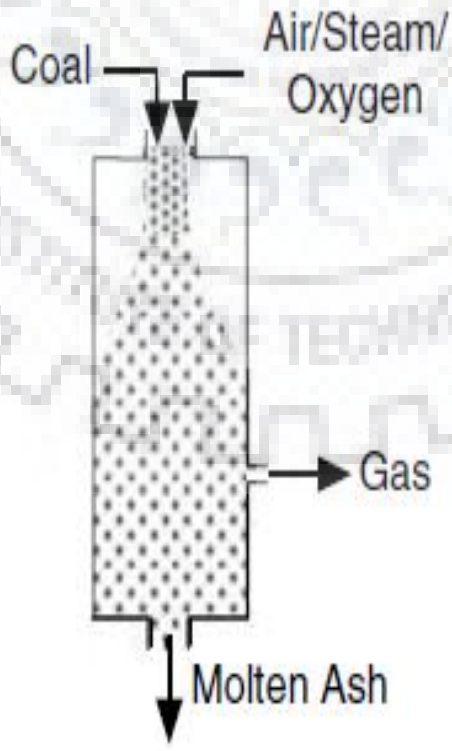

Figure 1.3: Schematic diagram of Entrained Bed Gasifier (Source: Basu, 2006)

An entrained flow gasifier gasifies the suspended pulverized solid fuel particle in the stream of the gasifying agents like oxygen and steam. It operated at very high temperature (above 2000 ^{0}C); therefore ash in the coal is removed as liquid slag and syn gas of the entrained bed gasifier contains no tar. An entrained bed gasifier can operate at pressure up to 35 bar (Basu, 2006). It can be used for larger capacity than the other types of the gasifiers and more commonly use for coal and refinery wastes. It handles the fine particles (80-100 µm) of the solid fuel. The high oxygen consumption is a drawback because it means lower thermal efficiency of the gasification process. Some of the slag particles can be carried by the product synthesis gas and deposited onto the downstream equipment, resulting in reduced performance and malfunction (Audus, 1993).

Table1.1: Some important features of different coal gasification process (Source: Basu, 2006)

S. No.	Feature	Fixed/Moving Bed	Fluidized Bed	Entrained Bed
1	Feed size	< 51 mm	< 6 mm	< 0.15 mm
2	Tolerance for fines	Limited	Good	Excellent
3	Tolerance for coarse	Very good	Good	Poor
4	Exit Gas Temperature	450-650 ^{0}C	800-1000 ^{0}C	> 1260 ^{0}C
5	Feed stock tolerance	Low-rank coal	Low-rank coal	Any coal
6	Oxidant requirement	Low	Moderate	High
7	Reaction zone temperature	1090 ^{0}C	800-1000 ^{0}C	> 1990 ^{0}C
8	Steam Requirement	High	Moderate	Low
9	Nature of ash produced	Dry	Dry	Slagging
10	Cold gas efficiency	80%	89.2%	80%
11	Application	Small capacities	Medium-size units	Large capacities
12	Problem areas	Tar production and utilization of fines	Carbon conversion	Raw gas cooling

As the coal gasification is emerged as a cleaner technology for production of gas which reduces the emission of greenhouse gases when used as a fuel for power and heat generation, more and more improvement in the gasification design are coming up. Therefore, detailed and in-depth understanding of its combustion and gasification behaviour is required. The kinetic information of coal conversion through pyrolysis makes it possible to predict its behaviour during conversion processes. Coals of different types

exhibit wide variation in their pyrolysis as well as gasification behaviour because of different extent of their coalification. Coals from different regions of the world have different characteristics regarding mineral content and coal matrix. Nearly 50% of the total world coal reserves are having high ash content; the beneficiation process is difficult for removal of the mineral matter from these coals that leads to the lower efficiency and greater environmental pollution by coal combustion.

Coal reserves are in better condition than oil and natural gas (Chavan et al., 2012); due to this reason in countries like India power production units are coal based which is responsible, to a large extent, in polluting our environment (Chandra and Chandra, 2004). Due to this, char gasification has been a subject of international interest for many years. Char gasification is commercially important not only for energy production, but also due to its applications in production of synthesis gas, ammonia, hydrogen, and methanol for various purposes. Also, by gasification coal can be converted directly to heat or to many other fuels including hydrogen and transportation fuels.

Gasification can also be used to capture the carbon for sequestration or for enhanced oil recovery from reservoirs. The gasification not only reduces the cost with increased efficiency for producing syngas but also substantially reduces emission of carbon dioxide and pollutant gases. The coal gasification process mainly consists of two steps, (i) pyrolysis and (ii) gasification; as gasification step has much lower reaction rate than that of pyrolysis, so the gasification becomes the rate controlling step (Shufen and Ruizheng, 1994; Liu et al., 2006). Gasification processes are particularly suitable for the utilisation of low-rank coal, because of its higher reactivity in comparison to high-rank coal (Li, 2007; Irfan et al. 2011; Kajitani et al., 2013). Gasification process can be carried out in different types of reactor, which are based on different models of the multi-phase reacting flow mechanisms (Abani and Ghoniem, 2013). Among these, steam gasification of char is the most promising method of char conversion (Vostrikov et al., 2007). Compared to the other gasifying agent, the water (steam) is found to be the environmentally clean and cheapest donor of H_2 and O_2.

Rate of gasification and the product quality, however, depends severely on the quality and structure of coal. The structure of coal changes with the coal types ranging from brown coal to subbituminous coal (Takeya, 1978). The size of the molecular structural unit varies with degree of coalification and this is why coal is considered to be an organic macro-molecular material. The rate of char gasification is affected by many other parameters such as concentration of gasifying agent, temperature, effective

diffusivity of gas in char, and porosity of char. Due to the reversible nature of many reactions involved in the gasification process, different reactions have different optimal operating conditions during the gasification of a char particle.

Gasification of char is one of the effective energy conversion methods for utilization of coal for producing gaseous fuel (Umeki et al., 2010). Since high fractions of combustible gases are preferred for the wider application of a gaseous fuel, the use of steam as a gasification agent appears to be excellent due to the absence of nitrogen. Also, the steam gasification has higher reactivity than the CO_2 gasification of char (Shufen and Ruizheng, 1994; Ye et al., 1998; Tremel and Spliethoff, 2013). It has been observed by many that the rate of the gasification increases with an increase in concentration of gasification agent (Kwon et al., 1988; Everson et al., 2006).

The size of the char particle also affects the rate of gasification. Since large particle has less surface area than the small one, the rate of conversion for the smaller particle is higher (Luo et al., 2001; Kajitani et al., 2006). The reaction temperature is expected to be another most important operating variable affecting the performance of a gasifier. Since the main gasification reactions are endothermic, an increase in temperature favors conversion. It has been observed in the present work that, especially carbon-steam reaction, which produces CO and H_2, and the Boudouard reaction which reduces the unwanted CO_2 to produce two molecules of CO are favors by higher temperature (Yadav and Kumar, 2014). For the quantitative analysis of these effects on the gasification of char particle, we have considered gasification of a char particle of 5, 7.5, and 10 mm, having different porosity, densities and ash content.

For the theoretical analysis suitable for better understanding of gasification process, the rate based modeling of gasification of a single particle becomes inhibitable. For the char gasification, a number of kinetic models have been proposed. The simplest of these models are homogeneous and shrinking-core model (Ye et al., 1998). In the homogeneous model, it is assumed that the particle size of char remains same but the density decreases during its gasification, whereas, in the shrinking-core model, the gaseous reactant are assumed to diffuse through the gas film and ash layer to reach the unreacted core surfaces. As reaction proceeds, the unreacted core of a char particle continues to shrinking (Wen, 1968). Based on the kinetic approach, many other researchers have also studied the modeling and simulation of coal gasification (Govind and Shah, 1984; Souza-Santos, 1989; Muller et al., 2003; Kim et al., 2014). The modeling of a single coal char particle deals to understanding the fundamental of the char

gasification (Qiao et al., 2012). The single char particle model was developed (Srinivas and Amundson, 1980; Haynes, 1982; Zygourakls et al., 1982; Samuilov et al., 2004), which was describing the effects of porous char structure and surface reaction kinetics in CO_2 gasification. In the present work, a staggered grid finite volume method (SGFVM) based numerical simulation technique is applied to solve gasification characteristics of a single char particle.

1.2 Objective of the Thesis

Considering the importance of the simulation study of a single char particle, the following objectives were set for the present work.

- To develop elementary reactions based gasification modelling of a single coal char particle to study its behaviour in different conditions.
- After model validation, to investigate the effect of following parameters on the compositions and heating values of the product gases:
  - ✓ Temperature
  - ✓ Particle size
  - ✓ Concentration of gasifying agents (steam and mixture of steam and CO_2)
  - ✓ Concentration of carbon in char
  - ✓ Initial porosity of the char particle
  - ✓ Ash content of the char

1.3 Layout of the Thesis

The outcomes of the research work are presented in the following sections beginning with the review of previously reported works followed by the model development and important results with suitable discussions. Results are grouped into two categories, (i) model validation, and (ii) parametric effects. Based on the results obtained, some conclusions have been made which is presented in the in the last chapter along with the scope of future work.

CHAPTER 2

LITERATURE REVIEW

As discussed earlier, considering the importance of gasification, many researchers have made theoretical as well as experimental work in this field. Most of the researchers have focussed their attention on various aspects of the process using coal or char. These works can broadly be classified in to two categories, viz., to study the effects of various operating parameters and the coal characteristics on the gasification process, and secondly the kinetic parameter estimation. A brief review of these works available in open literature is being presented in the following paragraphs.

2.1 Effects of Coal Characteristics and Operating Parameters

Effects of operating parameters on carbon conversion are significantly different for different grades of coal due to remarkably different characteristics of coal obtained from different sources. The increasing degree of coalification, that occurs as a coal matures from peat to anthracite, is referred as the ranking of a coal. With the passage of time and burial pressure, the rank of coal as well as its carbon content also increases. Obviously, this coal ranking plays a significant role in gasification.

2.1.1 Effect of coal rank

The effect of coal rank on the coal-char gasification has been concluded by many researchers. Ye et al. (1998) observed that the high inherent content of inorganic matter increase the reactivity of the low-ranked Bowmans coal, however, after the removal of the inherent inorganic constituents, the low as well as high rank coal have similar reactivity because the presence of inherent inorganic constituents acts as a catalyst for low rank coal (%C < 80) (Guo and Zhang, 1986; Molina and Mondragon, 1998). Li et al. (2010) studied the reactivity of three different Chinese coals of the category lignite, bituminous and anthracite. They concluded that the reactivity of the coal decreases with the increasing coal rank (Miura et al., 1989; Yang and Watkinson, 1994; Wornat et al., 1996; Ye et al., 1998; Everson et al., 2008; Zhao et al., 2010). This is due to the higher concentration of active sites, porosity and presence of inherent inorganic matter (Tomita, 1991). Since the lower rank coals contain higher amounts of functional groups with oxygen, such as hydroxyl, carbonyl, and ethers, with increasing rank, progressively fewer functional

groups are present, the oxygen content is reduced and the ring system becomes more polycondensed (Dorrestijn et al., 2000). The degree of aromatization in coal structure increases with the increase in the rank of coal (Gupta, 2007). Takarada et al. (1985) studied 34 different coals from eight countries and observed that the reactivity of the coal is controlled by the parameters like concentration of active sites, porosity and presence of inherent inorganic matter. They concluded that the reactivity of the high rank coals (caking coals) are low as compared to the low rank coals (non-caking coals) (Kyotani, 1993; Wall et al., 2002; Liu and Niksa, 2004).

Cakal et al. (2007) studied four different lignite sample at two temperatures, 875 ^{0}C and 1000 ^{0}C, under CO_2 atmosphere and found that at 875 ^{0}C the reactivity sequence is given as: Elbistan > Soma > Seyitomer > Tuncbilek as shown in Figure 2.1(a), which indicates that at 875 ^{0}C, the variation of reactivity with conversion for all four lignite sample have similar sequence; (increasing trend up to a certain conversion followed by a decreasing trend), however, at 1000 ^{0}C lignite sample behave quite differently. In cases of Tuncbilek and Soma lignite, the reactivity increases monotonously as conversion increases at higher temperature while Elbistan and Seyitomer lignite give maximum conversion at lower temperature. The reactivity sequence at 1000 ^{0}C is given as: Tuncbilek > Soma > Elbistan > Seyitomer which is shown in Figure 2.1(b). Tomeczek and Gil (2010) studied the hydrogasification reaction of chars from two coals of different rank for the temperature up to 1173 K and pressure up to 8 MPa. They found that the lignite char is more reactive than the subbituminous coal char at the same temperature (1273 K). According to Irfan et al. (2011) "A plausible explanation for such an enhanced reactivity of coal at higher temperatures may be a significant improvement in the internal surface area (or pore size) during pyrolysis and gasification and/or the catalysis of mineral impurities (inherent inorganic matter) which become more effective at relatively high temperatures. As stated previously, it is known that the rate of gasification depends on the accessibility of the reactant gas to the internal surface of porous coal where active sites reside."

The char particles of the coal as well as biomass have nearly the same reactivity (Lu et al., 2008) because these particles contain carbon and ash. Some researchers (Evans and Emmons, 1977; Blackham et al., 1994; Warnat et al., 1996; Blasi et al., 1999) have studied the reactivities of the biomass and coal char and reported that there is only a slight difference in the reactivities of these two char. The reason of this difference in the reactivity is due to the microstructure (porosity) of the char particle (Xu et al., 2011).

Hence, the kinetic data obtaining from biomass char can be used for coal char and vicevarsa.

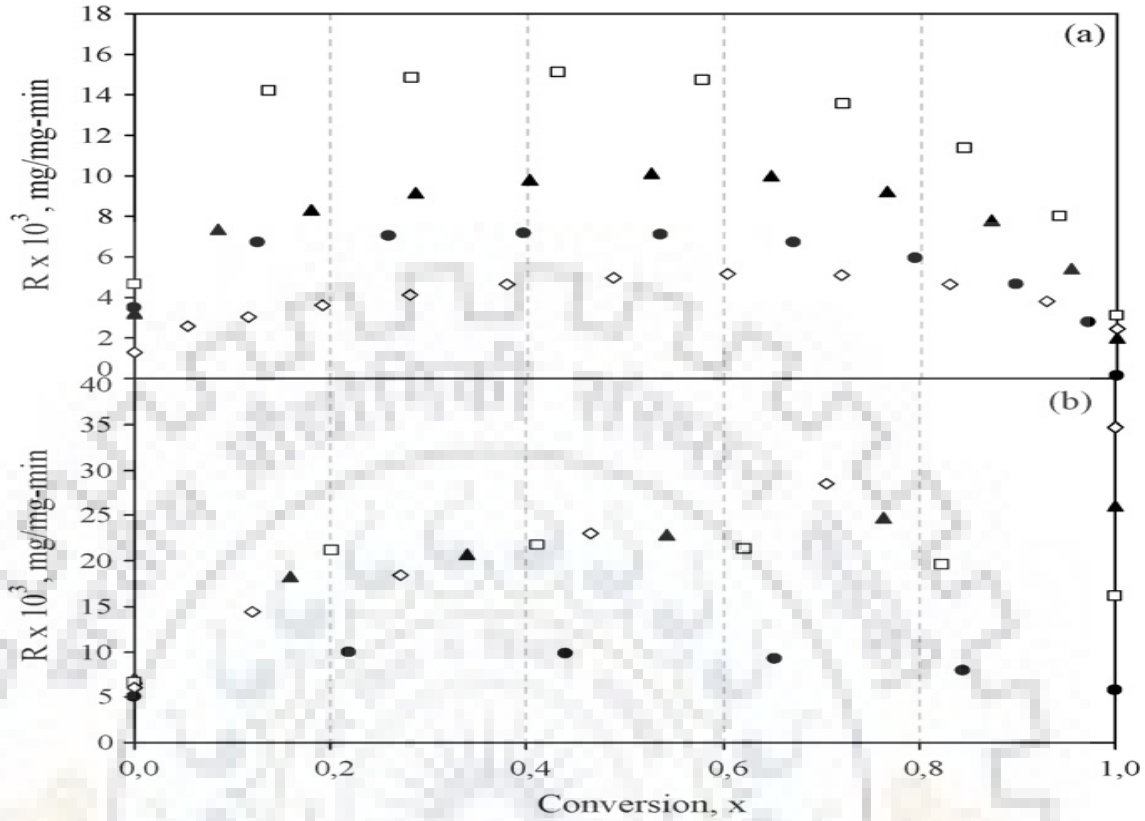

Figure 2.1: Variation of CO_2-gasification reactivities with conversion (a) at 875 ^{0}C and (b) at 1000 ^{0}C. (▲) Soma, (●) Seyitomer, (□) Elbistan and (◇) Tuncbilek (Source: Cakal et al., 2007)

Beamish et al. (1998) tested the reactivity of chars formed from New Zealand coals, of the rank ranging from lignite to high volatile bituminous by Thermogravimetric analysis. They pointed out that the lowest rank subbituminous coal chars have similar reactivities to the lignite coal chars. They also found that chars from low rank coal are more reactive than chars from high rank coal. Cai et al. (1996) analysed five coal samples (Linby, Pittsburg No.8, Illinois No.6, SBN and APCS) and concluded that the lower rank Illinois No.6 gave more reactive char compared to the higher rank Linby and Pittsburg No.8 coals because lower rank coals have high hydrogen and oxygen content and low carbon content. Similar thermogravimetric analysis was made by Morgan et al. (1986) to study the burning profile of coal. They found that the reactivity difference between vitrinite (vitrinite mean random reflectance 0.5%-1.5%) and inertinite decreases with increasing rank. They also include the burning performance of 9 coals and correlate them with the rank and maceral composition. They concluded that the maceral reactivity decreases as rank increases (Heek and Muhlen, 1987).

Brown et al. (1986) studied the effect of coal rank on the reactivity of four coals (Pittsburg No.8 bituminous, Illinois No.6 bituminous, Wyoming subbituminous and Texas lignite) in an entrained flow gasifier at atmospheric pressure. They also concluded that the low rank coals have higher reactivity and vice-versa, and the higher reactivity of low rank coals contribute to higher conversion (Gale et al., 1996). Kwon et al. (1988) investigated the effect of coal rank on the rate of conversion of char gasification in a thermobalance reactor using four coals (lignite to semianthracite). They plotted a graph between the reactivity of chars and carbon content of the coal and also compared the data obtained by different researchers. Finally they found that the reactivity increases with decreasing coal rank (Knight and Sergeant, 1982); they also concluded that the surface area of the char decreases with coal rank.

2.1.2 Effect of particle size

Kumar and Ghoniem (2013) studied the impact of coal particle size on the carbon conversion; they found that the fine particle of coal speeds up the conversion and the particle smaller than 36 µm undergo complete conversion. The fine particle of the size between 20 µm and 44 µm gives approximately the same intrinsic gasification rate at lower temperature but at higher temperature (>1200 ^{0}C), the coal size 20 µm has higher gasification reactivity than the 44 µm size of coal (Kajitani et al., 2006) which is shown in Figure 2.2. The chemical and physical properties of coal depend on particle size, however, the extent of which varies among different coals (Palmer et al., 1990).

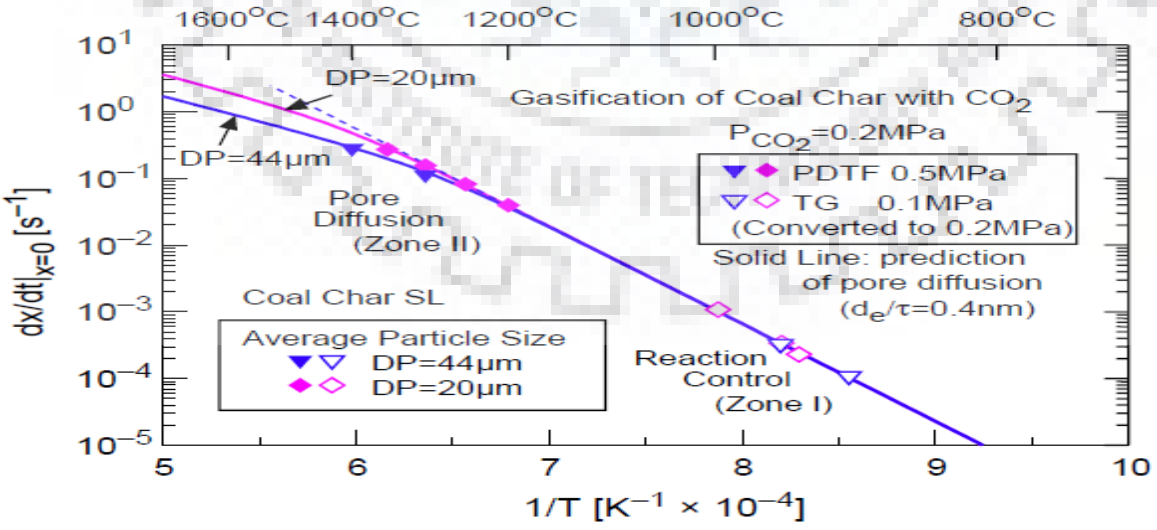

Figure 2.2: Influence of particle size on gasification rate (Source: Kajitani et al., 2006)

Huang and Watkinson (1996) studied the effect of particle size on the carbon conversion of two coals (Highvale and Coal Valley) at a constant temperature of 900 ^{0}C. They included the three particle size for each coal in their studies. For the Highvale coal, particle sizes were 0.85-1.4 mm, 1.4-2.0 mm and 2.36-3.0 mm and for Coal Valley the particle sizes were 1.0-2.0 mm, 2.0-2.36mm and 2.36-3.0 mm. They concluded that for Highvale coal, the lower size coal particle gives higher conversion compared to the coals of higher size but for the Coal Valley, there is no variation in conversion with coal particle size up to a carbon conversion of 60%; above this value there are slightly higher conversion for larger particles, they also correlate the relation between particle size and conversion as:

$$d_p = d_{p0}(1-x)^{0.333} \qquad (2.1A)$$

Luo et al. (2001) generalized the above correlation which shows the relationship between particle size and conversion as:

$$d_p = d_{p0}(1-x)^{\alpha} \qquad (2.1B)$$

Where α is diameter variation parameter.

Morgan et al. (1986) determined the burning profiles of coal for different sizes (63 µm, 75 µm and 125 µm) by thermogravimetric analysis and correlated the size of coal to the reactivity. They pointed out that the reactivity increases with decreasing the size of coal particle (Zhuo et al., 2000); this is due to the increasing surface area of particles (Fung et al., 1988), same trend between the reactivity and particle size of coal was also observed by Wen and Chaung (1979) for Illinois No.6 coal. For small difference in the particle sizes of coal sample, many researchers observed that the particle size has no significance impact on the gasification rate (Badzioch and Hawksley, 1970; Katta and Kealrns, 1981; Molina and Mondragon, 1998; Paviet et al., 2007). Brown et al. (1986) correlated the effect of coal particle size on the carbon conversion of the Utah coal having sizes 71 µm and 50 µm. They showed that the lower particle size gives higher conversion and vice-versa (Zhu et al., 2008). They also pointed out that the carbon conversion is approximately proportional to the square root of the coal particle size. Ye et al. (1998) examined the effect of particle size on the carbon conversion for Bowmans coal during steam and carbon dioxide gasification at a reaction temperature of 765 ^{0}C. They pointed out that for Bowmans coal, the gasification rate are independent of the particle size for both the gasification agents (for homogeneous model) and the reaction rate increases with decreasing particle size (for shrinking core model). Linares et al. (1977) studied the different sizes of coal for lignite, PSOC-87, LV bituminous char and PSOC-127. They

concluded that the reactivity is approximately same for 40×100, 100×150 and 200×325 mesh fraction for lignite and PSOC-87 but for LV bituminous char and PSOC-127, reactivity increases four times when particle size is reduced from 40×100 to 200 × 325 meshes (Linares-Solano et al., 1979), however, for the same variation of mesh fraction of particle, the reactivity increases with decreasing the mesh fraction of particle for POSC-87 and PSOC-127 coals (Hippo and Walker, 1975). Knight and Sergeant (1982) analysed the effect of reactivity of four Australian coals having the particle sizes 422-211 µm, 211-104 µm and <104 µm. They pointed out that the reactivity increases with decreasing the particle size of coal char, but for a small difference in the particle size of coal, the rate of reaction has little bearing on the size of particle. The similar observations were made Feldkirchner and Linden (1963) for size of -16, +20, -40 and +50 sieve sizes. Gremyachkin and Mazanchenko (2011) investigated the effect of coal char inner surface area and the gasifying agents. They concluded that for particles with large inner surface, the main oxidizer with steam and for small inner surface, steam and CO_2 play equal role.

2.1.3 Effect of catalyst

The coal gasification reaction rate are influence by the presence of foreign material (minerals) (Gomez and Mahinpey, 2015) which are more effective for low rank coals (Everson et al., 2006) and at low temperature because at higher temperature diffusional effect become appreciable. The same is discussed in detail by Ochoa et al. (2001). The measurement of coal reactivity with mineral matter can be evaluated by measuring the gasification rate of coal in both cases, i.e., in the presence of the mineral matter and after removal of the mineral matter (demineralization) with acid-washed (Vamvuka et al., 2006). Difference in the reactivity is due to the presence of mineral material in varying proportion in different coal, however, after the demineralization, some coals like Pocahontas No.3 coal char shows enhanced gasification rate; Sharma et al. (2002) pointed out that this means that some other factor is controlling the rate. They also observed a similar trend for high rank coal, with the increase in the porosity. Haga and Nishiyama (1988) studied the effect of Ni-catalyst on the steam gasification. They showed that the specific reactivity of a Ni-loaded char depends on the crystallinity of bulk carbon at high temperature (>700 ^{0}C).

The most important inherent catalysts are alkali and alkaline earth cations like Ca, K and Na (Kayotani et al., 1993; Liu and Niksa, 2004). The gasification reactivity follows

the order Na > K > Ca > Ni with the same anions (Ye el al., 1998). The combined effect of different cations is found to be less than for the sum of the individual cations.

Huang and Watkinson (1996) studied the effect of minerals on the gasification rate of Highvale coal. They concluded that after removal of minerals from the coal, the reactivity decreases four times. Similar results were also obtained by Calemma and Radovic (1991) for Italian Sulcis coal, but in case of the chars derived from higher rank coal, mineral matter removal increases the reactivity (Linares-Solano et al., 1979). Many researchers advocated that the influence of minerals on the gasification rate of lower rank coal are more effective because the rate of coal gasification for lower rank can be controlled by the minerals in the coal (Hashimoto et al., 1986; Heek and Muhlen, 1987; Miura et al. 1989). For small size of coal char, the reactivity is higher due to the higher content of the inherent mineral matter which catalyses the reaction of gasification (Fung et al., 1988; Zhu et al. 2008). Since the mineral matter increase the cross linking reactions that decreases both tar yield and hydrogen yield which results in increasing intrinsic char reactivity for lignite coal (Gale et al., 1996). The char gasification rate depends on the alkali index also. Greater the alkali index lead to higher reactivity in the Chinese anthracite coal because greater the alkali index, higher is the catalytic effect (Zhang et al., 2006). A linear relationship between the alkali index and the gasification rates for both H_2 and CO_2 gasification was observed in case of Greek lignite samples (Skodras and Sakillaropoulas, 2002) where alkalinity index is defined as:

$$Alkali\ Index = \frac{Mole\ fractions\ of\ basic\ compounds}{Mole\ fraction\ of\ acid\ compounds} \times Ash\ content\ (wt\%)$$

Some coal also contain trace amount of Fe with alkali and alkaline earth metals like Na and Ca, the co-loading of alkali and alkaline earth metals with Fe enhances the reactivity of char which has been reported by many researchers (Ohme and Suzuki, 1996; Irfan et al., 2011). They also proposed the following mechanism of iron catalyst for oxygen transfer.

$$Fe_mO_n + CO_2 \rightarrow Fe_mO_{n+1} + CO$$

$$Fe_mO_{n+1} + C \rightarrow Fe_mO_n + CO$$

Presence of organic and inorganic sulphur can strongly inhibit the catalytic activity of inherent mineral matter through the formation of inactive sulphides (Calemma and Radovic, 1991). Wells and Smoot (1991) correlated reactivity in terms of structure of the chars, which in turn is correlated with the fuel properties. The relative order of importance was observed to be “catalytic elements > porosity > hydrogen types > cluster size”.

2.1.4 Effect of gas composition

The effects of gas composition on the rate of gasification have been the subject of research of many researchers. It is generally observed that initially on increasing the gasification agents, the rate of gasification increases but after a certain level, there is no further increase in the gasification rate. Liu and Niksa (2004) reported that initially the rate of gasification is proportional to the increase in the CO_2 and H_2O mole fraction from 8 to 25% and 4 to 16% respectively. Upon further increases from 25 to 48% for CO_2; no effect on the rate was observed in a PDTF (Pressurized drop tube furnace) at 1300 ^{0}C and 0.5 MPa but Kwon et al. (1988) and Knight and Sergeant (1982) pointed out that on increasing the concentration of CO_2 even above 20%, the reactivity of char increases (Gomez et al., 2014). Liu and Niksa (2004) also concluded that at the same mole fraction of these gasification agents, the CO_2 gasification rate is about four times slower than the rates of steam gasification for Newlands char which is shown in Figure 2.3. The similar result was observed by Everson et al. (2006) that the rate of gasification increase with H_2O mole fraction from 10 to 20% for South African inertinite-rich (high-ash) coals. Tremel and Spliethoff (2013), Ye el al. (1998) and Shufen and Ruizheng (1994) also reported that the reaction rate of the char-H_2O reaction is higher than that for char-CO_2 reaction. Karimipour et al. (2013) conducted experiments to analysed the effect of coal feed rate, coal particle size, and steam/O_2 ratio on the quality of syn gas produced from fluidized bed gasification of lignite coal. They found that by the variations of feed rate from 0.036 to 0.063 g/s, for the particle sizes of 70 to 500 μm, and steam/O_2 ratio 0.5 to 1.0, the carbon conversion, H_2/CO ratio, CH_4/H_2 ratio, gasification yield, and gasification efficiency are found to range from 91%-97%, 0.776-1.268, 0.0517-0.0703, 3.4-3.7 m^3gas/kg coal, and 56%-67%, respectively. Katta and Kearlns (1977) observed that the higher conversion takes place through steam gasification. Hence, it is important to establish the char reactivities in the steam atmosphere rather than the other. Also they found that char reactivity decreases with increasing heat treatment temperature, however, magnitude of the effect depend on the coal rank. Tremel and Spliethoff (2013) pointed out that on an average; the char-H_2O reaction is about 3-6 times faster than the char-CO_2 reaction (Matsui et al., 1985). Mann et al. (2004) also pointed out that the steam gasification rates are several times faster than CO_2 gasification rates. Vostrikov et al. (2007) studied the kinetics of coal conversion in supercritical water under the pressure of 30 MPa and the temperature range of 500-750 ^{0}C. They found that the coal gasification in SCW without oxidants is the weakly endothermic process**.** The addition of CO_2 into SCW decreases the

conversion rate and increases the CO yield. Juntgen (1984) showed that the pyrolysis reactions of high rank coal interpreted in terms of parallel first order reaction is related to coal functional groups. In the presence of hydrogen at a temperature greater than 500 ^{0}C, additional reaction of partial hydrogenation with subsequent hydrocracking will occur, which increased the yield of aromatic tar, BTX, methane, and H_2O. Murphy and Shaddix (2006) studied the combustion kinetics of the coal chars over oxygen concentrations ranging from 6 to 36 mol% and temperature range of 1320 to 1800 K. They found that apparent reaction order varies from 0.1 under near-diffusion-limit oxygen-depleted conditions to 0.5 under oxygen-enriched conditions.

Zhuo et al. (2000) studied the gasification rate of char derived from the high ash Daw Mill coal sample in CO_2 and steam atmosphere at different pressure up to 30 bar in different types of gasifiers like WMR (Wire mess reactor), FBR (Fluidised bed reactor) and HRR (Hot-rod reactor). They concluded that the rate of gasification with steam is higher than the CO_2 and gasification rate increased with reactive gas pressure. The addition of the steam to the gasifier, increased coal moisture which ultimately led to decreased hydrogen concentration and CO/CO_2 ratio. Hence higher H_2O/coal ratio, decreased the CO/CO_2 ratio (Gutierrez and Watkinson, 1982), lowers hydrogen concentration and carbon conversion (Brown et al., 1986) because the addition of steam decreases the reaction temperature. Li et al. (2010) observed the reaction order for gasification reaction of Huolinhe lignite, Shenmu bituminous and Jincheng anthracite coals with CO_2 and H_2O experimentally in a self-made pressurized fixed-bed reactor at increased pressure (up to 1.0 MPa). On increasing the partial pressure above 1.5 MPa (or above the atmospheric pressure), the gasification rate tends to become zero order reaction with respect to the partial pressure of reacting gas (Schmal et al., 1983; Sha et al., 1990; Molina and Mondragon, 1998; Ahn et al., 2001). The results are described by the shrinking core model during CO_2 and H_2O gasification and the orders of reactions for steam gasification were reported to be 0.49, 0.46, and 0.43 respectively; for CO_2 gasification the reaction order were 0.31, 0.28, and 0.26 respectively. Tay et al. (2013) has studied the gasification of a Victorian brown coal in a novel fluidised-bed/fixed-bed reactor at 800 ^{0}C in the atmosphere containing reducing (H_2O) and oxidizing (CO_2 & O_2) gasifying agents. They observed that the presence of steam are important for the evolution of char structure and also improved the retention of Mg and Ca during gasification by changing the physico-chemical forms of Ma and Ca; the char-H_2O gasification followed a different reaction pathway from the char-CO_2 gasification. The char gasification with

steam enhances the production of H_2 (Xu et al., 2011; Cempa-Balewicz et al., 2013, Mostafavi et al., 2014) through water gas shift reaction (Pahuja and Saraf, 1978; Singh and Saraf, 1980; Adams II and Barton, 2010; Adams II and Barton, 2011(a); Adams II and Barton, 2011(b)) while with CO_2 gasification improves the CO formation in the product gas (Liu et al., 2006). Daggapati et al. (2011) also studied the underground coal gasification by using mixture of oxygen and steam as the feed gas and obtained the higher concentration of hydrogen in product gas.

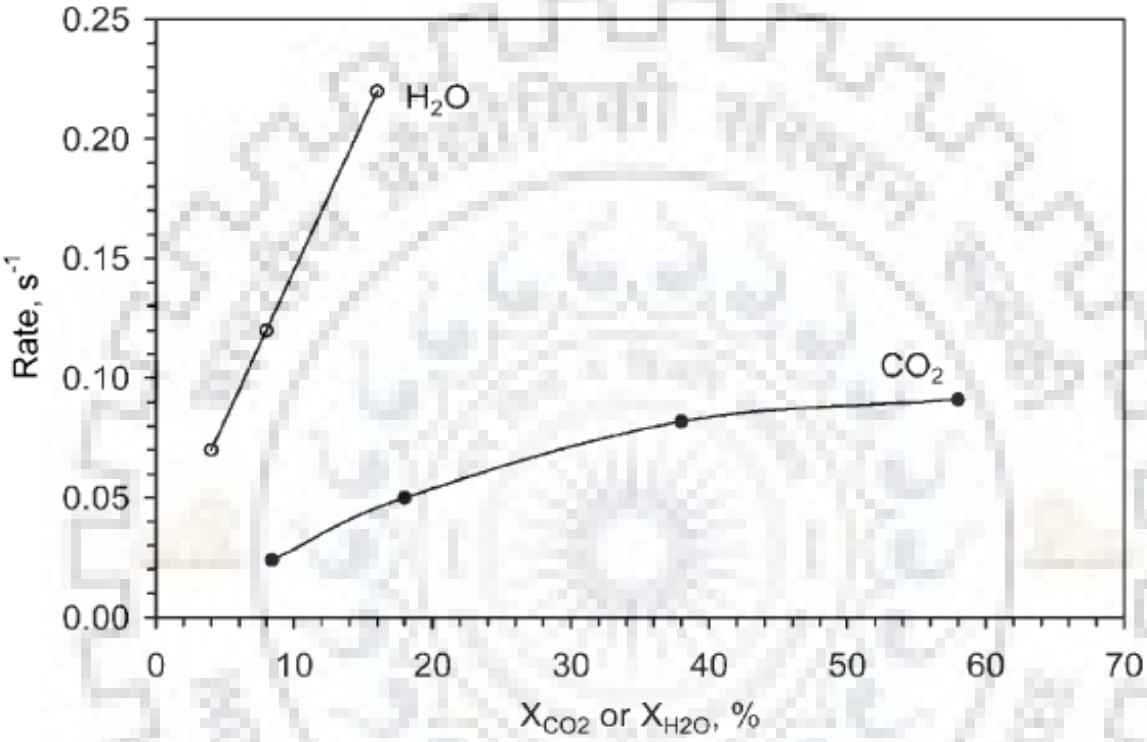

Figure 2.3: (○) CO_2 and (●) steam gasification rates for Newlands bituminous char at 1300 ^{0}C and 0.5 MPa in a PDTF (Source: Liu and Niksa, 2004)

Zhang et al. (2006) investigated the gasification reactivities of six Chinese anthracite chars with steam and CO_2 in the pressure range 0.02-0.1 MPa and temperature rage 920-1050 ^{0}C by using thermogravimetric analysis. They calculated the relative reactivity ratios of steam to CO_2 at 1000 °C and found that these ratios are 6.71, 14.20, 9.41, 11.08, 14.46, and 8.83 for Jincheng, Yangquan, Rujigou, Hunan, Guangdong and Longyan chars, respectively. Umemoto et al. (2013) also, used thermogravimetric analysis to measure the reactivity of SF char, MN char and DT char experimentally at 1223 K and 0.1 MPa with different concentration of H_2O. They founded that on increasing the concentration of H_2O, the char gasification rate increase.

Varying gas composition was used to establish the kinetic parameter for C-H_2O and C-CO_2 by many researchers. Katta and Kealrns (1981) found that the rate constants of

C-CO_2 reaction are about 2.5-5 times lower than the C-H_2O reaction over a temperature range of 950 to 1040 ^{0}C. Velez et al. (2009) worked on the co-gasification of Colombian biomass and coal blends (6-15 wt%) in a fluidized bed at atmospheric pressure. The fuel gases obtained from this blending were found to contain up to 15% more hydrogen. Further increasing the biomass fraction, increase the hydrogen content but decreased the energy efficiency of the process.

2.1.5 Effect of porosity (or pore size)

Porosity of the particle facilitates gas transport inside the particle volume and hence affects rate of gasification considerably. Gupta and Bhatia (2000) studied variation of the reactivity with porosity and pore surface area of char. They proposed following correlations to evaluate the porosity as well as the pore surface area of the char.

$$\varepsilon_\mu = 1 - \exp(-V_{\mu E}) \quad (2.2)$$

$$S_\mu = S_{\mu E}(1 - \varepsilon_\mu) \quad (2.3)$$

These equations indicate that on increasing the non-overlapped pore volume per unit volume of solid ($V_{\mu E}$), thus with increase in the porosity there is reduction in the surface area of pore. This in turn reduces pore surface area, reactivity, and conversion of char. Similar observation was made by Adschiri et al. (1986) that the gasification varies linearly with the pore surface area during gasification. Koranyi (1989) also founded a linear relationship between reactivity and microporosity. Char conversion, which varies from zero to unity, is related to the porosity (Gupta and Bhatia 2000; Singer and Ghoniem, 2011) by

$$X = \frac{\varepsilon_\mu - \varepsilon_{\mu 0}}{1 - \varepsilon_{\mu 0}} \quad (2.4)$$

Katta and Kealrns (1981) pointed out that the reactivities are proportional to the pore surface area above 0.003 μm in diameter of pores. On the other hand, Hurt et al. (1991) observed that the roles of microporous surface are significant for subbituminous coal char in the CO_2 gasification. However, the rate of coal char gasification is insensitive even to very large changes in microporous surface area occurring during heat treatment reaction. Ochoa et al. (2001) studied the effect of reactivity of subbituminous and high volatile bituminous coals in terms of microporosity. They concluded that the subbituminous char are more reactive as compared to the high volatile bituminous char due to the more disordered structure and micropores. Sharma et al. (2002) pointed out that the rate of gasification increases for high rank coal due to increase in porosity after

creation of additional poroses during demineralization, but for lower rank coals (having higher reactivity) the porosity is already higher (Li et al., 2010). Kwon et al. (1988) proposed a reason for higher reactivity of low rank coal; since the lower rank coals have higher concentration of macro and meso pore whereas in high rank coals microporosity predominates, due to this reactivity of lower rank coal are higher than high rank coal (Linares-Solano et al., 1979). The porosity enhances the ability of a reacting gas to diffuse into internal surface of the micropores. On the other hand, carbon deposition blocks the pores of char, 2.6% deposition of carbon by weight, reduces the open porosity from 35.6 to 23.8% (Kamishita et al., 1977). The porosity is also affected by the temperature. Bale et al. (1986) studied the changes in pore volume of North Dakota lignite by small angle X-ray scattering after heat treatment in argon. They observed that a larger increase in pore volume following thermal treatment in a nitrogen atmosphere in the temperature range of 400-700 ^{0}C. Heek and Muhlen (1987) observed that the porosity remains constant up to temperature of about 300 to 400 ^{0}C. After this value, the porosity of lower rank coal reduces and passes through minimum in the range 600-700 ^{0}C, but for high rank coal the porosity remains constant. Jenkins et al. (1973) also observed that porosity increases up to 600 ^{0}C; beyond this value (above 600 ^{0}C) the concentration of active pores decreases and also degradation of reactive chemical structures occur which results in decreased reactivity. Gale et al. (1996) studied the intrinsic reactivity of swelling and non-swelling coal with respect to porosity. They concluded that the reactivity of coal decrease with increasing porosity of non-swelling coal. Some researchers also studied the effect of pressure on the porosity. Wall et al. (2002) observed that at high pressure pyrolysis, most of the char particles are of a high porosity (Shurtz et al., 2012), low surface area and a non-uniform porous structure which influence the apparent char reactivity (Liu et al., 2000). Wu et al. (2006) studied the porosity changes with the char conversion. The porosity of the char increases at low carbon conversion due to the opening of closed pores and enlargement of existing pores simultaneously, while porosity decreases at high carbon conversion because the neighbouring pores amalgamating and pore disappearing due to the consumption of carbonaceous chars. Ng et al. (1998) found that the open porosity, total pore volume, micropore volume, N_2 and CO_2 surface areas, gasification reactivity and apparent compressibility of chars decreases with increase in carbon content of coals. Dwivedi and Upadhyay, (1977) reanalyzed the effect of voidage on mass transfer factor for particle-fluid system in fixed and fluidized bed and also developed correlations for the

various situations and Pugsley and Beruti (1996) used the circulating fluidized bed for the same.

2.1.6 Effect of heating rate

The char gasification reactivity gets affected by the heating rate during the coal pyrolysis (de-volatilization) (Ahuja et al., 1996(a); Ahuja et al., 1996(b); Shurtz and Fletcher, 2013). Otto et al. (1979) studied the effect of heating rate on the char reactivity of North Dakota lignite at rate of 20 ^{0}C/min. They observed that on higher heating rate during de-volatilization, resulted in an aggravated contact loss between the coal minerals and the char surface. Cai et al. (1996) studied the effect of heating rate on reactivity during pyrolysis of chars (Srivastava and Jalan, 1994; Srivastava et al., 2006) prepared under atmospheric pressure for Linby, Pittsburgh No.8 and Illinois No.6 coals at 1000 ^{0}C and Tilmanstone coal at 950 ^{0}C. They observed that the char reactivities increase with heating rate up to about 1000 K/s and to level off between 1000 to 5000 K/s (Gibbins et al., 1990). The increases in reactivities are found to be higher for lower rank coal. Since chars from rapidly heated coals have higher concentration of feeder pores and surface area, porosity and reactivity of such chars are high (Adschiri et al., 1986). Schmal et al. (1985) investigated the spontaneous heating of coal piles theoretically. The unsteady state model takes into account the oxygen depletion and production of heat by chemisorptions of oxygen in the coal, transport of oxygen by diffusion and convection. Li et al. (1993) observed the pyrolysis of mecaral concentrates of Linby coal for product yields and structures of tars in the temperature range 400 to 900 °C and heating rate between 1 to 1000 K/s. They found that the yield increases with increasing heating rate.

Zhuo et al. (2000) studied the effect of heating rate on the reactivity of the char during gasification. They observed that at slow heating rate (10 K/s) the lower conversion is due to poor gas-solid contact. Also, slow heating rate required long exposure times at temperature near 1000 ^{0}C. Gibbins-Matham and Kandiyoti (1988) examined the effect of heating rates between 1-1000 K/s on coal pyrolysis. They concluded that an increase in heating rate from 1 to 1000 K/s increases pyrolysis volatile yields from a number of coal types. Luo et al. (2001) studied the effect of rapid and slow heating of coal on the reactivity of coal char and concluded that reactivity increases with increase in heating rate during carbonization. They also observed that the effect of rapid heating (930-2600 K/s) on the char reactivities are several times higher than the low heating rate (5-40 K/s) (Peng et al. 1995). During slower heating (longer residence time), the additional hydrogenating

effects may occur (Heek and Muhlen, 1987). Rathnam et al. (2009) studied the reactivity of four pulverised Australian coals under simulated air (O_2/N_2) and oxy-fuel (O_2/CO_2) atmospheres using a DTF (drop tube furnace) maintained at heating rate of 25 K/s. They concluded that for char-CO_2 reaction, reactivity increases when temperature exceeds about 1030 K (or high heating rate). From 1000 ^{0}C to 1400 ^{0}C, char indicates a strong tendency of increasing reaction rate (Liu et al., 2006). Liu et al. (2004) studied char pyrolysis at low temperature and low heating rates with thermogravimetric analyzer. They found that low heating rate (longer residence time) led to lower reactivity. Kasaoka et al. (1987) observed the effect of heating rate on the char reactivity in steam gasification by gravimetric method using 12 coals ranging from 61.1 to 93.4 wt% C. They concluded that the heating rate (5-420 K/min) during carbonization and pyrolysis of coal below 1000 ^{0}C have less effect on the reactivity of the char. Carbonization above 1100 ^{0}C, however, reduced the char reactivity by a factor 7 to 10 at 1300 ^{0}C compared to 900-1000 ^{0}C. Karabulut et al. (1999) found that the reactivity decreases between 400-600 ^{0}C of the char samples, but above 600 ^{0}C the rates of gasification reactions started to increase.

Gale et al. (1996) observed that char intrinsic reactivity decreases with increasing pyrolysis temperature between 850 and 1627 K and heating rates between 10^4-10^5 K/s; this is due to ordering, flattering, or smoothing of carbon layered planed during depletion of nonaromatic components in the char matrix during de-volatilization. Miura et al. (1989) reported that char-CO_2 reactivity increases with decrease in C content because of the development of pore structure and increase of active sites due to stripping of volatile matter present in the char during the early stage of gasification. They also reported that the reactivity increases with increase in heating rate because higher heating rates increases the number of active sites by reducing the development of graphite-like structure. This is due to the fact that the rate constant is several times higher for rapid heating as compared to the slow heating (Bayarsaikhan et al., 2005). Tremel and Spliethoff (2013) observed the effect of char preparation on the gasification rate of char sample for two different coals in a pressurised entrained flow reactor and a pressurized thermogravimetric analyser. They performed two different types of experiment. In first experiments, the reaction rate was examined at constant temperature of 750 ^{0}C. After that the heating rate was kept constant at 10 K/min and temperature was increased from 600 to 1000 ^{0}C at 0.5 MPa. They found that the reaction rates are depending on char preparation conditions as well as reactant gas. They observed that the reaction rate decreases in CO_2 atmosphere for char sample which were prepared at higher temperature. Radovic et al. (1983) pointed out that coal char

deactivation is due to increased undesirables of pyrolysis which results decrease in the active surface area of the chars. Roberts et al. (2003) observed the effect of pressure and heating rate on the apparent reaction rates of char in CO_2, H_2O, and O_2 atmosphere for three Australian black coals in a pressurized thermogravimetric analyzer. They concluded that chars made at high pressure and high heating rates have apparent reaction rates in CO_2, H_2O, and O_2 that are orders of magnitude faster than those of char made from the same coal at atmospheric pressure and slow heating rate conditions. Guizani et al. (2013) pointed out that at low heating rate (5 ^{0}C/min), the char yield is 24.8% which is much lower than high heating rate (100 K/s). The char yield decreases slightly when increasing the reaction temperature from 9.89% at 850 ^{0}C to 7.87% at 950 ^{0}C. Since the heating rate also affect the activation energy and pre-exponential factor, both parameter decreases with increasing the heating rates. There is a difference of 60 kJ/mol in the value of activation energy at heating rates 5 and 30 ^{0}C/min (Sima-Ella et al., 2005). Fushimi et al. (2003) examined the reaction mechanism of steam gasification with rapid heating (100 K/s) by using thermobalance reactor with a micro GC and a mass spectrometer for Yallourn brown coal and Taiheiyo subbituminous coal. They concluded that above 600 ^{0}C, the evolution of CO decreases and the evolution of H_2 and CO_2 increases, but above 750 ^{0}C, increase in the evaluation of CO as well as gasification efficiency was observed in case of rapid heating. Gibbins and Kandiyoti (1989) observed that high heating rate gives larger yield of both tar and total volatiles above 400-800 ^{0}C, these increase in the tar and total volatile is due to the increasing heating rate between 1 K/s to 1000 K/s.

2.1.7 Effect of temperature

The reaction temperature is expected to be one of the most important operating variables affecting the performance of coal gasifier. Since the main gasification reactions are endothermic, an increase in temperature favours the reaction. However, many researchers worked on the low temperature gasification for low rank coal because low rank coal have high reactivity (Hurt et al., 1986; Kovacik et al., 1990; Sharma et al., 2002; Tay et al., 2013). It is generally observed that for the low rank coal conversion is more sensitive at lower temperature. Kwon et al. (1988) reported that for an increase in temperature from 700 to 800 ^{0}C, there is a seven fold increase in the carbon conversion, on further increasing the temperature from 800 to 900 ^{0}C (Mani et al., 2011), the carbon conversion for Australian lignite char doubles. Ye et al. (1998) studied the gasification of South Australian low rank coal having higher reactivity with steam and with CO_2 at

atmospheric pressure and at temperature between 714 and 892 ^{0}C (low temperature) and they suggested that the gasification rate follows the homogeneous model which is shown in Figure 2.4 below. The gasification rate increases with increasing the temperature (Hedman et al., 1983) for low temperature gasification (Bayarsaikhan et al., 2006) which is also shown in the same figure.

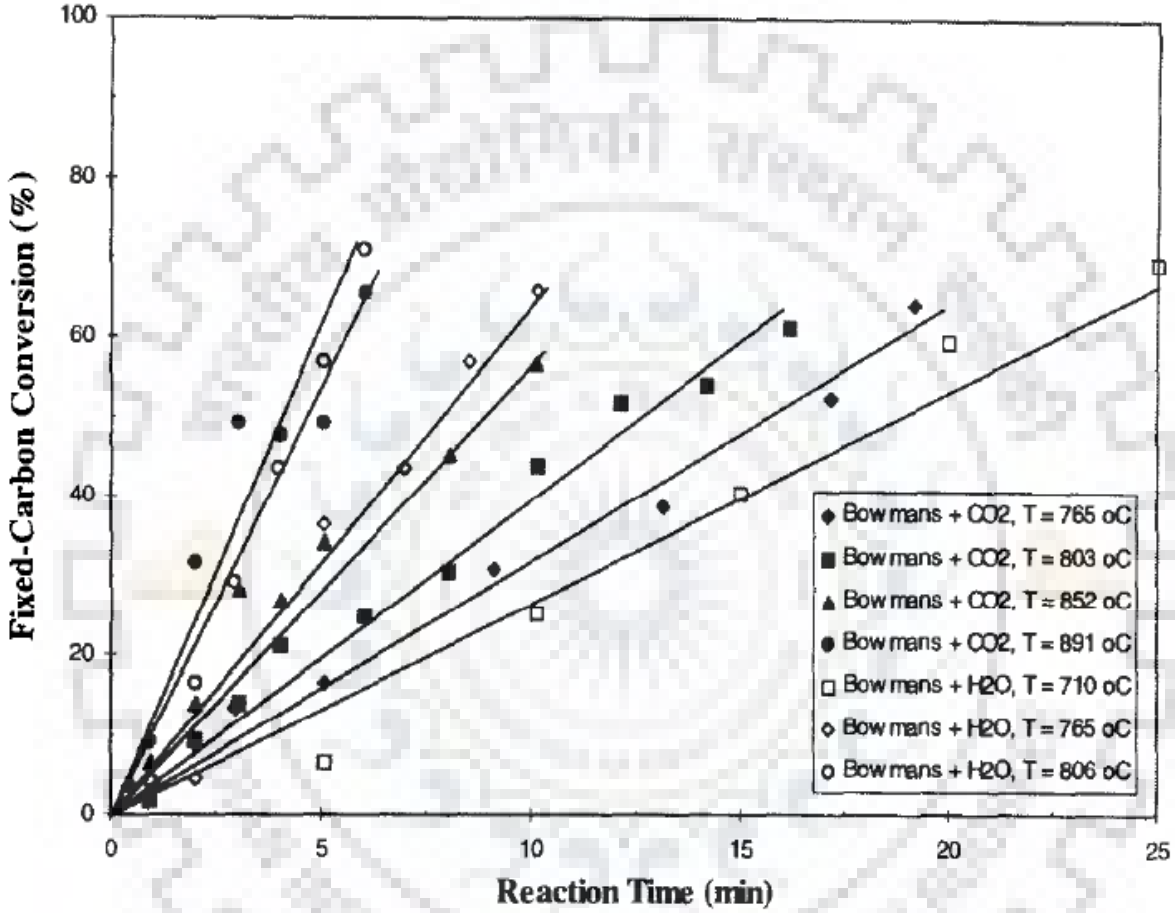

Figure 2.4: Fixed-carbon conversion versus reaction time for CO_2 and H_2O gasification of Bowmans coal at different temperatures (particle size fraction: 1.6-2.4 mm) (Source: Ye et al., 1998)

Ochoa et al. (2001) observed the CO_2 gasification of chars derived from Argentinean low-rank coals in the temperature range 1173-1433 K. They identified two regions: below 1333 K, kinetic control prevails for chars (Tremel and Spliethoff, 2013), and above 1333 K, diffusional effects (pore diffusion) become significant and affect the overall reaction rates. Similarobservation was made by many other researchers also (Adschiri et al., 1986; Kayotani et al., 1993; Kajitani et al., 2006; Umemoto et al., 2013). Watanabe and Otaka (2006) observed the temperature dependency of reaction rate. The

change in the rate-determining step from a chemical reaction control to pore diffusion limitation is shown in Figure 2.5.

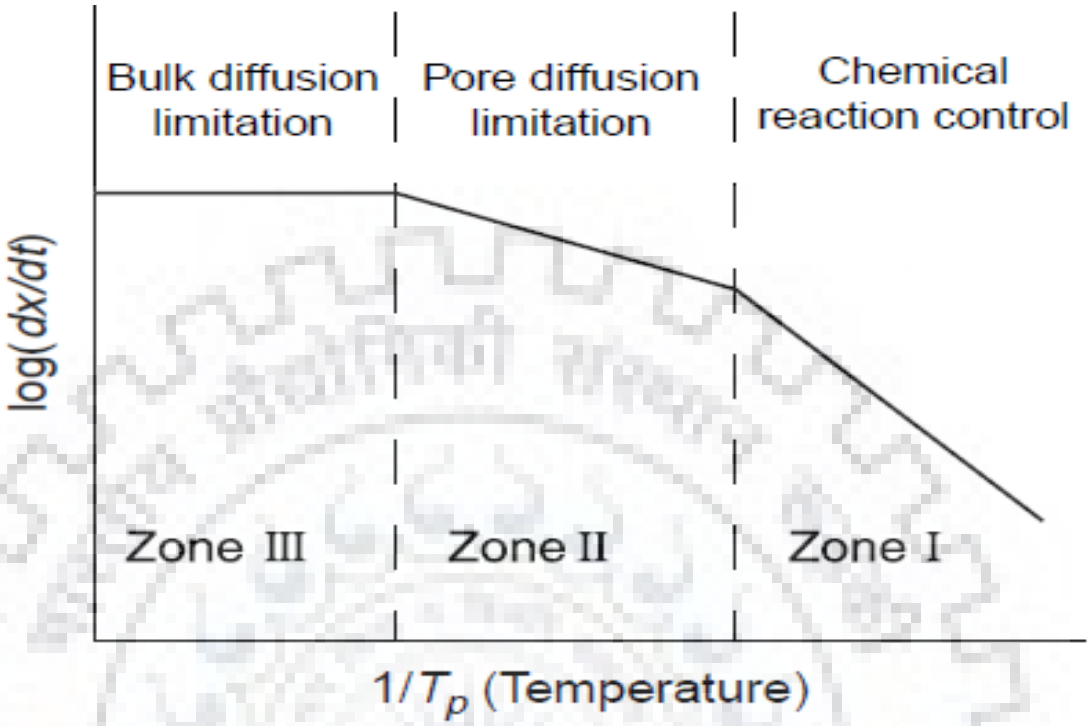

Figure 2.5: Temperature dependency of reaction rate (Source: Watanabe and Otaka, 2006)

Liu and Niska (2004) studied the effect of gas temperature variation from 800 to 1500 ^{0}C on the gasification rates. They found that the extents of conversion increased in uniform increments of roughly 15% per 100 ^{0}C as temperature increased from 800-1000 ^{0}C and further increasing to 1100 ^{0}C, the conversion increases only by 2.5% because the reaction shifted from kinetic control region to diffusional control region where pore diffusion is the rate controlling mechanism (Figure 2.6).

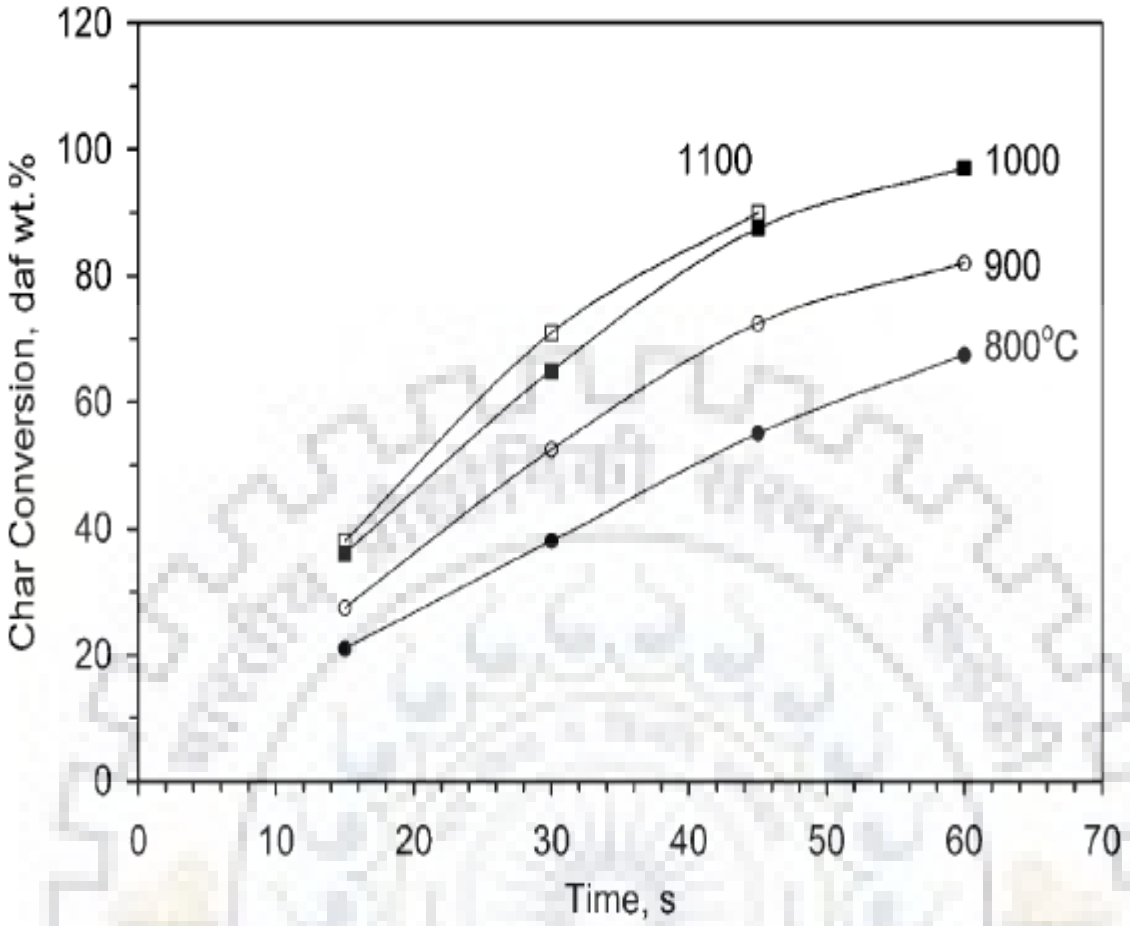

Figure 2.6: Char conversion histories of Roto subbituminous char at (●) 800, (○) 900, (■) 1000, and (□) 1100 ^{0}C and 0.78 MPa under 76% H_2O in a PDTF (Source: Liu and Niska, 2004)

Upon increasing the temperature from 800 to 1250 K, the reaction mechanism changes from chemical reaction controlled regime (27 kcal/mole) to gas film diffusion control (2.3 kcal/mole) (Lee et al., 1998). Guell et al. (1993) studied the CO_2 gasification reactivities of Pittsburg No.8 coal for temperature between 750 to 1200 ^{0}C (Audley, 1987). They also point out that the rates reached a maximum at about 20 to 40% conversion at around 900 ^{0}C. Rathnam et al. (2009) observed increased char reactivity at temperatures exceeding about 1030 K for char-CO_2 reaction in a thermogravimetric analyzer. Brown et al. (1986) studied four coals of varying rank in an entrained flow gasifier at atmospheric pressure. They concluded that at higher temperature (>1500 K) resulted in higher H_2 and CO concentration due to the endothermic reaction of steam-char pyrolysis (Kim et al., 2000). The entrained flow gasifier operates at higher temperatures with small particle which attains a high carbon conversion even for low residence time (Liu et al., 2004; Harris et al., 2006). Wen and Chaung (1979) pointed out that to achieve high conversion either recycling the unreacted hydrocarbon or to provide high temperature atmosphere to

enhance the gasification rates is required. Miura et al. (1989) proposed a relation between gasification reactivity (R), temperature (T), and pressure (P) as:

$$R \propto P^n e^{-E/RT} \quad (2.5)$$

where E is the activation energy and n is the order of reaction. This relation is used mainly for the comparison of chars of similar conditions because pyrolysis conditions affect the reactivity of char. Karabulut et al. (1999) found that the reactivities decreases between 400-600 ^{0}C of the coal char samples, and above 600 ^{0}C the rates of gasification reactions started to increase. Liu et al. (2006) pointed out that all chars demonstrate a strong tendency to increase the reaction rate with temperature between 1000 ^{0}C and 1400 ^{0}C; but between 1500 ^{0}C and 1600 ^{0}C different chars demonstrated different temperature dependencies. Schmal et al. (1982) reported a kinetic study of the gasification of Brazilian coal with steam using a thermobalance for temperature between 800 and 1000 ^{0}C at atmospheric pressure. They pointed out that 1100 to 1200 ^{0}C is the best temperature for this reaction because the reactivity is higher and CO_2 content of product is very low. They concluded that Charqueadas coal is more reactive as compared to the other coals in the range of 700 to 1040 ^{0}C and atmospheric pressure. Everson et al. (2008) observed the gasification kinetics with CO_2 in a thermogravimetric analyzer at 87.5 kPa and 287.5 kPa and temperature between 850 and 900 ^{0}C with 1 mm diameter particles. They plotted the graph between conversion and time at different temperature like 850, 863, 875, and 900 ^{0}C with different mole % of CO_2 at two pressure 87.5 kPa and 287.5 kPa. They found that on increasing the temperature from 850 to 900 ^{0}C, the conversion increases but the residence time decreases. Matsui et al. (1985) analysed the char-steam gasification in a fluidized-bed reactor over a temperature range of 1096 to 1311 K at atmospheric pressure. They observed that the reactivity of coal increases with increasing reaction temperature. Chejne and Hernandez (2002) developed a numerical algorithm to simulate the coal gasification process in fluidized bed. They also used the model to optimise the gasification process by changing different parameters such as air, particle size distribution, coal type, and the geometry of the reactor. Katta and Kealrns (1981) observed the rates of C-H_2O and C-CO_2 reactions in a laboratory fluidized bed over a temperature range of 920-1040 °C at 1013 kPa. They observed that below 1100 ^{0}C, the gasification reactions are chemically controlled and above this temperature, the diffusion effects become important. Sun et al. (2004) studied the CO_2 gasification of maceral chars using CAHN TG-151 pressurized thermobalance under different operating conditions and concluded that with increasing temperature and pressure, the gasification rate of maceral char increases. The temperature

also affects the formation of surface area (Gao et al., 2010). Higher temperature generates activated carbons with lower surface area (Arenas and Chejne, 2004). Leppalahti and Koljonen (1995) reviewed for the nitrogen evolution from coal (Collings et al., 1993; Collings and Mann, 1994). The fuel nitrogen is liberated mainly during ammonia gasification. It is probably affected by several parameters, including gasification temperature, heating rate, pressure, residence time of fuel in the reactor. Thus, increasing temperature leads to higher heating rate in pyrolysis which increases de-volatilization rate and hence to lower ammonia formation.

2.1.8 Effect of pressure

Liu and Niska (2004) observed that the pressure variation can be confusing to unravel because they can affect gasification both directly and indirectly, i.e., by directly changing reactant partial pressures and indirectly, by changing transport rate (Irfan et al., 2011). They found that effect of pressure from 0.1 to 3.0 MPa on conversion of a bituminous char with two cases of fixed gas compositions (i) for 80% steam, and (ii) for 100% CO_2 (Figure 2.7). For steam gasification, the extents of char conversion for all pressures increases rapidly during initial 15 s, after that further gasification take place much more slowly. The same trend was observed for CO_2 gasification. Lee et al. (1991) observed the rapid heating conditions in two entrained flow furnaces at pressure from 0.1 to 3.8 MPa for pyrolysis of Illinois no.6 bituminous coal. Upon increasing the pyrolysis pressure, the overall release rates of volatile was found to be lowered. Also, on increasing the pressure above 0.8 MPa, reduced the swelling and number and size of holes formed on the particle surfaces (Yang et al., 2014).

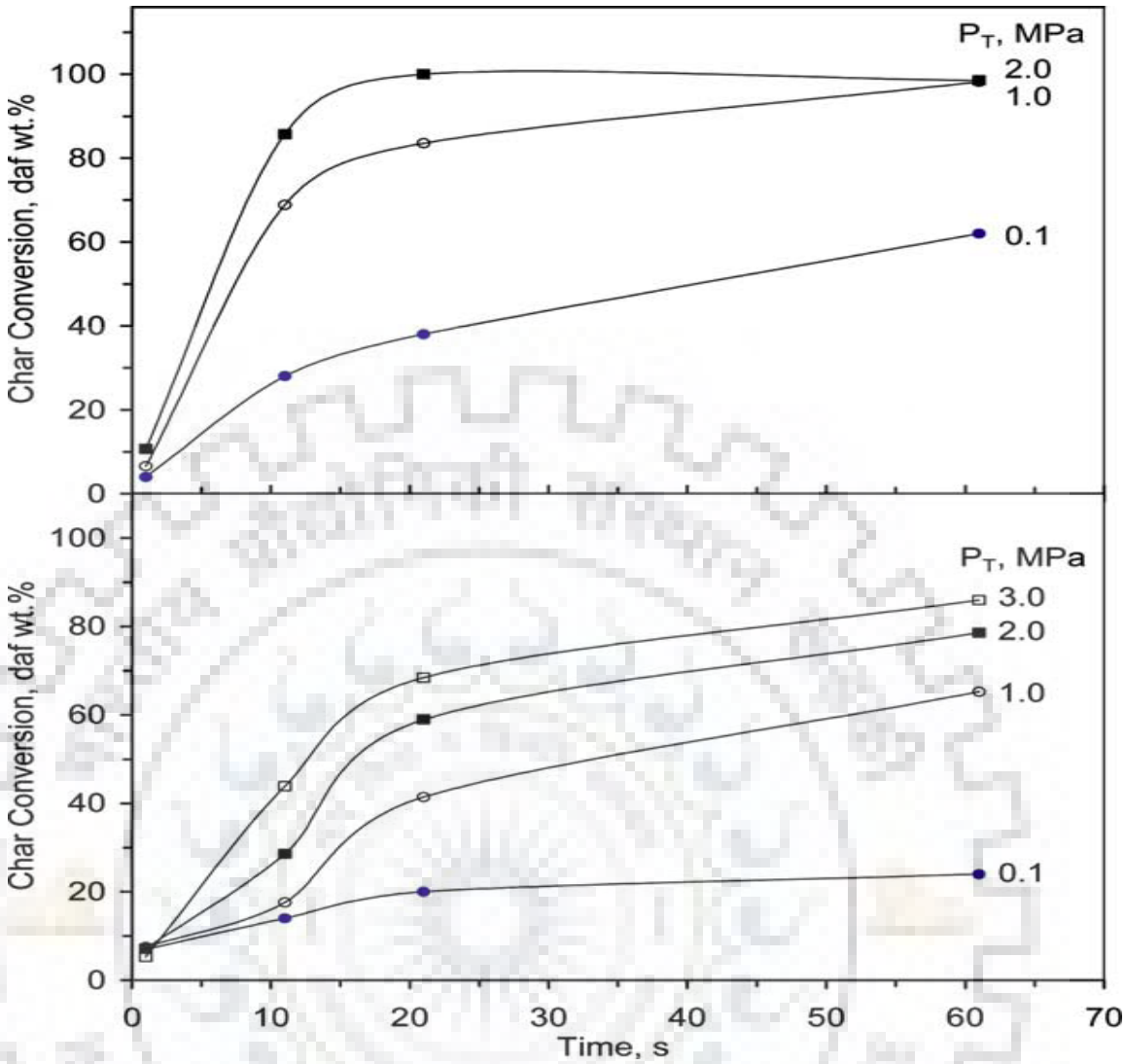

Figure 2.7: Char conversion histories for Daw Mill bituminous char gasification under (upper) 80% steam and (lower) 100% CO_2 at 1000 ^{0}C and (●) 0.1, (○) 1.0, (■) 2.0 and (□) 3.0 MPa in a WMR (Source: Liu and Niska, 2004)

Roberts and Harris (2000) measured the intrinsic reaction rates of two Australian coal chars with O_2, CO_2 and H_2O at increased pressure (up to 30 atm) by using a pressurized thermogravimetric analyzer. They found that the reaction order in CO_2 and H_2O varying from 0.5 to 0.8 at atmospheric pressure and decrease at pressures above approximately 10 atm (Cetin et al., 2004). They also studied the effect of pressure on the activation energy and pre-exponential factor. They observed that the activation energy is not significantly affected by the pressure but the frequency factor does change with pressure. The variations of hydro-pyrolysis pressure also affect the reactivity of the char. They observed that at 700 ^{0}C (or > 700 ^{0}C), the reactivity of coal char decreases as hydrogen pressure increased from 2.5 to 40 bars (Muhlen et al., 1986), and increased with further increase in pressure due to gradual erosion of the unreactive surface-deposited char

by hydro-gasification reactions. The same trend obtained for Pittsburgh No.8 coal char prepared at 2.5 and 70 bars under similar conditions (Cai et al., 1996). Zhuo et al. (2000) observed the steam gasification of Daw Mill coal in the three bench-scale reactors (Wire mess, Fluidised bed and Fixed bed) with 60 s holding time at peak temperature of 1000 ^{0}C. They found that for both CO_2-gasification and steam gasification, conversions monotonically increased with pressure.

Li et al. (2010) studied the gasification of three Chinese coals (Huolinhe lignite, Shenmu bituminous coal, and Jincheng anthracite) with CO_2 and H_2O in a self-made pressurized fixed-bed reactor at increased pressures (up to 1.0 MPa). They observed that the char gasification reactivity increases with increasing partial pressure of CO_2 and steam (Kovacik et al., 1990). This conclusion is consistent with their earlier study (Liu et al., 2000) where they found that with increase in partial pressure of CO_2, the rate of gasification increases at constant temperature.

When the gasification reaction is controlled by pore diffusion, the rate decreases with increasing total system pressure (Tremel and Spliethoff, 2013), and for chemical kinetics controlled gasification, there is no pressure dependency. The gasification rates increases with increasing the pressure up to 10 atm and level off with further increase in pressure (Schmal et al., 1983). The reactivities of the char obtained by pyrolysis are also affected by the pyrolysis pressure. The reactivities of the coal char decreases with increasing the pyrolysis pressure (Sha et al., 1990; Messenbock et al., 2000; Cetin et al., 2005). Sha et al. (1990) concluded that the reaction rates of C-H_2O and C-CO_2 increase with increasing the P_{H2O} and P_{CO2}, respectively, up to 1-1.5 MPa and then tend to have a zero order with respect to partial pressure of reacting gas. Nozaki (1992) also observed that the gasification rate is first order with respect to CO_2 below atmospheric pressure and zero order at elevated pressure. Thiele and Haslam (1927) also reported similar behaviour in their classic paper that the reaction is of the zero order, the pressure of the steam has little effect on the composition of the fixed gases produced; and the reaction is a negative order as increase in pressure lowers the CO content of the fixed gases very much (Sheikh, 1985).

Goyal et al. (1989) studied the gasification kinetics of Western Kentucky bituminous coal under different operation conditions. They observed that, at steam partial pressure of 3.9-14.2 atm, the rate of gasification for these chars is independent of the steam partial pressure in the temperature range of 925-1038 ^{0}C. Zhang et al. (2006) investigated the gasification reactivities of six typical Chinese anthracite chars with steam

and CO_2 at 0.02-0.1 MPa and 920-1050 ^{0}C by using thermogravimetric analyzer. They found that the gasification rate increases with increasing steam (or CO_2) partial pressure (Katta and Kealrns, 1981). This is due to the increase in number of steam (or CO_2) molecules diffusing to and becoming adsorbed on the char surface. Yang et al. (2007) investigated the influence of pressure during coal pyrolysis and gasification reactivity of resultant coal chars. They found that higher pressure is favourable for the initial char gasification, while lowering the pyrolysis pressure reduces gasification rate. The gasification reactivity of solid char first decreased with increasing pyrolysis pressure from ambient to 1.5 MPa; after that, it increased and got the maximum value at 5 MPa. Mann et al. (2004) observed that the rate of gasification is proportional to the steam partial pressure. They also point out that the general trends show a linear increase in reaction rate at low partial pressures and level off at higher pressure due to the inhibiting effects of the product gases H_2 and CO. Many researchers pointed out that the rate of gasification with respect to CO_2 (or steam) is approximately first order at low pressure but approaches zero order at high pressure (Juntgen, 1981; Adschiri et al., 1986; Kwon et al., 1988; Molina and Mondragon, 1998). Sun et al. (2004) studied the changes of gasification conversion of vitrinite and inertinite char at temperature of 1223 K under different pressures. They found that on increasing the pressures from 0.1 to 3 MPa, the complete gasification time decreases from 2.1 h to 23 min and 2.4 h to 24 min for vitrinite and inertinite char respectively due to the increase in gasification rate. Roberts and Harris (2007) studied the char gasification reaction kinetics at high pressure. They found that the rate of reaction for a mixture of CO_2 and H_2O is not the algebraic sum of the two pure-gas reaction rates; rather, it is a complex combination of two that appears to be dependent on the blocking of reactant site by relatively slower C-CO_2 reaction. Hong et al. (2000) observed that Langmuir rate equation is more suitable for modelling the effects of pressure on the char reactivity.

The char gasification with H_2O and CO_2 has been studied for a wide range of coal char types at different temperature and pressure ranges by using different experimental methods. A brief summary is presented in Table 2.1.

Table 2.1: Published experimental studies on coal gasification reactivity at pressure

Samples	Reactant gas	Temperature (^{0}C)	Pressure	Particle size	References	Method
Coal D, Coal Y	O_2,CO_2, H_2O	560-940	1-30 atm	-1.0+0.6 mm	Robets and Harris (2000)	PTGA
Bituminous coal	CO_2	≤1400	≤0.7MPa	20-44 μm	Kojitani et al. (2006)	PDTF
Lignite, Bituminous, Subbitumin-ous coal	CO_2, H_2O, H_2,CO	800-1500	0.02-3.0 MPa	50-725 μm	Liu and Niska (2004)	PTGA, PDTF, WMR
Subbitumin-ous coal	H_2O	850	0.25-0.8 atm	0.3-1.0 mm	Lee et al. (1998)	Thermobal-ance reactor
Linby and Pittsburgh No.8 coals	CO_2, H_2	700-850	≤150 bar	--	Guell et al. (1993)	TGA
Daw Mill (Washed)	H_2O, CO_2	1000	1-30 bar	106-152 μm	Zhuo et al. (2000)	WMR
Lignite, Bituminous, Anthracite	H_2O, CO_2	900-1000	≤1.0 MPa	<0.178 mm	Li et al. (2010)	PFBR
Pine char	CO_2	800-1000	1-20 bar	300 μm	Cetin et al. (2005)	TGA
Lignite, Bituminous, Subbitumin-ous coal	CO_2, H_2O, H_2, O_2	800-900	1-7.0 MPa	420-840 μm	Sha et al. (1990)	Pressurized thermal balance
Illinois No.6 coal	H_2O, O_2	>1000	24-50 atm	200-600 μm	Wen and Chaung (1979)	Entrainment gasifier
Daw Mill, Illinois No.6, Rietspruit, El cerrejon and Drayton coal	CO_2	1000	1-30 atm	106-150 μm	Messen-bock et al. (2000)	WMR
Australian coal	O_2	1100-1500	2.0 MPa	-180+45 μm	Harris et al. (2006)	Entrained-flow gasifier
Coal R, Coal A	H_2O, CO_2	≤1600	≤2.5 MPa	--	Tremel and Spliethoff (2013)	PiTER, PRETA
Bituminous coal	H_2O, H_2	925-1038	4-28 atm	-20+40 μm	Goyal et al. 1989	Fluidized-bed gasifier

Coal char	CO_2	827-1727	≤7 MPa	100 µm	Liu et al. (2000)	Entrained-flow gasifier
Subbitumin-ous coal	H_2O	850-1000	1-15 atm	35-48 µm	Schmal et al. (1983)	FBR
Bituminous coal	CO_2	≤1000	≤5 MPa	--	Yang et al. (2007)	PTGA
Bituminous coal	H_2O, CO_2	800-1000	1-70 bar	--	Muhlen et al. (1985)	FBR
Lignite char	CO_2	800-1000	1-25 atm	100-630 µm	Adanej et al. (1985)	FBR
Coal char	CO_2	850-900	87.5, 287.5 kPa	1 mm	Everson et al. (2008)	FBR
Bituminous char	H_2, H_2O	<927	≤172 bar	-16+20 µm	Feldkirch-ner and Linden (1963)	Semi-flow reactor
Maceral chars	CO_2	850-900	0.1-3.0 MPa	< 50 µm	Sun et al. (2004)	CAHN TG-151 pressurized thermobala-nce

PTGA: Pressurized Thermogravimetric Analyzer
WMR: Wire Mess Reactor
PFBR: Pressurized Fluidized-bed Reactor
PiTER: Pressurised Entrained flow Reactor
PRETA: Pressurised Thermogravimetric Analyser
PDTF: Pressurized Draft-tube Furnace
TGA: Thermogravimetric Analyzer
FBR: Fluidized-bed Reactor

2.2 Mechanism and Rate Law

Both design and practicing engineers needs better understanding of the process that they handle. Mechanism of the gasification reaction along with the knowledge of rate constants is of great importance for this purpose. Considering this, large numbers of researchers have used their experimental findings to establish reaction kinetics of the gasification reaction. Some of them are being presented in the following sections.

2.2.1 Mechanism and kinetics for coal char with CO_2

The char is widely used to test the reactivities of the chars produced from different types of coals and different processes. The CO_2 is not used industrially as much as steam in the gasification processes but it is more preferred at laboratory scale because the char-CO_2 reactions are slow, easy to measure and analyse different operating parameters. For

smaller char particles (< 500 μm) and lower temperature (< 1050 ^{0}C), the char-CO_2 is controlled by the chemical reaction rate and occurs nearly uniformly throughout the interior surfaces of the char particles (Tremel and Spliethoff, 2013) but for higher temperature (> 1050 ^{0}C), the diffusional effects (pore diffusion) become significant and affect the overall reaction rates observed by many researchers (Adschiri et al., 1986; Kayotani et al., 1993; Kajitani et al., 2006; Umemoto et al., 2013). This indicates that the temperature has great influence on the rate of reaction. The effect of pressure on the char-CO_2 gasification reaction has been studied by many researchers (Adanej et al., 1985; Liu et al., 2000; Messenbock et al., 2000; Sun et al., 2004; Cetin et al., 2005; Koyitani et al., 2006; Yang et al., 2007; Everson et al., 2008).

To design the coal gasifiers, the kinetic data of the coal gasification is required. A number of researchers have worked on the kinetics of coal gasification (Kwon et al., 1988; Kyotani et al., 1993; Liu et al., 2000; Kajitani et al., 2006; Liu et al., 2006). The uncatalysed CO_2 gasification of char is an endothermic reaction (Kwon et al., 1988; Molina and Mondragon, 1998), which is given as:

$$C + CO_2 \leftrightarrow 2CO \qquad \Delta H = +159.7\,\frac{kJ}{mole} \tag{2.6}$$

The rate of this reaction is relatively slow and easy to measure. This equation has been frequently used for the measurement of the CO_2 gasification rate. The reaction rate is also interpreted by the following oxygen-exchange mechanism (Roberts and Harris, 2008):

$$C_f + CO_2(g) \leftrightarrow C(O) + CO(g) \tag{2.7}$$

$$C(O) \rightarrow CO(g) \tag{2.8}$$

where C_f is an available active site and $C(O)$ is an occupied site.

The reactivity, R_C, is expressed as:

$$R_C = \frac{k_1 P_{CO_2}}{1 + k_2 P_{CO} + k_3 P_{CO_2}} \tag{2.9}$$

where k_1, k_2 and k_3 are rate constants and P_{CO}, P_{CO_2} are the partial pressure of each gas. Ignoring the retarding effect of CO, the reaction rate with respect to CO_2 concentration is approximately first order at low pressure but approaches zero order at high pressure (>1.5 MPa) (Sha et al., 1990). Kajitani et al. (2006) observed the inhibition effect of CO on the gasification rate by using pressurized TGA and L-H type rate equation. The rise in partial pressure of CO reduces the gasification rate (Liu and Niksa, 2004). Inhibition effect of CO during CO_2 gasification was also studied by Everson et al. (2006) in TGA for two different types of coals which is shown in Figure 2.8 below at 1173 K.

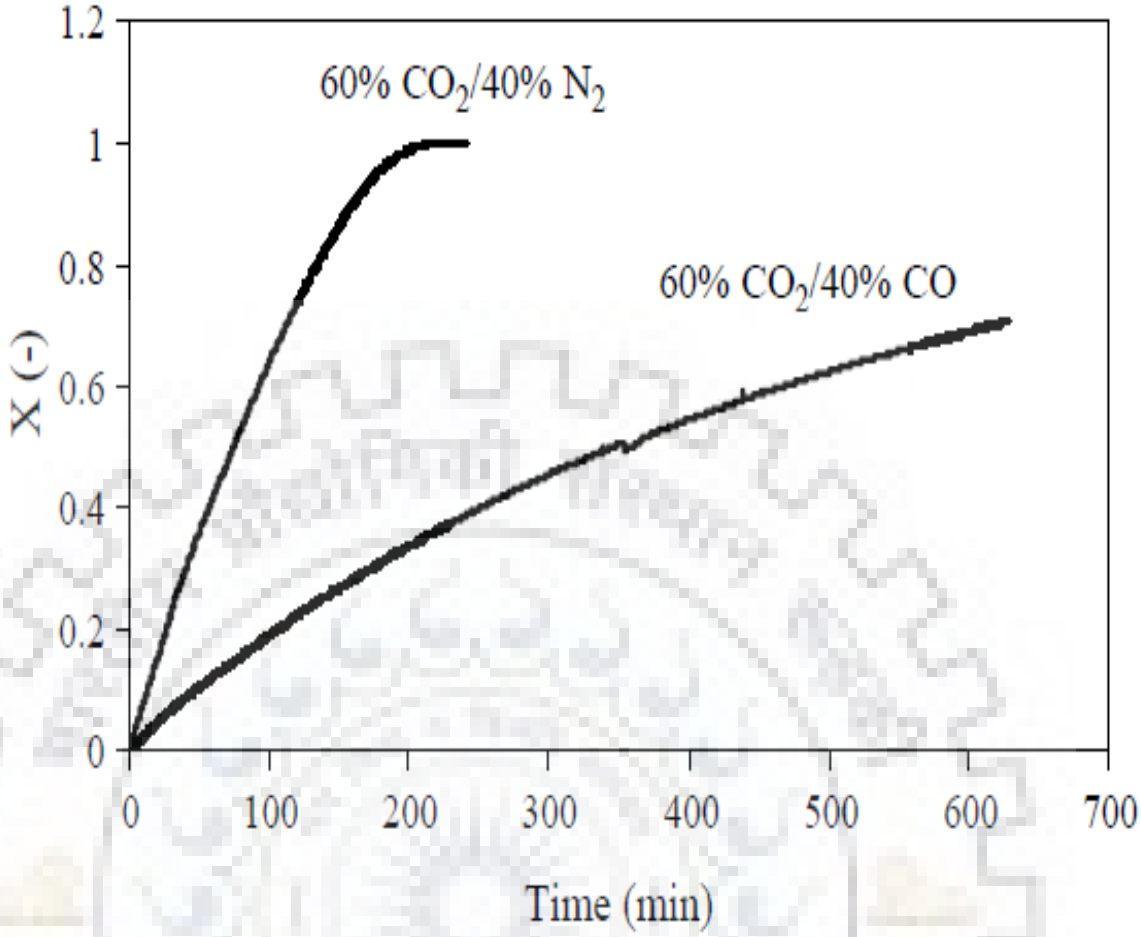

Figure 2.8: Inhibition effect of carbon monoxide during carbon dioxide gasification at 1173 K (Source: Everson et al., 2006)

Muhlen et al. (1985) added two more steps showing the inhibition of gasification by CO (Liu et al., 2000; Wall et al., 2002; Irfan et al., 2011) as following:

$$C(CO) + CO_2 \leftrightarrow 2CO + C(O) \quad (2.10)$$

$$CO + C(CO) \leftrightarrow 2C_f + CO_2 \quad (2.11)$$

With increasing CO_2 pressure, the concentrations of oxygen complexes C(O) and C(CO) on the carbon surface approach unity, indicating C(O) and C(CO) saturation; then pressure effect becomes insignificant. The complex Langmuir–Hinshelwood type expression is given as:

$$R_C = k_1 P_{CO_2} + k_4 P_{CO_2}^2 / (1 + k_2 P_{CO} + k_3 P_{CO_2}) \quad (2.12)$$

The temperature effect of reactant gas and product gas inhibition is mostly described by negative activation energies i.e., at higher temperature, the inhibition is less significant (Tremel and Spliethoff, 2013).

Kajitani et al. (2006) used two reaction rate equations for char-CO_2 reaction i.e., n^{th} order and Langmuir-Hinshelwood (L-H) type reaction rate equations. In the n^{th} order reaction rate equation, the overall char gasification rate is proportional to the n^{th} power of the carbon dioxide partial pressure and follows the Arrhenius equation as:

$$R_{char} = A_0 e^{-E/RT} P_{CO2}^{n} \quad (2.13)$$

where A_0 is a frequency factor, E is the activation energy, R is the universal gas constant, T is temperature, n is reaction order and P_{CO2} is the partial pressure of CO_2.

Compared to the n^{th} rate equation, the Langmuir–Hinshelwood type equation:

- ✓ does not involve the pressure order which is uncertain for the n^{th} order equation;
- ✓ is derived from reaction mechanism, whereas the n^{th} order equation is empirical;
- ✓ accounts for the inhibiting effect of H_2 and CO, which are considerably present at high pressures.

In order to explain the variation in the dependency of the gasification rate on partial pressure, the L-H type rate equation is applied (Liu et al., 2000; Kajitani et al., 2006)

$$R_C = S \frac{k_1 P_{CO2} + k_4 P_{CO2}^2}{1 + k_2 P_{CO2} + k_3 P_{CO}} \quad (2.14)$$

where S is the surface area per unit volume of the char particle and it is defined as (Kajitani et al., 2002 and 2006):

$$S = S_0 (1 - x) \sqrt{1 - \psi \ln(1 - x)} \quad (2.15)$$

where S_0 is the initial surface area, x is the conversion ratio of the char. ψ is a dimensionless parameter indicating initial pore structure and is calculated as (Kajitani et al., 2002):

$$\psi = \frac{4\pi L_0 (1 - \varepsilon_0)}{S_0} \quad (2.16)$$

where L_0 is pore length and ε_0 is the initial porosity of the solid. If the value of ψ is 0, it means the char is very porous, and larger the value of ψ means that the pore in the char grows with the progress of char gasification (Figure 2.9).

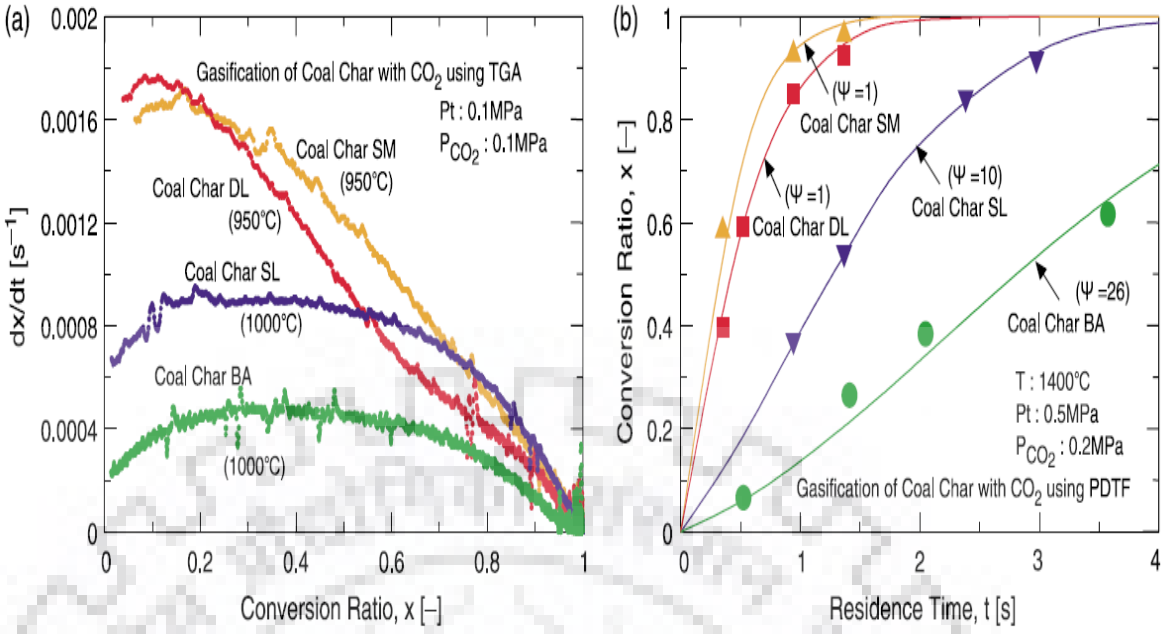

Figure 2.9: Results of gasification rate with CO_2 using PDTF and TGA. (a) Gasification using TGA. (b) Gasification using PDTF at 1400 ^{0}C (Source: Kajitani et al., 2006)

Liu et al. (2000) defined the intrinsic reaction rate as the ratio of the apparent reaction rate to the internal surface area of the particle. On this basis, the equations (2.14) and (2.15) are identified as the intrinsic reaction rates. The temperature-dependent constants k_1, k_2, k_3 and k_4 of equation (2.15) obtained from elemental reactions (2.17)-(2.21) (Liu et al., 2000).

$$C_f + CO_2 \leftrightarrow C(O) + CO \quad (2.17)$$

$$C(O) \rightarrow CO \quad (2.18)$$

$$CO + C_f \leftrightarrow C(CO) \quad (2.19)$$

$$CO_2 + C(CO) \rightarrow 2CO + C(O) \quad (2.20)$$

$$CO + C(CO) \rightarrow CO_2 + 2C_f \quad (2.21)$$

where C(O) and C(CO) denotes the oxygen complexes on the carbon surface and C_f is available active sites.

The temperature-dependent constants can be represented in an Arrhenius type equation, as given below:

$$k_j = A_j e^{-E_j/RT} \quad (2.22)$$

Kajitani et al. (2006) considered the following elementary reactions and reaction rate constants k_j (j=1, 2, 3, 4) applied to the Arrhenius equation (2.22):

$$CO_2 \xrightarrow{i_1} CO + (O) \quad (2.23)$$

$$CO \underset{i_3}{\overset{i_2}{\leftrightarrow}} (CO) \quad (2.24)$$

$$C + (O) \overset{i_4}{\rightarrow} CO \quad (2.25)$$

$$CO_2 + (CO) \overset{i_5}{\rightarrow} 2CO + (O) \quad (2.26)$$

$$CO + (CO) \overset{i_6}{\rightarrow} CO_2 + C \quad (2.27)$$

The rate constants are defined as:

$k_1 = i_1; k_2 = i_1/i_4 + i_5/i_3; k_3 = i_2/i_3 + i_6/i_3; k_4 = i_1 i_5/i_3$

Some other researchers also used the same mechanism but they developed different rate equations (Nozaki, 1992; Wall et al., 2002; Everson et al., 2006; Kajitani et al., 2006).

A combined oxidation-gasification mechanism was developed by Liu and Niksa (2004) that includes three combustion reactions and four reactions for gasification. The eight step mechanism includes two reversible reactions therefore a total of following ten heterogeneous reactions were obtained.

Combustion:

$$2C + O_2 \rightarrow C(O) + CO \quad (2.28)$$

$$C + C(O) + O_2 \rightarrow CO_2 + C(O) \quad (2.29)$$

$$C(O) \rightarrow CO \quad (2.30)$$

Gasification:

$$C + CO_2 \leftrightarrow C(O) + CO \quad (2.31)$$

$$C(O) \rightarrow CO \quad (2.32)$$

$$C + H_2O \leftrightarrow C(O) + H_2 \quad (2.33)$$

$$C(O) \rightarrow CO \quad (2.34)$$

$$C + 2H_2 \rightarrow CH_4 \quad (2.35)$$

where C(O) is the oxide complex on the carbon surface. Since CO_2 and steam gasification involve oxide complexes with the same nominal composition, but these complexes disrobed at different rates. The ratio of the desorption rates, $\gamma = {}^{k_{32}}/_{k_{34}}$, in the rate expression depend on temperature but not pressure. This variation is invoked after an earlier version of CBK/G with a common oxide complex which failed to describe the different asymptotic limits for steam and CO_2 gasification at the highest pressure. From above reaction mechanism, the following rate expression can be derived.

$$R_{C-Comb} = (k_{28}k_{29}P_{O_2}^2 + k_{28}k_{30}P_{O_2})/(k_{28}P_{O_2} + k_{30}/2) \quad (2.36)$$

CO/CO_2 from combustion= $k_3/k_2P_{O_2}$ (2.37)

$$R_{C-Gas} = (k_{34} + k_{32})\theta + k_{35}P_{H_2} \quad (2.38)$$

$$R_{C-Total} = R_{C-Comb} + R_{C-Gas} \quad (2.39)$$

$$R_{O_2} = -(k_{28}k_{30}\,P_{O_2}/2 + k_{28}k_{29}P_{O_2}^2)/(k_{28}P_{O_2} + k_{30}/2) \quad (2.40)$$

$$R_{H_2O} = -\frac{k_{34}k_{33}P_{H_2O}}{k_{34} + \gamma k_{31}P_{CO_2} + \gamma k_{31}^{'}P_{CO} + k_{33}P_{H_2O} + k_{33}^{'}P_{H_2}} \quad (2.41)$$

$$R_{CO_2} = -\frac{k_{34}k_{31}P_{CO_2}}{k_{34} + \gamma k_{31}P_{CO_2} + \gamma k_{31}^{'}P_{CO} + k_{33}P_{H_2O} + k_{33}^{'}P_{H_2}} + k_{29}k_{28}P_{O_2}^2/(k_{28}P_{O_2} + k_{30}/2) \quad (2.42)$$

$$R_{CO} = k_{28}k_{30}P_{O_2}/(k_{28}P_{O_2} + k_{30}/2) + 2R_{CO_2} + R_{H_2O} \quad (2.43)$$

$$R_{H_2} = R_{H_2O} - 2k_{35}P_{H_2} \quad (2.44)$$

$$R_{CH_4} = k_{35}P_{H_2} \quad (2.45)$$

where

$$\theta = \frac{k_{31}P_{CO_2} + k_{33}P_{H_2O}}{k_{34} + \gamma k_{31}P_{CO_2} + \gamma k_{31}^{'}P_{CO} + k_{33}P_{H_2O} + k_{33}^{'}P_{H_2}} \quad (2.46)$$

The rate constants k_i, $i = 28 - 35$, have the Arrhenius form.

The above mechanism and rate expressions are based on following assumptions:

1. The mechanism assumes different but coexisting surface oxides C(O) for CO_2 and H_2O gasification. The desorption rates of these C(O) are different, so that the CO_2 and steam gasification rates saturate to different limits at very high pressure.
2. The mechanism neither include CO chemisorption nor the reactions of C(CO), which give rise to quadratic higher order terms in Langmuir-Hinshelwood rate expression in some other mechanism (Muhlen et al., 1985).

The total rate of char gasification for mixtures of CO_2, H_2O, CO, H_2 (Muhlen et al., 1985; Liu and Niksa, 2004; Irfan et al., 2011) is:

$$R_{C-Gas} = R_{C-CO_2} + R_{C-H_2O} + R_{C-CO} + R_{H_2} \quad (2.47)$$

By using above equations, equation (2.47) becomes as:

$$R_{C-Gas} = \frac{k_{28}P_{CO_2} + k_{35}P_{CO_2}^2 + k_{36}P_{H_2O} + k_{38}P_{H_2O}^2 + k_{39}P_{H_2O}P_{H_2} + k_{31}P_{H_2}}{1 + k_{29}P_{CO_2} + k_{30}P_{CO} + k_{37}P_{H_2O} + k_{32}P_{H_2}} \quad (2.48)$$

According to published results (Everson et al., 2006; Guizani et al., 2013; Umemoto et al., 2013) there are two possible surface mechanisms that may occur:

1. The carbon-steam and carbon-carbon dioxide reactions occur at common active sites (Ye et al., 1998).
2. The carbon dioxide and steam reactions occur at separate active sites.

Since both the reactions are surface reaction controlled, and the respective rate equations are the following (Everson et al., 2006; Irfan et al., 2011)

$$R_{C-1} = \frac{k_{30}K_{CO_2}P_{CO_2} + k_{34}K_{H_2O}P_{H_2O}}{1 + K_{CO_2}P_{CO_2} + K_{CO}P_{CO} + K_{H_2O}P_{H_2O} + K_{H_2}P_{H_2}} \quad (2.49)$$

$$R_{C-2} = \frac{k_{30}K_{CO_2}P_{CO_2}}{1 + K_{CO_2}P_{CO_2} + K_{CO}P_{CO}} + \frac{k_{34}K_{H_2O}P_{H_2O}}{1 + K_{H_2O}P_{H_2O} + K_{H_2}P_{H_2}} \quad (2.50)$$

A comparison between experimental results for coal-char and prediction using the two mechanisms is shown in Figure 2.10. From the figure it is clear that the overall reaction rate is best described with the assumption that the reactions proceed on the separate sites.

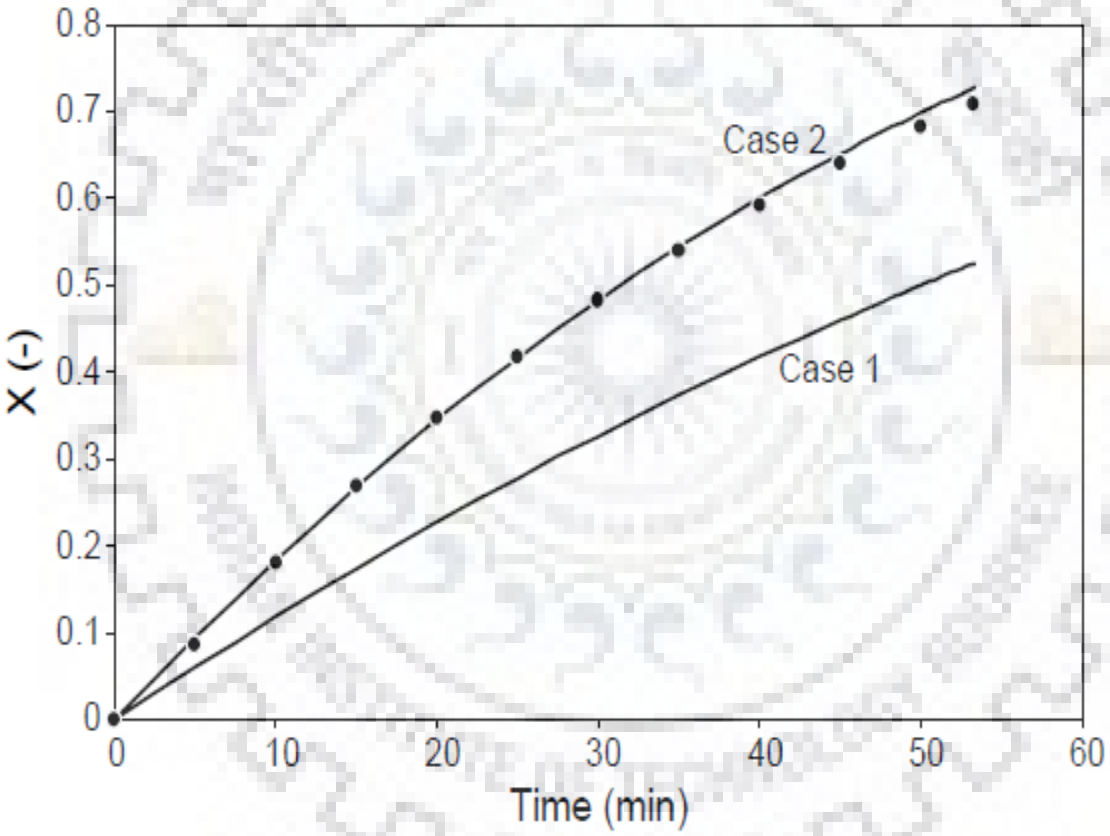

Figure 2.10: Coal-char gasification with multi-component mixture for coal-char A at 1223 K. Case 1 involves Rate 1 (same site) and Case 2 involves Rate 2 (separate sites), full lines represent models and the symbolic line represents experimental points (Source: Everson et al., 2006)

Liu and Niksa (2004) and Irfan et al. (2011) showed that the rate constant k_{35}, k_{38} and k_{39} of the quadratic term in equation (2.48) are small compared to k_{28} and k_{36} in the first order terms at temperatures above 900 ^{0}C. The rate constants of the quadratic terms are 3-5 orders of magnitude smaller than those for first order terms in an entrained flow

gasifier in the temperature ranges of 1500 ^{0}C to 2000 ^{0}C, and for fluidized bed gasifier at temperature below 900 ^{0}C, only k_{39} is comparable to the constants for the first order terms.

The CO_2 gasification rate R_{C-CO_2} can be expressed without the quadratic terms from equation (2.42) as follow:

$$R_{C-CO_2} = \frac{k_{34}k_{31}P_{CO_2}}{k_{34} + \gamma k_{31}P_{CO_2} + \gamma k_{31}^{'}P_{CO} + k_{33}P_{H_2O} + k_{33}^{'}P_{H_2}} \tag{2.51}$$

which can be simplifies to:

$$R_{C-CO_2} = \frac{K_{1a}P_{CO_2}}{1 + K_2P_{CO_2} + K_3P_{H_2O}} \tag{2.52}$$

where $K_{1a} = k_{31}k_{34}/\omega$, $K_2 = (\gamma k_{31} - 2\gamma k_{31}^{'} D_{CO_2}/D_{CO})/\omega$,

$K_3 = (k_{33} - k_{33}^{'} D_{H_2O}/D_{H_2} - \gamma k_{31}^{'} D_{H_2O}/D_{CO})/\omega$, and

$\omega = k_{34} + \gamma k_{31}^{'}\left(P_{CO,S} + 2P_{CO_2,S} D_{CO_2}/D_{CO} + P_{H_2O,S} D_{H_2O}/D_{CO}\right) + k_{33}^{'}(P_{H_2,S} + P_{H_2O,S}\frac{D_{H_2O}}{D_{H_2}})$

For the effectiveness factor of Langmuir-Hinshelwood type rate expression, we first determine the effective reaction order for R_{CO_2} (Liu and Niksa, 2004; Irfan et al., 2011) as follow:

$$n_{CO_2} = 1 - \frac{K_2\bar{P}_{CO_2}}{1 + K_2\bar{P}_{CO_2} + K_3\bar{P}_{H_2O}} \tag{2.53}$$

where $\bar{P}_{CO_2} \approx P_{CO_2,S}$ and $\bar{P}_{H_2O} \approx P_{H_2O,S}$ are the mean partial pressure of CO_2 and H_2O within the porous char particles and the Thiele modulus is defined as:

$$\phi_{CO_2} = \frac{d_P}{2}(\rho\nu_{C-CO_2}\frac{n_{CO_2} + 1}{2D_{CO_2}}\frac{R_{CO_2,S}}{C_{CO_2,S}})^{0.5} \tag{2.54}$$

where ρ is apparent density of char, ν is a stoichiometric coefficient whose subscript denotes the gasification reaction; $R_{CO_2,S}$ and $C_{CO_2,S}$ are the reaction rate and the molar concentration of CO_2 at the partial surface, respectively, and n_{CO_2} is the effective reaction order.

The effective diffusivity (D) appearing in equation (2.54) is calculated as products of the continuum diffusion coefficients and the ratio of the total porosity to tortuosity. The tortuosity is re-scaled by the percentage of pore-volume in macropores. Knudsen diffusion through micropores is omitted (Liu et al., 2000; Irfan et al., 2011).

The total porosity of the char particle is expressed as sum of the macro-, meso- and micro-porosity, which is written as:

$$\varepsilon_T = \varepsilon_a + \varepsilon_e + \varepsilon_i \tag{2.55}$$

where ε_a, ε_e and ε_i are the macro-, meso- and micro-porosity, respectively. The effective diffusion rate in the particle is, therefore, the sum of the contribution from the macro-, meso- and micro-pores. For a given initial macro-, meso- and micro-pore size and porosity, the effective diffusivity can be calculated as (Liu et al., 2000; Irfan et al., 2011):

$$D_{eff} = \varepsilon_a^2 D_a + \varepsilon_e^2 D_e + (1-\varepsilon_a-\varepsilon_e)^2 D_i + 2\varepsilon_a(1-\varepsilon_a-\varepsilon_e)\frac{2}{\left(1/D_a\right)+\left(1/D_i\right)}$$
$$+ 2\varepsilon_e(1-\varepsilon_a-\varepsilon_e)\frac{2}{\left(1/D_e\right)+\left(1/D_i\right)} + 2\varepsilon_a\varepsilon_e\frac{2}{\left(1/D_a\right)+\left(1/D_e\right)} \quad (2.56)$$

where D_a, D_e and D_i denotes the effective diffusivity for macro-, meso- and micro-pores, respectively, which is given as (Singh and Saraf, 1977):

$$D_a = \frac{1}{\left(1/D_{AB}\right)+\left(1/D_{k,a}\right)},\ D_e = \frac{1}{\left(1/D_{AB}\right)+\left(1/D_{k,e}\right)} \text{ and } D_i = \frac{1}{\left(1/D_{AB}\right)+\left(1/D_{k,i}\right)}$$

where D_{AB} is the molecular diffusion calculated by $D_{AB} = \frac{0.000000266T^{2/3}}{(P_T\sigma_{AB}^2\Omega_{AB}\sqrt{(1/M_A+1/M_B)})}$ and Knudsen diffusion $D_{k,a}$, $D_{k,e}$ and $D_{k,i}$ are strongly dependent on the macro-pore, meso-pore and micro-pore radii, respectively, which is given as:

$$D_{k,a} = \frac{2}{3}R_a\sqrt{\frac{8RT}{\pi M_A}},\ D_{k,e} = \frac{2}{3}R_e\sqrt{\frac{8RT}{\pi M_A}} \text{ and } D_{k,i} = \frac{2}{3}R_i\sqrt{\frac{8RT}{\pi M_A}}$$

The effectiveness factor is defined as the actual rate of conversion in a pore divided by the theoretical rate if there were no diffusion limitations in the pore (under the chemical reaction control) (Jensen, 1975; Liu et al., 2000; Liu and Niksa, 2004; Irfan et al., 2011; Singer et al., 2011). Many researchers have reported the correlation for effectiveness factor (Senneca et al., 1996; Liu et al., 2000; Liu and Niksa, 2004; Everson et al., 2005; Kajitani et al., 2006; Irfan et al., 2011; Singer et al., 2011; Umemoto et al., 2013).

Liu and Niksa (2004) derived the effectiveness factor for R_{C-CO_2} as follow (Irfan et al., 2011):

$$\eta_{CO_2} = \frac{1}{\phi_{CO_2}}\left[\frac{1}{\tanh(\phi_{CO_2})} - \frac{1}{\phi_{CO_2}}\right] \quad (2.57)$$

The overall rate of char-CO_2 reaction in high temperature zone (mediation by internal pore diffusion) is given as (Liu and Niksa, 2004; Irfan et al., 2011):

$$R_{C-CO_2} = \eta_{CO_2}\frac{k_{34}k_{31}P_{CO_2,S}}{k_{34}+\gamma k_{31}P_{CO_2,S}+\gamma k_{31}^{'}P_{CO,S}+k_{33}P_{H_2O,S}+k_{33}^{'}P_{H_2,S}} \quad (2.58)$$

The η_{CO_2} varies from 0.2 to 1.0 under typical entrained flow gasification condition.

The effectiveness factor η_{CO_2} can be correlated with the modified Thiele number ϕ_M and the correction factor f_c conducted by Kajitani et al. (2006) and Umemoto et al. (2013) is given in equation (2.57) as:

$$\eta_{CO_2} = f_c \frac{1}{\phi_M}\left[\frac{1}{\tanh(3\phi_M)} - \frac{1}{3\phi_M}\right] \tag{2.59}$$

$$f_c = \left(1 + \frac{\sqrt{1/2}}{2\phi_M^2 + 1/2\phi_M^2}\right)^{0.5(1-n_{obs})^2} \tag{2.60}$$

For the n^{th} order reaction rate equation

$$\phi_M = L_P \sqrt{\frac{(n+1)}{2}\frac{k_m C_{As}^{n-1}}{D_{eA}}} \tag{2.61}$$

with

$$n_{obs} = n \tag{2.62}$$

For the L-H type reaction rate equation,

$$\phi_M = L_P \sqrt{\frac{v_0 k_{1m}}{2D_{eA}}} \frac{k_{2m}C_{As}}{1 + k_{2m}C_{As}} \sqrt{\frac{1}{k_{2m}C_{As} - \ln(1 + k_{2m}C_{As})}} \tag{2.63}$$

And

$$n_{obs} = \frac{1}{1 + k_{2m}C_{As}} \tag{2.64}$$

where L_P is the characteristics length of the char particle, correlated in terms of the particle diameter D_P, and D_{eA} is the effective diffusion coefficient of CO_2 in the char particle, C_{As} is the mol concentration of CO_2 at surface of the char particle and k_m, $k_{1m}$and k_{2m} are intrinsic reaction rate coefficients per unit volume of the char particle.

Parallel pore mode was used to express D_{eA} (Kajitani et al., 2006; Irfan et al., 2011) as:

$$D_{eA} = \frac{\varepsilon}{\tau} D_N \tag{2.65}$$

ε is the porosity of char particle and τ is the tortuosity factor of the pore. D_N is the diffusion coefficient including molecular diffusion and Knudsen diffusion, and Knudsen diffusion coefficient is proportional to average pore diameter d_e. Same correlation for effectiveness factor was also proposed by the Senneca et al. (1996) by eliminating the correction factor term f_c which is shown in equation (2.59).

Everson et al. (2005) proposed the effectiveness factor which is different at different reaction during two periods of combustion. They designated the first period when the reaction rate is fastest (near the surface) as compared to the interior of the particle, in

this period, the concentration depletes near the surface thus forming ash layer. After this period, the ash layer thickness increase with a decreasing porous core of coal (or char).

For first period, the effectiveness factor is given as:

$$\eta_1 = \frac{3}{\phi^2}(\phi coth\phi - 1) \tag{2.66}$$

and for the second period, the effectiveness factor is given as:

$$\eta_2 = \frac{3}{(\phi\xi_m)^2}(\phi\xi_m coth\xi_m - 1) \tag{2.67}$$

where $\xi_m = r_m/R_0$, is the dimensionless shrinking unreacted core radius, r_m is the radius of shrinking unreacted core, and R_0 is the initial particle radius.

For the simple pore-scale, the effectiveness factor of steady state reaction-diffusion equation (on which the Thiele modulus ϕ is based) is given by Singer et al. (2011) for i^{th} pore as:

$$\eta_i = \frac{tanh\phi_i}{\phi_i} \tag{2.68}$$

Liu et al. (2000) correlated the effectiveness factor with modified Thiele modulus as follow (Irfan et al., 2011):

$$\eta_{CO_2} = \left|\frac{3\sqrt{2}}{\phi_M}\left(\frac{1+AP_{CO_2,S}}{P_{CO_2,S}+2BP_{CO_2,S}^2}\right)\left\{\frac{1}{A}\left[B\left(P_{CO_2,S}^2 - P_{CO_2,0}^2\right) + C\left(P_{CO_2,S} - P_{CO_2,0}\right) + Dln\left|\frac{1+AP_{CO_2,S}}{1+AP_{CO_2,0}}\right|\right]\right\}^{1/2}\right| \tag{2.69}$$

where ϕ_M represents the modified Thiele modulus and can be expressed as:

$$\phi_M = R_0\left(\frac{K_1 SRT}{VD_{eff,CO_2}M_c}\right)^{1/2} \tag{2.70}$$

The change in CO_2 partial pressure along the partial radial distance is given by many researchers (Roberts and Starrefield, 1965; 1966; Liu et al., 1999).

The internal CO_2 partial pressure gradients along the particle radial distance are obtained as follows:

$$\frac{dP_{CO_2}}{dr} = -\left|\sqrt{2}\frac{\phi_M}{R_0}\right|\left\{\frac{1}{A}\left[B\left(P_{CO_2}^2 - P_{CO_2,0}^2\right) + C\left(P_{CO_2} - P_{CO_2,0}\right) + Dln\left|\frac{1+AP_{CO_2}}{1+AP_{CO_2,0}}\right|\right]\right\}^{1/2} \tag{2.71}$$

where $P_{CO_2,0}$ is the partial pressure of CO_2 at the particle centre, which can be obtained by solving equation (2.71) using Runga-Kutta method (Liu et al., 2000; Irfan et al., 2011). A, B, C, and D in equation (2.59) and (2.71) are the constants, and are defined as:

$A = K_2, \quad B = K_4/2K_1, \quad C = 1 - (K_4/K_1K_1), \quad$ and $\quad D = -\left((1/K_2) - (K_4/K_1K_2^2)\right)$, respectively.

K_1, K_2 and K_4 are the modified reaction constants and are defined as: $K_1 = k_1/\omega$, $K_2 = \left(k_2 - k_3\gamma\, D_{eff,CO_2}/D_{eff,CO}\right)/\omega$ and $K_4 = k_4/\omega$, and intermediate constant ω is expressed as $\omega = 1 - k_3\left(P_{CO,S} + P_{CO_2,S}\gamma\, D_{eff,CO_2}/D_{eff,CO}\right)$, where D_{eff,CO_2} and $D_{eff,CO}$ are the effective diffusivities of CO_2 and CO in the particle, respectively, and γ is the reaction stoichiometry.

2.2.2 Mechanism and kinetics for coal char gasification with steam

The kinetic studies of the char-steam reaction are of great importance for the design of gasification plants since steam is used widely in industry for the gasification processes due to its high reaction rates as compared to the carbon dioxide. To design the coal gasification plant, the kinetic data of the coal gasification is required. A number of research papers are available in open literature on the kinetics of coal gasification with steam (Muhlen et al., 1985; Peng et al., 1995; Wall et al., 2002; Paviet et al., 2007; Umemoto et al., 2013). The char-steam reaction is an endothermic reaction (Molina and Mondragon, 1998) which is given as:

$$C_f + H_2O \leftrightarrow C(O) + H_2 \qquad +118.9\frac{kJ}{mol} \tag{2.72}$$

This reaction has been frequently used for the analysis of the H_2O gasification rate. The procedure being followed for the evaluation of the overall reaction rate model for the steam gasification with and without hydrogen are the same as those described in equation (2.29) and (2.30) for CO_2 gasification reactions. A L-H type reaction rate equation used by the researchers (Liu et al., 2000; Everson et al., 2006) is similar to the reaction rate equations for CO_2.

The widely used reaction mechanism for char-steam gasification is as follows (Molina and Mondragon, 1998; Everson et al., 2006):

$$C_f + H_2O \leftrightarrow C(O) + H_2 \tag{2.73}$$

$$C(O) \rightarrow CO \tag{2.74}$$

where C_f is an available active site and $C(O)$ is an occupied site.

The reactivity R_{C-H_2O} is expressed as (Long and Sykes, 1948; Muhlen et al., 1985; Peng et al., 1995; Paviet et al., 2007; Umemoto et al., 2013):

$$R_{C-H_2O} = \frac{k_1 P_{H_2O}}{1 + k_2 P_{H_2O} + k_3 P_{H_2}} \tag{2.75}$$

The char-steam gasification reactions at high pressures can be explained using following reactions (Muhlen et al., 1985; Wall et al., 2002):

$$H_2O + C \leftrightarrow C(OH) + C(H) \tag{2.76}$$

$$C(OH) + C(H) \rightarrow C(O) + C(H_2) \tag{2.77}$$

$$C(O) \rightarrow CO \tag{2.78}$$

$$C(H_2) + H_2O + C \rightarrow CH_4 + C(O) \tag{2.79}$$

and the rate equation can be derived from equation (2.76-2.79) as:

$$R_{C-H_2O} = \frac{k_4 P_{H_2O} + k_7 P_{H_2O} P_{H_2} + k_8 P_{H_2O}^2}{1 + k_2 P_{H_2O} + k_3 P_{H_2}} \tag{2.80}$$

Bayarsaikhan et al. (2006) studied the inhibition of steam gasification by H_2. The atmosphere in the fluidized bed prevents the progress of steam gasification of the char beyond certain level of conversion, which depend on bed temperature. It is generally believed that H_2 retards steam gasification of chars obtained from coal as well as other carbonaceous materials (Juntgen, 1981; Yang and Yang, 1985; Yang and Duan, 1985; Huttinger and Merdes, 1992; Bayarsaikhan et al., 2006). Retardation of gasification by CO, if any, may not be as significant as that by H_2. Figure 11 plots reciprocal of k_{ncg} (rate constant for non-catalytic gasification) against square root of P_{H_2}, showing a linear relationship between them.

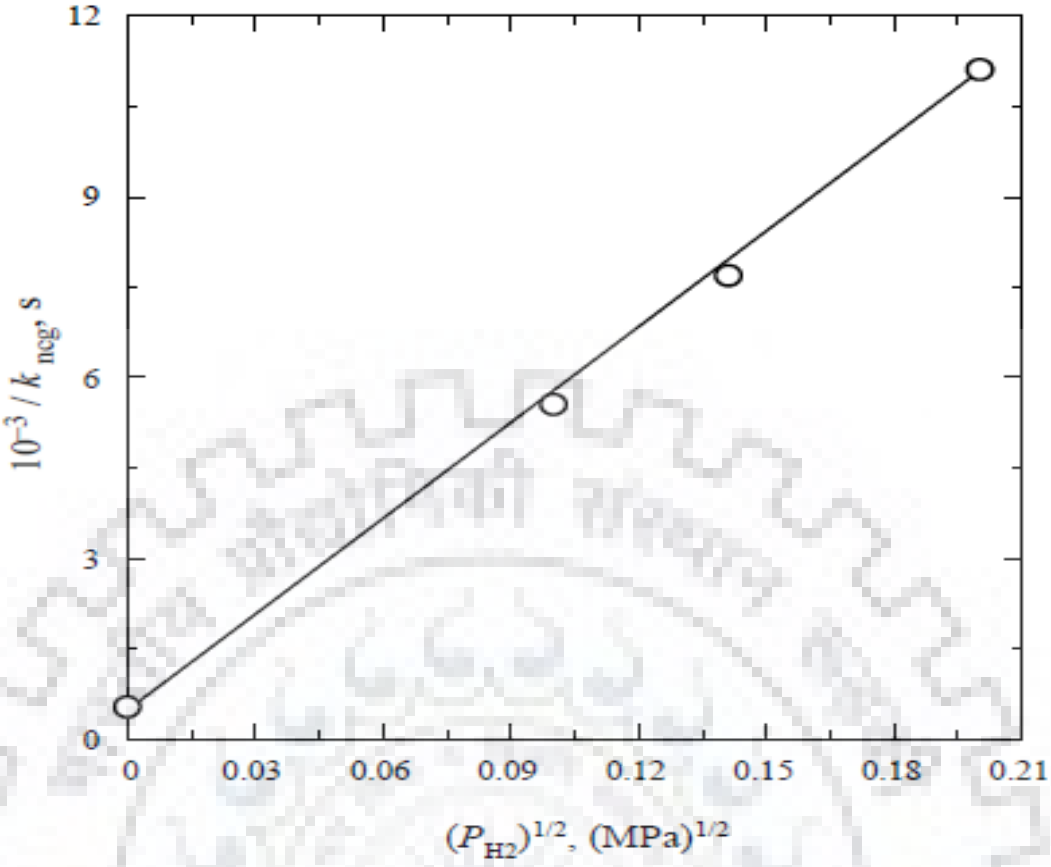

Figure 2.11: Relationship between reciprocal k_{ncg} and square root of P_{H_2} for in situ steam gasification in drop-tube/fixed-bed reactor at 1173 K and $P_{H_2O} = 53\ kPa$ (Source: Bayarsaikhan et al., 2006)

This relationship indicates that the non-catalytic gasification is governed by a so-called dissociative chemisorption mechanism (Yang and Duan, 1985; Yang and Yang, 1985; Huttinger, 1988; Lussier et al., 1998) that involves the following mechanisms:

$$C_f + H_2O \xrightarrow{i_1} C(O) + H_2 \tag{2.81}$$

$$C_f + {}^1/_2\, H_2 \underset{j_2}{\overset{i_2}{\longleftrightarrow}} C(H) \tag{2.82}$$

$$C(H) \xrightarrow{i_3} C_f + H \tag{2.83}$$

$$C(O) \xrightarrow{i_4} CO \tag{2.84}$$

$C(O)$ and $C(H)$ are carbon atoms on the char surface, which are bonded to the oxygen and hydrogen, respectively, through chemisorption. The rate of desorption of $C(O)$ is expressed as (Yang and Duan, 1985; Yang and Yang, 1985; Huttinger, 1988; Bayarsikhan et al., 2006):

$$R_{C-H_2O} = \frac{k_1 P_{H_2O}}{1 + k_2\sqrt{P_{H_2}} + k_3 P_{H_2O}} \tag{2.85}$$

k_1, k_2, and k_3 are the functions of two or more rate constants for elementary reactons (2.81) to (2.84), which is given as: $k_1 = i_1$, $k_2 = i_2/j_2$, and $k_3 = i_1/i_4$. The linear relationship between k_{ncg} and square root of P_{H_2} indicates that k_{ncg} is proportional to the term $1/\sqrt{P_{H_2}}$ appearing in equation (3.85), in other words, the gasification is inhibited by dissociative chemisorptions of H_2 (Bayarsaikhan et al., 2006). Presence of H_2 hinders the gasification reactions by blocking the active sites rather than by removing surface oxygen (Spinal et al., 2009).

The steam gasification reactions are also given by Liu and Niksa (2004) which are given in equations (2.33) and (2.34). From these reaction mechanisms, the rate expression for char-CO_2 gasification was given in equation (2.41). The steam gasification rate R_{C-H_2O} is expressed without the quadratic terms from equation (2.41) as follows (Liu and Niksa, 2004):

$$R_{C-H_2O} = \frac{k_{33}k_{34}P_{H_2O}}{k_{34} + \gamma k_{31}P_{CO_2} + \gamma k_{31}^{'}P_{CO} + k_{33}P_{H_2O} + k_{33}^{'}P_{H_2}} \tag{2.86}$$

which simplifies to:

$$R_{C-H_2O} = \frac{K_{1b}P_{H_2O}}{1 + K_2P_{CO_2} + K_3P_{H_2O}} \tag{2.87}$$

where $K_{1b} = k_{33}k_{34}/\omega$; $K_2 = (\gamma k_4 - 2\gamma k_4^{'} D_{CO_2}/D_{CO})/\omega$,

$K_3 = (k_6 - k_6^{'} D_{H_2O}/D_{H_2} - \gamma k_4^{'} D_{H_2O}/D_{CO})/\omega$ and

$\omega = k_7 + \gamma k_4^{'}\left(P_{CO,S} + 2P_{CO_2,S} D_{CO_2}/D_{CO} + P_{H_2O,S} D_{H_2O}/D_{CO}\right) + k_6^{'}(P_{H_2,S} + P_{H_2O,S}\frac{D_{H_2O}}{D_{H_2}})$

For the effectiveness factor of Langmuir-Hinshelwood type rate expression, first the effective reaction order for R_{C-H_2O} is determined as follows (Liu and Niksa, 2004):

$$n_{H_2O} = 1 - \frac{K_3\bar{P}_{H_2O}}{1 + K_2\bar{P}_{CO_2} + K_3\bar{P}_{H_2O}} \tag{2.88}$$

The Thiele modulus is defined as (Liu and Niksa, 2004):

$$\phi_{H_2O} = \frac{d_P}{2}(\rho\nu_{C-H_2O}\frac{n_{H_2O} + 1}{2D_{H_2O}}\frac{R_{H_2O,S}}{C_{H_2O,S}})^{0.5} \tag{2.89}$$

where $R_{H_2O,S}$ and $C_{H_2O,S}$ are the reaction rate and molar concentration of H_2O at the particle surface, and n_{H_2O} is effective reaction order.

The effectiveness factor is defined as the ratio of the actual rate to the rate if the concentration of the gasification agents were uniform throughout the char particle (Liu and Niksa, 2004; Irfan et al., 2011). The effectiveness factor can also be defined as the ratio of surface participating in the reaction to the total amount of surface available for reaction,

and is commonly used as an indicator of the extent that observed reaction rates are limited by pore diffusion control (Roberts and Harris, 2000).

Then the effectiveness factor for R_{C-H_2O} becomes (Liu and Niksa, 2004):

$$\eta_{C-H_2O} = \frac{1}{\phi_{C-H_2O}}\left[\frac{1}{\tanh(\phi_{C-H_2O})} - \frac{1}{\phi_{C-H_2O}}\right] \tag{2.90}$$

Similar to the CO_2 gasification, the effectiveness factor η_{H_2O} has a correlation with the modified Thiele number ϕ_M and the correction factor f_c as reported by Kajitani et al. (2006) and Umemoto et al. (2013), which is given in the following equation:

$$\eta_{C-H_2O} = f_c \frac{1}{\phi_M}\left[\frac{1}{\tanh(3\phi_M)} - \frac{1}{3\phi_M}\right] \tag{2.91}$$

$$f_c = \left(1 + \frac{\sqrt{1/2}}{2\phi_M^2 + 1/2\phi_M^2}\right)^{0.5(1-n_{obs})^2} \tag{2.92}$$

For the nth order reaction rate equation

$$\phi_M = L_P \sqrt{\frac{(n+1)}{2}\frac{k_m C_{As}^{n-1}}{D_{eA}}} \tag{2.93}$$

$$n_{obs} = n \tag{2.94}$$

For the L-H type reaction rate equation

$$\phi_M = L_P \sqrt{\frac{v_0 k_{1m}}{2D_{eA}}} \frac{k_{2m}C_{As}}{1 + k_{2m}C_{As}} \sqrt{\frac{1}{k_{2m}C_{As} - \ln(1 + k_{2m}C_{As})}} \tag{2.95}$$

$$n_{obs} = \frac{1}{1 + k_{2m}C_{As}} \tag{2.96}$$

where L_P is the characteristics length of the char particle, correlated in terms of the particle diameter D_P, and D_{eA} is the effective diffusion coefficient of H_2O in the char particle, C_{As} is the mol concentration of H_2O at surface of the char particle and k_m, $k_{1m}$and k_{2m} are intrinsic reaction rate coefficients per volume of the char particle.

Parallel pore mode was used to express D_{eA} (Kajitani et al., 2006; Irfan et al., 2011) as:

$$D_{eA} = \frac{\varepsilon}{\tau} D_N \tag{2.97}$$

where ε is the porosity of char particle and τ is the tortuosity factor of the pore. D_N is the diffusion coefficient including molecular diffusion and Knudsen diffusion, and Knudsen diffusion coefficient is proportional to average pore diameter d_e.

The total porosity (ε_T) as well as effective diffusivity (D_{eff}) can be obtained from equation (2.55) and (2.56), respectively.

Wakao and Smith (1964) determined the diffusivity in porous catalyst pellets and observed that the diffusivity is a function of effectiveness factor. The catalytic effectiveness factor has been developed for kinetic expression of the Langmuir-Hinshelwood type by Roberts and Satterfield (1966). They found that the region in which effectiveness factor is greater than unity can theoretically occur in an isothermal pellet which is actually encountered in a number of hydrogenation reactions. Hong et al. (2000) modelled using an m^{th} order intrinsic reaction rate in conjunction with an effectiveness factor for intraparticle diffusion of gas species.

The overall rate of char-steam gasification in high temperature zone (mediation by internal pore diffusion) is given (Liu and Niksa, 2004) as:

$$R_{C-H_2O} = \eta_{C-H_2O} \frac{k_{18} k_{17} P_{H_2O}}{k_{18} + \gamma k_{15} P_{CO_2} + \gamma k_{15}^{'} P_{CO} + k_{17} P_{H_2O} + k_{17}^{'} P_{H_2}} \quad (2.98)$$

The η_{C-H_2O} will vary from 0.2 to 1.0 under typical entrained flow gasification condition.

2.2.3 Activation energies and rate constants

Recent studies based on the thermal analyses suggest that activation energy is the predominant factor in the reactivity equation (Sima-Ella et al., 2005). Activation energy, affects the temperature sensitivity of the reaction rate, whereas pre-exponential factor is related more to material structure. Reaction with high activation energy needs a high temperature or a long reaction time (Liu et al., 2004). For coal pyrolysis, high activation energy means that the reaction needs more energy from surroundings. Essenhigh and Mishra (1990) correlated the pre-exponential factor and activation energy for both steam and CO_2 gasification, assuming that they are auto correlated. Ergun (1961) described three distinct ranges of temperature, which is based on the variation in the activation energy. They observed that at low temperature (chemically controlled), the reaction rates follow the true activation energy but at intermediate temperature (pore diffusion controlled), observed activation energy is half of the true value and at high temperature (boundary diffusion control), the activation energy approaches to zero.

Gupta and Bhatia (2000) estimated the activation energy and pre-exponential factors for different char samples by using the random pore model. They found that the values of the activation energies for the various samples are similar. Roberts and Harris (2000) measured the activation energy and frequency factor for char D and char Y reacting with O_2, CO_2, and H_2O at atmospheric pressure and 10 atm in the absence of all diffusion limitations. They found that, the activation energy is not significantly affected by pressure,

but the frequency factor does change with pressure. The higher reactivity chars have lower activation energy (Ochoa et al., 2001). Otto et al. (1979) pointed out that the reaction rate varies exponentially with the activation energy but only directly with the number of sites. Thus, at 850 ^{0}C, a decrease in the activation energy by 21 kJ/mol is equivalent to a 10-fold increase in the reaction site density. The carbon deposition also affects the activation energy. An increase in the carbon deposition leads to reduction in pore aperture which increases the activation energy but decreases the diffusion coefficient (Kamishita et al., 1977). With the increase of coal rank, the activation energy increase slightly with steam, but the activation energy with CO_2 increases considerably (Liu et al., 2000; Everson et al., 2008). Similar conclusion that the activation energy with CO_2 is higher than that with steam was made by Li et al. (2010) and Zhang et al. (2006) using six anthracite chars. The activation energy values were reported between 213 and 250 kJ/mol for steam gasification and between 146 and 202 kJ/mol for CO_2 gasification. Activation energy increased with the carbon content of the parent coal. The lower activation energy is attributed to the effect of diffusional resistance to CO_2 passing through the ash layer and film of gas to reach the unreacted carbon (Kwon et al., 1988). Osafune and Marsh (1988) studied the gasification kinetics of five chars with CO_2 at 1273 K from coals of different rank. They found that at 1273 K, values of first order rate constant for the surface reaction, decreased from 0.13 to 0.0090 cm/s with increasing rank of parent coal, activation energies varied between 175 and 195 kJ/mol. Frequency factor decreased with decreasing rate from 3.0×10^6 to 2.5×10^5 cm/s. The activation energy is a function of the temperature, decreasing from about 30 kcal/mole at 1300 K to about 10 kcal/mole at 1800 K (Field, 1969).

The activation energy of char produced at 1400 ^{0}C is slightly higher than that produced at 1600 ^{0}C, this results in a higher pre-exponential factor of the 1400 ^{0}C char (Tremel and Spliethoff, 2013). The activation energy is hardly affected by the heat treatment during pyrolysis, but the pre-exponential factor is significantly influenced. Pre-exponential factor of the char produced at 1600 ^{0}C deviate by a factor of 20. The value of apparent activation energy increases with the increase of pyrolysis temperature, which also tells us that the increase of pyrolysis temperatures diminishes the steam gasification reactivity (Wu et al., 2006). The lignite has low apparent activation energy and therefore high reactivities to steam (Juntgen, 1981). In the majority of cases, the presence of ash constituents or impurities accelerates gasification and reduces the overall activation energy (Knight and Sergeant, 1982). Sun et al. (2004) studied the kinetics of CO_2 gasification of Shenmu maceral chars by using CAHN TG-151 pressurized thermobalance under different

conditions. They pointed out that with increasing gasification, the activation energy increased for all the samples, which indicates the gasification reactivities of the chars gradually decreases due to the decrease in reactive sites. Activation energies and pre-exponential factors reported in some literatures for the steam gasification reaction and CO_2 gasification reaction of coals and coal chars are shown in Table 2.2 and Table 2.3, respectively.

Table 2.2: Activation energies and pre-exponential factors reported by some literatures for the steam gasification reaction of coals and coal chars

Samples	Reaction Temperature (^{0}C)	Activation energy (kJ/mole)	Pre-exponential factor	Reference
Kentucky No.9	1040-1430	82.76	4.5 L^3 $mole^{-1}$ t^{-1}	Jensen (1975)
Coal	1100-1300	121.42	50 m/h	Biba et al. (1978)
Coal	>1100	175.1	247 sec^{-1}	Wen and Chang (1979)
Lignite Coal	800-850	123.3	6×10^5 min^{-1}	Juntgen (1981)
Brazilian Coal	800-1000	165.11	1350 mole cm^{-2} min^{-1} atm^{-n}	Schmal et al. (1982)
Sub bituminous Coal	850-1000	163.02	--	Schmal et al. (1983)
Coal	823-1038	146.5	3.98×10^5 s^{-1} $(mole/cm^3)^{-0.45}$	Matsui et al. (1985)
Lignite Char	750-1000	138.3	1.03×10^4 min^{-1}	Shufen and Ruizheng (1992)
Coal Valley	900	131.68	28.045 s^{-1} $KPa^{-0.351}$	Huang and Watkinson (1996)
High Vale		56.51	0.074 s^{-1} $KPa^{-0.542}$ $mm^{0.489}$	
Lignite Coal	750-850	121	--	Liliedahl and Sjostrom (1997)
Bowmans Coal	714-892	131	261276 min^{-1}	Ye et al. (1997)

Sub bituminous Coal	750-900	162.5	6474.7 s^{-1} atm^{-1}	Lee et al. (1998)
Char D	900	227	8×10^{4} g g^{-1} s^{-1} atm^{-n}	Roberts and Harris (2000)
Char Y		221	5×10^{6} g g^{-1} s^{-1} atm^{-n}	
Bituminous coal	727-1727	1.15×10^{5}	0.0782 kg $Pa^{-0.5}$ s^{-1} m^{-2}	Chen et al. (2000)
Datong Coal	>1000	147	1.33 m s^{-1} K^{-1}	Choi et al. (2001)
Lignite Coal	815-950	83.6	1.4×10^{7} s^{-1}	Mann et al. (2004)
Anthracite Char	920-1050	239.8-246.9	3.09×10^{8}-4.15×10^{8} min^{-1}	Zhang et al. (2006)
Coal Char	900-1200	127.17-196.55	9.27×10^{2}-3.39×10^{5} min^{-1}	Wu et al. (2006)
Coal	500-1500	103-214	$1.3\times10^{3.1}$ sec^{-1}	Vostrikov et al. (2007)
HLH Coal	950	114.39	4.68×10^{3} s^{-1} MPa	Li el al. (2010)
SM coal		126.96	1.05×10^{4} s^{-1} MPa	
JC coal		138.72	1.9×10^{4} s^{-1} MPa	

Table 2.3: Activation energies and pre-exponential factors reported by some literatures for the CO_2 gasification reaction of coals and coal chars

Samples	Reaction Temperature (^{0}C)	Activation energy (kJ/mole)	Pre-exponential factor	Reference
Coal	1100-1300	360.065	0.2×108 m/h	Biba et al. (1978)
Coal	>1100	175.1	247 sec^{-1}	Wen and Chaung (1997)
Lignite Char	800-1000	140	1.16×10^4 min^{-1} atm^{-1}	Adanez et al. (1983)
Yallourn Char	870-1286	180	3.0×10^6 cm/s	Osafune and Marsh (1988)
Taiheiyo Char		175	2.1×10^6 cm/s	
Markham Char		195	2.5×10^6 cm/s	
Victoria Char				
Cynheidre Char		190	4.6×10^6 cm/s	
Lignite Char	800-950	149.1	4.93×10^4 min^{-1}	Shufen and Ruizheng (1994)
Lignite Char	750-850	155	--	Liliedahl and Sjostrom (1996)
Bowmans Coal	714-892	91.0	1327 min^{-1}	Ye et al. (1997)
Bituminous coal	727-1727	1.125×10^5	0.0732 kg $Pa^{-0.5}$ s^{-1} m^{-2}	Chen et al. (2000)
Char D	940	209	2×10^4 g g^{-1} s^{-1} atm^{-n}	Roberts and Harris (2000)
Char Y		223	1×10^6 g g^{-1} s^{-1} atm^{-n}	
Coal Char	827-1727	170-250	--	Liu et al. (2000)
Datong Coal	>1000	162	4.40 m s^{-1} K^{-1}	Choi et al. (2001)
SS005, 017,021, 026, 033 Char	1000-1400	45, 174, 200, 45, 128	--	Liu et al. (2006)

Anthracite Char	920-1050	151.5-201.2	9.17×10^{3}-9.8×10^{5} min^{-1}	Zhang et al. (2006)
Coal Char BA	1000-1400	257	2.54×10^{7} s^{-1} $MPa^{-0.56}$	Kajitani et al. (2006)
Coal Char SL		280	6.59×10^{8} s^{-1} $MPa^{-0.43}$	
HLH Coal	950	120.46	4.68×10^{3} s^{-1} MPa	Li el al. (2010)
SM coal		168.63	1.05×10^{4} s^{-1} MPa	
JC coal		209.36	1.9×10^{4} s^{-1} MPa	

2.2.4 Reactions models for coal-char gasification with CO_2 and steam

Mathematical models form an important part of the design process and are used as a predictive tool for assessing commercial prospects. However, detailed knowledge of rates of competing gasification reactions is required when setting up mathematical models of the process. Mehta and Aris (1971) observed that the zeroth order reactions may be approached in heterogeneous reaction when the surface is almost completely covered, while at low coverage reaction may be of first order due to diffusion and reaction in porous slab. The negative orders have been used to represent inhibitory effects and apparent orders of reaction, due to lumping in complex reaction schemes.

Gupta and Bhatia (2000) investigated the modification of discrete random pore model (Ochoa et al., 2001) by including an additional rate constant which takes into account the different reactivity of the initial pore surface having attached functional groups and hydrogen. It is seen that the variations of the reaction rate and surface area with conversion are better represented by the present approach than earlier random pore models (Bhatia and Vartak, 1996).

Most of the random pore models designate the pores a priori, whether in kinetic control or in complete diffusion control, but a particular pore size cannot be in mixed control and cannot switch from one regime to the other with time or with location (Singer et al., 2011). Fung and Kim (1984) studied the reactivities of eight Canadian coal-derived chars of four different ranks thermogravimetrically at 500 ^{0}C; results were represented by shrinking core model in which initial stage of the reaction is kinetically controlled by chemical reaction and the later stage by gas diffusion through ash but effect of diffusion was not rather strong (Wu et al., 2006). The shrinking core model is suitable for the chemical reaction control (Schmal et al. 1982; Kwon et al., 1988; Shufen and Ruizheng,

1994) as well as for noncatalytic gas-solid reactions (Do, 1982). The char-CO_2 gasification under chemical control conditions was satisfactorily described by the random capillary model and the random pore model (Ochoa et al., 2001). The random pore model imparts the correct form to the predicted rate reduction with conversion (Liu and Niksa, 2004). The random pore model (RPM) is based on the initial structural data of the solid reactant (Paviet et al., 2007). The RPM is also used to predict a particle structure parameter (Liu et al., 2000). Structural models such as random capillary model (RCM) and RPM are also used in coal gasification (Huang and Watkinson, 1996). A RCM, considers randomly oriented and overlapping pores (Liu et al., 2000). The RPM does not apply at elevated temperatures because it assumes a reaction regime of chemical control (Liu et al., 2004). Lizzio et al. (1990) analysed the gasification reactivity profiles of two chars. They found that both char (Bituminous and Saran char) were obtained in kinetically controlled regime for CO_2 gasification. Everson et al. (2008) observed that the random pore model also accounts for the intra-particle structure changes. The structural effects in addition to the intrinsic kinetics have been evaluated by many models for predicting overall rates includes the shrinking core model (SCM), capillary/random pore model, percolation models and grain models (Guizani et al., 2013). The SCM has a structure factor (Everson et al., 2005) depending on the initial char properties (surface area and porosity) whereas random pore model accounts for surface area variations during reaction dependent on the initial structural properties (Bhatia and Vartak, 1996; Everson et al., 2005). Park and Levenspiel (1975) used a one parameter model to represent the reaction of nonporous solid with gas.

It views that cracks form at the pellet surface and penetrate in to the interior. As a result the virgin core shrinks leaving behind a grainy structure which then reacts away according to the shrinking core model. Percolation models account for connectivity properties associated with the pore behaviour which include opening/closing of pores and disintegration of chars (Everson et al., 2008). The development of the mean specific surface area during gasification cannot be described by the RPM probably because of the ash melting, but by an empirical correlation can be used for better predictability (Tremel and Spliethoff, 2013). The Random Pore Model has the advantage that the difference of coal type is expressible in not only in terms of the reaction constant but also the reaction process using the structure parameter (Watanabe and Otaka, 2006). Lee et al. (1998) studied the coal gasification in a fluidized-bed reactor and observed that the overall gasification process involves pyrolysis in the free board region and combustion and steam

gasification in the main bed region, where the following reaction were assumed to occur (Lee et al., 1998; Kim et al., 2000):

Combustion reaction:

$$C + \alpha O_2 \rightarrow 2(1-\alpha)CO + (2\alpha - 1)CO_2 \quad (2.99)$$

Steam gasification reactions (Matsui et al., 1985; Kim et al., 2000):

$$C + H_2O \rightarrow CO + H_2 \quad (2.100)$$

$$CO + H_2O \rightarrow CO_2 + H_2 \quad (2.101)$$

$$C + 2H_2O \rightarrow CO_2 + 2H_2 \quad (2.102)$$

$$C + \beta H_2O \rightarrow (2-\beta)CO + (\beta - 1)CO_2 + \beta H_2 \quad (2.103)$$

Here α is mechanism factor which takes the value 0.5 when CO is transported away from the char particle and 1.0 when CO_2 is transported away during char combustion (Shirazi et al., 2013). The factor α is a function of char-particle diameter and temperature. The values are

$$\alpha = (P+2)/(2P+2) \qquad for\ d_c < 0.005\ cm \quad (2.104)$$

and

$$\alpha = \frac{P+2}{2P+2-P((d_c-0.005)/0.095)} \qquad for\ 0.005 < d_c < 0.1\ cm \quad (2.105)$$

where $P = 2500exp[-5.19 \times 10^7/RT]$ and d_c is the char particle diameter. In equation (2.103), $(2-\beta)/\beta$ represents the fraction of steam consumed represented by the reaction (2.100) and $2(\beta-1)/\beta$ represents the fraction of steam consumed by reaction (2.102). Matsui et al. (1985) determined β experimentally to be in the range of 1.5-1.1 at 750-900 ^{0}C (Kim et al., 2000). They found β decreases with increasing temperature.

Most of the initial porosities of the chars produced in the fluidized bed were relatively high; the change in gasification rate of the char can be approximately expressed by the volume model for most of the chars (Adschiri et al., 1986).

Li et al. (2010) studied the effect of pressure by shrinking core model for three Chinese chars during steam and CO_2 gasification. In this model, reaction rate equations and kinetic parameters at high temperature and pressure were obtained for each char. Since the steam can enter the microporous network of the chars and therefore the rate can be modelled by either the shrinking core model or the homogeneous model. If the reaction follows the shrinking core model, the reaction rate is proportional to the reaction surface area of shrinking core (or dependent on particle size) (Ye et al., 1998). If the reaction follows the homogeneous model, the reaction rate is particle size independent. The validity of the shrinking core model can be attributed to the core having an exceptional

low porosity (high inertinite parent coal) and consequently negligible penetration of gases (Everson et al., 2006).

Everson et al. (2006) evaluated the overall reaction rate models by using experimental results of isothermal reaction obtained at atmospheric pressure within the temperature range of 1073-1223 K. They used the following general model (Everson et al., 2006; Irfan et al., 2011):

$$\frac{dX}{dt} = rf(X) \tag{2.106}$$

where r being the intrinsic reaction rate and $f(X)$ the structure factor.

The structural factor depends on the initial surface area, porosity and the conversion only, which is given as (Everson et al., 2006a; 2006b; Irfan et al., 2011) as:

$$f(X) = \frac{S_0(1-X)^{2/3}}{(1-\varepsilon_0)} \tag{2.107}$$

By using equation (2.107), equation (2.106) becomes as:

$$\frac{dX}{dt}\frac{1}{(1-X)^{2/3}} = r\frac{S_0}{(1-\varepsilon_0)} \tag{2.108}$$

After separation of variables and after integrating the following correlation was obtained:

$$F(X) = r\frac{S_0}{(1-\varepsilon_0)}t \tag{2.109}$$

With

$$F(X) = \int_0^X \frac{dX}{f(X)} \tag{2.110}$$

Thus, a linear plot of $F(X)$ versus t (for constant partial pressure of gas) is a suitable test for validity of the shrinking core model, shown in Figure 2.12 and 2.13. The slope of these lines at different conditions will give the value of the intrinsic reaction rate r for kwon values of S_0 and ε_0.

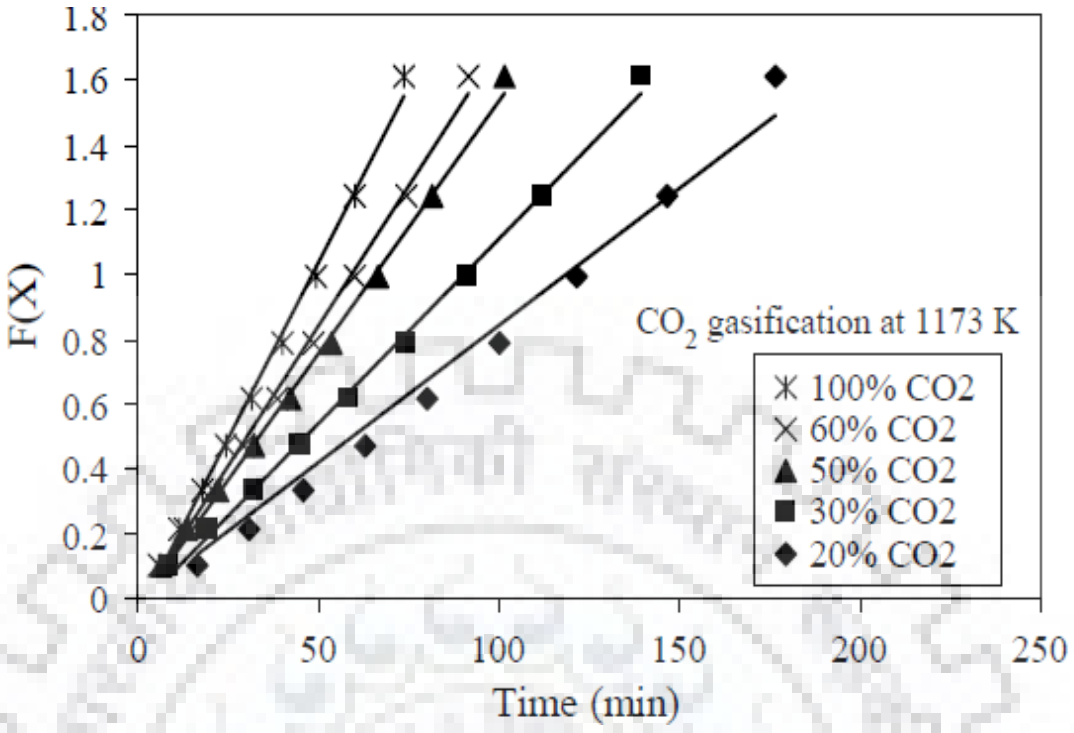

Figure 2.12: Validation of shrinking core model for coal-char B with carbon dioxide gasification at 1173 K (Source: Everson et al., 2006).

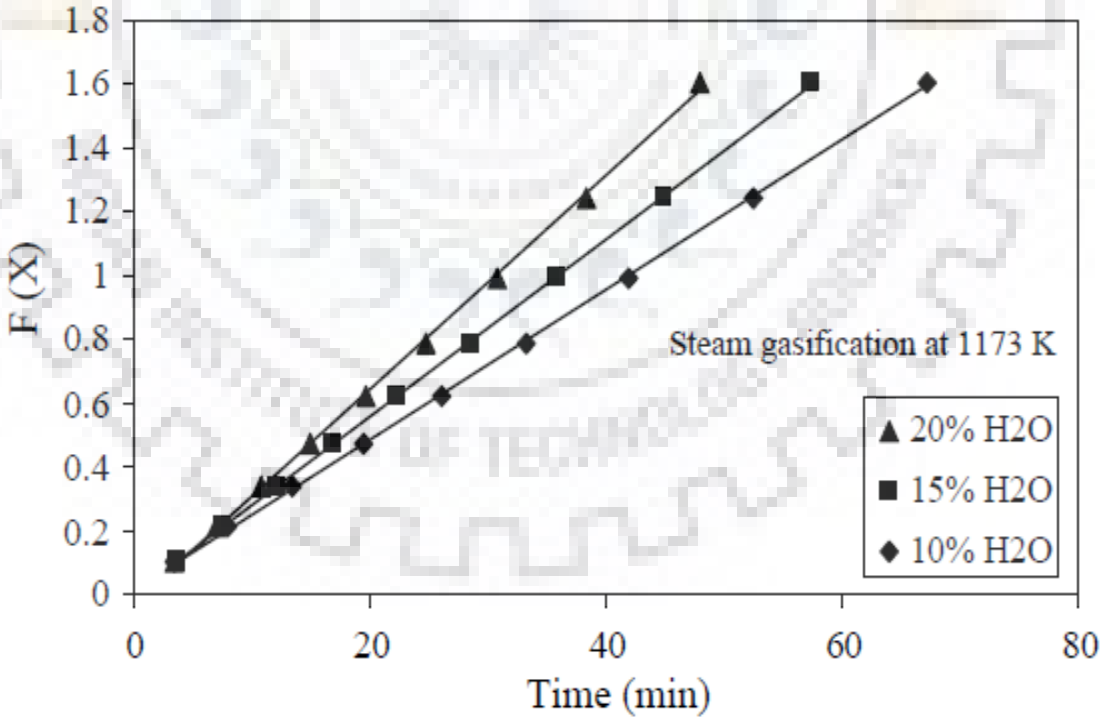

Figure 2.13: Validation of shrinking core model for coal-char B with steam gasification at 1173 K (Source: Everson et al., 2006)

Liu et al. (2006) observed that the grain model and the random pore model are the most popular models to describe the variation of gasification rates with conversion (or time).

The variation of the reaction rate with conversion of the char during gasification is given as:

$$r_c = \frac{dX}{dt} = r_0 F(X) \tag{2.111}$$

where r_0 is the initial rate of gasification and $F(X)$ is a function of carbon conversion X.

The random pore model gives (Mandapati et al., 2012; Silbermann et al., 2013):

$$\frac{dX}{dt} = r_0(1-X)\sqrt{1-\psi ln(1-X)} \tag{2.112}$$

where ψ is a parameter that accounts for the effect of pore structure of char particle. They found that the random pore model ($\psi = 2.5$) best described the experimental data (Liu et al., 2006).

Pores in the surfaces of the char particles are considered to widen rapidly from micropores in to mesopores with the progress of reaction. In respect of such changes in specific surface area, a comparison was made between a grain model and random pore model. The grain model (Kajitani et al., 2006) assumes that a char particle is an aggregation of smaller grains, each of which follows the unburned core model. Assuming that grains are sphere of uniform size, the equation to calculate specific surface area S is expressed as follows (Kajitani et al., 2006):

$$S = S_0(1-X)^{2/3} \tag{2.113}$$

where S_0 means the initial specific surface area and X indicates a conversion ratio of the char.

The reaction rate is expressed as follows (Zhang et al., 2006):

$$\frac{dX}{dt} = k_g(1-X)^{2/3} \tag{2.114}$$

In random pore model, it is assumed that char particle is porous and the internal surfaces of such pores serve as reaction interfaces (Kajitani et al., 2006). The random pore model was chosen by many researchers since the char is characterised by the presence of fine pores and cracks (Everson et al., 2006; Irfan et al., 2011), which can contribute to intra-particle gas penetration and subsequently particle structure changes. The specific surface area is given as (Bhatia and Vartak, 1996; Ziv and Kantorovich, 2001; Everson et al., 2006; Kajitani et al., 2006; Shadhukhan et al., 2010; Irfan et al., 2011; Tremel and Spliethoff, 2013):

$$S = S_0(1-X)\sqrt{1-\psi ln(1-X)} \tag{2.115}$$

and the reaction rate is (Everson et al., 2006; Irfan et al., 2011)

$$\frac{dX}{dt} = \frac{r_s(1-X)S_0\sqrt{1-\psi ln(1-X)}}{(1-\varepsilon_0)} \tag{2.116}$$

ψ being the structural parameter characteristics of the initial char structure defined as (Zolin et al., 1998):

$$\psi = \frac{4\pi L_0(1-\varepsilon_0)}{S_0^2} \tag{2.117}$$

Therefore, equation (2.116) can be written in terms of dimensionless parameter as follows (Bhatia and Vartak, 1996; Kajitani et al., 2006; Zhang et al. 2010)

$$\frac{dX}{d\tau} = (1-X)\sqrt{1-\psi ln(1-X)} \tag{2.118}$$

with

$$\tau = \frac{r_s S_0 t}{(1-\varepsilon_0)} \tag{2.119}$$

Relationships for the fractional carbon conversion X in terms of time t or dimensionless time τ (implicit or explicit) obtained by integration of equation (2.116) and by using equation (2.117) are as follows:

$$t = \frac{2(1-\varepsilon_0)}{r_s S_0 \psi}\left(\sqrt{1-\psi ln(1-X)} - 1\right) \tag{2.120}$$

In terms of dimensionless time (τ), in implicit form reduces to:

$$\tau = \frac{2}{\psi}\left(\sqrt{1-\psi ln(1-X)} - 1\right) \tag{2.121}$$

and explicitly as:

$$X = 1 - exp\left[-\tau\left(1+\frac{\psi\tau}{4}\right)\right] \tag{2.122}$$

On introducing the time factor as:

$$t_f = \frac{r_s S_0}{(1-\varepsilon_0)} \tag{2.123}$$

equation (2.122) becomes:

$$X = 1 - exp\left[-t_f t\left(1+\frac{\psi t_f t}{4}\right)\right] \tag{2.124}$$

A power rate law (n^{th} order) for the intrinsic reaction rate r_s given by equation (2.125) was used together with the Arrhenius equation for the temperature dependence, the equation becomes:

$$r_s = k_{s0} exp\left(-{}^{E}/_{RT}\right) P_{Gas}^{n} \tag{2.125}$$

where P_{Gas}^{n} is the partial pressure of the gasifying agents.

The RPM can represent the behaviour of a system that shows a maximum at certain conversion levels (X<0.393) as well as one that does not have any maximum (Zhang et al., 2010). When $\psi = 0$, the RPM becomes the same as the volumetric model, and for $\psi = 1$, it approaches to the shrinking core model for the cases of n≤1. In this regards, the RPM is more flexible than the volumetric and shrinking models.

The char consumption rate for C-CO_2 reactions, in the regime where kinetic control can be assumed, is written as (by use of equation (2.10)) (Kumar and Ghoniem, 2013)

$$\dot{m}_p = k_s P_g = m_0 S_0 (1-X)\sqrt{1-\psi ln(1-X)}\,\frac{k_1 P_{CO_2}}{1+k_2 P_{CO}+k_3 P_{CO_2}} \qquad (2.126)$$

where m_0 is the initial char mass of the particle, S_0 is the initial surface area (m^2/kg).

Similar expression for the C-H_2O reaction, in the kinetics-controlled regime, is written as (Kumar and Ghoniem, 2013) (by use of equation (2.80))

$$\dot{m}_p = k_s P_g = m_0 S_0 (1-X)\sqrt{1-\psi ln(1-X)}\,\frac{k_1 P_{H_2O}}{1+k_2\sqrt{P_{H_2}}+k_3 P_{H_2O}} \qquad (2.127)$$

where P_{H_2O} and P_{H_2} are the free stream partial pressures of H_2O and H_2, respectively, in the vicinity of the particle.

Different researches proposed different model for the coal char-CO_2 and coal char-steam gasification which are summarized in Table 2.4.

Table 2.4: Different model with their developed equations for coal-char gasification by different researchers

Model	Equation	Reference
Random pore model	$\frac{dx}{dt} = k_p(1-x)\sqrt{1-\psi \ln(1-x)}$	Kajitani et al. (2006)
Gibson-Euker model	$\frac{dx}{dt} = k(1-x)\left(P_{H_2O} - \frac{P_{H_2}P_{CO}}{K}\right)$	Huang and Watkinson (1996)
Volumetric reaction model	$\frac{dx}{dt} = k_v\beta(x,t)C_{S,0}^n(1-x)^m$	
Shrinking core model	$\frac{dx}{dt} = k\exp(E/_{-RT})P^n(1-x)^{2/3}$	Lee et al. (1998)
	$\frac{dx}{dt} = kP_{gas}^n(1-x)^{2/3}$	Li et al. (2010)
	$\frac{dx}{dt} = kP_{CO_2}^n(1-x)^{2/3}$	Ahn et al. (2001)
The Johnson model	$\frac{dX}{dt} = K(1-X)^{2/3}\exp(-\alpha X^2)$	Goyal et al. (1988)
Homogeneous model	$\frac{dX}{dt} = k\,(1-X)$	Ye et al. (1998)
Grain model	$\frac{dx}{dt} = k_g(1-x)^{2/3}$	Kajitani et al. (2002)
Random pore model	$\frac{dx}{dt} = k_p(1-x)\sqrt{1-\psi \ln(1-x)}$	
Shrinking core model	$\frac{dx}{dt} = k'P_{H_2O}^n(1-x)^{2/3}$	Zhang et al. (2006)
Homogeneous model	$\frac{dx_c}{dt} = k(1-x_c)$	Guo and Zhang (1986)
Volumetric model	$\frac{dx}{dt} = k\,(1-x)$	Zhang et al. (2010)
Shrinking core model	$\frac{dx}{dt} = \frac{k_s C^n S_0}{(1-\epsilon_0)}(1-x)^m$	Zhang et al. (2010)
Random pore model	$\frac{dx}{dt} = k_p(1-x)\sqrt{1-\psi \ln(1-x)}$	

Shrinking core model	$\frac{dX}{dt} = kP_{H_2O}^{n}(1-X)^{2/3}$	Kim et al. (2000)
Random pore model	$\frac{dx}{dt} = k_p(1-x)\sqrt{1-\psi_i \ln(1-x)}$	Watanabe and Otaka (2006)
Volumetric model	$\frac{dx}{dt} = k_v(1-x)$	Adschiri et al. (1986)
Random pore model	$\frac{dX}{dt} = \frac{r_s(1-X)S_0\sqrt{1-\psi \ln(1-X)}}{(1-\epsilon_0)}$	Everson et al. (2008)
The Dutta and Wen model	$\frac{dx}{dt} = \left(1 \pm 100x^{v\beta}\exp(-\beta x)\right)kC_g(1-x)$	Molina and Mondragon (1998)
Modified volumetric model	$\frac{dx}{dt} = a^{1/b}b\,(1-x)[-\ln(1-x)]^{b-1/b}$	
The Adschiri and Furusawa model	$\frac{dx}{dt} = S_{(x)}k = k(1-x)$	
Shrinking reacted core model	$X = \frac{3}{(\phi)^2}(\phi\coth\phi - 1)k_V C_{A0}t$	Everson et al. (2006)

2.3 Specific Surface Area

The specific surface areas of coal char increases rapidly with progress of reaction and peaks with a conversion ratio of about 0.4 (Kajitani et al., 2002). Specific surface areas can be measured with nitrogen gas adsorption isotherm at 77 K by the BET method (Ramasamy et al., 2014), but this method is difficult to apply for very low porosity (<0.5 nm) because of restrictive activated diffusion effect which is shown in Figure 14(a). This drawback can be eliminated with carbon dioxide gas adsorption isotherms at 273 K (Kopyscinski et al., 2014), to evaluate micro-pores more exactly, which is shown in Figure 14(b). The adsorption isotherms were analysed by the Dubinin-Astakhov method (D-A method).

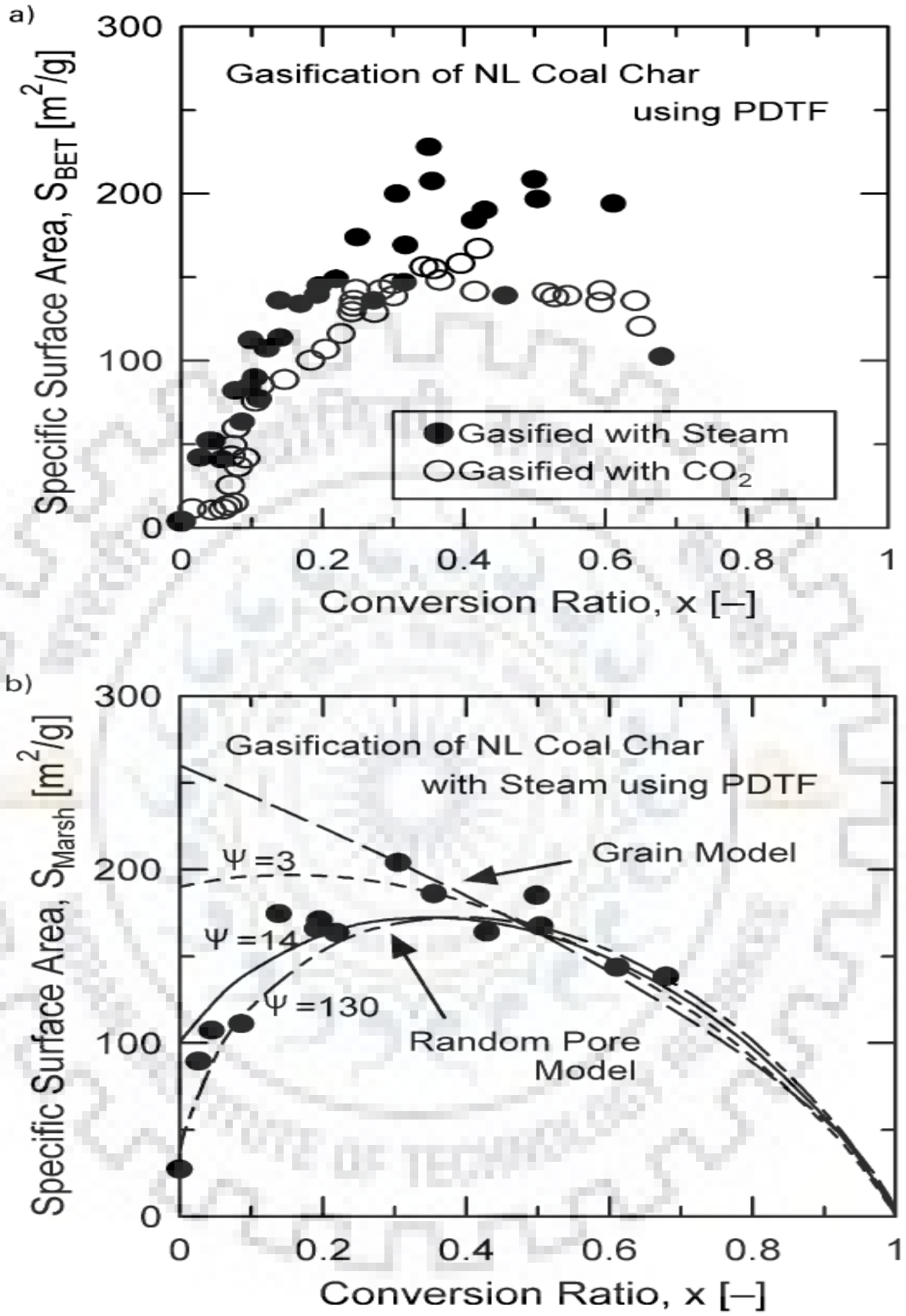

Figure 2.14: Specific surface area of NL sampled char. (a) surface area by BET method (absorbate: N_2). (b) Surface area including micro pore by D-A method (absorbate: CO_2) (Source: Kajitani et al., 2002)

2.4. Summary

The above discussion reveals that considering importance of the coal (or coal char) gasification, many researchers have paid their attention on experimental as well as theoretical investigation. However, there are many gaps. Particularly the mathematical models developed so far have limited applicability perhaps due to lack of deeper understanding of the gasification processes occurring at the microscopic level. Considering this, in the present work an attempt has been made to investigate steam gasification inside a single char particle using basic reaction mechanism but with greater detailed and flexibility of changing physic-chemical properties of reactant and product species.

CHAPTER 3

MATHEMATICAL MODEL DEVELOPMENT

A mathematical model representing gasification of a single coal char particle was developed. In this chapter, details of the model are being discussed in four sections. The first section of this chapter deals with the model development of coal char particle in terms of balance equations followed by the discussion about the kinetics of the gasification reactions in the second section. The third section describes selection of suitable correlations for the porosity and effective diffusivity in terms of changing particle properties as the carbon conversion proceeds. Finally the computational strategy for solving all model equations is discussed in the fourth section.

3.1 Mathematical Modeling of a Single Coal Particle

Gasification is the main commercial technologies of coal processing where non-catalytic heterogeneous reaction between carbon and gasifying media takes place. A successful design and optimal operation of any commercial unit consisting of various processes, which proceed at various rates, depend on better understanding of the key processes. In case of coal (or coal char) gasification, the most important parameter is the behavior and history of each individual particle in the gasifier. Considering this, in the present work, gasification of a single spherical particle is being considered for theoretical study. Our task is to formulate a coal gasification model able to predict the single coal char particle behavior during its gasification. This model includes simultaneous intra-particle diffusion and reaction. The mathematical model take into account the heterogeneous and homogeneous reactions mechanism and solid phase structure such as porosity. The developed model used the pre-exponential factor and activation energies from the literature.

For development of the model, following assumptions are made:

- ✓ Isothermal condition: Temperature within the particle is uniform through.
- ✓ Constant pressure: Pressure within the particle is constant and transfer of reactant and product species take place due to molecular diffusion only.
- ✓ Particle size remains constant: It is assumed that there is no shrinkage or no flaking of the ash layer produced after gasification.

- ✓ No solid product is formed: No solid product other than ash is formed after reaction is complete.
- ✓ Particle is free from volatile compounds since the beginning of the process
- ✓ Porosity depends on the carbon content: Porosity of reacted and unreacted core of a particle is represented as a function of carbon concentration and the initial mass of the particle.

Mathematical modeling for the steam gasification of a single coal char particle involves the mole balances of the gasifying agent as well as the product gas species through an infinitesimal spherical volume element with radius increment, Δr and in the time interval of Δt. For this model development, it is assumed that the char particle is a regular sphere of known initial size, and a constant concentration of the gasifying agent is maintained outside the particle surface. The developed model equation is a nonlinear partial differential equation which is solved by using the staggered grid finite volume method similar to that proposed by Kumar and Upadhyay (2000). Here we take the concentration of various species at nodes represented by C_i (Figure 3.1) and molar flux is calculated across the boundaries of volume elements represented by r_i and r_{i-1} in the same figure.

3.1.1 Material balance for gasifying species

Assuming a spherical co-ordinate system with the origin at the centre of the particle, the flux of the gasifying agent will have a negative sign as the gasifying agent is diffusing inward.

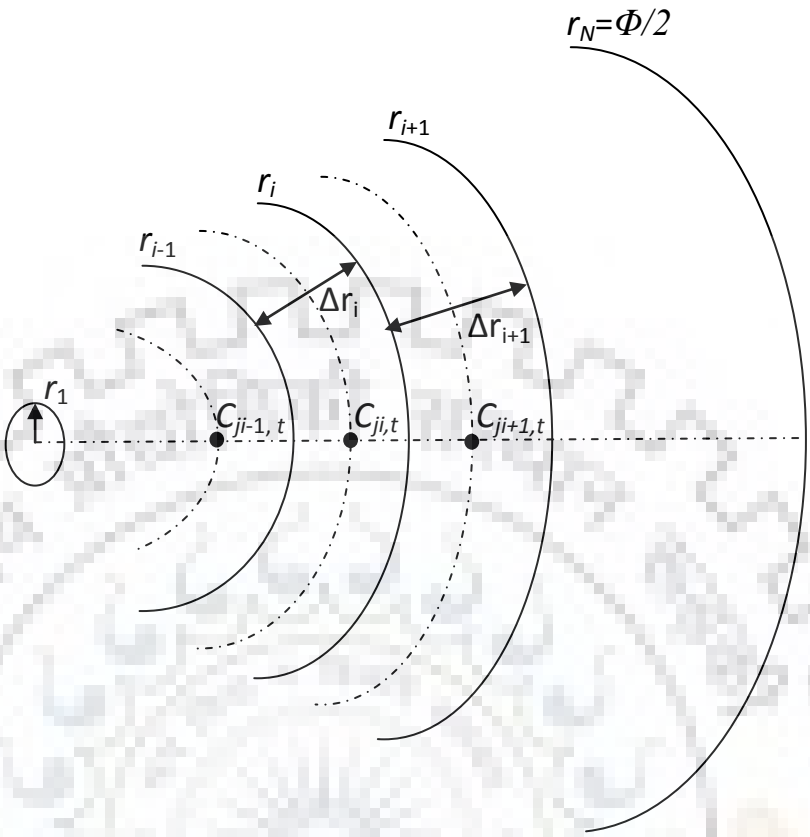

Figure 3.1: Spherical volume elements inside the char particle ($C_{ji,t}$ is the concentration of j^{th} component in the i^{th} volume element at time t)

Performing a molar balance for the gasifying agent over the i^{th} volume element bounded between r_{i-1} and r_i (Figure 3.1), we have:

$$\text{Rate of moles in through } i^{\text{th}}\text{face} - \text{Rate of moles out through } (i-1)^{\text{th}}\text{face}$$
$$= \text{Rate of moles accumulated in the } i^{\text{th}} \text{ volume element}$$
$$- \text{Rate of moles generated in the } i^{\text{th}} \text{ volume element}$$

$$\text{Rate of moles in through } i^{\text{th}}\text{face} = -A_{r_i} D_{ei} \left.\frac{\partial C}{\partial r}\right|_{r_i}$$

$$\text{Rate of moles out through } (i-1)^{\text{th}}\text{face} = -A_{r_{i-1}} D_{e(i-1)} \left.\frac{\partial C}{\partial r}\right|_{r_{i-1}}$$

$$\text{Rate of moles accumulated in the } i^{\text{th}} \text{ volume element} = V_{r_i} \left.\frac{\partial C}{\partial t}\right|_{C_i}$$

$$\text{Rate of moles generated in the } i^{\text{th}} \text{ volume element} = R_{i,t} V_{r_i}$$

Applying these terms in the molar balance expression, finally we have:

$$A_{r_i} D_{ei} \left.\frac{\partial C}{\partial r}\right|_{r_i} - A_{r_{i-1}} D_{e(i-1)} \left.\frac{\partial C}{\partial r}\right|_{r_{i-1}} = V_{r_i} \left.\frac{\partial C}{\partial t}\right|_{C_i} - V_{r_i} R_{i,t}\big|_{C_i} \tag{3.1}$$

$$4\pi r_i^2 D_{ei} \left.\frac{\partial C}{\partial r}\right|_{r_i} - 4\pi r_{i-1}^2 D_{e(i-1)} \left.\frac{\partial C}{\partial r}\right|_{r_{i-1}} = \frac{4}{3}\pi (r_i^3 - r_{i-1}^3) \left[\left.\frac{\partial C}{\partial t}\right|_{C_i} - R_{i,t}\right] \tag{3.2}$$

For the limiting case of $\Delta r (= r_i - r_{i-1})$ tending to zero, the above equation reduces to the non-linear partial differential equation (Nigam et al., 1982; Nigam et al., 1983; Ahuja, 2010)

$$\frac{\partial C}{\partial t} = \frac{1}{r^2}\frac{\partial}{\partial r}\left[r^2 D_e \frac{\partial C}{\partial r}\right] + R_j \tag{3.3}$$

The solution of this non-linear partial differential equation (3.3) may be obtained using the staggered grid finite volume method by substituting following derivatives in terms of finite differences in equation (3.2):

$$\left.\frac{\partial C}{\partial t}\right|_{C_i} = \frac{C_{i,t+\Delta t} - C_{i,t}}{\Delta t} \tag{3.4}$$

The concentration gradient is given as

$$\left.\frac{\partial C}{\partial r}\right|_{r_i} = \frac{C_{i+1,t} - C_{i,t}}{(\Delta r_i + \Delta r_{i+1})/2} \tag{3.5}$$

$$\left.\frac{\partial C}{\partial r}\right|_{r_{i-1}} = \frac{C_{i,t} - C_{i-1,t}}{(\Delta r_i + \Delta r_{i-1})/2} \tag{3.6}$$

Applying equation (3.4), (3.5), and (3.6) in equation (3.2) which leads to the following algebraic equation:

$$\frac{r_i^2 D_{e(i+1)}(C_{i+1,t} - C_{i,t})}{(\Delta r_i + \Delta r_{i+1})/2} - \frac{r_{i-1}^2 D_{ei}(C_{i,t} - C_{i-1,t})}{(\Delta r_i + \Delta r_{i-1})/2} = \frac{1}{3}(r_i^3 - r_{i-1}^3)\left[\frac{C_{i,t+\Delta t} - C_{i,t}}{\Delta t} - R_{i,t}\right] \tag{3.7}$$

Rearranging equation (3.7); the resultant expression can be obtained as:

$$C_{i,t+\Delta t} = C_{i,t} + R_{i,t}\Delta t + \frac{6}{(r_i^3 - r_{i-1}^3)}\left[\frac{r_i^2 D_{e(i+1)}(C_{i+1,t} - C_{i,t})}{\Delta r_i + \Delta r_{i+1}} - \frac{r_{i-1}^2 D_{ei}(C_{i,t} - C_{i-1,t})}{\Delta r_i + \Delta r_{i-1}}\right]\Delta t \tag{3.8}$$

The term $R_{i,t}$ (with positive sign) is the rate of generation of steam in i^{th} volume element which is based on the rate of reaction of the steam.

As evident from equation (3.3), for solving this equation three boundary conditions (two at known *r*, and one at known *t*) are required, which may be taken as:

B. C. I (t): $\quad at\ t = 0\ (for\ all\ r) \qquad C = 0$ (3.9)

B. C. II (r): $\quad at\ r = \Phi/2\ (for\ all\ t) \qquad C = C_0$ (3.10)

B. C. III (r): $\quad at\ r = 0\ (for\ all\ t) \qquad \dfrac{\partial C}{\partial r} = 0$ (3.11)

Substituting B.C. III, i.e., $\left.\frac{\partial C}{\partial r}\right|_{r=0} = 0$; equation (3.8) reduces to

$$4\pi r_1^2 D_{e1} \left.\frac{\partial C}{\partial r}\right|_{r_1} = \frac{4}{3}\pi r_1^3 \left[\left.\frac{\partial C}{\partial t}\right|_{r_1} - R_{1,t}\right] \tag{3.12}$$

The values of derivatives given in equations (3.4) and (3.5) for central volume element becomes:

$$\left.\frac{\partial C}{\partial t}\right|_{C_1} = \frac{C_{1,t+\Delta t} - C_{1,t}}{\Delta t} \tag{3.13}$$

and

$$\left.\frac{\partial C}{\partial r}\right|_{r_1} = \frac{C_{2,t} - C_{1,t}}{r_1(\Delta r_1 + \Delta r_2)} \tag{3.14}$$

Applying equation (3.13) and (3.14) in the equation (3.12) and rearranging, the resultant expression can be obtained as:

$$C_{1,t+\Delta t} = C_{1,t} + R_{1,t}\Delta t + \frac{6D_{e1}\Delta t}{r_1(\Delta r_1 + \Delta r_2)}\left(C_{2,t} - C_{1,t}\right) \tag{3.15}$$

The term $R_{1,t}$ is function of concentration which is based on the rate of reaction of steam (reactant) at the centre of the particle.

3.1.2 Material balance for product species

Performing a molar balance for any j^{th} species over the i^{th} volume element bounded between r_{i-1} and r_i (Figure 3.1), we have:

$$\text{Rate of moles in through } i^{\text{th}}\text{face} - \text{Rate of moles out through } (i-1)^{\text{th}}\text{face} = \text{Rate of moles accumulated in the } i^{\text{th}} \text{ volume element} - \text{Rate of moles generated in the } i^{\text{th}} \text{ volume element}$$

$$\text{Rate of moles in through } i^{\text{th}}\text{face} = -A_{r_{ij}} D_{eji} \left.\frac{\partial C_j}{\partial r}\right|_{r_i}$$

$$\text{Rate of moles out through } (i-1)^{\text{th}}\text{face} = -A_{r_{(i-1)j}} D_{ej(i-1)} \left.\frac{\partial C_j}{\partial r}\right|_{r_{i-1}}$$

$$\text{Rate of moles accumulated in the } i^{\text{th}} \text{ volume element} = V_{jr_i} \left.\frac{\partial C_j}{\partial t}\right|_{C_j}$$

$$\text{Rate of moles generated in the } i^{\text{th}} \text{ volume element} = V_{jr_i} R_{ji}\big|_{C_j}$$

Finally, we have

$$A_{r_i} D_{eji} \left.\frac{\partial C_j}{\partial r}\right|_{r_i} - A_{r_{i-1}} D_{ej(i-1)} \left.\frac{\partial C_j}{\partial r}\right|_{r_{i-1}} = V_{jr_i} \left.\frac{\partial C_j}{\partial t}\right|_{C_j} - V_{jr_i} R_{ji,t}\big|_{C_j} \tag{3.16}$$

The method of solution of this non-linear partial differential equation may be same as that of equation (3.8), which is given by following algebraic equation:

$$\frac{r_i^2 D_{ej(i+1)} (C_{j(i+1),t} - C_{ji,t})}{(\Delta r_i + \Delta r_{i+1})/2} - \frac{r_{i-1}^2 D_{eji} (C_{ji,t} - C_{j(i-1),t})}{(\Delta r_i + \Delta r_{i-1})/2} = \frac{1}{3}(r_i^3 - r_{i-1}^3)\left[\frac{C_{ji,t+\Delta t} - C_{ji,t}}{\Delta t} - R_{ji,t}\right] \tag{3.17}$$

Rearranging equation (3.17); the resultant expression can be obtained as:

$$C_{ji,t+\Delta t} = \left(C_{ji,t} + R_{ji,t}\Delta t\right) + \frac{6}{(r_i^3 - r_{i-1}^3)}\left[\frac{r_i^2 D_{ej(i+1)}(C_{j(i+1),t} - C_{ji,t})}{(\Delta r_i + \Delta r_{i+1})} - \frac{r_{i-1}^2 D_{eji}\left(C_{ji,t} - C_{j(i-1),t}\right)}{(\Delta r_i + \Delta r_{i-1})}\right]\Delta t \quad (3.18)$$

where C_j is the concentration of product gases, which are H_2, CO, CO_2, and CH_4. The term $R_{ji,t}$ is the rate of generation of j^{th} component in i^{th} volume element.

Similar to equation (3.3), for solving equation (3.18) for product species, three boundary conditions (two at known *r*, and one at known *t*) are required, which may be taken as:

B. C. I : $at\ t = 0, \quad C_j = 0 \quad (for\ all\ r, and\ j = H_2, CO, CO_2, CH_4)$ (3.19)

B. C. II : $at\ r = \Phi/2\ , \ C_j = C_{j0} \quad (for\ all\ t, and\ j)$ (3.20)

B. C. III : $at\ r = 0, \quad \frac{\partial C_j}{\partial r} = 0 \quad (for\ all\ t, and\ j)$ (3.21)

Applying BC III for the product species at centre of the coal char particle, equation (3.16) reduces to:

$$4\pi r_1^2 D_{ej1}\left.\frac{\partial C_j}{\partial r}\right|_{r_1} = \frac{4}{3}\pi r_1^3\left[\left.\frac{\partial C_j}{\partial t}\right|_{r_1} - R_{j1,t}\right] \quad (3.22)$$

and equation (3.18) becomes

$$C_{j1,t+\Delta t} = \left(C_{j1,t} + R_{j1,t}\Delta t\right) + 6D_{ej1,t}\left[\frac{\left(C_{j2,t} - C_{j1,t}\right)}{r_1(\Delta r_1 + \Delta r_2)}\right]\Delta t \quad (3.23)$$

The value of $R_{j1,t}$ (function of concentration) is based on the rate of reactions of the product species at the centre of the particle.

3.1.3 Material balance on solid reactant (carbon)

Performing a molar balance for the product species over the i^{th} volume element bounded between r_{i-1} and r_i (Figure 3.1), we have:

$$\text{Rate of moles in through } i^{\text{th}}\text{face} - \text{Rate of moles out through } (i-1)^{\text{th}}\text{face}$$
$$= \text{Rate of moles accumulated in the } i^{\text{th}} \text{ volume element}$$
$$- \text{Rate of moles generated in the } i^{\text{th}} \text{ volume element}$$

$$\text{Rate of moles in through } i^{\text{th}}\text{face} = 0$$

$$\text{Rate of moles out through } (i-1)^{\text{th}}\text{face} = 0$$

$$\text{Rate of moles disappeared in the } i^{\text{th}} \text{ volume element} = V_{r_i} \left.\frac{\partial C_C}{\partial t}\right|_{C_{Ci}}$$

$$\text{Rate of moles consumed in the } i^{\text{th}} \text{ volume element} = V_{r_i} R_{Ci,t}$$

Applying these terms in the balance expression, we have

$$0 = V_{r_i} \left.\frac{\partial C_C}{\partial t}\right|_{C_{Ci}} - V_{r_i} R_{Ci,t} \tag{3.24}$$

On rearranging we have

$$\left.\frac{\partial C_C}{\partial t}\right|_{C_{Ci}} = R_{Ci,t} \tag{3.25}$$

The term $R_{Ci,t}$ is based on the reaction rates depending on the conditions prevailing in the i^{th} volume element which varies non-linearly with time. Therefore, the solution of equation (3.25) is also obtained by using the staggered grid finite volume method, giving

$$\frac{C_{Ci,t+\Delta t} - C_{Ci,t}}{\Delta t} = R_{Ci,t} \tag{3.26}$$

Finally, on rearranging the equation (3.26), we have

$$C_{Ci,t+\Delta t} = C_{Ci,t} + R_{Ci,t}\Delta t \tag{3.27}$$

The required boundary condition for carbon gasification (equation 3.25) can be taken as

$$\text{B. C. I}: \quad at\ t = 0, \quad C_C = C_{C0} \quad (for\ all\ r) \tag{3.28}$$

3.2 Kinetics of the Steam Gasification of Coal Char

The rate of the gasification reaction mainly depends on the reactivity of the fuel, gasifying medium, and temperature and pressure of the process. Different reactions are favored at different operating conditions in the gasifier reactor. In this work the main gasification reactions are water-gas, Boudouard reaction and water gas shift reaction. Methanation reaction and methane steam reforming reaction are described along with the parameters affecting the process. The reaction rate correlations found in scientific articles are presented and examined mainly as a function of temperature.

Here, we consider the heterogeneous non-catalytic reaction systems involving only solid-gas reactions and the homogeneous gas phase reactions. The coal char particle is spherical in shape and small in size. Since the particle is small, the temperature variation in the radial direction within the particle is neglected. The over-all reaction rates are influenced not only by the rate of chemical reactions occurring in or at surface of solid, but also by the mass transfer rates of gas through the solid as well as across the gas-film surrounding the solid, which in turn depend on factors such as surface features, porosity, etc.

Heterogeneous gas-solid reactions involving in a single coal particle are governed by an intricate coupling of transport phenomena and chemical kinetics. The overall reaction scheme can be described by following steps:

(1) Diffusion of mass (reactant and product gases) across the boundary layer surrounding the solid particle;
(2) Diffusion of mass through the porous structure of particle;
(3) Reaction of gases with solid surfaces within the particle.

In the gasification of the coal, following three types of reaction take place:

3.2.1 Devolitalization of coal

$$Coal \rightarrow C(Solid) + H_2O, H_2, CO, CO_2, CH_4 \tag{3.29}$$

After the devolitalization of coal, all the volatiles and moisture is removed. The heterogeneous chemical reactions include the char-steam gasification, char-CO_2, and char-hydrogen gasification followed by the homogeneous reactions (gas phase reactions).

3.2.2 Heterogeneous reaction between coal char and gases

Steam Gasification of char (R1): The steam gasification is the partial oxidation of carbon by steam. Steam reacts with the heated carbon according to the following endothermic reaction:

R1: Steam Gasification of char $C + H_2O \rightarrow CO + H_2 \quad \Delta H = 131.4 \frac{kJ}{mol}$ (3.30)

Hydrogasification (R2): The formation of the methane could take place in steam gasification by hydrogasification, which is given as:

R2: Hydrogasification $C + 2H_2 \rightarrow CH_4 \quad \Delta H = -75 \frac{kJ}{mol}$ (3.31)

The Boudouard reaction (R3): produces carbon monoxide by the reaction of coal char and carbon dioxide according to the following endothermic reaction:

R3: Boudouard reaction $C + CO_2 \rightarrow 2CO \quad \Delta H = 172 \frac{kJ}{mol}$ (3.32)

3.2.3 Homogeneous reaction

Methane-Steam Reforming (R4): Methane formed due to the hydro-gasification reaction (R2), may further react with steam through steam reforming reaction which is widely used and studied for the production of the hydrogen in industry for synthesis of ammonia. This reaction is highly endothermic.

R4: Methane steam reforming $CH_4 + H_2O \rightarrow CO + 3H_2 \quad \Delta H = 206.4 \frac{kJ}{mol}$ (3.33)

Water gas shift reaction (R5): This reaction is endothermic in nature and increases the hydrogen to carbon monoxide ratio in the gas therefore this reaction is extensively used and studied in the manufacturing of synthesis gas. Since the water gas shift reaction is the reversible reaction, the equilibrium constant is inversely proportional to the reaction temperature and reaction is favoured kinetically at higher temperature and thermodynamically at lower temperature. The reaction is not affected by the system pressure because there is no variation in the volume of the species.

R5: Water gas shift reaction $CO + H_2O \leftrightarrow CO_2 + H_2 \quad \Delta H = -41.7 \frac{kJ}{mol}$ (3.34)

3.2.4 Rate of reactions

In this work the five main gasification reactions as proposed by Muller et al. (2003) along with their reaction kinetics obtained from various sources are given in Table 1. The modelling and simulation of char gasification studies have been carried out by many researchers (Souza-Santos, 1989, Muller et al., 2003; Kim et al., 2014) using different combinations of these reactions and their respective rate kinetics. There are numerous possible ways through which kinetics of the gasification reactions R1 to R5 can be represented. Table 3.1 presents the rate kinetics being used in the present work with their respective source.

The overall volumetric rate of formation of each j^{th} component $R_j = \frac{dC_j}{dt}$, may be presented individually in terms of rates of reactions (γ) of above reactions:

$$R_C = \frac{dC_C}{dt} = -\gamma_1 - \gamma_2 - \gamma_3 \tag{3.35}$$

$$R_{H_2O} = \frac{dC_{H_2O}}{dt} = -\gamma_1 - \gamma_4 - \gamma_5 \tag{3.36}$$

$$R_{H_2} = \frac{dC_{H_2}}{dt} = \gamma_1 + 3\gamma_4 + \gamma_5 - 2\gamma_2 \tag{3.37}$$

$$R_{CO} = \frac{dC_{CO}}{dt} = \gamma_1 + 2\gamma_2 + \gamma_4 - \gamma_5 \tag{3.38}$$

$$R_{CH_4} = \frac{dC_{CH_4}}{dt} = \gamma_2 - \gamma_4 \tag{3.39}$$

$$R_{CO_2} = \frac{dC_{CO_2}}{dt} = -\gamma_3 + \gamma_5 \tag{3.40}$$

The rate of reaction with respect to the reacting species is given (for the above mentioned five reactions) as:

$$\gamma = kC_A^n C_B^m \tag{3.41}$$

where *m* and *n* are the reaction order with respect to the components A and B.

Table 3.1: Kinetic parameters for steam gasification of coal char from different sources

Reaction No.	Reaction Rate (mol/m^{3}s)	Parameters	Reference
R1	$\gamma_1 = k_1 C_C C_{H_2O}$	$k_1 = 2 \times 10^5 \exp\left(-6000/T\right)$	Corella and Sanz (2005)
R1	$\gamma_1 = k_1 C_s C_{H_2O}^{0.7}$	$k_1 = 10^6 \exp\left(-26112.6/T\right)$	Groeneveld and Swaaij (1980)
R2	$\gamma_2 = k_2 (6/d_p) C_{H_2}$	$k_2 = 2.05 \times 10^3 \exp\left(-27697.14/T\right)$	Mendes et al. (2008)
R3	$\gamma_3 = k_3 S_{Char} C_{CO_2}^{0.83}$	$k_3 = 7.2 \exp\left(-20000/T\right)$	Corella and Sanz (2005)
R3	$\gamma_3 = k_3 C_s C_{CO_2}^{0.7}$	$k_3 = 10^6 \exp\left(-26112.6/T\right)$	Groeneveld and Swaaij (1980)
R4	$\gamma_4 = k_4 \left(C_{CH_4} C_{H_2O} - \frac{C_{CO} C_{H_2}^2}{k_{4w}} \right) \frac{M_C}{\rho_C F_C}$	$k_4 = 7.301 \times 10^{-2} \exp\left(-36150/RT\right)$ $k_{4w} = 5.12 \times 10^{-14} \exp\left(27347/T\right)$	Mendes et al. (2008)
R4	$\gamma_4 = k_4 C_{CH_4}$	$k_4 = 312 \exp\left(-30000/RT\right)$	Govind and Shah (1984)
R4	$\gamma_4 = k_4 C_{CH_4} C_{H_2O}$	$k_4 = 3.1 \times 10^5 \exp\left(-15000/T\right)$	Inayat et al. (2010)
R5	$\gamma_5 = k_5 \left(C_{CO} C_{H_2O} - \frac{C_{CO_2} C_{H_2}}{k_{5w}} \right)$	$k_5 = 10^6 \exp\left(-6370/T\right)$ $k_{5w} = 520 \exp\left(-7230/T\right)$	Corella and Sanz (2005); Inayat et al. (2010)
R5	$\gamma_5 = k_5 \left(C_{CO} C_{H_2O} - \frac{C_{CO_2} C_{H_2}}{k_{5w}} \right)$	$k_5 = 2.78 \exp\left(-1510/T\right)$ $k_{5w} = 0.0265 \exp\left(3968/T\right)$	Chejne and Hernandez (2002)
R5	$\gamma_5 = k_5 \left(C_{CO} C_{H_2O} - \frac{C_{CO_2} C_{H_2}}{k_{5w}} \right)$	$k_5 = 2.778 \exp\left(-12560/RT\right)$ $k_{5w} = 0.0265 \exp\left(32910/RT\right)$	Daggupati et al. (2012) Mendes et al. (2008)

3.3 Porosity and Effective Diffusivity

The coal char particle is surrounded by the gasifying medium. As reaction start, the diffusion-reaction of coal char particle at the outer most surface will begins. Depending on the rate of conversion, carbon content of the reacting layer begins to deplete leaving behind completely or partially converted ash layer which changes the diffusivity of the gasifying agent and hindered the counter diffusion of product gases and also altered the porosity of the char particle.

Due to this, the rate of gasification of single coal char particle is only moderately affected by the ambient pressure level, but the main rate controlling parameters during coal char gasification are diffusivity of gas in coal char, gasification temperature, and particle size (Bliek et al., 1986). Since the rate of conversion of coal char strongly influence the porosity of coal char, which influence the diffusivity dependency on the coal char conversion and porosity of the char particle during course of the reactions.

The diffusion of the gases in the coal char particle may seriously affected the coal char gasification rate (Samdani et al., 2012). Since the formation of ash during the conversion of carbon in the coal char alters the diffusion rate of gases in the coal char particle it also influences the overall reaction rate of gasification. Therefore, modeling the variation of the diffusion coefficient in the coal char particle during the course of reaction as well as position within the coal char particle is necessary. The model includes the effective transport properties and chemical reaction rate as a function of position and time within the coal char particle.

During the diffusion of reactant gas into the pores of the coal char particle, if the length of the mean free path of gas molecules is larger than the micro-pore diameter, the collision becomes more frequent between pore wall and gas molecules which reduces the overall diffusivity of gas into coal char due to lack of gas transport by the narrow space within the pore, this phenomena is called Knudsen Diffusion. But in this model, the length of mean free path of gas molecules is significantly less than the micro-pore diameter of the pore. Therefore, it is necessary to account for the diffusivity of the gas molecules into the coal char particle.

The Knudsen Diffusion coefficient (D_{jK}) of j^{th} component in the pores of the coal char is given as:

$$D_{jK} = \frac{d_m}{3}\sqrt{\frac{8R_gT}{\pi MW_j}} \tag{3.42}$$

where d_m is the mean pore diameter.

The binary diffusion coefficient of component for species *j* in species *l* is given as:

$$D_{jl} = \frac{0.001858T^{3/2}\sqrt{\frac{1}{MW_j}+\frac{1}{MW_l}}}{P\sigma_{jl}^2\Omega_D} \tag{3.43}$$

The initial effective diffusivity can be evaluated by use of Knudsen diffusion coefficient and binary diffusion coefficient, which is given as:

$$\frac{1}{D_{ej}^0} = \frac{1}{D_{jK}} + \frac{1}{D_{jl}} \tag{3.44}$$

The porosity in coal char particle has significant influence on other properties also. The pore size and pore volume distribution in the coal char particle affects the extent and ease of diffusion-reaction within the pore. During gasification, the chemical reaction occurs between the reactant gas and coal char surfaces, mostly which is located in the pores of the particle. The product gases are formed during reaction must be able to escape rapidly from the pores of the char to be filled by the fresh reactant of gas for the further reaction. The particle porosity also affects the control process of diffusion-reaction within the pores of the char particle. At very high initial porosity, the process shift towards the chemically controlled process.

During gasification both the particle internal structure and its porosity are changed (Zygourakls, 1982; Morell et al., 1990). Due to the porosity variation other parameters also changes. These changes correspond to decrease of particle mass. The porosity variation is proportional to the changes of in the amount of carbon in the coal particle. If the linear relation between the carbon conversion and the particle porosity is assumed, the following expression can be made for porosity changes during reactions (Gil et al., 2011):

$$\varepsilon_P = \varepsilon_0 + X(1-\varepsilon_0) \tag{3.45}$$

where ε_0 is the initial solid particle porosity and *X* is the fractional reduction in particle mass.

The initial porosity of the char particle can be calculated through the relationship between bulk density and the solid density (Avnimelech et al., 2001; Mermoud et al., 2006) giving

$$\varepsilon_0 = \left(1 - \frac{\rho_b}{\rho_s}\right) \tag{3.46}$$

where ρ_b is the bulk density which is the ratio of the mass of the char (including moisture) to its total volume and ρ_s is the solid density which is the ratio of the mass of dry solid to the volume of the solid char. The solid phase density measures the density of carbon and ash in the char particle.

The fractional reduction in the particle mass, *X*, is given as:

$$X = 1 - \frac{m(t)}{m_0} \tag{3.47}$$

where m_0 is the initial mass of particle and $m(t)$ is the mass of particle at time *t* including ash.

The overall reaction rate of coal char particle gasification depends on the ease with which the gasifying agent (H_2O) approaches its internal surface. The accessibility of internal surface of coal char particle for gasifying reactant is closely related to the porosity, which is related to effective diffusivity of gases in solid.

The effective diffusivity of gas species in the particle can be calculated by the parallel model, which is given (Abashar and Elnashaie, 1993; Gomez-Barea et al., 2005; Lu et al., 2008; Adams II and Barton, 2009; Huo et al., 2014) as:

$$D_{ej} = \frac{D_{ej}^0 \varepsilon}{\tau} \tag{3.48}$$

where τ is the tortuosity factor

The porosity and tortuosity strongly depend on the coal char structure and nature of the coal char. They changes with progress of the reactions.

The empirical correlation is given by many researchers (Zajdlik et al., 2001; Holikova et al., 2005; Gomez-Barea and Ollero, 2006) for the variation of effective diffusivity with the porosity of the char particle, which is given as:

$$\frac{D_{ej}}{D_{ej}^0} = \left(\frac{\varepsilon_P}{\varepsilon_0}\right)^{\propto} \tag{3.49}$$

where $\propto$ is equal to 2 for random pore size distribution and D_{ei}^0 is the initial effective diffusivity of gas in solid phase. Hence equation (3.49) becomes:

$$\frac{D_{ej}}{D_{ej}^0} = \left(\frac{\varepsilon_P}{\varepsilon_0}\right)^2 \tag{3.50}$$

Values of the initial diffusivity (D_{ej}^0) of various species used in present work are listed in Table 3.2.

Table 3.2: The initial diffusivity of all the gaseous components in unburned char particle

Component	Diffusivity (m^2/s)	Reference
H_2O	2×10^{-5}	Massman (1997); Buczek (2012)
H_2	1.41×10^{-5}	Shi et al. (2010)
CO	2.147×10^{-5}	Ollero et al. (2002)
CO_2	1.67×10^{-5}	Ollero et al. (2002)
CH_4	2.93×10^{-11}	Olague and Smith (1989)

3.4 Numerical Methodology

The problem of char gasification of a single particle defined by equation (3.8-3.15) and equation (3.18-3.23) is a two dimensional problem of a spatial coordinate *r* and a temporal coordinate *t*.

Solution of the problem begins with the application of boundary condition I (equation 3.9 and 3.19) to all the nodal variables $C_{ji,t}$ at t=0, i.e. assigning values to all the concentration nodes on the leftmost column of Figure 3.2(a). Starting from the outermost volume element (between $r_{N\text{-}1}$ and r_N) the rate of formation/consumption of individual species and corresponding flux are evaluated for all the volume elements (reaction and flux nodes) between the time interval 0 and Δt sequentially. Assuming these rates of reactions and fluxes to be the average value between time interval 0 and Δt, concentration of each volume

elements at the time t=Δt is calculated using equation (3.8) and equation (3.23). The process is repeated iteratively until the final time is attained.

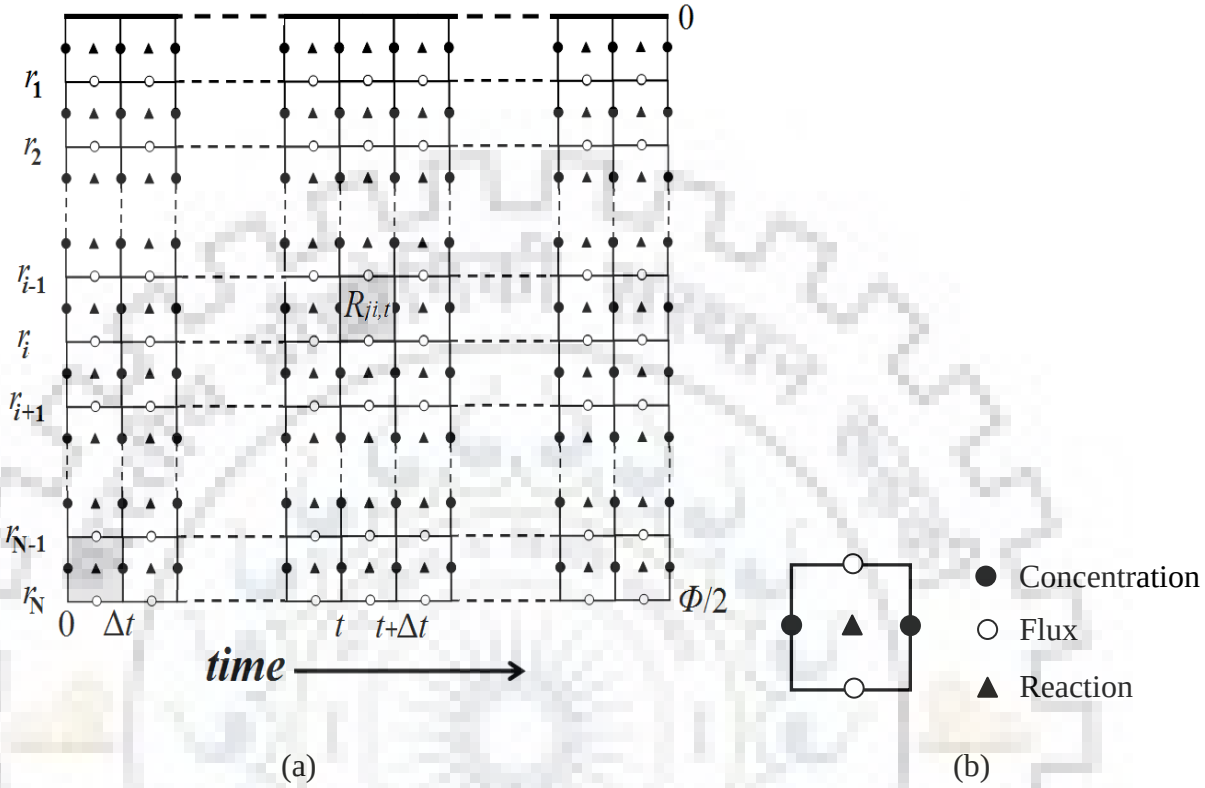

Figure 3.2: (a) Spatiotemporal grid for unsteady state char gasification of a single particle, (b) Staggered grid nodal configuration

The flow diagram for the overall solution of the MATLAB program is shown in Figure 3.3. In this algorithm, solution begins with assigning variables their boundary conditions at t=0. Then concentration and reaction rate are calculated sequentially beginning from particle surface to centre of the particle. Material balance for each volume element is made for a small time interval Δt (0.00001 second in this case) and their resulting concentration is predicted at time t+Δt. The same sequence of calculation is repeated (from particle surface to the centre of the particle) for the regular time interval (Δt) till the final time set for the analysis is attained.

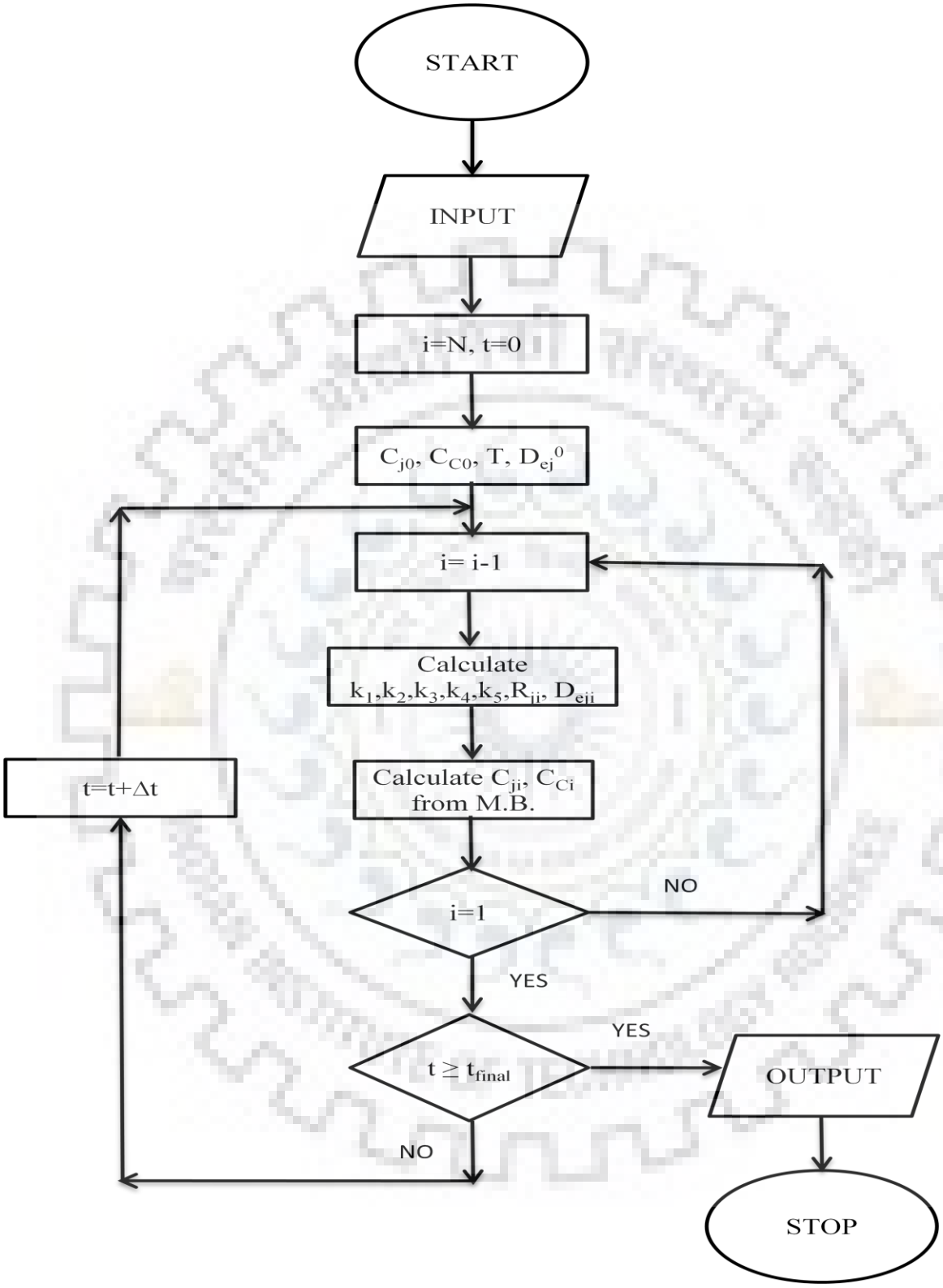

Figure 3.3: Flow diagram for solution of material balance

CHAPTER 4

RESULTS AND DISCUSSION

As discussed in previous chapters, the material balance equations were combined with reaction kinetics to obtain the moles of each component coming out of any volume element *i* (=1 to N) of the char particle. Thus, the model could predict the yield pattern along the radial direction of char particle at a specified time as well as the overall yield and conversion as a function of time. To validate the model results, experimental data of Mermoud et al. (2006) is used. Also, the heat effects of reactions are analyzed to validate assumption of constant temperature within a particle before the discussion about the parametric effects on gasification.

4.1 Model Validation

4.1.1 Comparison with experimental results

Due to unavailability of experimental data for the gasification of single coal or coal-char particle of size greater than 5 mm, the experimental results of steam gasification of a single 10 mm wood charcoal reported by Mermoud et al. (2006) is used to validate the results of the present simulation model for the steam gasification for two cases of temperature and steam concentrations (Figure 4.1 and 4.2). The properties of charcoal particle used for model validation are shown in Table 4.1.

It is evident from Figure 4.1 and 4.2 that the predicted and experimental results are in good agreement at lower temperatures. At higher temperature, however, predicted result follows experimental values only during initial period of gasification (up to 500 sec). After 500 sec, the experimental result continues to follow a constant rate of conversion (linear X vs. t plot), but the model results are concave downward. This difference is due to uneven shrinking size of the char particle during gasification of wood char (Mermoud et al., 2006) and the constant size of spherical char particle assumed in the present model. Due to this, model predicted rate of conversion decreases with time because of the decrease in surface area due to the collapse of two pores by gasification of the pore wall which is in tune with the observation made by many researchers (Wang et al., 2009; Xu et al., 2011).

Table 4.1: Properties of char sample used for the model validation (Source: Mermoud et al., 2006)

Analysis of Sample			
Proximate Analysis		Ultimate Analysis	
Components	wt%	Components	wt%
Ash	0.38	C	44.16
Volatile Matter	82.45	H	5.48
Fixed Carbon	17.17	O (by difference)	50.36
Properties of char particle			
Diameter of Particle, mm	Solid Density, kg/m^3	Bulk Density, kg/m^3	Porosity, %
10	1900	507	73

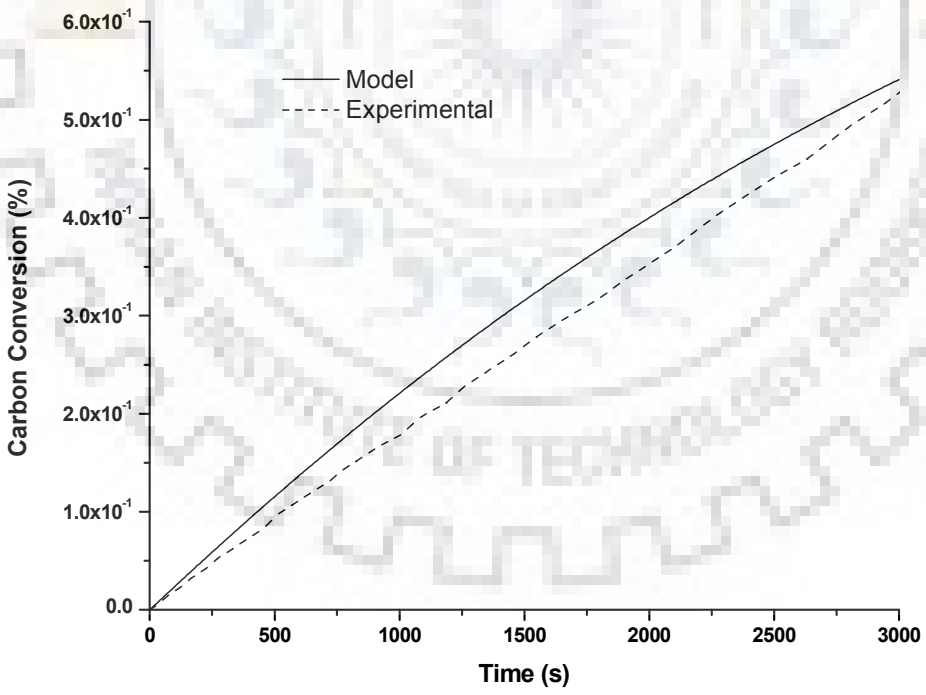

Figure 4.1: Comparison between model and experimental results at 830 ^{0}C and steam partial pressure of 0.2atm

Further, it has been observed (discussed later in the §4.2.2) that at lower temperature, gasification of a char particle follows progressive reaction model and with increase in temperature the mechanism shifts gradually to shrinking core model. Therefore, at lower temperature, gasification takes place everywhere inside the char particle leading to significant conversion without appreciable change in particle size (i.e., experimental condition remains closer to the model assumption of constant particle size), leading to better match of model result. On the other hand, at higher temperature, change in particle size with conversion is fast (due to shrinking core) that leads to deviation in the experimental and predicted result after a short time (less than 500 sec).

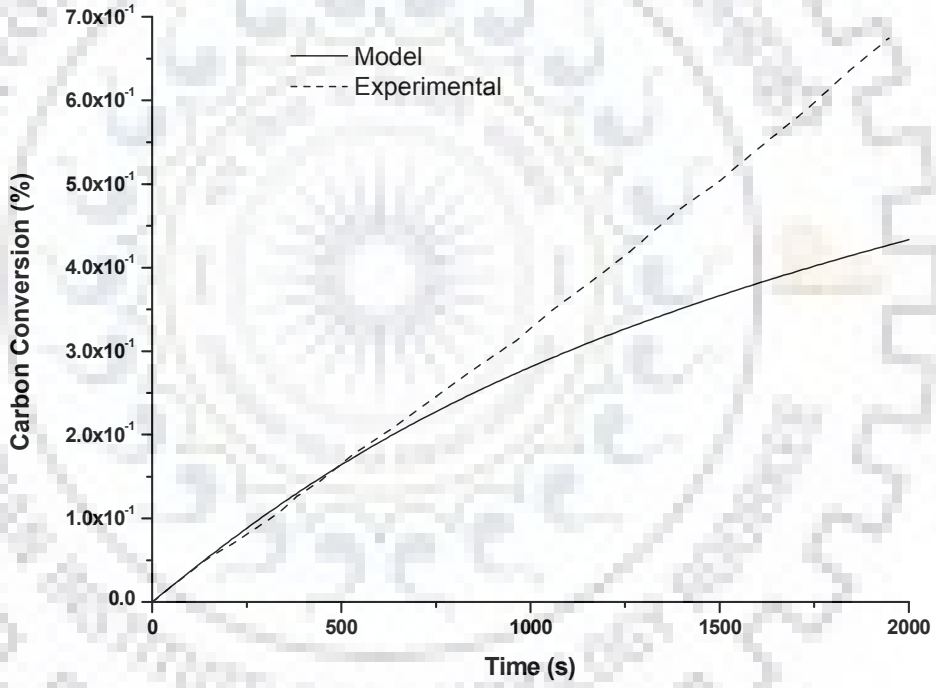

Figure 4.2: Comparison between model and experimental results at 930 ^{0}C and steam partial pressure of 0.1atm

4.1.2 Validity of constancy of temperature

Assumption of constant temperature inside a small char particle is widely accepted for small particle, for large particles. However, temperature variation within the particle was calculated by applying energy balance on the heat effects (absorption/generation) of the gasifying reaction. Figure 4.3 shows the radial variation in the overall rate of heat consumed due to all the reactions. This requirement of heat is accomplish by heat conduction through the particle and heat convection at the outer surface.

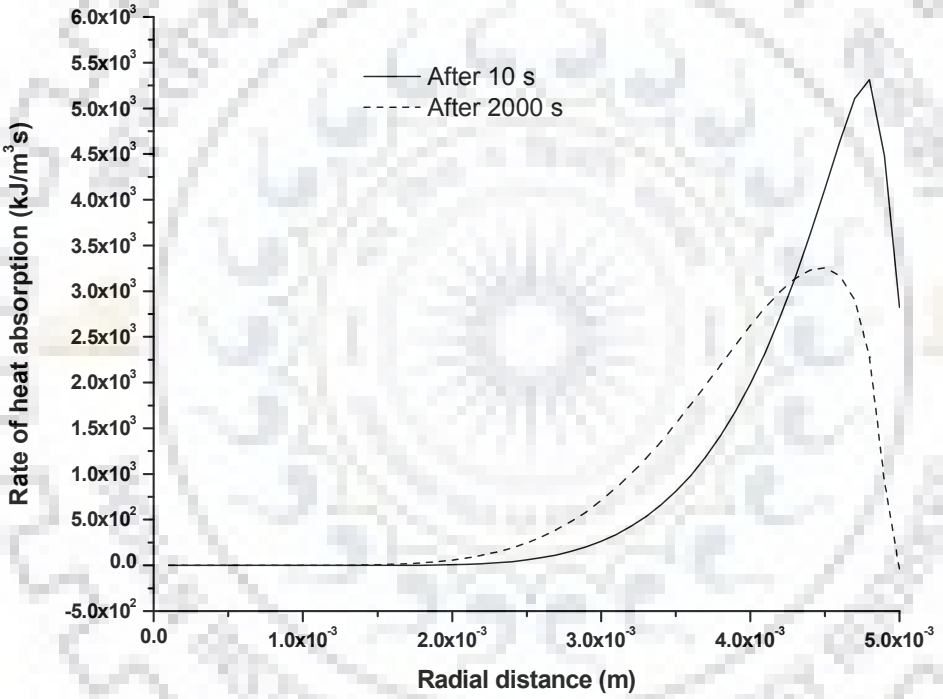

Figure 4.3: Rate of heat consumption inside the particle assuming constant temperature (1100 K)

To calculate required temperature difference at a redial position r_i to achieve this heat transfer, following equation was used.

$$\Delta T = Q\left[\frac{\Phi/2 - r_i}{4\pi(\Phi/2)r_i k_{char}} + \frac{1}{4\pi(\Phi/2)^2 h_{steam}}\right]$$

where Q is the total heat required in the particle volume from r=0 to r_i. Values of thermal conductivity k_{char} and heat transfer coefficient of steam, h_{steam} were taken as 0.2 W/m K, and 6000 W/m^{2}K, respectively.

Radial variation in ΔT is presented in Figure 4.4. Obviously, there is no significant variation in the temperature profile (maximum variation is 0.007 K from the outer temperature); therefore, the assumption of constant temperature inside the particle can be used safely to avoid excessive computational load.

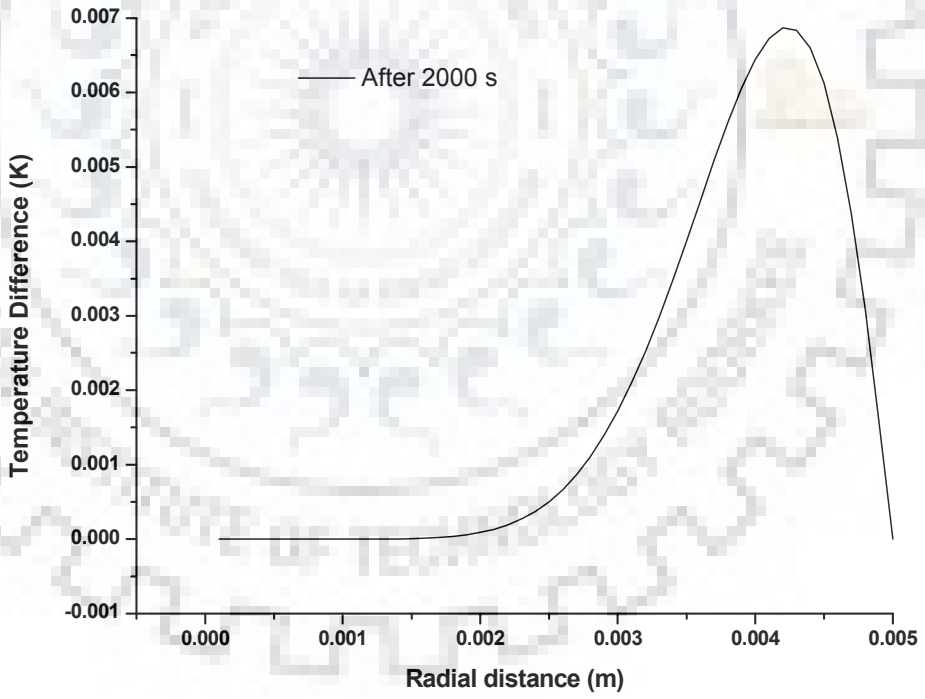

Figure 4.4: Difference in temperature at a radial position inside the particle with respect to ambient temperature

4.2 Parametric Effects on Gasification

In this unsteady state modelling study, the effects of steam concentration, carbon concentration in the char, temperature, particle size, initial porosity, ash content in char, and effect of mixture of steam and CO_2 on the synthesis gas formation have been studied. It has been observed that in all cases, with the passage of time, conversion increases which results in an increase in the porosity of the reacted outer surface of the char particle leading to enhanced effective diffusivity of the steam and products through this outer layer. The change in diffusivity alters the rate of approach of gasification agent and the rate of removal of products in a complex way. In the following section, the parametric effects on the reaction mechanism and product quality are being discussed. The properties of coal particle of Umaria Coalfield M.P., India, used for parametric studied on gasification are shown in Table 4.2.

Table 4.2: Properties of coal particle used for the parametric study of gasification (Source: Singh, 2010)

Analysis of coal particle				
Sample	Proximate Analysis			
	Moisture content (wt%)	Volatile matter (wt%)	Ash content (wt%)	Fixed carbon content (wt%)
Umaria Coalfield (Sub-bituminous rank)	6.27	29.84	16.87	47.43
Properties of coal char particle				
Sample	Particle Size (mm)	Particle Density (kg/m3)	Bulk Density (kg/m3)	Porosity (%)
Coal char particle	10	1411	1051.9	25.45

4.2.1 Effect of steam concentration

The rate of steam gasification of coal char particle is proportional to the steam concentration. The carbon consumption rate inside the char particle increases with the steam concentration leading to the increase in carbon conversion inside the coal char particle in radial direction as shown in Figure 4.5. Since the rate of carbon consumption is proportional to the steam concentration, this cause the increase in the overall carbon conversion with the steam concentration. With increase in temperature, however, the consumption pattern of carbon changes drastically. As shown in Figure 4.6, virtually no conversion take place near the center of the particle indicating that all the steam entering the particle is consumed before it reaches up to the center.

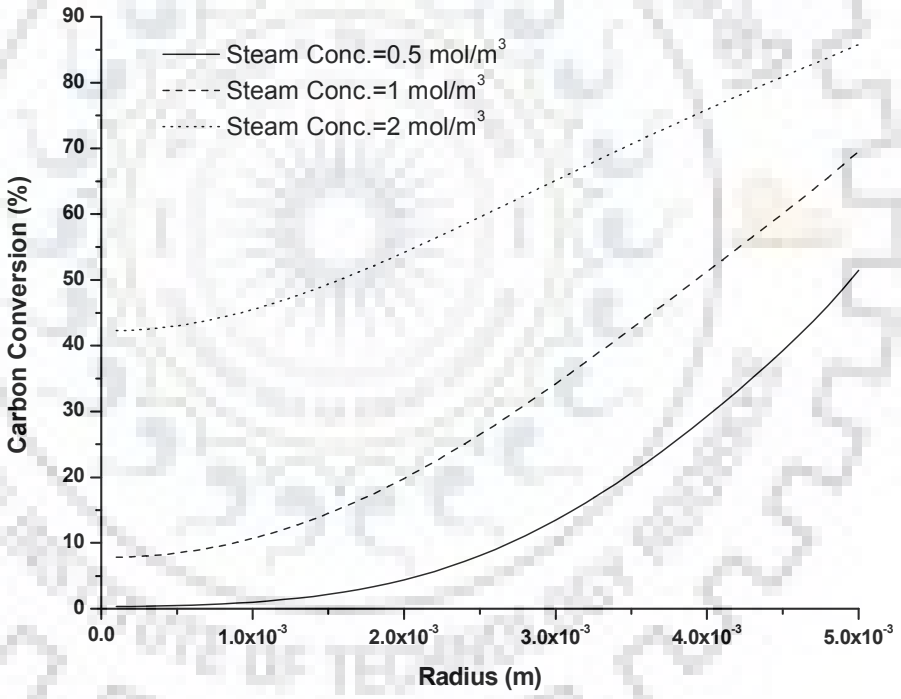

Figure 4.5: Carbon conversion profile in the char particle at 1100 K for different steam concentration

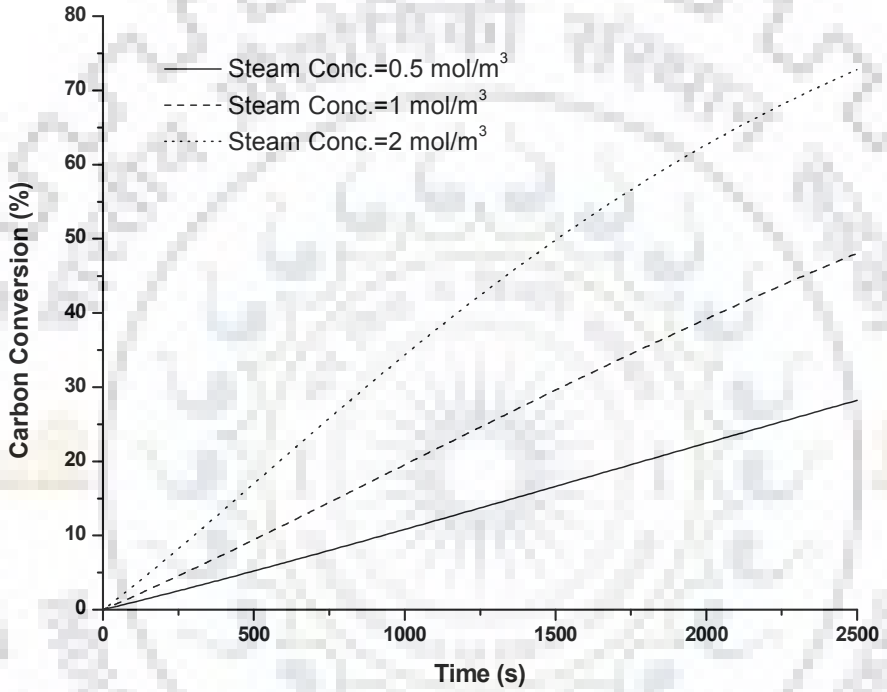

Figure 4.6: Carbon conversion with time for different steam concentration at 1100 K

Since the synthesis gas produced by coal gasification is an intermediate for feeding many different processes, its required composition, particularly H_2/CO ratios is significantly different. For example, in Fischer Tropsch synthesis applied to Gas-to-Liquid (GTL) applications, the required H_2/CO ratio is about 2.0 (mole/mole) and for aldehydes productions via hydroformylation, the required H_2/CO ratio is 1.0 (mole/mole). The ratio H_2/CO is also the key variable in the design of the synthesis gas plants. Similarly, the ratio of CO/CO_2 is used to measure the efficiency of the process and the extant of completion of the gasification reaction, therefore used to measure the effectiveness of the process.

The outward flux ratio of H_2/CO increases 1.6 folds (Figure 4.7) while the CO/CO_2 ratio decreases with increasing the steam concentration from 0.5 to 2 mol/m^3, as shown in Figure 4.8. In this figure, however, the initial variation is not clear seen; due to this, a logarithmic plot (x-axis) of the same data is shown in Figure 4.9. Evidently, a quick initial adjustment in the CO/CO_2 ratio is observed. Considering this, all subsequent graphs are presented on logarithmic time scale.

The overall flux of hydrogen, CO, and CO_2, is presented in Figure 4.10. to Figure 4.12, respectively. It is evident that there is about two folds increase in CO flux (Figure 4.11) whereas the corresponding increment in the fluxes of both H_2 and CO_2 is approximately 3 folds (Figure 4.10 and Figure 4.12, respectively) under same conditions. This is because of the fact that water gas reaction (R1) enhances production of H_2 and CO but CO is further consumes by the water gas shift reaction (R5) to produce CO_2 and H_2.

Since the Boudouard reaction (R3), which enhances production of CO, is favoured at higher temperature, the prevailing temperature (1100 K) appears to be not sufficiently high so that it can increase the production of CO leading to the decrease in the CO/CO_2 ratio with time. Hence for obtaining high yield of hydrogen, the steam concentration should be high.

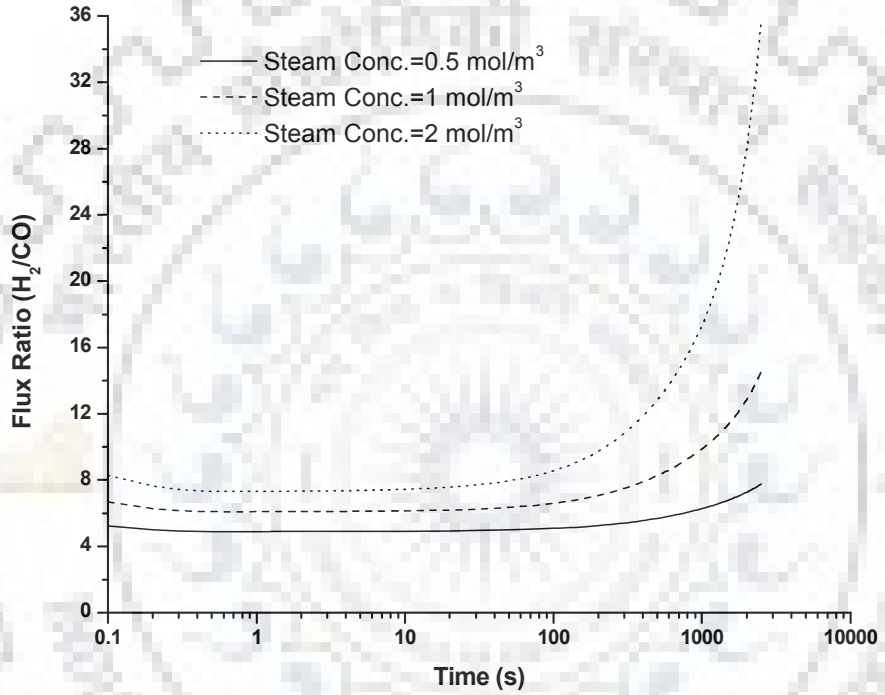

Figure 4.7: Flux ratio of H_2/CO for different steam concentration at 1100 K (logarithmic *x*-axis)

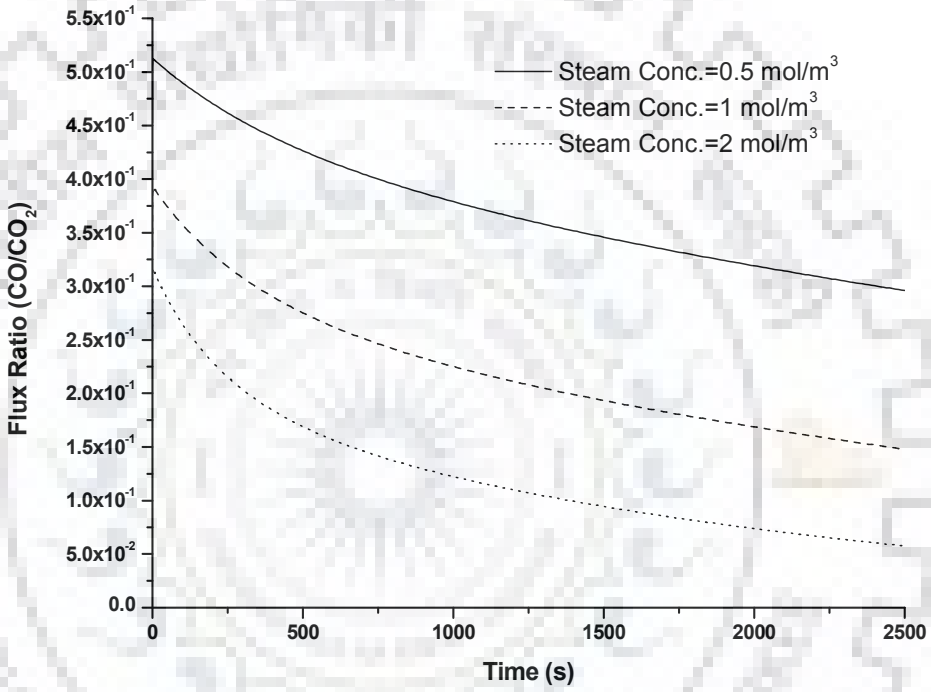

Figure 4.8: Flux ratio of CO/CO_2 for different steam concentration at 1100 K

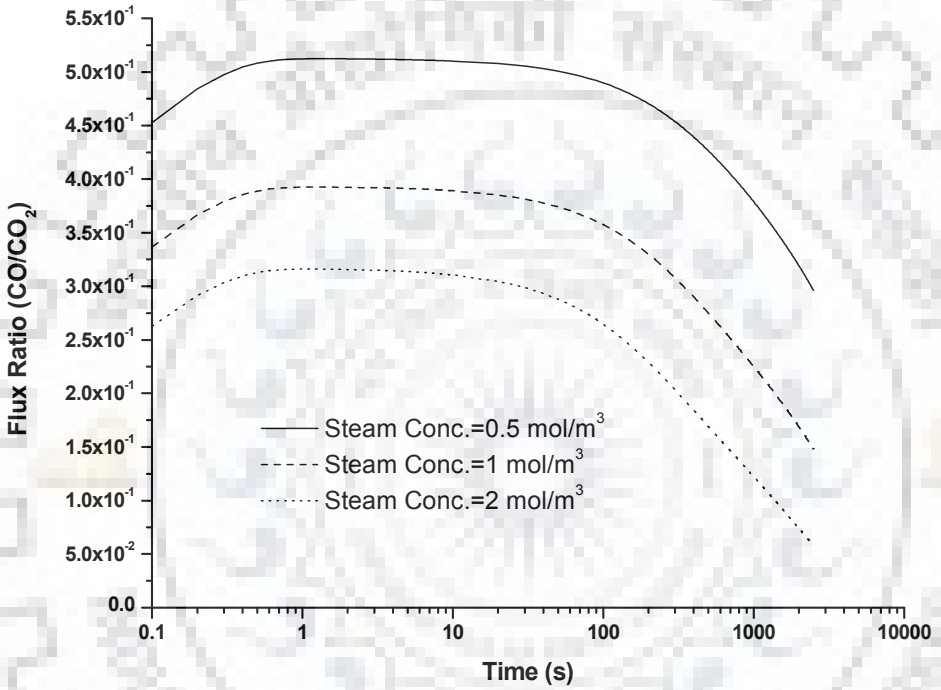

Figure 4.9: Flux ratio of CO/CO_2 for different steam concentration at 1100 K (logarithmic *x*-axis)

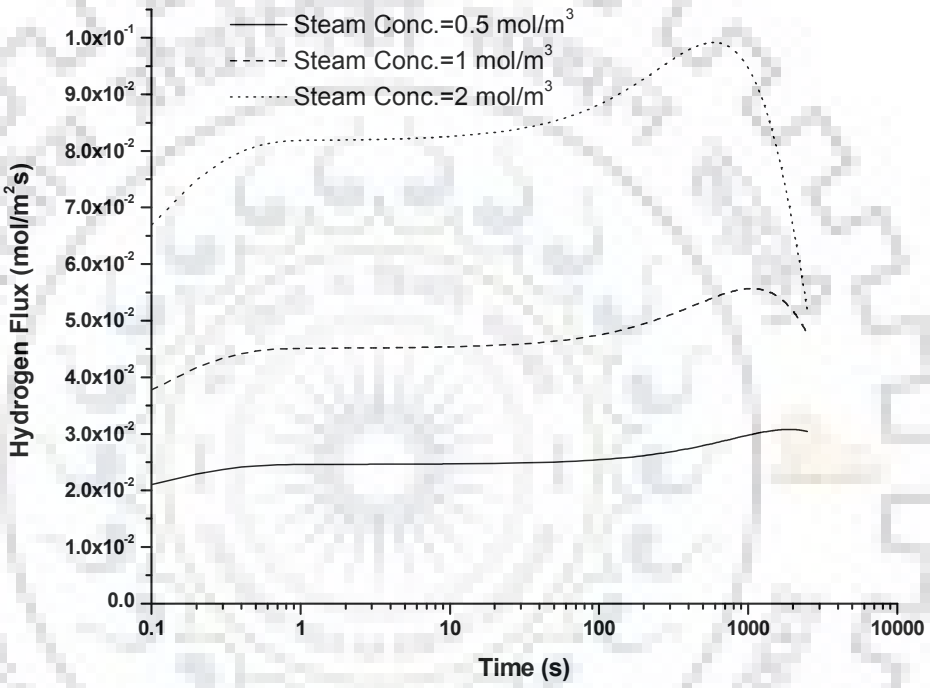

Figure 4.10: Hydrogen Flux from outer surface of char particle for different steam concentration at 1100 K (logarithmic *x*-axis)

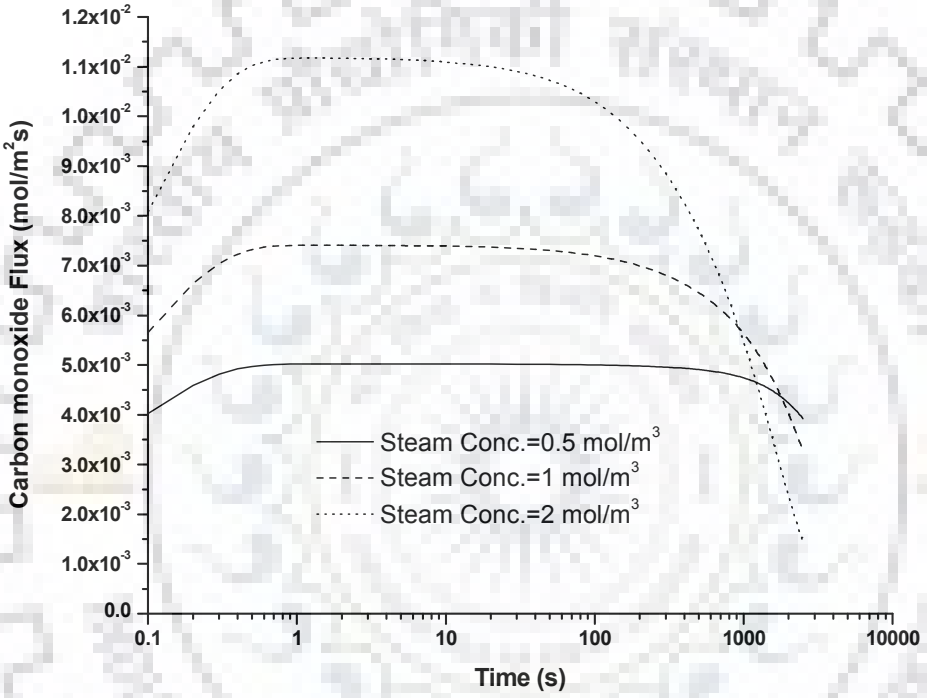

Figure 4.11: Carbon monoxide Flux from outer surface of char particle for different steam concentration at 1100 K (logarithmic *x*-axis)

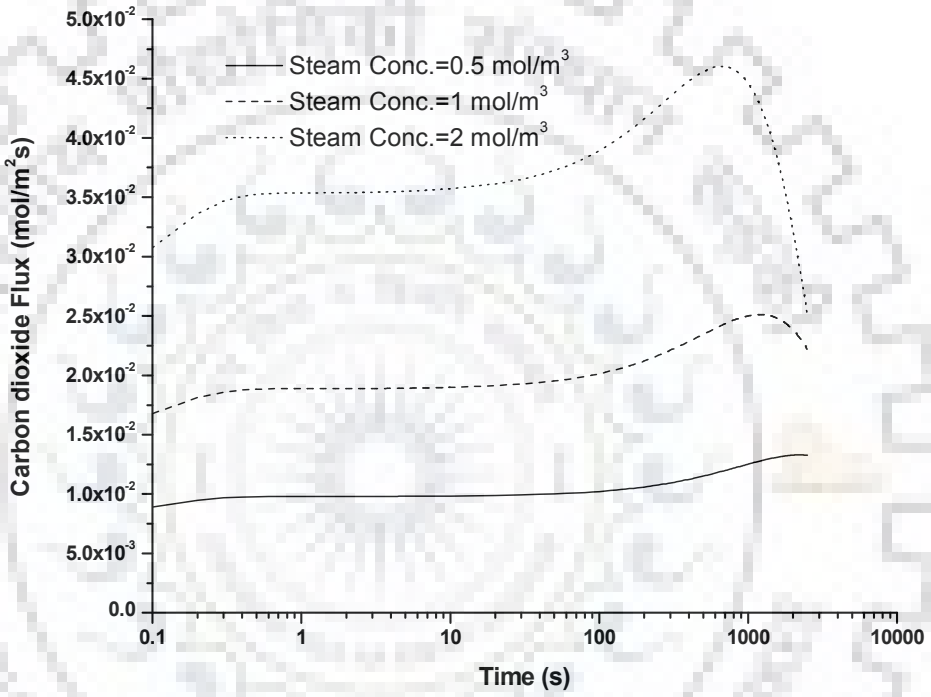

Figure 4.12: Carbon dioxide Flux from outer surface of char particle for different steam concentration at 1100 K (logarithmic *x*-axis)

4.2.2 Effect of temperature

The temperature is an operating parameter that directly affects the efficiency of the process. The rate constants are temperature dependent which changes the rate of reactions leading to the variation in the composition of the gaseous product. Since the main gasification reactions are strongly endothermic, therefore higher reaction temperature is expected to increase the reaction rate inside the char particle. Figure 4.13 and Figure 4.14 show, respectively, carbon concentration and conversion inside the particle for different time interval at constant temperature of 1000 K. The analysis for the effect of temperature is carried out at constant steam concentration of 1 mol/m^3 and other parameters are same as those shown in Table 4.2. The initial carbon concentration of the solid particle was 87.63 kmol/m^3. Evidently, carbon concentration begins to decline from very beginning (10 s) indicating that gasification take place everywhere inside the particle.

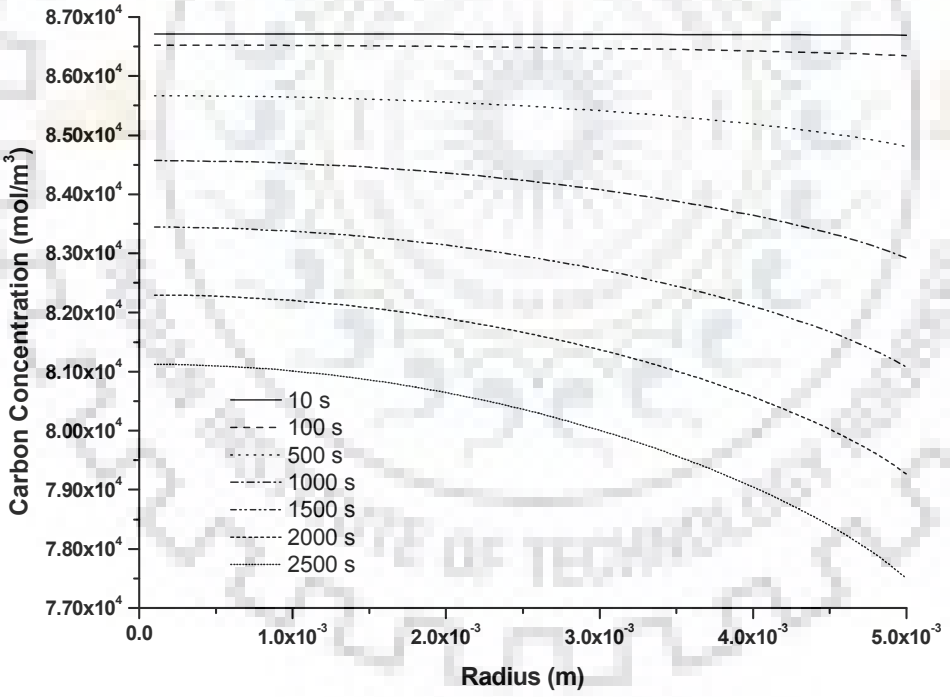

Figure 4.13: Carbon concentration profile in the char particle for different time interval at 1000 K

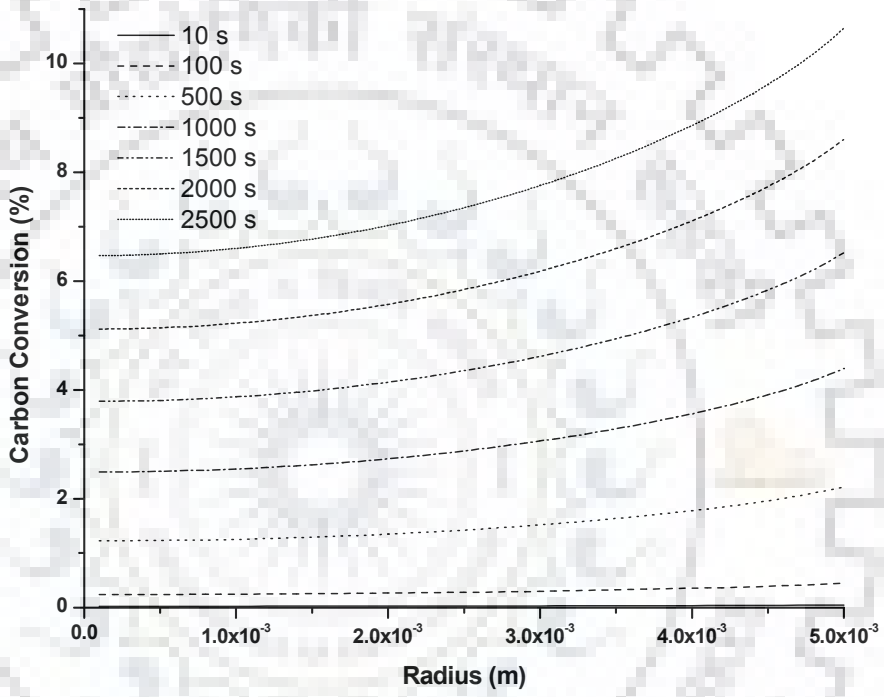

Figure 4.14: Carbon conversion profile in the char particle for different time interval at 1000 K

The other parameters remaining constant, when the temperature was increased from the lower (<1100 K) to the higher temperature (>1100 K), the carbon conversion becomes higher at the outer surface of char particle while towards the centre it is minimal. Since at lower temperature (1000 K), the reaction kinetic becomes the controlling step, the conversion follows the progressive reaction model leading to carbon conversion inside the coal char particle up to its center (Figure 4.15). On increasing the temperature from 1000 K to 1100 K, the carbon conversion near the centre begins to decline in comparison with the outer surface of char particle because of slowly shifting of progressive reaction model to shrinking core model, which can be clearly seen in Figure 4.15. At temperature 1200 K (Figure 4.16), the reaction tend to follow the shrinking core model where initially carbon conversion takes place at the outer surface of the char particle, without affecting the carbon conversion near the centre of particle till 2000 seconds that resembles shrinkage of unreacted core with a reaction front of about 3.5×10^{-3} m.

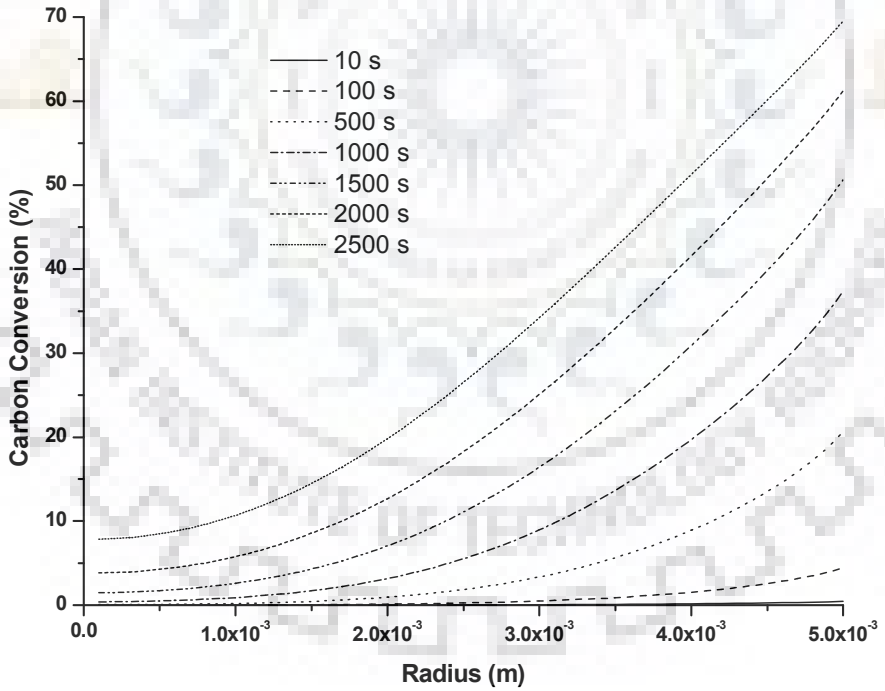

Figure 4.15: Carbon conversion profile in the char particle for different time interval at 1100 K

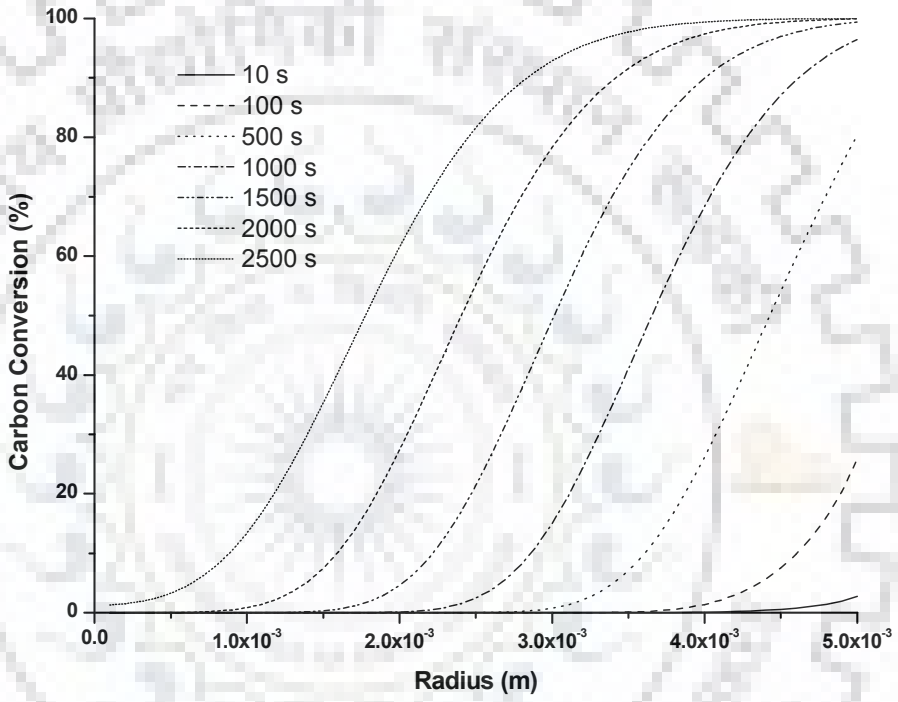

Figure 4.16: Carbon conversion profile in the char particle for different time interval at 1200 K

At still higher temperatures (Figures 4.17 and 4.18), diffusional resistances (pore diffusion) become more prominent showing more sharp reaction front of about $2.5x10^{-3}$ and $2.5x10^{-3}$ m at 1300 K and 1400 K, respectively. Also, higher temperature leads to the rate of shrinkage of unreacted carbon core in char particle to increase. Figure 4.19 shows the carbon conversion profile inside the char particle at different temperature after a constant time of 2500 seconds. At lower temperature (1000 K), the carbon conversion profile inside the char particle is nearly flat because of homogeneous conversion of carbon inside the particle. The rate of carbon conversion of char particle increases with the increase in temperature due to increase in the rate constant.

Figure 4.20 shows an asymptotic increase in conversion with time. This indicates that although at lower temperature homogeneous reaction takes place, but the rate of reaction is low. Therefore, the time duration for complete conversion shown in Figure 4.20 reduces considerably at higher temperature. At high value of rate constant, nature of the gasification process shift towards the diffusion controlled regime.

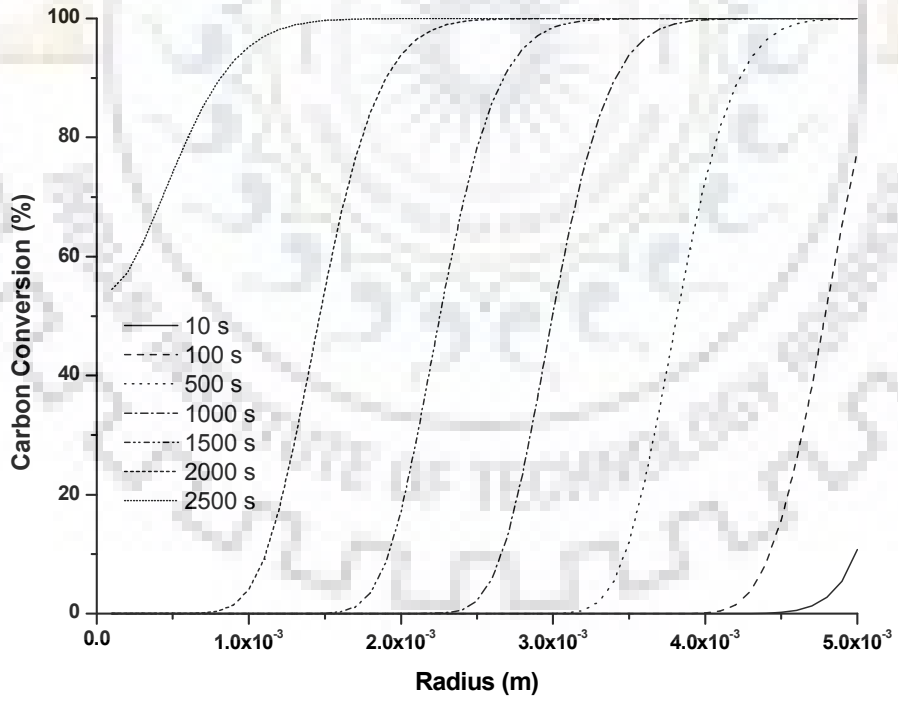

Figure 4.17: Carbon conversion profile in the char particle for different time interval at 1300 K

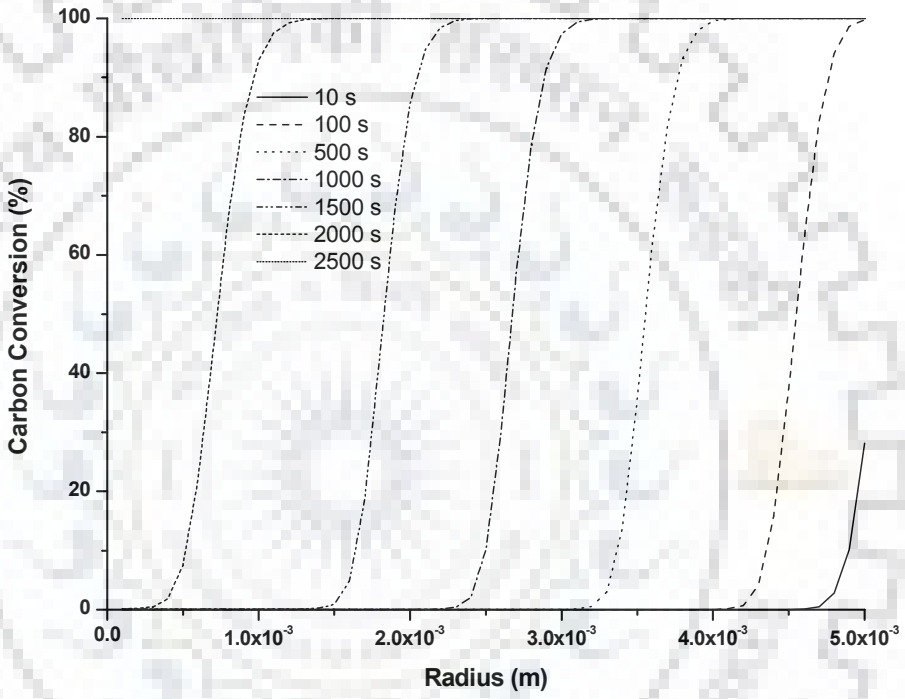

Figure 4.18: Carbon conversion profile in the char particle for different time interval at 1400 K

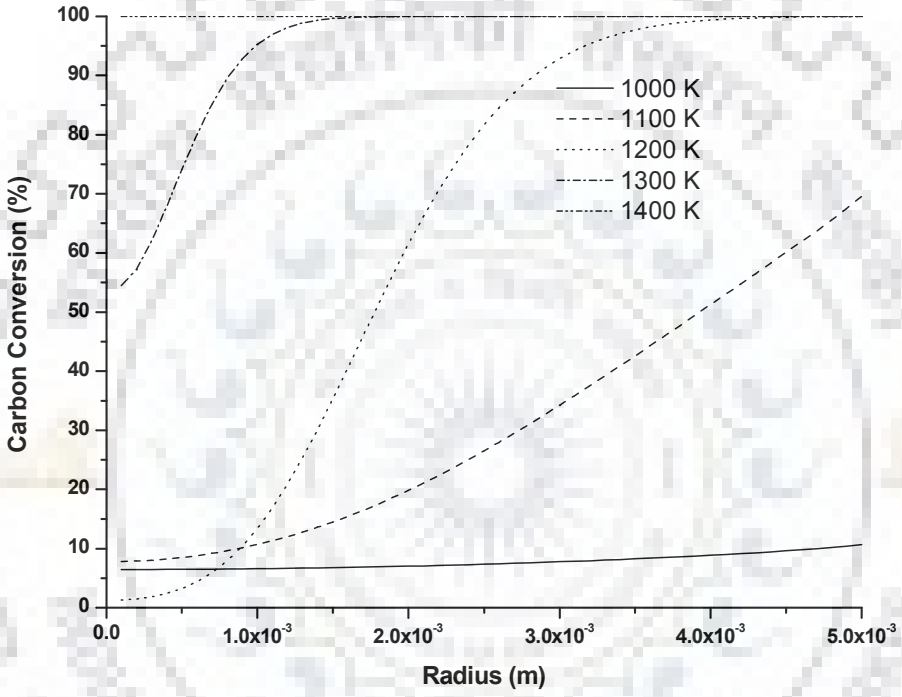

Figure 4.19: Carbon conversion profile in the char particle for different temperature after 2500 second

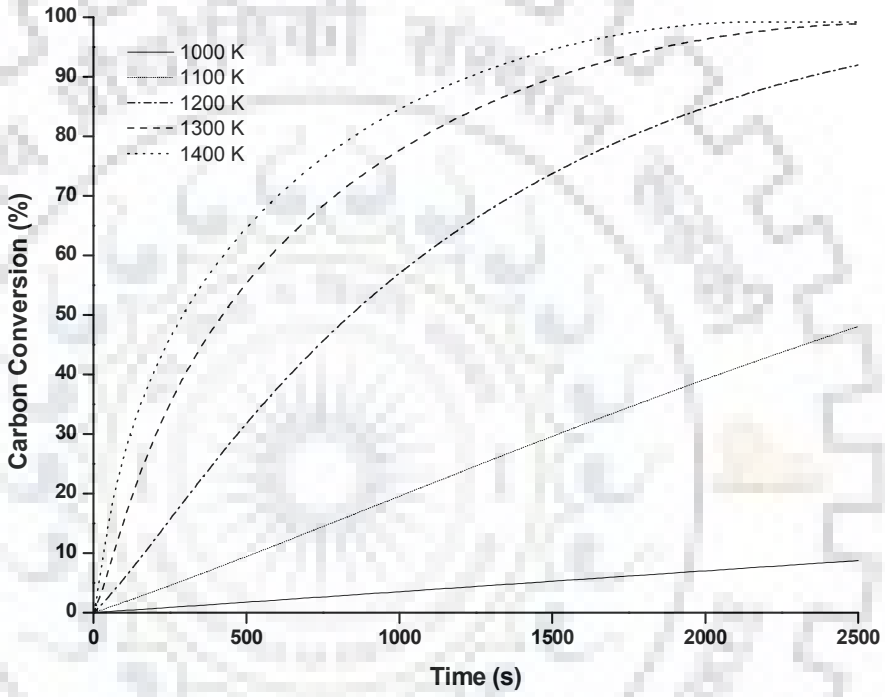

Figure 4.20: Carbon conversion with time for different temperature

The rate of consumption of carbon depends not only on the rate of approach of gasification agent but also on the concentration of products like hydrogen, carbon dioxide, and carbon monoxide. With the passage of time, carbon concentration profile, as well as, conversion profiles of various species within the particle changes that affects overall rate of production. Figures 4.21 to 4.26 compares variation in molar flux of H_2, CO, and CO_2 coming out of the particle with passage of time at different temperatures in the range from 1000 K to 1400 K with and without ash content, whereas effect of temperature on variation in fluxes of H_2, CO, CO_2 and CH_4 are presented in Figures 4.27 to 4.30.

When the reaction temperature is 1000 K, the reaction rates are slow and steam diffuses deep into the char particle and all the reactions continue throughout the particle. The steam gasification reaction (R1) produce sufficient amount of CO that further reacts with steam through water gas shift reaction (R5) to form CO_2 and H_2. Thus, although small in amount, but production of all the species continues for a longer period at almost the same rate (Figure 4.21).

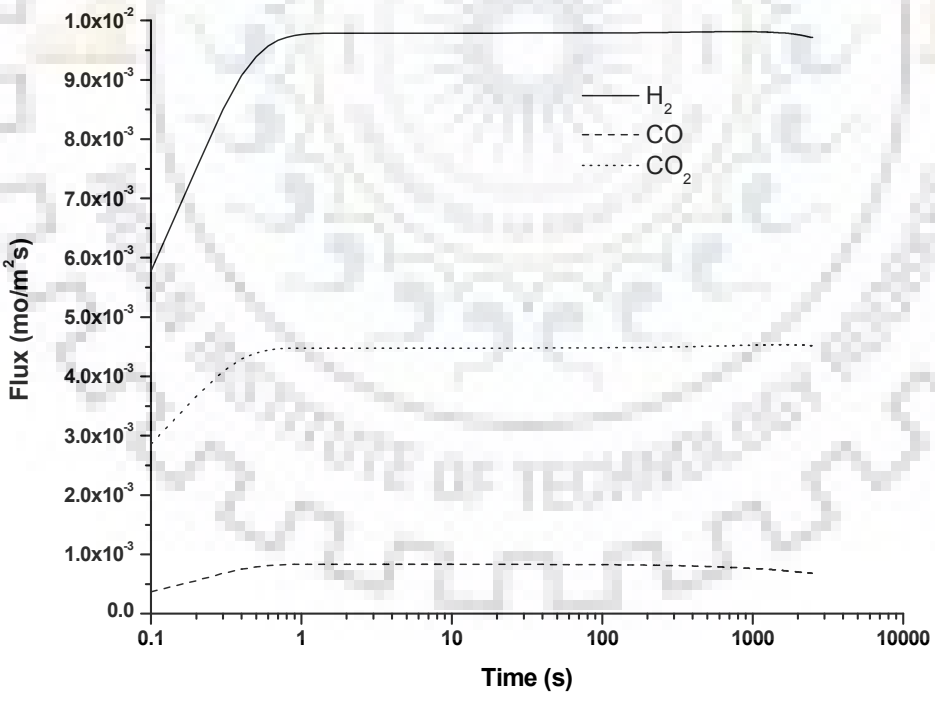

Figure 4.21: Flux of product gases from outer surface of char particle at 1000 K (logarithmic *x*-axis)

Further increasing the temperature to 1100 K (Figure 4.22), the rate of gasification reaction increases leading to the increase in molar flux of H_2, CO, and CO_2 from outer surface of char particle. It is also evident from this figure that after an initial adjustment period of about 100 seconds, rate of production of H_2 and that of CO decreases sharply.

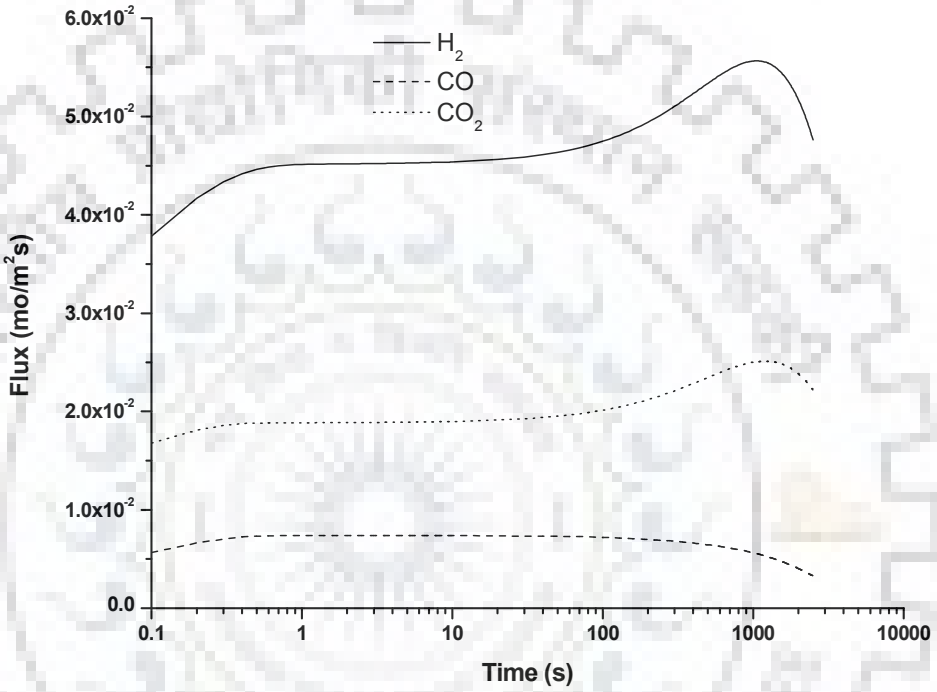

Figure 4.22: Flux of product gases from outer surface of char particle at 1100 K (logarithmic *x*-axis)

Upon further increase in reaction temperature to 1200 K (Figure 4.23) and 1300 K (Figure 4.24), the overall fluxes of all the species increases but the increase in CO production rate with increasing temperature is more prominent in the initial phase, i.e., <10 seconds (Figure 4.28) as compared to CO_2 (Figure 4.29) such that the initial rate of formation of CO and CO_2 in the product gas becomes narrower (Figure 4.23). This may be because of the Boudouard reaction (R3) which is favoured at high temperature producing more CO by consuming CO_2. However, with the passage of time, formation of CO decreases and that of the CO_2 increases to some extent, indicating significant conversion through water gas shift reaction (R5) at 1200 K. Upon further increase in temperature up to 1300 K, all the reactions become faster and rates of production of each species increases in the initial phase.

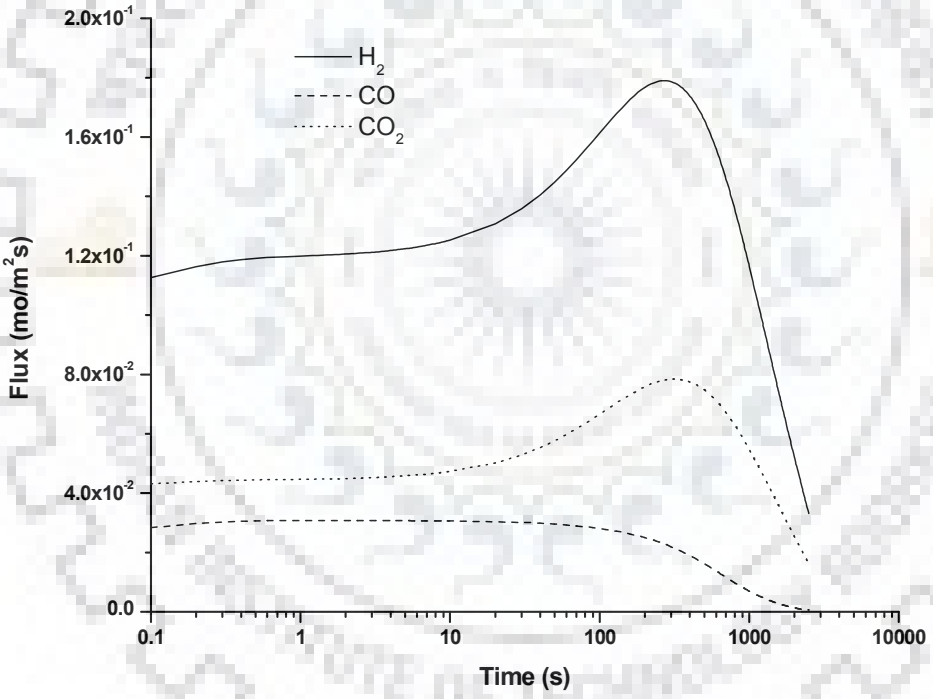

Figure 4.23: Flux of product gases from outer surface of char particle at 1200 K (logarithmic *x*-axis)

It is clear from Figure 4.24 and Figure 4.29 that molar flux of carbon monoxide start to decline from very beginning of the reaction (after 10 second and CO_2 flux increases up to 100 second (Figure 4.29) due to the water gas shift reaction, but after 100 second CO_2 flux declines because of the formation of ash layer on the outer surface leading to an increase in the diffusional resistance of char particle that reduces the rate of reaction. This is evident from the Figure 4.26 that if we considered the char particle without ash content, CO flux begins to decline along with the H_2 flux after 100 second.

At temperature of 1400 K (Figure 4.25), rate of production of CO is approximately three folds higher than the CO_2 production rate because of the Boudouard reaction (R3), and it continues to increase up to 15 seconds as compared to 10 seconds in case of 1300 K. After 15 second it begins to decline and H_2 and CO_2 flux increases up to 40 second due to water gas shift reaction (R5). Hence, removal of the ash layer from the particle surface at time interval of 100 second for low ash content char and 10 second for high ash content char (>25%) may give higher CO flux in the product gas composition.

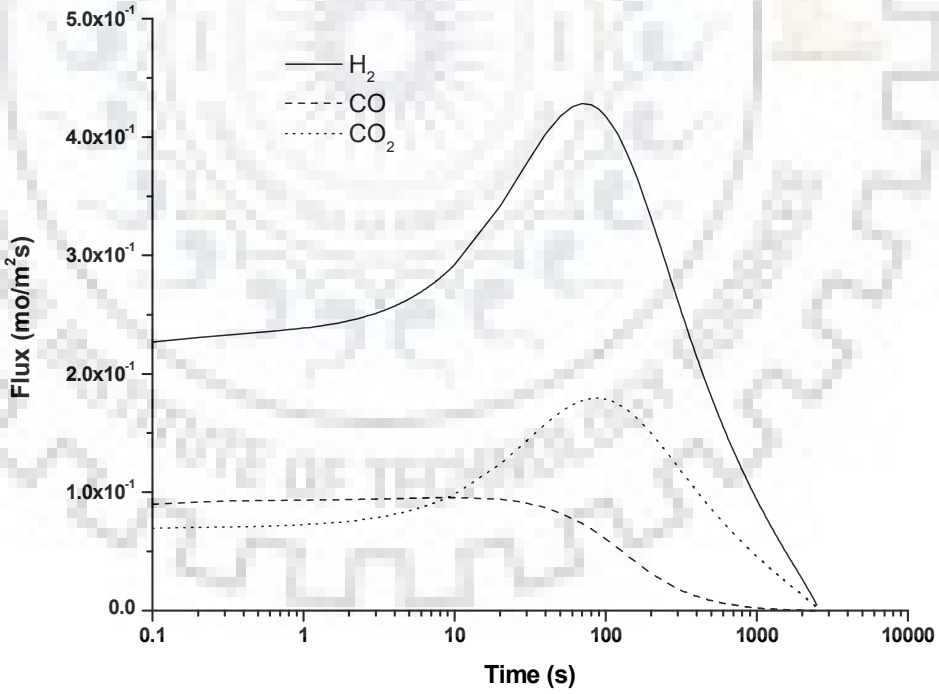

Figure 4.24: Flux of product gases from outer surface of char particle at 1300 K (logarithmic *x*-axis)

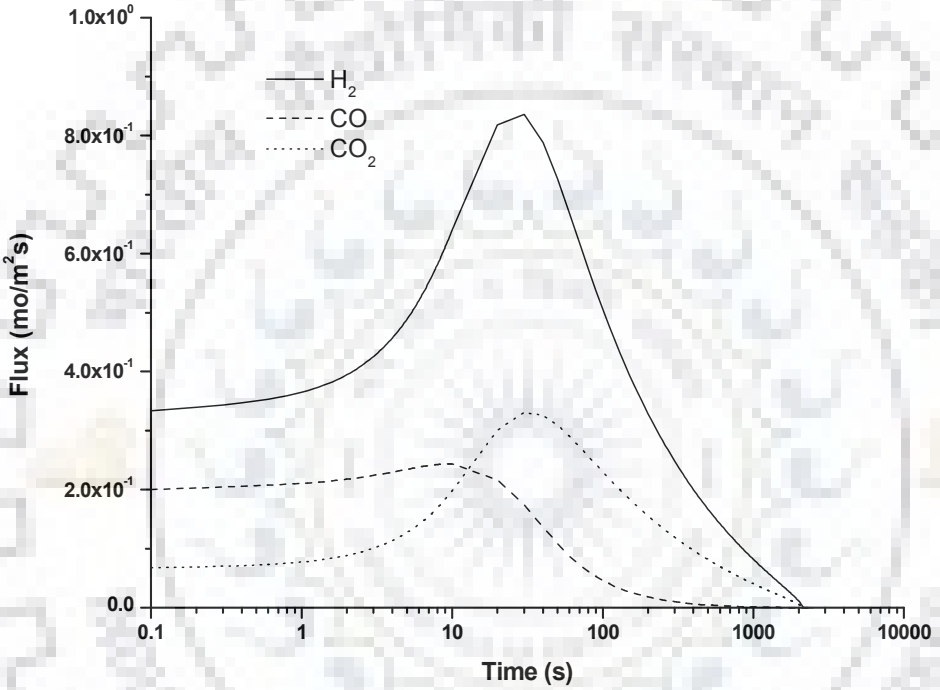

Figure 4.25: Flux of product gases from outer surface of char particle at 1400 K (logarithmic *x*-axis)

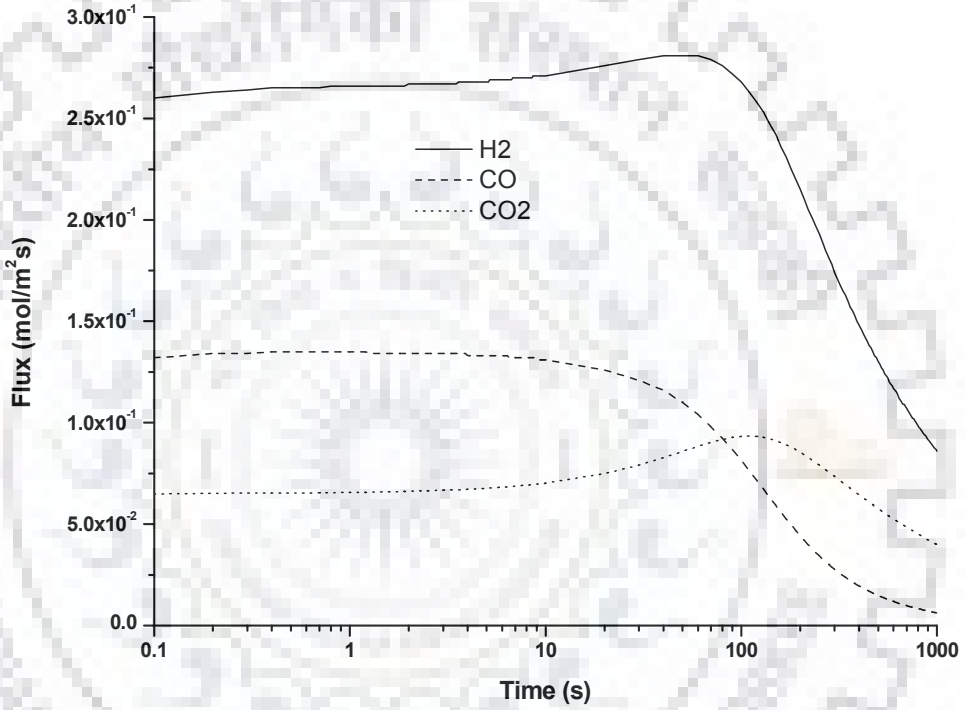

Figure 4.26: Flux of product gases from outer surface of char particle (no ash content) at 1300 K (logarithmic *x*-axis)

The rate of production of all gases (H_2, CO, CO_2, and CH_4) increases with increasing temperature because the main reactions are endothermic. The H_2 flux from the outer surface of char particle (Figure 4.27) is less temperature sensitive than that of the CO flux (Figure 4.28) because of Boudouard reaction is more favourable at higher temperature range leading to decrease in the CO_2 flux after a temperature of 1300 K shown in Figure 4.29. The rate of production of CH_4 is negligibly small in the temperature range from 1000 K to 1400 K shown in Figure 4.30; therefore analysis of CH_4 production is omitted in further study. Above discussed results indicate that for obtaining high yield of H_2 and CO in the product gases, the temperature should be kept high.

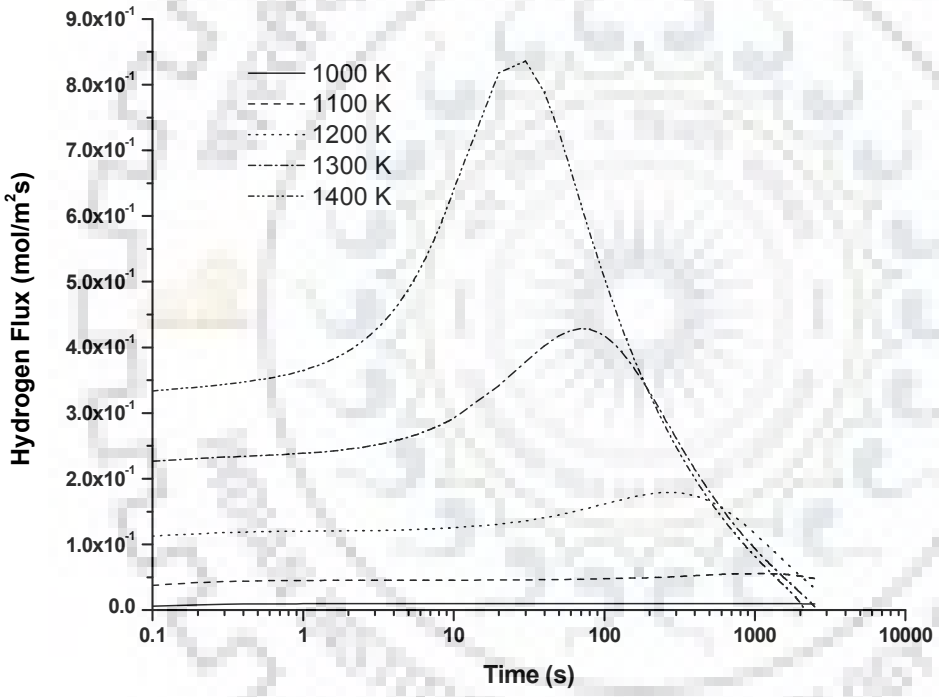

Figure 4.27: Hydrogen Flux from outer surface of char particle for different temperature after 2500 second (logarithmic *x*-axis)

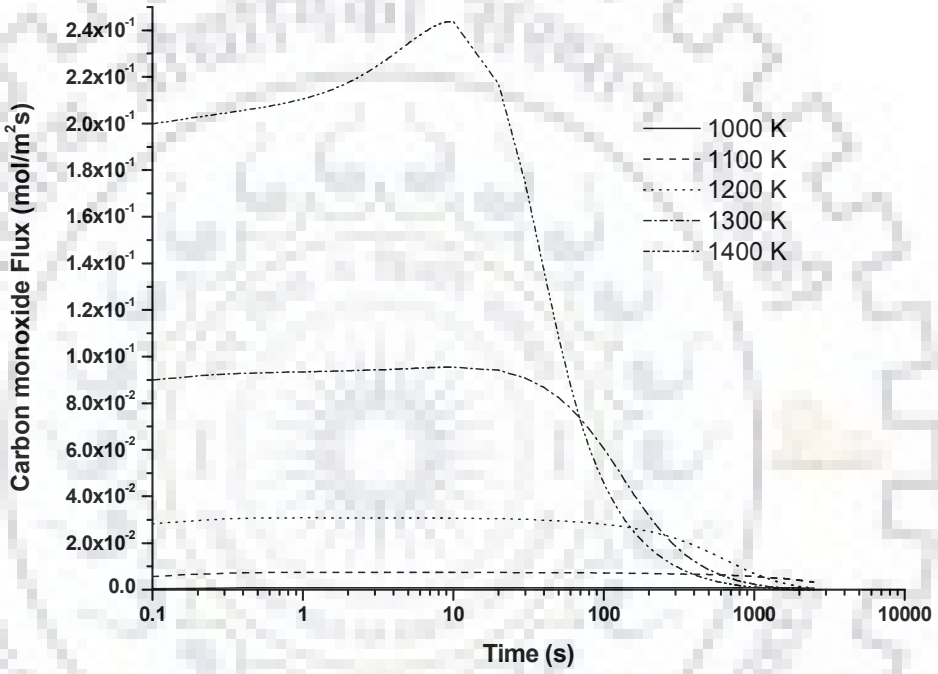

Figure 4.28: Carbon monoxide Flux from outer surface of char particle for different temperature after 2500 second (logarithmic *x*-axis)

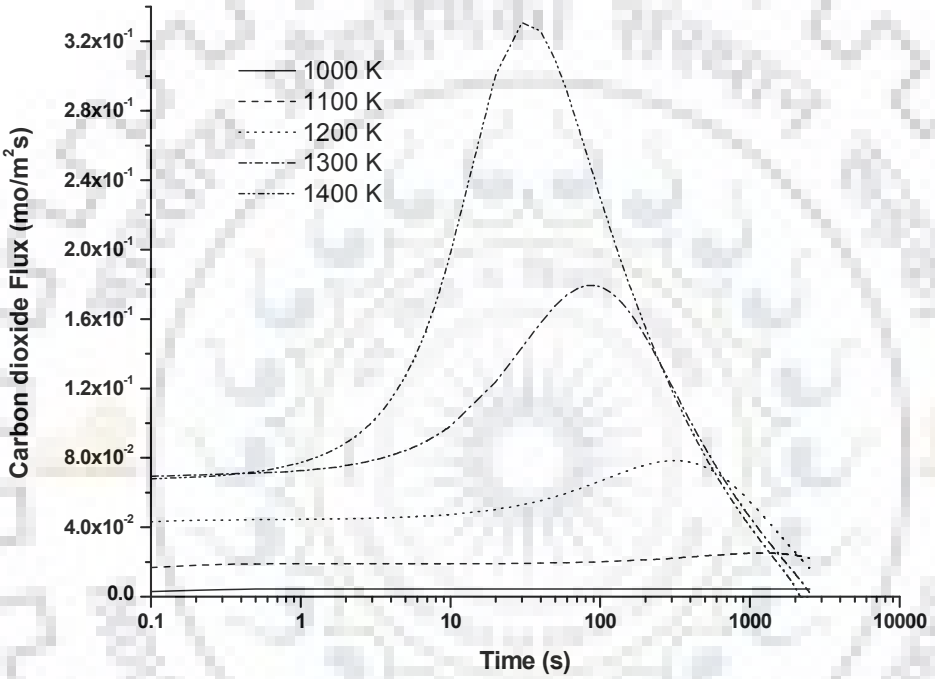

Figure 4.29: Carbon dioxide Flux from outer surface of char particle for different temperature after 2500 second (logarithmic *x*-axis)

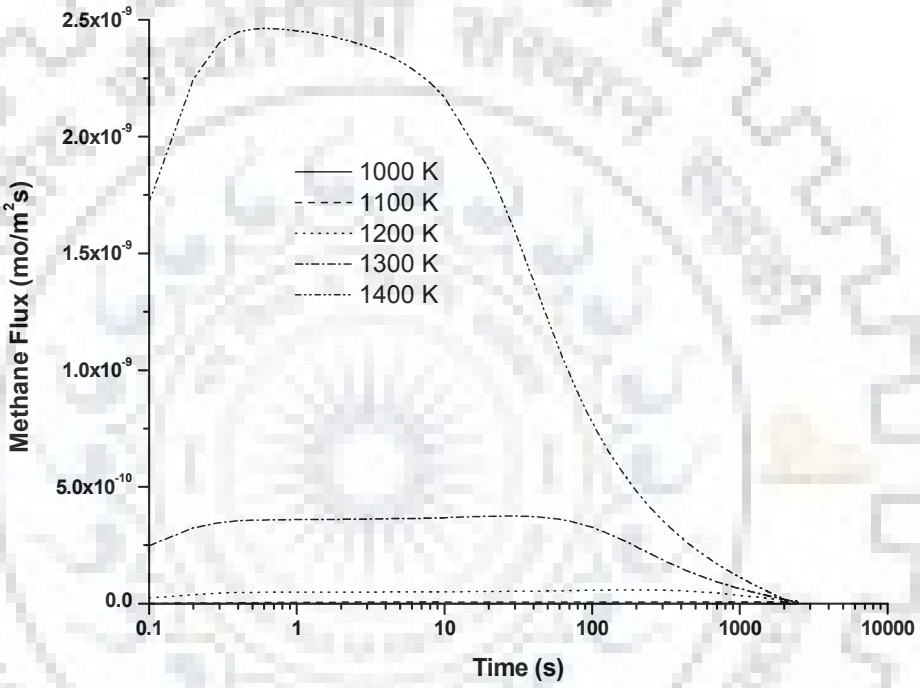

Figure 4.30: Methane Flux from outer surface of char particle for different temperature after 2500 second (logarithmic *x*-axis)

4.2.3 Effect of carbon concentration in char

Carbon concentration directly affects the rate of gasification of the char particle. Apparently, a higher carbon concentration should lead to higher conversion, however, the simulation results reveal that if the parameters like size, density, and porosity of the particle remain unchanged, the rate of percent conversion is high for low char concentration but low at high char concentration (Figure 4.31). To understand this phenomenon, cumulative local carbon consumption (up to 1000 seconds) is also plotted in the same figure.

Clearly, the consumption near the particle surface is more for charcoal with higher carbon concentration. But, near the center, carbon consumption is high when its concentration is low. This is because of the fact that keeping density constant, reduction in carbon concentration ultimately leads to increase in the diffusivity of gasifying agent. Therefore availability of gasifying agent in the core region is more when carbon concentration is less. The analysis for this section was carried out at constant particle size (10 mm), steam concentration (1 mol/m^3), char particle porosity (20 %), and temperature (1000 K).

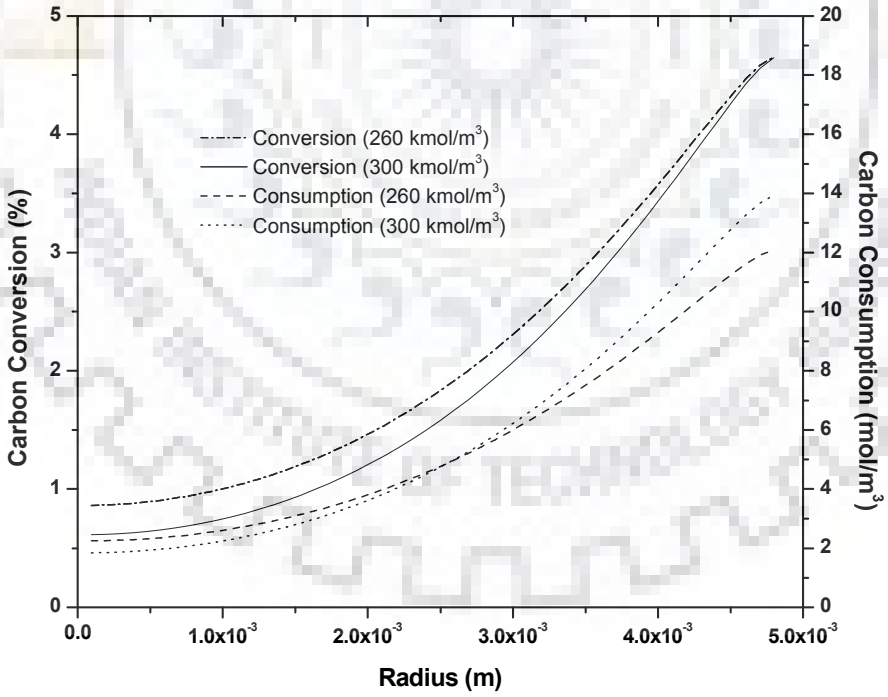

Figure 4.31: Effect of carbon concentration on the conversion of char at 1000 K after 1000 Second

4.2.4 Effect of size of char particle

The selection of particle size for gasification depends on the gasifier types and also composition of constituent in the char particle including moisture, volatile matter, and ash. Different sizes of char particles show different characteristics during the gasification reaction because of different reactivity of the char particle. The difference in the reactivity of char particle is due to the change in the surface area with the size of the char particle. The particle sizes used for this analysis are 5, 7.5, and10 mm at the reaction temperature of 1100 K with steam concentration of 1 mol/m^3. The overall rate of conversion increases with a decrease in the particle size (Figure 4.32) because of lower initial mass and increase in specific surface area of char particle.

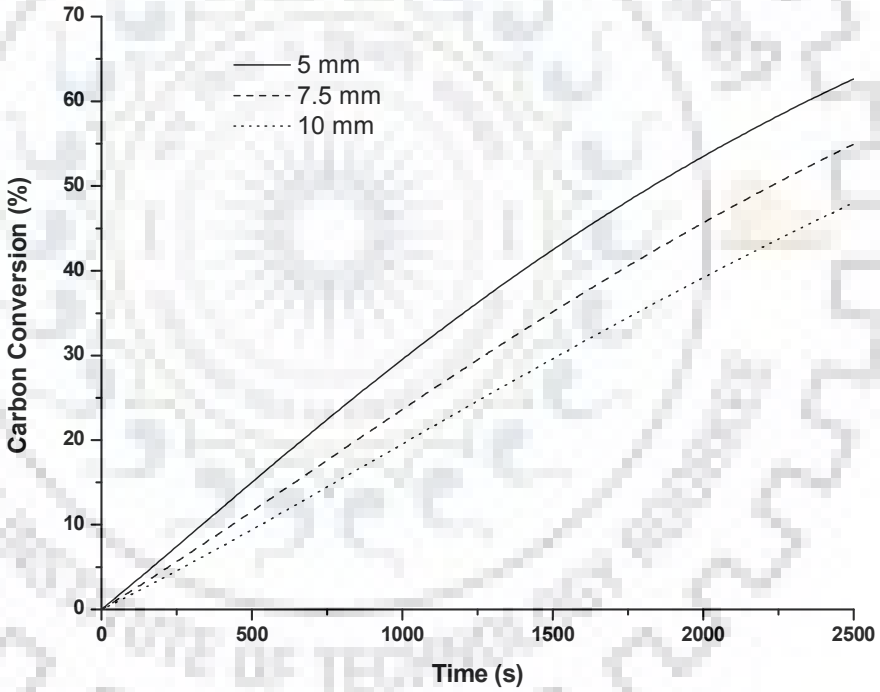

Figure 4.32: Carbon conversion with time for different particle size at 1100 K

Also, in a smaller particle, the steam diffuses deep in the char particle and reactions continue throughout the particle following the progressive reaction model even at relatively higher temperature. In the case of large particle, however, reactions take place at the outer surface of the particle and steam does not reach deep into the particle follow the shrinking core model. Hence in the smaller char particle kinetics controlled reaction prevails while in the larger char particle diffusional effects (pore diffusion) become controlling step. On the other hand, larger char particles give higher production rates of H_2, CO, and CO_2 than the small size char particle. For increase in the char particle sizes from 5 mm to 10 mm, initially H_2 production rate increases 3.5 folds (Figure 4.33), CO production rate enhances approximately 5 folds (Figure 4.34), and CO_2 production rate is enhanced 4 times (Figure 4.35). The H_2, CO, CO_2 production rates begins to decline sharply for larger char particle after 1000 second because of decrease in the available specific surface area for reaction due to the ash formation on the surface leading to decrease in the reaction rates.

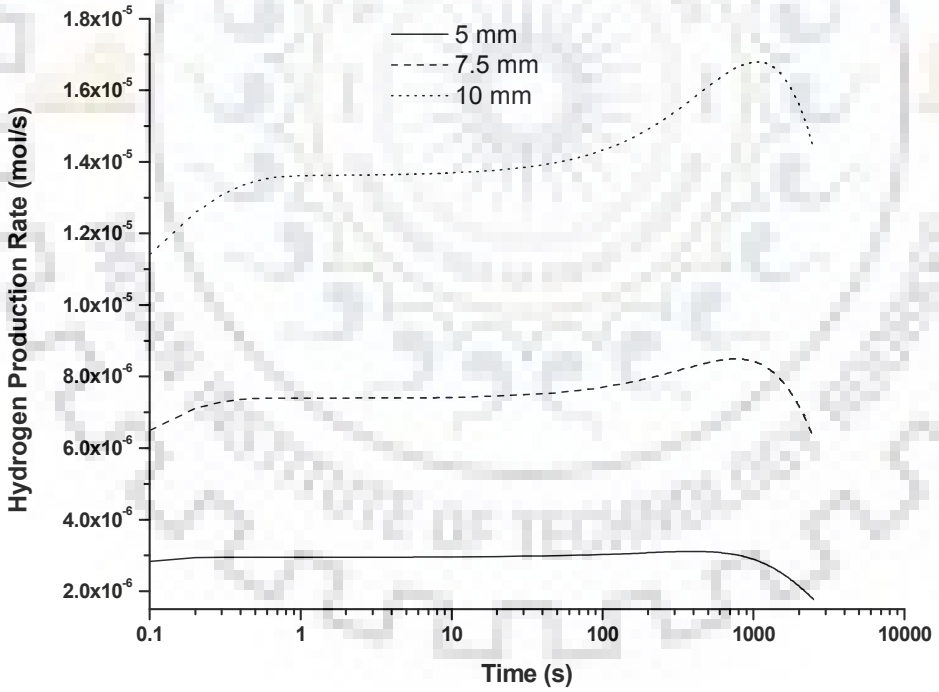

Figure 4.33: Hydrogen production rate from the outer surface of char particle for different particle size at 1100 K (logarithmic *x*-axis)

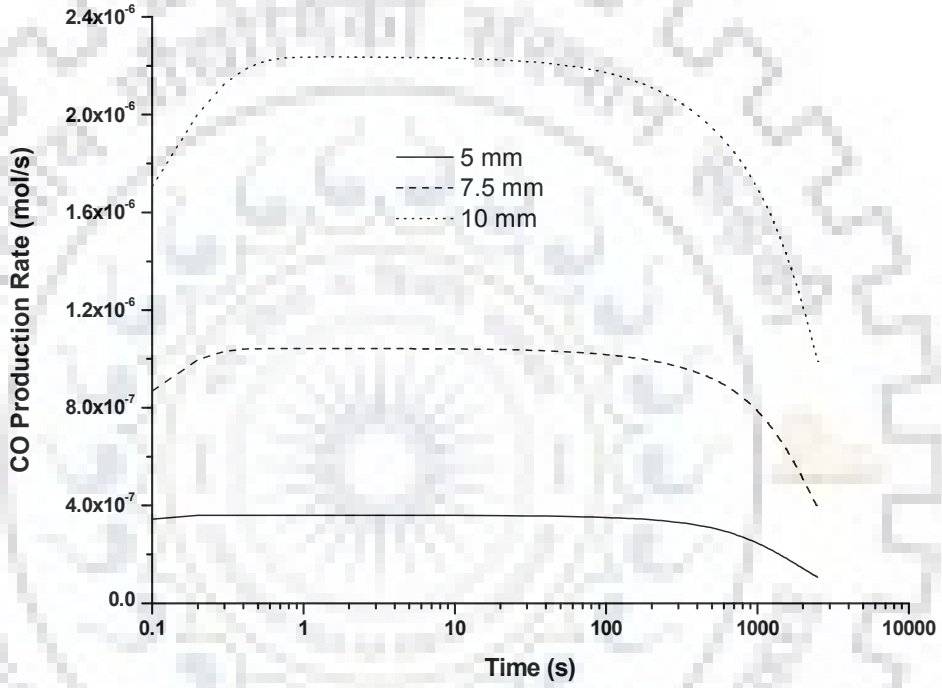

Figure 4.34: CO production rate from the outer surface of char particle for different particle size at 1100 K (logarithmic *x*-axis)

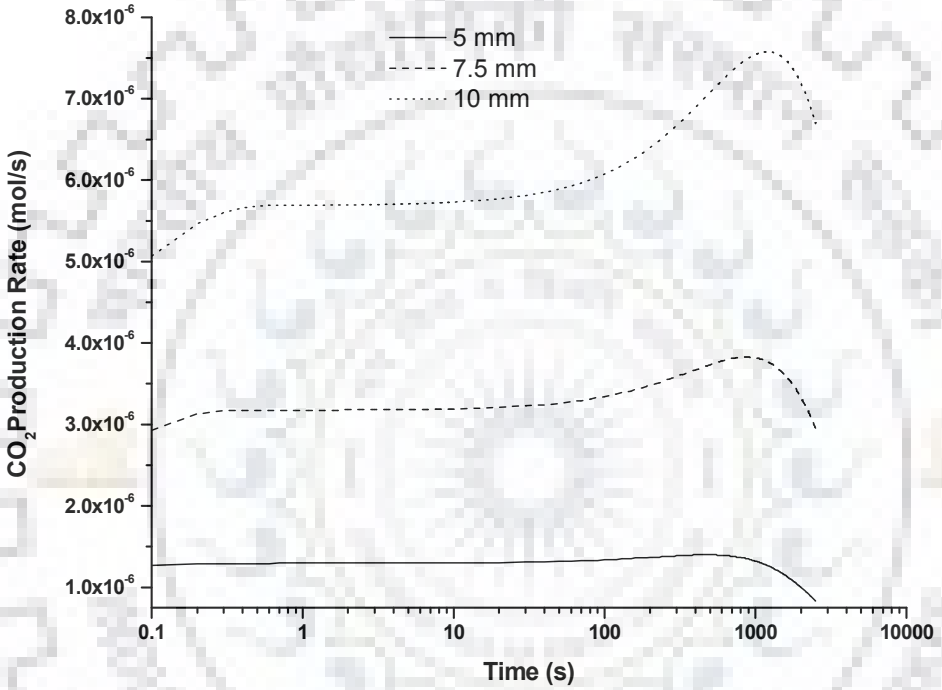

Figure 4.35: CO_2 production rate from the outer surface of char particle for different particle size at 1100 K (logarithmic *x*-axis)

Due to 5 fold increase in CO production rates while the H_2 production rates increases only approximately 4 times with the increase in particle size from 5 mm to 10 mm, the flux ratio of H_2/CO decreases with increase in the particle size (Figure 4.36). Similarly the flux ratio of CO/CO_2 enhances with the particle sizes (Figure 4.37) because of steeper increase in the CO production rate as compared to CO_2 production rates for increase in char particle sizes.

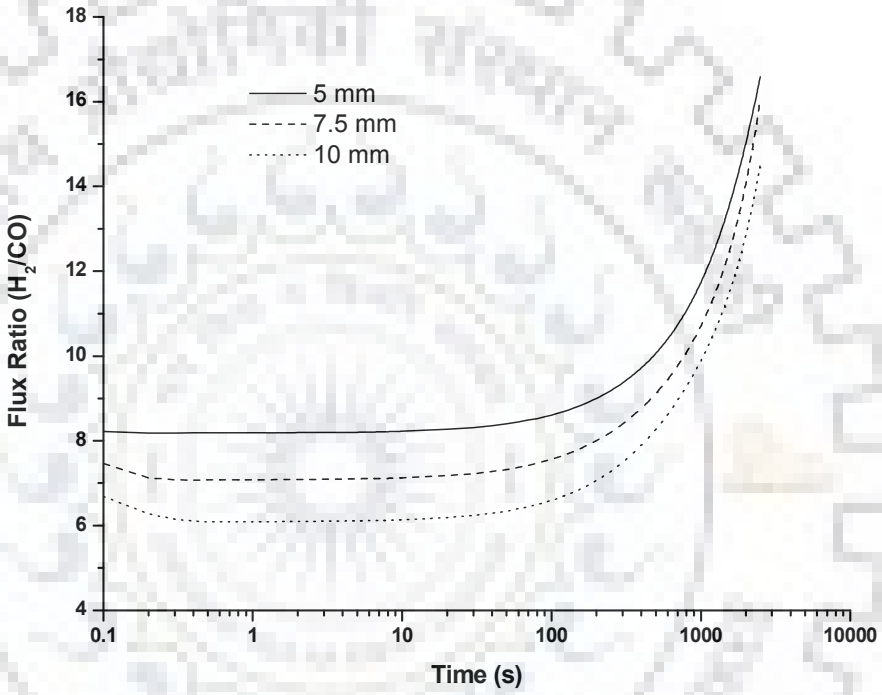

Figure 4.36: Flux ratio of H_2/CO for different particle size at 1100 K (logarithmic *x*-axis)

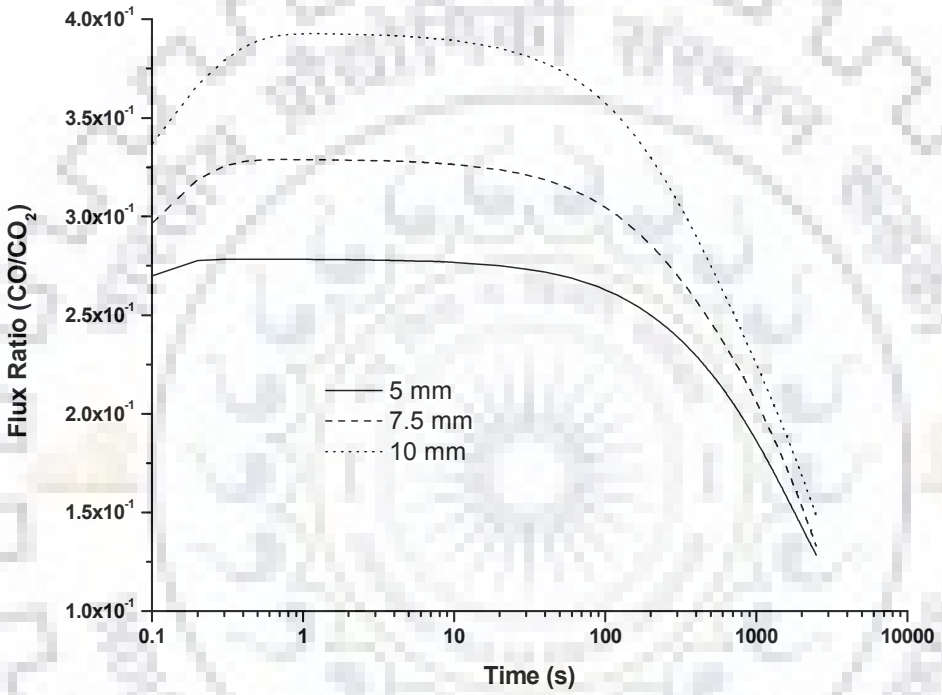

Figure 4.37: Flux ratio of CO/CO_2 for different steam concentration at 1100 K (logarithmic *x*-axis)

4.2.5 Effect of initial porosity of char particle

The porosity and the pore size distribution influence reaction and diffusion rates during the course of gasification of coal char particle. The carbon conversion in the char particle affects the formation of new pore during gasification which changes the porosity of the char particle leading to change in the diffusion rates. In this section, results with the initial porosities of 0.2545, 0.4, and 0.5 at constant temperature of 1100 K and char particle of 10 mm are discussed. The initial porosity of char particle affects the total conversion only in the initial phase of gasification, in the other words, the time required to reaches complete conversion is almost the same for all initial porosity values.

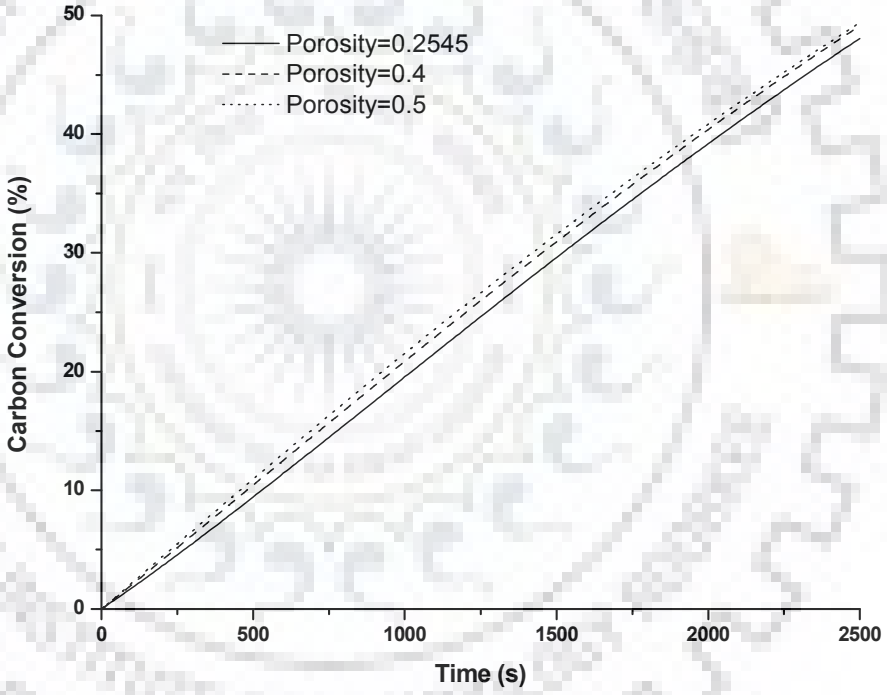

Figure 4.38: Carbon Conversion with time for different initial porosity of char particle at 1100 K

The variation of initial porosity is more prominent towards the low porosity range. For higher initial porosity, curves between total conversion and time get closer to each other (Figure 4.38). This is because of diffusional resistance (pore diffusion) becomes rate controlling step and Knudson diffusivity becomes less prominent at higher porosity.

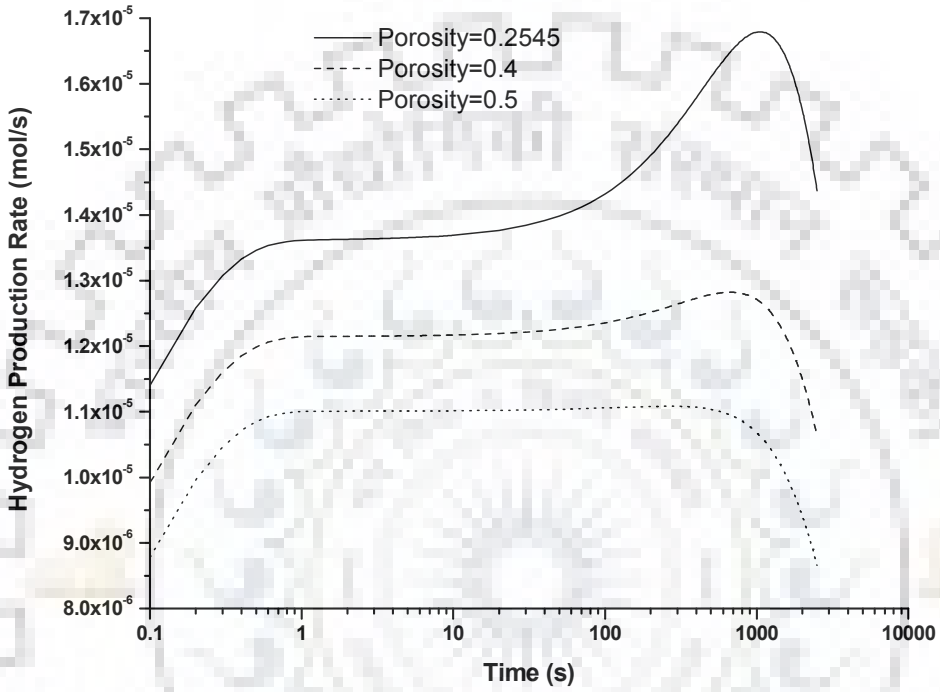

Figure 4.39: Hydrogen production rate from the outer surface of char particle for different porosity at 1100 K (logarithmic *x*-axis)

Nature of the curves for overall fluxes of H_2, CO, and CO_2 are similar to those obtained for the analysis of the effects of particle size, however, in this case there is a decrease in production with increase in porosity. For lower initial porosity of char particle, surface reaction takes place with more amount of carbon available for reaction leading to the higher production rate of H_2, CO, and CO_2 as compared to the higher initial porosity. The production rate of H_2 increases nearly 1.3 folds (Figure 4.39), CO approximately 1.6 folds (Figure 4.40) and increase in CO_2 production rate is close to 1.25 folds (Figure 4.41) with a decrease in initial porosity from 0.5 to 0.25. The production rates of all the components (H_2, CO, and CO_2) begin to decline sharply after 1000 seconds.

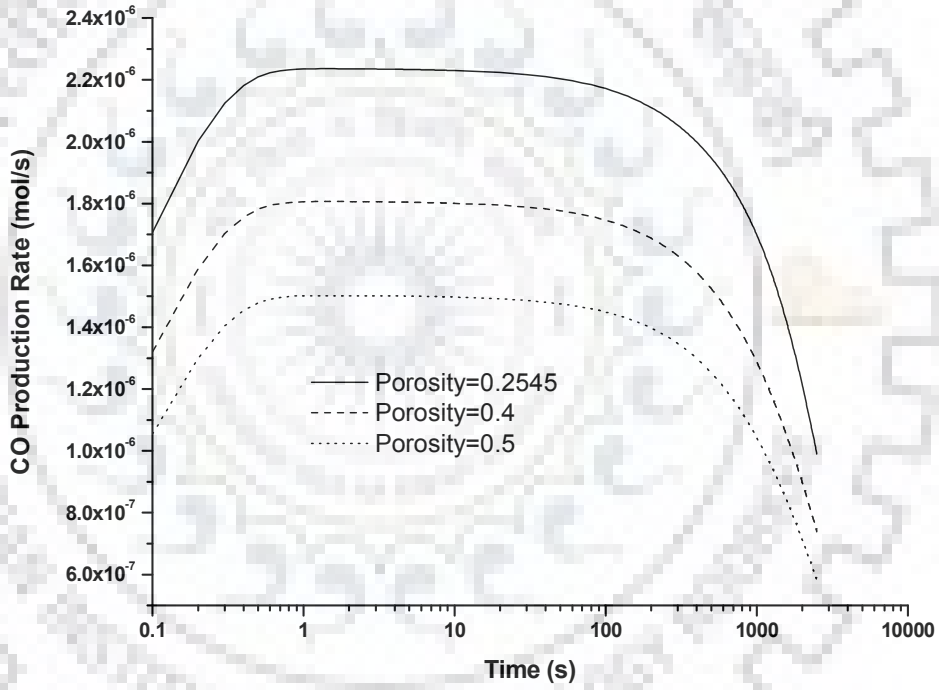

Figure 4.40: CO production rate from the outer surface of char particle for different porosity at 1100 K (logarithmic *x*-axis)

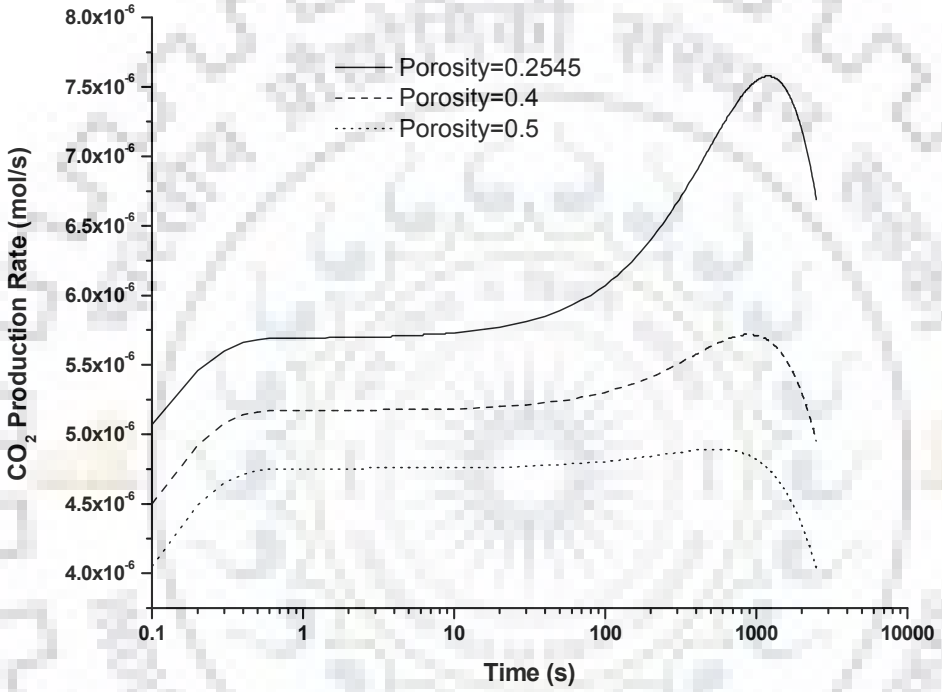

Figure 4.41: CO_2 production rate from the outer surface of char particle for different porosity at 1100 K (logarithmic *x*-axis)

Since increase in CO production rate is nearly 1.6 folds while the increase in H_2 production rate is approximately 1.3 folds and that of CO_2 is close to 1.25 folds with the decrease in initial porosity of char particle from 0.5 to 0.25, the flux ratio of H_2/CO increases (Figure 4.42) but flux ratio of CO/CO_2 decreases (Figure 4.43) with increase in initial porosity of char particle. Due to nearly same time requirement for complete conversion of char particle of different initial porosity, the flux ratios of H_2/CO and CO/CO_2 remains the same for all initial porosity of char particle after a certain period of time (≈2500 s).

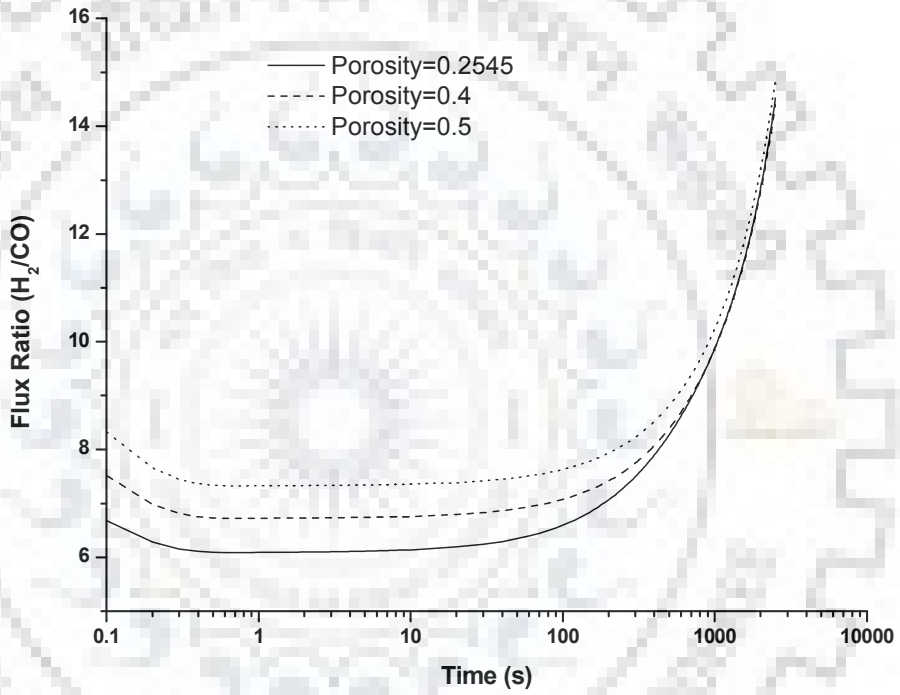

Figure 4.42: Flux ratio of H_2/CO for different initial porosity of char particle at 1100 K (logarithmic *x*-axis)

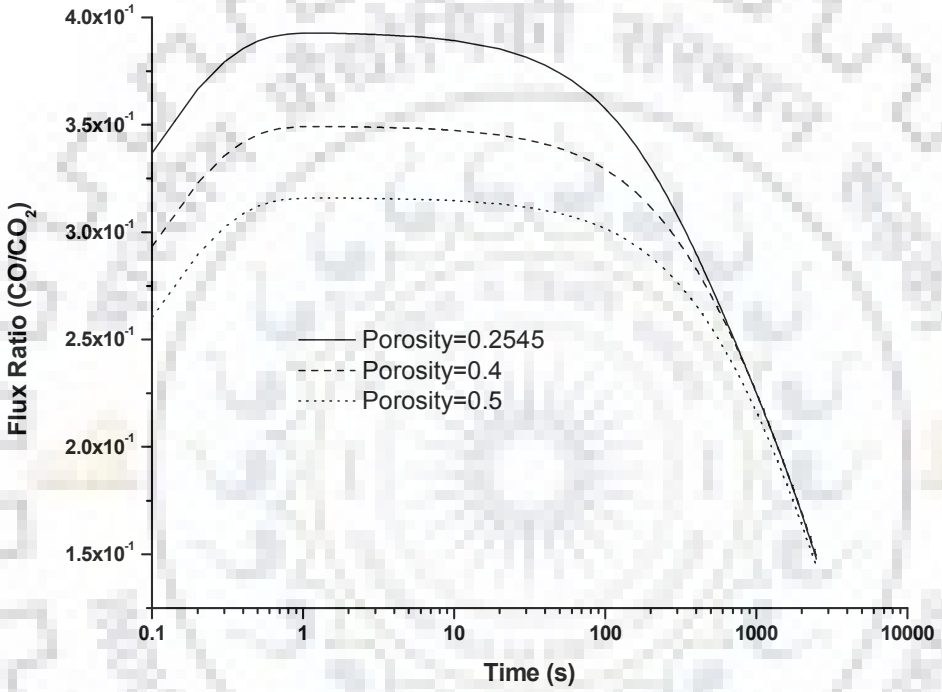

Figure 4.43: Flux ratio of CO/CO_2 for different initial porosity of char particle at 1100 K (logarithmic *x*-axis)

4.2.6 Effect of ash content in the char

Since the reactivity data of coal char particle with high ash content is limited, the study on the effect of ash content in the coal char particle on the gasification is important for the design of a gasifier to use high ash content coal char. Because of this, in the present work, the effect of ash content on the conversion rate and overall rate of generation of gaseous components from the outer surface of the coal char particle are also included. For this analysis, the ash content in the char particle are taken as 26.4%, 40%, and 50% and other parameter like temperature (1100 K), particle size (10 mm), and steam concentration (1 mol/m^3) are kept constant. The carbon conversion near the surface of the particle for different ash content in the char particle is nearly same whereas towards the centre of the char particle, because of the available specific surface area for the gasification reactions, conversion is significantly high (Figure 4.44). The study also reveals that although product yield decline but the overall carbon conversion of high ash content coal char is higher than lower one (Figure 4.45).

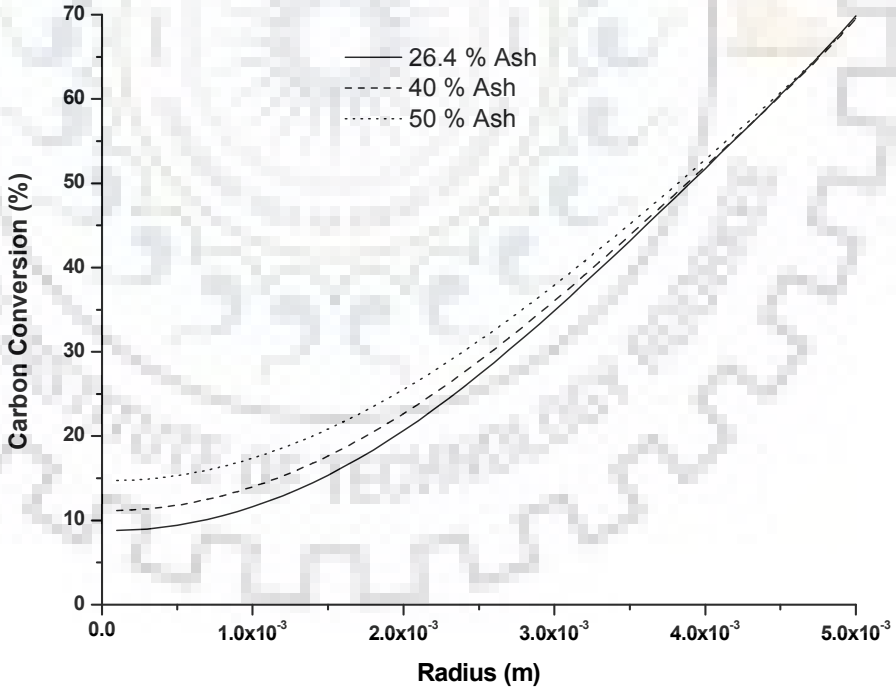

Figure 4.44: Carbon conversion profile in the char particle for different ash content in the char particle at 1100 K

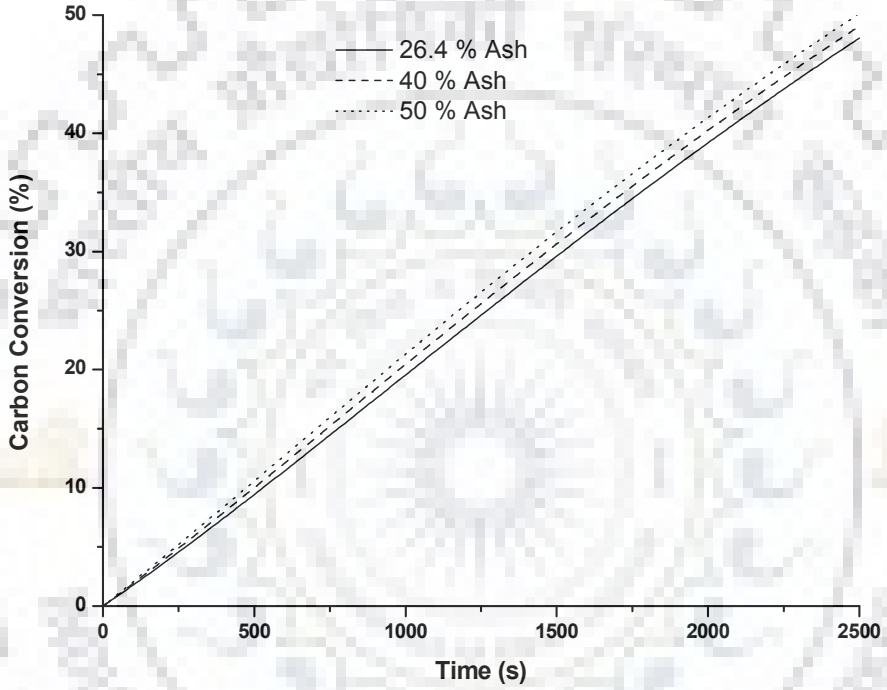

Figure 4.45: Carbon Conversion with time for different ash content in the char particle at 1100 K

The rate of production of H_2, CO, and CO_2 decreases with increasing the ash content in the char because of decrease in the concentration of carbon. On the other hand, carbon conversion increases with the increase in the ash content in char because of increase in the available active specific surface area of char particle for gasification (Figure 4.45). For the low ash content char, pore diffusion becomes significant leading to the gasification reactions to take place on the surface which enhance the production rates of H_2 (Figure 4.46), CO (Figure 4.47), and CO_2 (Figure 4.48) and production rates of H_2, CO, and CO_2 begin to decline after 1000 second because of decline in the specific surface area for the gasification reactions due to formation of ash layer on the surface of the char.

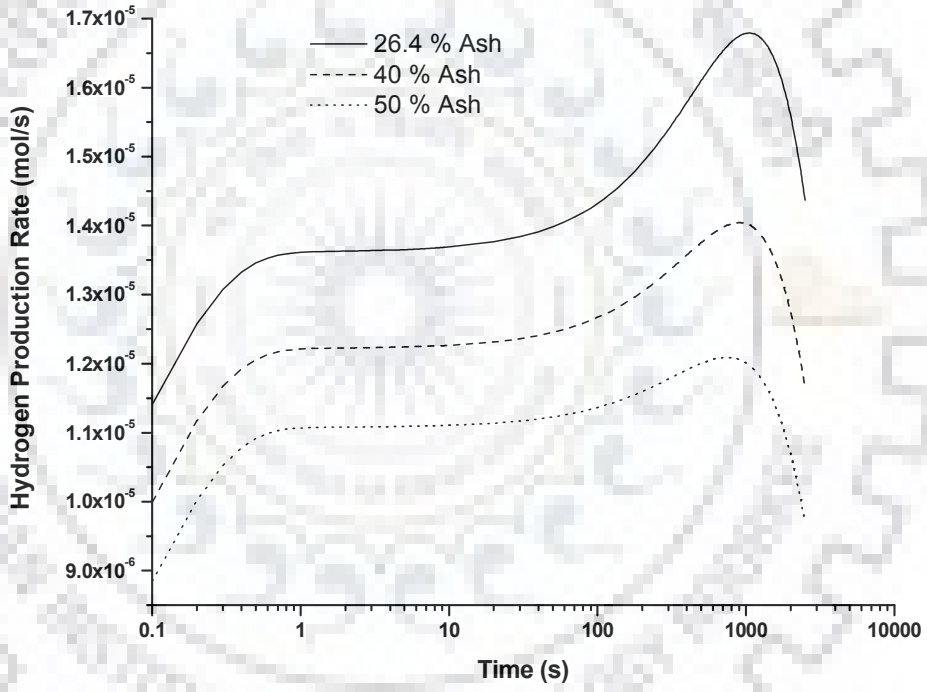

Figure 4.46: H_2 production rate from the outer surface of char particle for different ash content at 1100 K (logarithmic *x*-axis)

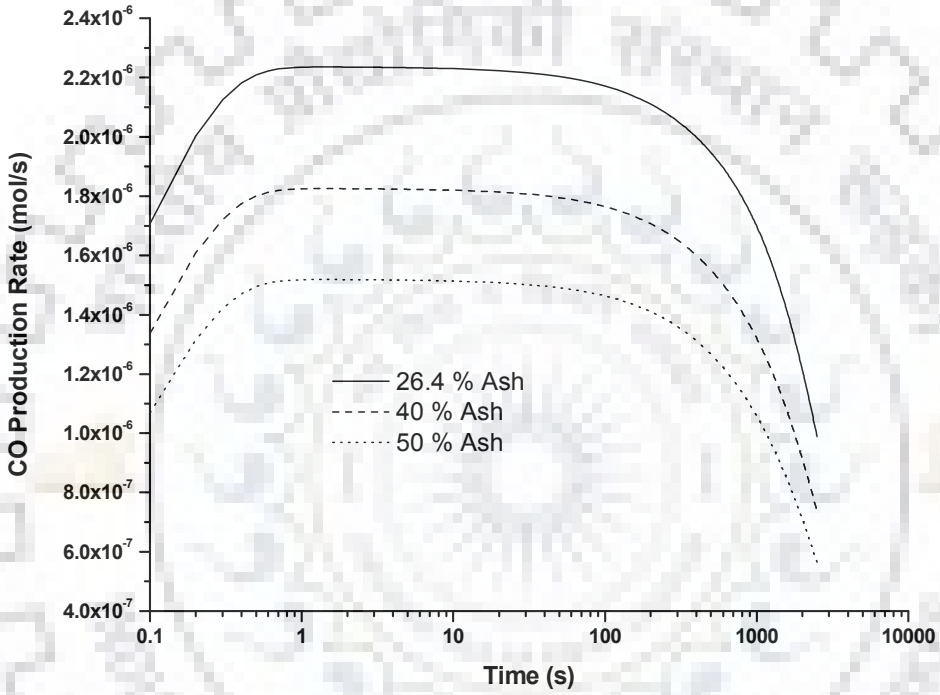

Figure 4.47: CO production rate from the outer surface of char particle for different ash content at 1100 K (logarithmic *x*-axis)

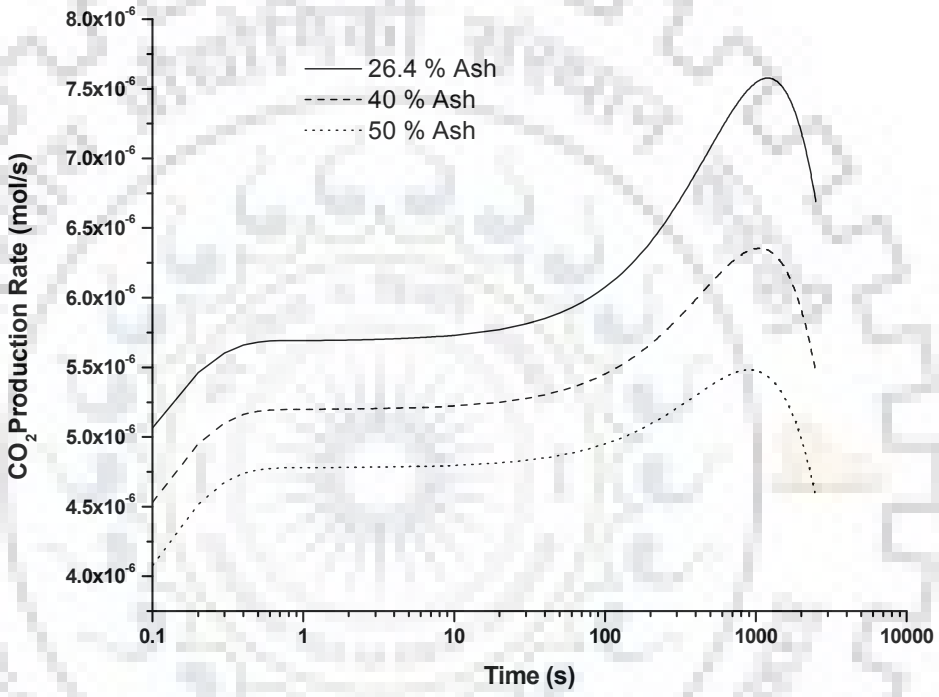

Figure 4.48: CO_2 production rate from the outer surface f of char particle for different ash content at 1100 K (logarithmic *x*-axis)

At higher ash contents, gasification becomes kinetic control which results in the homogeneous reactions inside the char particle and the rate of production of gases (H_2, CO, and CO_2) begins to decline after 1000 second. The rate of production of H_2 and CO_2 decline approximately 1.2 times while the CO decreases nearly 1.5 folds for the increase in ash content from 26.4% to 50% in the char particle. Due to this reason, the flux ratio of H_2/CO increases with the ash content in the char (Figure 4.49) while the ratio CO/CO_2 decreases with increase in the ash content (Figure 4.50). The ratio H_2/CO increases while CO/CO_2 decreases sharply after 1000 second because of sharp decrease in the CO production rate.

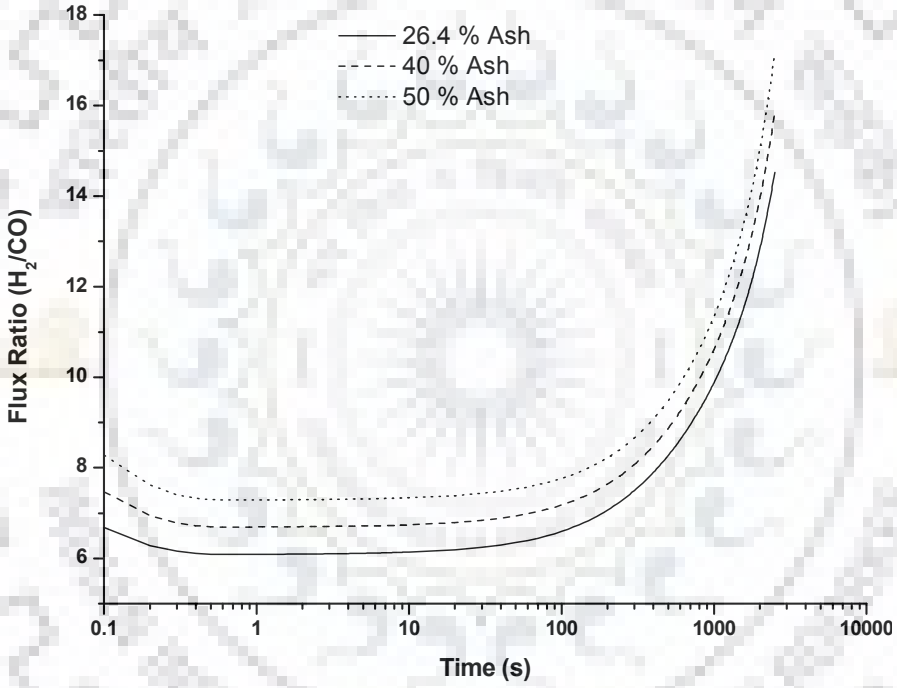

Figure 4.49: Flux ratio of H_2/CO for different ash content in the char particle at 1100 K (logarithmic *x*-axis)

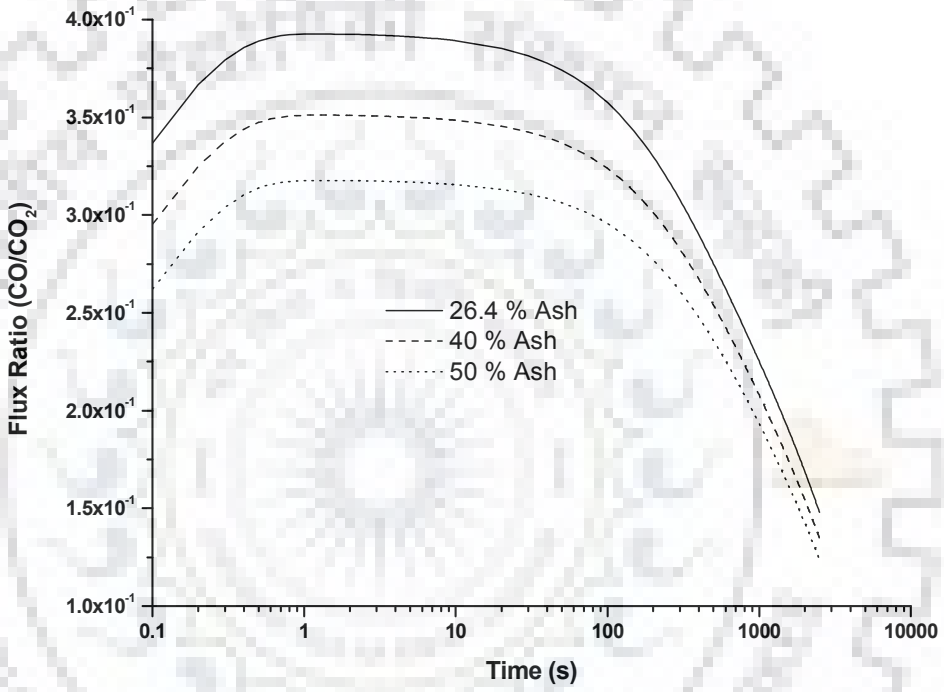

Figure 4.50: Flux ratio of CO/CO_2 for different ash content in the char particle at 1100 K (logarithmic *x*-axis)

4.2.7 Effect of mixture of steam and CO_2

The unsteady state coal char gasification with varying composition of steam and CO_2 as gasifying agent for the 10 mm char particle, with initial porosity 0.2545, and constant temperature of 1100 K was simulated using above discussed model (in Chapter 3). In this section, the effects of composition of gasifying agent on the synthesis gas production and minimization of CO_2 emission have been studied. During coal char gasification, the rate of carbon conversion depends on the gasifying agent concentration, different composition of reactant gases give the different carbon conversion inside the particle (Figure 4.51).

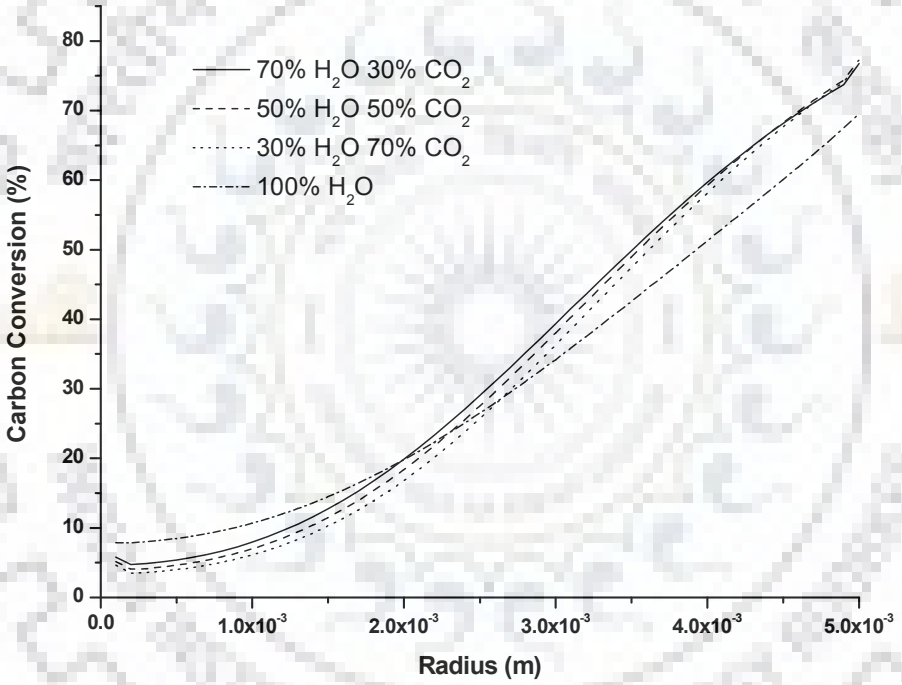

Figure 4.51: Carbon conversion profile in the char particle for different fraction of Steam and CO_2 concentration at 1100 K

Here, it is also observed that the overall rate of carbon conversion in the char particle is higher for mixtures of steam and CO_2 as compared to steam alone (Figure 4.52). It is also observed that mixture of 70 % steam and 30 % CO_2 gives the highest carbon conversion.

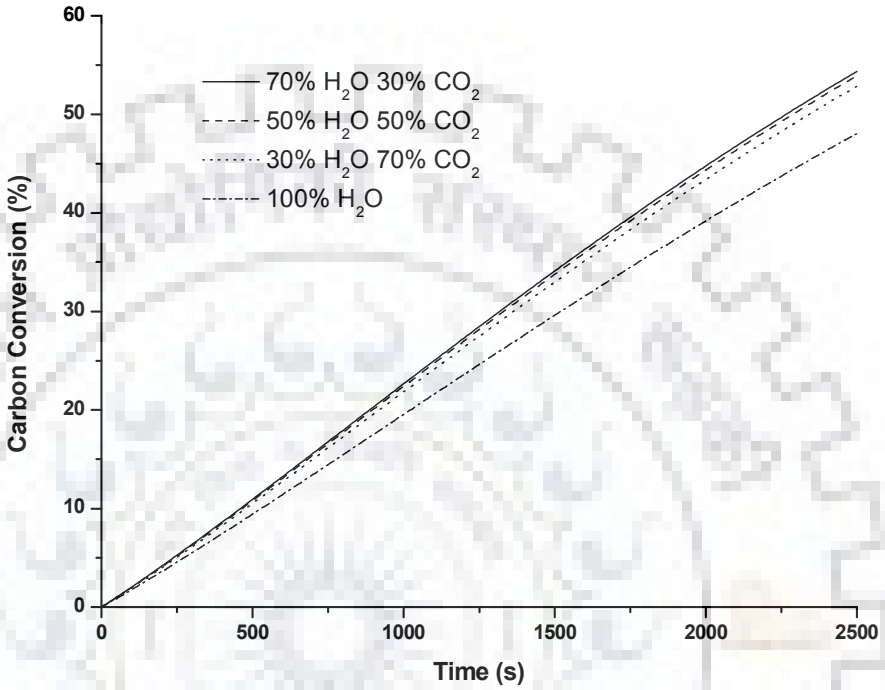

Figure 4.52: Carbon conversion with time for different fraction of Steam and CO_2 concentration at 1100 K

Net hydrogen flux from outer surface of the char particle, however, increases with increasing the composition of steam in the gasifying agent due to the water gas reaction (R1). As shown in Figure 4.53, initially, hydrogen flux sharply increases because of increase in the specific surface area and after about 1000 s the flux begins to decline due to the reduction in the specific surface area leading to reduced reaction rate.

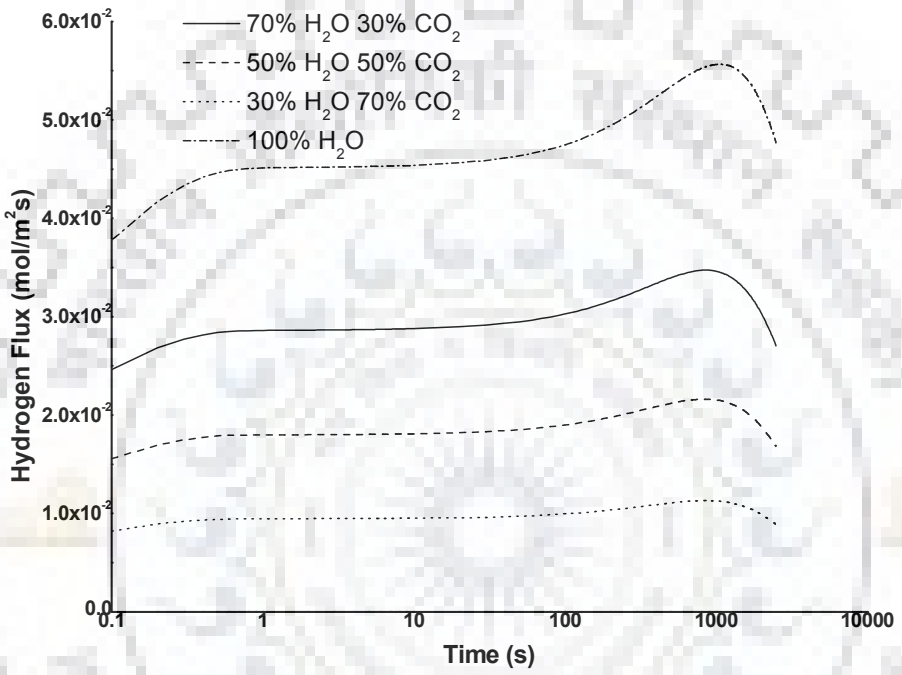

Figure 4.53: Hydrogen Flux from the outer surface of char particle for different fraction of Steam and CO_2 concentration at 1100 K (logarithmic *x*-axis)

Similar to the nature of hydrogen flux, the overall flux of carbon monoxide and CO_2 from the outer surface increases with an increase in the composition of CO_2 in the gasifying agent (Figure 4.54) because of the Boudouard reaction (R3) is favoured by CO_2 concentration. In case of pure steam, the CO is formed from the water gas reaction (R1) but it gets converted to CO_2 and H_2 by the homogeneous water gas shift reaction (R5) leads to lower flux of CO (Figure 4.54) and higher flux of CO_2 (Figure 4.55). The CO_2 flux is observed to be minimum for the reactant gas composition of 70 % steam and 30 % CO_2 and also synthesis gas obtaining in this case has the higher heating value (dry basis) in comparison to the other cases shown in Table 4.3

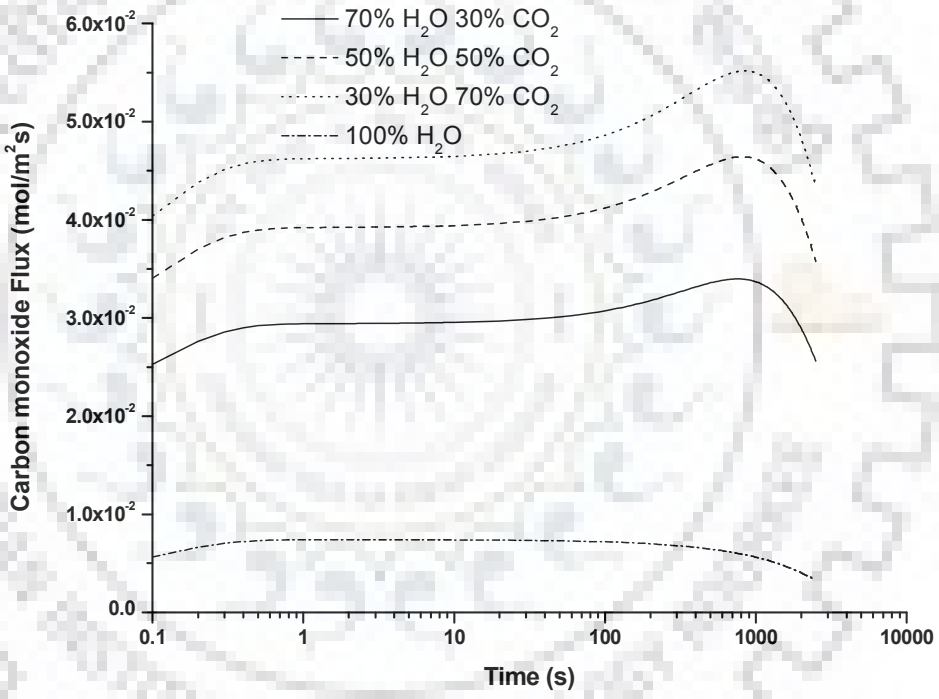

Figure 4.54: CO Flux from the outer surface of char particle for different fraction of Steam and CO_2 concentration at 1100 K (logarithmic *x*-axis)

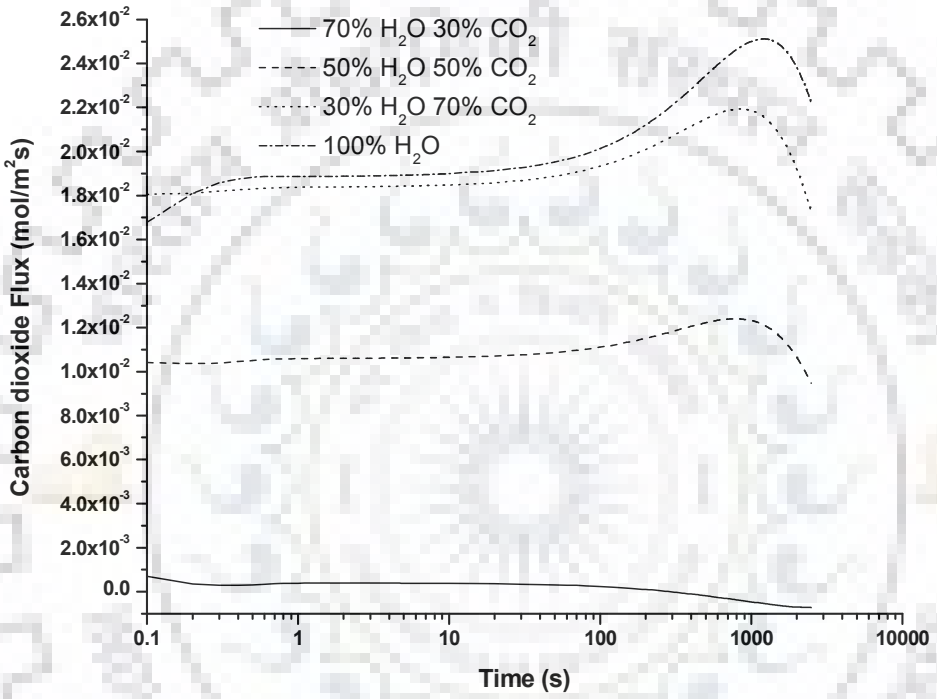

Figure 4.55: CO_2 Flux from the outer surface of char particle for different fraction of Steam and CO_2 concentration at 1100 K (logarithmic *x*-axis)

Table 4.3 shows the synthesis gas composition and their higher heating values for different fraction of gasifying agents (Steam and CO_2) in both cases (dry and wet). The fraction of H_2 increases in the synthesis gas with increase in the steam fraction in gasifying agents whiles the increase in the CO_2 fraction increasing the CO composition in the synthesis gas. From the Table 4.3, it is also clear that the fraction of 70 % steam and 30 % CO_2 enhanced the heating value of synthesis gas and reduces the CO_2 fraction in the product gases.

Table 4.3: Synthesis gas composition and their HHV at different gasifying agent composition

Gasifying agent composition	Synthesis Gas Composition							HHV of Synthesis Gas	
	Wet (%)				Dry (%)			Wet	Dry
	H_2O	H_2	CO	CO_2	H_2	CO	CO_2	(kJ/mol)	(kJ/mol)
100 % H_2O	39.2	39.2	3.9	17.6	64.5	6.4	29	123.23	202.75
70 % H_2O 30 % CO_2	**33.4**	**33.4**	**32.57**	**0.46**	**50.3**	**48.9**	**0.7**	**188.023**	**282.683**
50 % H_2O 50 % CO_2	21.20	21.20	45.46	12.13	26.9	57.7	15.4	189.41	240.39
30 % H_2O 70 % CO_2	11.33	11.33	55.33	22.0	12.78	62.4	24.8	189.138	213.315
HHV (Higher heating value) of H_2=286 kJ/mol and CO=283.24 kJ/mol									

CHAPTER 5

CONCLUSIONS AND RECOMMENDATIONS

In the present research work a new technique for modeling the single char particle gasification has been developed. The model incorporated a more realistic kinetic scheme for the gasification reactions using Arrhenius type reaction rate constants.

5.1 Conclusions

- Rate of char gasification increases with increasing steam concentration and also the steam gasification of char particle enhanced the yield of hydrogen.
- The rate of gasification increases with increasing the temperature. At lower temperature (upto 1100 K), the gasification follow the progressive reaction model while at higher temperature (> 1100 K), the gasification follows the shrinking core model. The highest concentration of CO and H_2 is obtained when the reaction temperature is greater than 1200 K.
- Removal of the ash layer from the particle surface at time interval of 100 second for low ash content char (<1%) and 10 second for high ash content char (>25%) may give higher CO concentration.
- The rate of percent conversion is high for low char concentration in the centre core of particle. Near the centre, carbon consumption is high when its concentration is low.
- The rate of conversion increases with decrease in particle size but rate of surface reaction of large particle is higher compared to smaller particle leading to the higher rate of production of gases (H_2, CO, and CO_2) from the outer surface of char particle.
- The porosity of the char particle affects the total conversion only in the initial phase of gasification. Time required to reach complete conversion is almost same for all initial porosity values. The variation of initial porosity is more prominent towards the low porosity range. The rate of production of gases from the outer surface of char particle is inversely proportional to the porosity. For constant time of conversion, the flux ratio

of H_2 to CO and CO to CO_2 remains the same for all initial porosity of char particle after 2500 second.

- The carbon conversion near the surface of char particle are nearly same for all char particle whereas towards the centre of the char particle, conversion is significantly high for high ash content char because of available specific surface area. The overall carbon conversion of high ash content char particle is higher. The rate of production of gases from the outer surface of char particle is inversely proportional to the ash content.

- The higher fraction of CO_2 in the gasifying medium enhanced the yield of CO. The highest fraction of H_2 and CO with lower CO_2 concentration (dry basis) is obtained when the gasifying agent composition is 70% steam and 30% CO_2. The synthesis gas obtained by 70% steam and 30% CO_2 has higher heating value.

5.2 Recommendations

- The proposed model can be used for analyzing the effects of various flow pattern of gasifying medium during the gasification of char particle.

- The proposed scheme can be used for the effect of removal of ash layers from char particle surface after a fixed time interval on the product gas yields.

- The proposed scheme can also be applied for changing pore structure of char particle during the progress of gasification.

- The present study incorporates inert ash content in the char particle. This model can be extended for study the effect of various minerals presents in the ash on the gasification.

REFERENCES

Abani N, Ghoniem AF. Large eddy simulations of coal gasification in an entrained flow gasifier. Fuel 2013; 104: 664-680.

Abashar ME, Elnashaie SS. Mathematical Modelling of Diffusion-Reaction, and Solution Algorithm for complex Reaction Networks in Porous Catalyst Pellets-Steam Reforming of Natural Gas. Mathematical and Computer Modelling 1993; 18: 85-100.

Adams II TA, Barton PI. A dynamic two-dimensional heterogeneous model for water gas shift reactors. International Journal of Hydrogen Energy 2009; 34: 8877-8891.

Adams II TA, Barton PI. Combining coal gasification and natural gas reforming for efficient polygeneration. Fuel Processing Technology 2011(a); 92: 639-655.

Adams TA II, Barton PI. Clean coal: A new power generation process with high efficiency, carbon capture and zero emissions. In: 20th European Symposium on Computer Aided Process Engineering. 2010: 991-996.

Adams TA II, Barton PI. Combining coal gasification, natural gas reforming, and solid oxide fuel cells for efficient polygeneration with CO_2 capture and sequestration. Fuel Processing Technology 2011(b); 92: 2105-2115.

Adanez J, Miranda JL, Gavilan JM. Kinetics of lignite-char gasification by CO_2. Fuel 1985; 64: 801-804.

Adschiri T, Shiraha T, Kojima T, Furusawa T. Prediction of CO_2 gasification rate of char in fluidized bed gasifier. Fuel 1986; 65: 1688-1693.

Ahn DH, Gibbs BM, Ko KH, Kim JJ. Gasification kinetics of an Indonesian sub-bituminous coal-char with CO_2 at elevated pressure. Fuel 2001; 80: 1651-1658.

Ahuja P. Introduction to Numerical Methods in Chemical Engineering, PHI Learning, New Delhi, 2010.

Ahuja P, Kumar S, Singh PC. A Model for Primary and Heterogeneous Secondary Reactions of Wood Pyrolysis. Chemical Engineering and Technology. (VCH, Weinheim, Germany) 1996(a); 19: 272-282.

Ahuja P, Singh PC, Upadhyay SN, Kumar S. Kinetics of Biomass and Sewage Sludge Pyrolysis: Thermogravimetric and Sealed Reactor Studies. Indian Journal of Chemical Technology 1996(b); 3: 306-312.

Arenas E, Chejne F. The effect of the activating agent and temperature on the porosity development of physically activated coal chars. Fuel 2004; 42: 2451-2455.

Audley GJ. An evaluation of methods for enhancing the CO_2-reactivity of a caking bituminous coal. Fuel 1987; 66: 1635-1641.

Audus H. Greenhouse gas release from fossil fuel power stations. IEA Greenhouse gas R&D programme (IEAGHG/SRI). March 1993.

Avnimelech Y, Ritvo G, Meijer LE, Kochba M. Water content, organic carbon and dry bulk density in flooded sediments. Aquacultural Engineering 2001; 25: 25-33.

Badzioch S, Hawksley PGW. Kinetics of Thermal Decomposition of Pulverized Coal Particles. Industrial and engineering chemistry process design and development 1970; 9: 521-530.

Bale HD, Carlson ML, Schobert HH. Thermal modification of the pore structure of a North Dakota lignite. Fuel 1986; 65: 1185-1189.

Basu P. Combustion and Gasification in Fluidized Beds. Taylor and Francis Group, LLC 2006.

Bayarsaikhan B, Hayashi J, Shimada T, Sathe C, Li CZ, Tsutsumi A, Chiba T. Kinetics of steam gasification of nascent char from rapid pyrolysis of a Victorian brown coal. Fuel 2005; 84: 1612-1621.

Bayarsaikhan B, Sonoyama N, Hosokai S, Shimada T, Hayashi J, Li CZ, Chiba T. Inhibition of steam gasification of char by volatiles in a fluidized bed under continuous feeding of a brown coal. Fuel 2006; 85: 340-349.

Beamish BB, Shaw KJ, Rodgers KA, Newman J. Thermogravimetric determination of the carbon dioxide reactivity of char from some New Zealand coals and its association with the inorganic geochemistry of the parent coal. Fuel Processing Technology 1998; 53: 243-253.

Bhatia SK, Vartak BJ. Reaction of microporous solids: The discrete random pore model. Carbon 1996; 34: 1383-1391.

Biba V, Macak J, Klose E, Malecha J. Mathematical Model for the Gasification of Coal under Pressure. Industrial and engineering chemistry process design and development 1978; 17: 92-98.

Blackham AU, Smoot LD, Yousefi P. Rates of oxidation of millimetre-sized char particles: simple experiments. Fuel 1994; 73: 602-612.

Blasi CD, Buonanno F, Branca C. Reactivities of some biomass chars in air. Carbon 1999; 37: 1227-1238.

Bliek A, Lont JC, Swaaij WPMV. Gasification of Coal-Derived Chars in Synthesis Gas Mixture under Intraparticle Mass Transfer-Controlled Conditions. Chemical Engineering Science 1986; 41: 1895-1909.

Brown BW, Smoot LD, Hedman PO. Effect of coal type on entrained gasification. Fuel 1986; 65: 673-678.

Buczek B. Properties of Active Carbon with various particle shapes obtained in Char-Steam Reaction. Chemical and Process Engineering 2012; 33: 335-344.

Cai HY, Guell AJ, Chatzakis IN, Lim JY, Dugwell DR, Kandiyoti R. Combustion reactivity and morphological change in coal chars: effect of pyrolysis temperature, heating rate and pressure. Fuel 1996; 75: 15-24.

Cakal GO, Yucel H, Guruz AG. Physical and chemical properties of selected Turkish lignites and their pyrolysis and gasification rates determined by thermogravimetric analysis. Journal of Analytical and Applied Pyrolysis 2007; 80: 262-268.

Calemma V, Radovic LR. On the gasification reactivity of Italian Sulcis coal. Fuel 1991; 70: 1027-1030.

Cempa-Balewicz M, Laczny MJ, Smolinski A, Iwaszenko S. Equilibrium Model of Steam Gasification of Coal. Journal of Sustainable Mining 2013; 12: 21-28.

Cetin E, Gupta R, Moghtaderi B. Effect of pyrolysis pressure and heating rate on radiata pine char structure and apparent gasification reactivity. Fuel 2005; 84:1328-1334.

Cetin E, Moghtaderi B, Gupta R, Wall TF. Influence of pyrolysis conditions on the structure and gasification reactivity of biomass chars. Fuel 2004; 83: 2139-2150.

Chandra A, Chandra H. Impact of Indian and imported coal on Indian thermal power plants. Journal of Scientific and Industrial Research 2004; 63: 156-162.

Chavan P, Datta S, Saha S, Sahu G, Sharma T. Influence of High Ash Indian Coals in Fluidized Bed Gasification under Different Operating Conditions. Solid Fuel Chemistry 2012; 46: 108–113.

Chejne F, Hernandez JP. Modelling and simulation of coal gasification process in fluidized bed. Fuel 2002; 81: 1687-1702.

Chen C, Horio M, Kojima T. Numerical simulation of entrained flow coal gasifiers. Part I: modeling of coal gasification in an entrained flow gasifier. Chemical Engineering Science 2000; 55: 3861-3874.

Choi YC, Li XY, Park TJ, Kim JH, Lee JG. Numerical study on the coal gasification characteristics in an entrained flow gasifier. Fuel 2001; 80: 2193-2201.

Collings ME, Mann MD, Young BC. Effect of Coal Rank and Circulating Fluidized-Bed Operating Parameters on Nitrous Oxide Emissions. Energy and Fuels 1993; 7: 554-558.

Collings ME, Mann MD. Empirical Modeling of N_2O Emissions from Circulating Fluidized-Bed Combustion. Energy and Fuels 1994; 8: 1083-1094.

Corella J, Sanz A. Modelling circulating fluidized bed biomass gasifier. A pseudo-rigorous model for stationary state. Fuel Processing Technology 2005; 86: 1021-1053.

Daggupati S, Mandapati RN, Mahajani SM, Ganesh A, Pal AK, Sharma RK, Aghalayam P. Compartment Modeling and Flow Characterization in Nonisothermal Underground Coal Gasification Cavities. Industrial and Engineering Chemistry Research 2012; 51: 4493-4508.

Daggupati S, Mandapati RN, Mahajani SM, Ganesh A, Sapru RK, Sharma RK, Aghalayam P. Laboratory studies on cavity growth and product gas composition in the context of underground coal gasification. Energy 2011; 36: 1776-1784.

Do DD. On the validity of the shrinking core model in noncatalytic gas solid reaction. Chemical Engineering Science 1982; 37: 1477-1481.

Dorrestijn E, Laarhoven LJJ, Arends IWCE, Mulder P. The occurrence and reactivity of phenoxyl linkages in lignin and low rank coal. Journal of Analytical and Applied Pyrolysis 2000; 54: 153-192.

Dwivedi PN, Upadhyay SN. Particle-Fluid Mass Transfer in Fixed and Fluidized Beds. Industrial and engineering chemistry process design and development 1977; 16: 157–165.

Ergun S. Kinetics of the reactions of carbon dioxide and steam with coke. Project coordinator, solid state physics, Pittsburg coal research centre, Bureau of mines, Pittsburg 1961; 1-9.

Essenhigh RH, Mishra MK. Autocorrelations of Kinetic Parameters in Coal and Char Reactions. Energy and Fuels 1990; 4: 171-177.

Evans DD, Emmons HW. Combustion of Wood Charcoal. Fire Research 1977; 1: 57-66.

Everson R, Neomagus H, Kaitano R. The modeling of the combustion of high-ash coal–char particles suitable for pressurised fluidized bed combustion: shrinking reacted core model. Fuel 2005; 84: 1136-1143.

Everson RC, Neomagus HWJP, Kaitano R, Falcon R, Cann VM. Properties of high ash coal-char particles derived from inertinite-rich coal: II. Gasification kinetics with carbon dioxide. Fuel 2008; 87: 3403-3408.

Everson RC, Neomagus HWJP, Kasaini H, Njapha D. Reaction kinetics of pulverized coal-chars derived from inertinite-rich coal discards: Gasification with carbon dioxide and steam. Fuel 2006; 85: 1076-1082.

Everson RC, Neomagus HWJP, Kasaini H, Njapha D. Reaction kinetics of pulverized coal-chars derived from inertinite-rich coal discards: Characterisation and combustion. Fuel 2006; 85: 1067-1075.

Feldkirchner HL, Linden HR. Reactivity of coals in high-pressure gasification with hydrogen with steam. I&CE Process Design and Development 1963; 2: 153-162.

Field MA. Rate of combustion on size-graded fractions of char from a low-rank coal between 1200 K and 2000 K. Combustion and Flame 1969; 13: 237-252.

Fung DPC, Fairbridge C, Anderson R. Gasification reactivity of Canadian anthracite and semi-anthracite chars. Fuel 1988; 67: 753-757.

Fung DPC, Kim SD. Chemical reactivity of Canadian coal-derived chars. Fuel 1984; 63: 1197-1201.

Fushimi C, Goto M, Tsutsumi A, Hayashi J, Chiba T. Steam gasification characteristics of coal with rapid heating. Journal of Analytical and Applied Pyrolysis 2003; 70: 185-197.

Gale TK, Bartholomew CH, Fletcher TH. Effects of Pyrolysis Heating Rate on Intrinsic Reactivities of Coal Chars. Energy and Fuels 1996; 10: 766-775.

Gao C, Vejahati F, Katalambula H, Gupta R. Co-gasification of Biomass with Coal and Oil Sand Coke in a Drop Tube Furnace. Energy and Fuels 2010; 24: 232-240.

Gibbins JR, Kandiyoti R. The effect of variations in time-temperature history on product distribution from coal pyrolysis. Fuel 1989; 68: 895-903.

Gibbins JR, Khogali K, Kandiyoti R. Relationship between results from conventional proximate analysis and pyrolysis yields under rapid-heating conditions. Fuel Processing Technology 1990; 24: 3-9.

Gibbins-Matham J, Kandiyoti R. Coal Pyrolysis Yields from Fast and Slow Heating in a Wire-Mesh Apparatus with a Gas Sweep. Energy and Fuels 1988; 2:505-511.

Gil S, Mocek P, Bialik W. Changes in total active centres on particle surfaces during coal pyrolysis, gasification and combustion. Chemical and Process Engineering 2011; 32:155-169.

Gomez A, Mahinpey N. A new model to estimate CO_2 coal gasification kinetics based only on parent coal characterization properties. Applied Energy 2015; 137: 126-133.

Gomez A, Silbermann R, Mahinpey N. A comprehensive experimental procedure for CO_2 coal gasification: Is there really a maximum reaction rate?. Applied Energy 2014; 124: 73-81.

Gomez-Barea A, Ollero P, Arjona R. Reaction-diffusion model of TGA gasification experiments for estimating diffusional effects. Fuel 2005; 84: 1695–1704.

Gomez-Barea A, Ollero P. An approximate method for solving gas–solid non-catalytic reactions. Chemical Engineering Science 2006; 61: 3725-3735.

Govind R, Shah J. Modeling and Simulation of an Entrained Flow Coal Gasifier. AlChE Journal 1984; 30:79-91.

Goyal A, Zabransky RF, Rehmat A. Gasification Kinetics of Western Kentucky Bituminous Coal Char. Industrial and engineering chemistry research 1989; 28: 1767-1777.

Gremyachkin VM, Mazanchenko EP. Interaction of a Porous Carbon Particle with Steam and Carbon Dioxide. Combustion, Explosion, and Shock Waves 2011; 47: 442-447.

Groeneveld MJ, Swaaij WPMV. Gasification of Char Particles with CO_2 and H_2O. Chemical Engineering Science 1980; 35: 307-313.

Guell AJ, Cai HY, Dugwell DR, Kandiyoti R. Combustion and Gasification reactivities of Hydropyrolysis chars: Effect of pressure and heating rate. Fuel Processing Technology 1993; 36: 259-265.

Guizani C, Sanz FJE, Salvador S. The gasification reactivity of high-heating-rate chars in single and mixed atmospheres of H_2O and CO_2. Fuel 2013; 108: 812-823.

Guo CT, Zhang LM. Kinetics of coal char gasification at elevated pressures. Fuel 1986; 65: 1364-1367.

Gupta JS, Bhatia SK. A modified discrete random pore model allowing for different initial surface reactivity. Carbon 2000; 38:47-58.

Gupta R. Advanced Coal Characterization: A Review. Energy and Fuels 2007; 21: 451-460.

Gutierrez LA, Watkison AP. Fluidized-bed gasification of some Western Canadian coals. Fuel 1982; 61: 133-138.

Haga T, Nishiyam Y. Influence of structural parameters on coal char gasification 2. N i-catalysed steam gasif ication. Fuel 1988; 67: 748-752.

Harris DJ, Roberts DG, Henderson DG. Gasification behaviour of Australian coals at high temperature and pressure. Fuel 2006; 85: 134-142.

Hashimoto K, Miura K, Ueda T. Correlation of gasification rates of various coals measured by a rapid heating method in a steam atmosphere at relatively low temperatures. Fuel 1986; 65: 1516-1523.

Haynes HW, JR. An Improved Single Particle Char Gasification Model. AIChE Journal 1982; 28: 517-521.

Hedman PO, Smoot LD, Fletcher TH, Smith PJ, Blackham AU. Prediction and Measurement of Entrained Flow Coal Gasification Processes. Interim Report Volume I prepared for U.S. DOE/METC, Contract No. DE-AC21-81MC16518, Combustion Laboratory, Brigham Young University (October, 1983).

Heek KHV, Muhlen HJ. Effect of coal and char properties on gasification. Fuel Processing Technology 1987; 15: 113-133.

Hippo E, Walker PL, Jr. Reactivity of heat-treated coals in carbon dioxide at 900^0C. Fuel 1975; 54: 245-248.

Holikova K, Zajdlik R, Markos J, Jelemensky L. Comparison of Single Coal Char Particle Combustion at Different Conditions. Chemical Papers 2005; 59: 413-420.

Hong J, Hecker WC, Fletcher TH. Improving the Accuracy of Predicting Effectiveness Factors for *m*th Order and Langmuir Rate Equations in Spherical Coordinates. Energy and Fuels 2000; 14: 663-670.

Huang J, Watkinson AP. Coal gasification in a stirred bed reactor. Fuel 1996; 75: 1617-1624.

Huo W, Zhou Z, Wang F, Wang Y, Yu G. Experimental study of pore diffusion effect on char gasification with CO_2 and steam. Fuel 2014; 131: 59-65.

Hurt RH, Longwell JP, Sarofim AF. Gasification reactivity of chars from low rank coal lithotypes. Fuel 1986; 65: 451-452.

Hurt RH, Sarofim AF, Longwell JP. The role of microporous surface area in the gasification of chars from a sub-bituminous coal. Fuel 1991; 70: 1079-1082.

Huttinger KJ. Mechanism of water vapor gasification at high hydrogen level. Carbon 1988; 26: 79-87.

Huttinger KL, Merdes WF. The carbon-steam reaction at elevated pressure Formations of product gases and hydrogen inhibitions. Carbon 1992; 30: 883-894.

Inayat A, Ahmad MM, Yusup S, Mutalib MIA. Biomass Steam Gasification with In-Situ CO_2 capture for Enriched Hydrogen Gas Production: A Reaction Kinetics Modelling Approach. Energies 2010; 3: 1472-1484.

Irfan MF, Usman MR, Kusakabe K. Coal gasification in CO_2 atmosphere and its kinetics since 1948: A brief review. Energy 2011; 36: 12-40.

Jenkins RG, Nandi SP, Walker PL, Jr. Reactivity of heat-treated coals in an air at 500 ^{0}C. Fuel 1973; 52: 288-293.

Jensen GA. The Kinetics of Gasification of Carbon Contained in Coal Minerals at Atmospheric Pressure. Industrial and engineering chemistry process design and development 1975; 14: 309-314.

Juntgen H. Reactivities of carbon to steam and hydrogen and applications to technical gasification processes-A Review. Carbon 1981; 19: 167-173.

Juntgen H. Review of the kinetics of pyrolysis and hydropyrolysis in relation to the chemical constitution of coal. Fuel 1984; 63: 731-737.

Kajitani S, Hara S, Matsuda H. Gasification rate analysis of coal char with a pressurized drop tube furnace. Fuel 2002; 81: 539-546.

Kajitani S, Suzuki N, Ashizawa M, Hara S. CO_2 gasification rate analysis of coal char in entrained flow coal gasifier. Fuel 2006; 85: 163-169.

Kajitani S, Tay HL, Zhang S, Li CZ. Mechanisms and kinetic modelling of steam gasification of brown coal in the presence of volatile–char interactions. Fuel 2013; 103: 7-13.

Kamishita M, Mahajan OP, Walker Jr PL. Effect of carbon deposition on porosity and reactivity of a lignite char. Fuel 1977; 56: 444-450.

Karabulut R, Sinag A, Misirlioglu Z, Canel M. Investigation on gasification properties of solid fuels. Communications de la Faculté des Sciences de l'Université d'Ankara. Séries B 1999; 45: 35-47.

Karimipour S, Gerspacher R, Gupta R, Spiteri RJ. Study of factors affecting syngas quality and their interactions in fluidized bed gasification of lignite coal. Fuel 2013; 103: 308-320.

Kasaoka S, Sakata Y, Shimada M. Effects of coal carbonization conditions on rate of steam gasification of char. Fuel 1987; 66: 697-701.

Katta S, Kealrns DL. Char Reactivities and Their Relationship to Pore Characteristics. Westinghouse R&D Center Pittsburgh, 1977; PA 15235: 19-28.

Katta S, Kealrns DL. Study of Kinetics of Carbon Gasification Reactions. Industrial and engineering chemistry fundamentals 1981; 20: 6-13.

Kim D, Choi S, Shaddix SR, Geier M. Effect of CO_2 gasification on char particle combustion in oxy-fuel conditions. Fuel 2014; 120: 130-140.

Kim YJ, Lee JM, Kim SD. Modeling of coal gasification in an internally circulating fluidized bed reactor with draught tube. Fuel 2000; 79: 69-77.

Knight AT, Sergeant GD. Reactivity of Australian coal-derived chars to carbon dioxide. Fuel 1982; 61: 145-149.

Kopyscinski J, Rahman M, Gupta R, Mims CA, Hill JM. K2CO3 catalyzed CO2 gasification of ash-free coal. Interactions of the catalyst with carbon in N2 and CO2 atmosphere. Fuel 2014; 117: 1181-1189.

Koranyi AD. The relationship between specific reactivity and the pore structure of coal chars during gasification. Carbon 1989; 27: 55-61.

Kovacik G, Oguztoreli M, Chambers A, Ozum B. Equilibrium calculations in coal gasification. International Journal of Hydrogen Energy 1990; 15: 125-131.

Kumar M, Ghoniem AF. Application of a validated gasification model to determine the impact of coal particle grinding size on carbon conversion. Fuel 2013; 108: 565-577.

Kumar V, Upadhyay SN. Computer simulation of membrane processes: ultrafiltration and dialysis units. Computers and Chemical Engineering 2000; 23: 1713–1724.

Kwon TW, Kim SD, Fung DPC. Reaction kinetics of char-CO_2 gasification. Fuel 1988; 67: 530-535.

Kyotani T, Kubota K, Cao J, Yamashita H, Tomita A. Combustion and CO_2 gasification of coals in a wide temperature range. Fuel Processing Technology 1993; 36: 209-217.

Lee CW, Scaroni W, Jenkins RG. Effect of pressure on the devolatilization and swelling behaviour of a softening coal during rapid heating. Fuel 1991; 70: 957-965.

Lee JM, Kim YJ, Lee WJ, Kim SD. Coal-gasification kinetics derived from pyrolysis in a fluidized-bed reactor. Energy 1998; 23: 475-488.

Leppalahti J, Koljonen T. Nitrogen evolution from coal, peat and wood during gasification: Literature review. Fuel Processing Technology 1995; 43: 1-45.

Li C, Zhao J, Fang Y, Wang Y. Effect of pressure on gasification reactivity of three Chinese coals with different ranks. Frontiers of Chemical Engineering in China 2010; 4: 385-393.

Li CZ, Bartle KD, Kandiyoti R. Characterization of tars from variable heating rate pyrolysis of maceral concentrates. Fuel 1993; 72: 3-11.

Li CZ. Some recent advances in the understanding of the pyrolysis and gasification behaviour of Victorian brown coal. Fuel 2007; 86: 1664-1683.

Liliedahl T, Sjostrom K. Modelling of char-gas reaction kinetics. Fuel 1997; 76: 29-37.

Linares A, Mahajan OP, Walker PL, Jr. Reactivities of heat-treated coals in steam. Material science department, Pennsylvania, State University, University park, 1977; Pennsylvania 16802: 1-3.

Linares-Solano A, Mahajan OP, Walker PL, Jr. Reactivity of heat-treated coals in steam. Fuel 1979; 58: 327-332.

Liu G, Benyon P, Benfell KE, Bryant GW, Tate AG, Boyd RK, Harris DJ, Wall TF. The porous structure of bituminous coal chars and its influence on combustion and gasification under chemically controlled conditions. Fuel 2000; 79: 617-626.

Liu G, Tate AG, Bryant GW, Wall TF. Mathematical modelings of coal char reactivity with CO_2 at high pressures and temperatures. Fuel 2000; 79: 1145-1154.

Liu GS, Niksa S. Coal conversion submodels for design applications at elevated pressures. Part II. Char gasification. Progress in Energy and Combustion Science 2004; 30: 679-717.

Liu GS, Tate AG, Rezaei HR, Beath AC, Wall TF. Modeling of Intra-Particle C-CO, Reaction: An Application of the Random Pore Model. Devlopments in chemical engineering and mineral processing 1999; 7: 525-536.

Liu H, Kaneko M, Luo C, Kato S, Kojima T. Effect of pyrolysis time on the gasification reactivity of char with CO_2 at elevated temperatures. Fuel 2004; 83: 1055-1061.

Liu H, Luo C, Kato S, Uemiya S, Kaneko M, Kajima T. Kinetics of CO_2/Char gasification at elevated temperatures Part I: Experimental results. Fuel Processing Technology 2006; 87: 775-781.

Liu Q, Hu H, Zhuo Q, Zhu S, Chen G. Effect of inorganic matter on reactivity and kinetics of coal pyrolysis. Fuel 2004; 83: 713-718.

Lizzio AA, Jiang H, Radovic LR. On the kinetics of carbon (char) gasification: reconciling models with experiments. Carbon 1990; 28: 7-19.

Long FJ, Sykes KW. The Mechanism of the Steam-Carbon Reaction. Mathematical and Physical Science 1948; 193: 377-399.

Lu H, Robert W, Peirce G, Ripa B, Baxter LL. Comprehensive Study of Biomass Particle Combustion. Energy and Fuels 2008; 22: 2826-2839.

Luo C, Watanabe T, Nakamura M, Uemiya S, Kojima T. Development of FBR measurement of char reactivity to carbon dioxide at elevated temperatures. Fuel 2001; 80: 233-243.

Lussier MG, Zhang Z, Miller DJ. Characterizing rate in inhibition in steam/hydrogen gasification via analysis of adsorbed hydrogen. Carbon 1998; 36: 1361-1369.

Mandapati RN, Daggupati S, Mahajani SM, Preeti Aghalayam, Sapru RK, Sharma RK, Anuradda Ganesh A. Experiments and Kinetic Modeling for CO_2 Gasification of Indian Coal Chars in the Context of Underground Coal Gasification. Industrial and Engineering Chemistry Research 2012; 51: 15041-15052.

Mani T, Mahinpey N, Murugan P. Reaction kinetics and mass transfer studies of biomass char gasification with CO_2. Chemical Engineering Science 2011; 66: 36-41.

Mann MD, Knutson RZ, Erjavec J, Jacobsen JP. Modeling reaction kinetics of steam gasification for a transport gasifier. Fuel 2004; 83: 1643-1650.

Massman WJ. A review of the molecular diffusivities of H_2O, CO_2, CH_4, CO, O_3, SO_2, NH_3, N_2O, NO, and NO_2 in air, O_2 and N_2 near STP. Atmospheric Environment 1998; 32: 1111-1127.

Matsui I, Kunii D, Furusawa T. Study of fluidized bed steam gasification of char by Thermogravimetrically obtained kinetics. Journal of Chemical Engineering Japan 1985; 18: 105-113.

Mehta BN, Aris R. Communications on the theory of diffusion and reaction – VII The isothermal p^{th} order reaction. Chemical Engineering Science 1971; 26: 1699-1712.

Mendes A, Dollet A, Ablitzer C, Perrais C, Flamant G. Numerical simulation of reactive transfer in spouted beds at high temperature: Application to coal gasification. Journal of Analytical and Applied Pyrolysis 2008; 82: 117-128.

Mermoud F, Golfier F, Salvador S, Steene LVD, Dirion JL. Experimental and numerical study of steam gasification of a single charcoal particle. Combustion and Flame 2006; 145: 59-79.

Messenbock RC, Paterson NP. Dugwell DR, Kandiyoti R. Factors governing reactivity in low temperature coal gasification. Part 1. An attempt to correlate results from a suite of coals with experiments on maceral concentrates. Fuel 2000; 79: 109-121.

Miura K, Hashimoto K, Silveston PL. Factors affecting the reactivity of coal chars during gasification, and indices representing reactivity. Fuel 1989; 68: 1461-1475.

Molina A, Mondragon F. Reactivity of coal gasification with steam and CO_2. Fuel 1998; 77: 1831-1839.

Morell JI, Amundson NR, Park SK. Dynamics of a Single Particle during Char Gasification. Chemical Engineering Science 1990; 45: 387-401.

Morgan PA, Robertson SD, Unsworth JF. Combustion studies by thermogravimetric analysis. 1. Coal oxidation. Fuel 1986; 65: 1546-1551.

Mostafavi E, Mahinpey N, Manovic V. A novel development of mixed catalyst–sorbent pellets for steam gasification of coal chars with in situ CO_2 capture. Catalysis Today 2014; 237: 111-117.

Muhlen HJ, Heek KHV, Juntgen H. Influence of pretreatment temperature and pressure on the char reactivity during hydrogasification. Fuel 1986; 65: 591-593.

Muhlen HJ, Heek KHV, Juntgen H. Kinetic studies of steam gasification of char in the presence of H_2, CO_2, and CO. Fuel 1985; 64: 944-949.

Muller R, Zedtwitz PV, Wokaun A, Steinfeld A. Kinetic investigation on steam gasification of charcoal under direct high-flux irradiation. Chemical Engineering Science 2003; 58: 5111-5119.

Murphy JJ, Shaddix CR. Combustion kinetics of coal chars in oxygen-enriched environments. Combustion and Flame 2006; 144: 710-729.

Ng SH, Fung DPC, Kim SD. Study of the pore structure and reactivity of Canadian coal-derived chars. Fuel 1988; 67: 700-706.

Nigam KM, Nigam KDP, Srivastava VK. An Approximate Solution for Diffusion and Reaction in a Non-Ideal Tubular Reactor. International communications in heat and mass transfer 1983; 10: 341-348.

Nigam KM, Srivastava VK, Nigam KDP. Homogeneous-Heterogeneous Reactions in a Tubular Reactor: An Analytical Solution. The Chemical Engineering Journal 1982; 25: 147-150.

Nozaki T, Adschiri T, Fujimoto K. Coal char gasification under pressurized CO_2 atmosphere. Fuel 1992; 71: 349-350.

Ochoa J, Cassanello MC, Bonelli PR, Cukierman AL. CO_2 gasification of Argentinean coal chars: a kinetic characterization. Fuel Processing Technology 2001; 74: 161-176.

Ohme H, Suzuki T. Mechanisms of CO_2 Gasification of Carbon Catalyzed with Group VIII Metals. 1. Iron-Catalyzed CO_2 Gasification. Energy and Fuels 1996; 10: 980:987.

Olague NE, Smith DM. Diffusion of gases in American coals. Fuel 1989; 68: 1381-1387.

Ollero P, Serrera A, Arjona R, Alcantarilla S. Diffusional effects in TGA gasification experiments for kinetic determination. Fuel 2002; 81: 1989-2000.

Osafune K, Marsh H. Gasification kinetics of coal chars in carbon dioxide. Fuel 1988; 67: 384-388.

Otto K, Bartosiewicz L, Shelef M. Catalysis of carbon-steam gasification by ash components from two lignites. Fuel 1979; 58: 85-91.

Pahuja KK, Saraf DN. Simulation and optimization of a water-gas shift reactor. Journal of the Institution of Engineers (India). Chemical Engineering Division 1978; 58: 60-68.

Palmer AD, Cheng M, Guolet JC, Furimsky E. Relation between particle size and properties of some bituminous coals. Fuel 1990; 69: 183-188.

Park JY, Levenspiel O. The cracking core model for the reaction of solid particles. Chemical Engineering Science 1975; 30: 1207-1214.

Paviet F, Bals O, Antonini G. Kinetic StudyVoafri ous Chars Steam Gasification. International Journal of Chemical Reactor Engineering 2007; 5: 1-14.

Peng FF, Lee IC, Yang RYK. Reactivities of in situ and ex situ coal chars during gasification in steam at 1000-1400 ^{0}C. Fuel Processing Technology 1995; 41: 233-251.

Pugsley TS, Berruti F. Apredective hydrodynamic model for circulating fluidized bed risers. Powder Technology 1996; 89: 57-69.

Qiao L, Xu J, Sane A, Gore J. Multiphysics modeling of carbon gasification processes in a well-stirred reactor with detailed gas-phase chemistry. Combustion and Flame 2012; 159: 1693-1707.

Radovic LR, Walker PL, Jr, Jenkins RG. Importance of carbon active sites in the gasification of coal chars. Fuel 1983; 62: 849-856.

Ramasamy S, Sripada PP, Khan MM, Tian S, Trivedi J, Gupta R. Adsorption Behavior of CO_2 in Coal and Coal Char. Energy Fuels 2014; 28: 5241-5251.

Rathnam RK, Elliott LK, Wall TF, Liu Y, Moghtaderi B. Differences in reactivity of pulverised coal in air (O_2/N_2) and oxy-fuel (O_2/CO_2) conditions. Fuel Processing Technology 2009; 90: 797-802.

Roberts D, Harris D. Char reactivity in gas mixtures: Towards an understanding of the C-CO-CO_2 reaction system. CSIRO Energy Technology 2008; Technical Note 35:1-13.

Roberts DG, Harris DJ, Wall TF. On the Effects of High Pressure and Heating Rate during Coal Pyrolysis on Char Gasification Reactivity. Energy and Fuels 2003; 17: 887-895.

Roberts DG, Harris DJ. Char gasification in mixtures of CO_2 and H_2O: Competition and inhibition. Fuel 2007; 86: 2672-2678.

Roberts DG, Harris DJ. Char Gasification with O_2, CO_2, and H_2O: Effects of Pressure on Intrinsic Reaction Kinetics. Energy and Fuels 2000; 14: 483-489.

Roberts GW, Satterfield CN. Effectiveness factor for porous catalysts: Langmuir-Hinsheluiood Kinetic Expressions for Bimolecular Surface Reactions. Industrial and engineering chemistry fundamentals 1966; 5: 317-325.

Sadhukhan AP, Gupta P, Saha RK. Modelling of combustion characteristics of high ash coal char particles at high pressure: Shrinking reactive core model. Fuel 2010; 89: 162-169.

Samdani G, Mahajani S, Ganesh A, Aghalayam P, Sapru RK, Mathur DK. Diffusion Modeling in TGA in Context of CO_2 Gasification of Char. COMSOL Conference Bangalore 2012.

Samuilov EV, Faminskaya MF, Golovina ES. Model and Calculation of the Gasification of a Single Carbon Particle. Combustion, Explosion, and Shock Waves 2004; 40: 77-84.

Schmal D, Duyzer JH, Heuven JW. A model for the spontaneous heating of coal. Fuel 1985; 64: 963-972.

Schmal M, Montelro JLF, Castellan JL. Kinetics of Coal Gasification. Industrial and engineering chemistry process design and development 1982; 21:256-266.

Schmal M, Montelro JLF, Toscani H. Gasification of High Ash Content Coals with Steam in a Semibatch Fluidized Bed Reactor. Industrial and engineering chemistry process design and development 1983; 22:563-570.

Senneca O, Russo P, Salatino P, Masi S. The relevance of thermal annealing to the evolution of coal char gasification reactivity. Carbon 1997; 35: 141-151.

Sha XZ, Chen YG, Cao J, Yang YM, Ren DQ. Effects of operating pressure on coal gasification. Fuel 1990; 69: 656-659.

Sharma A, Kadooka H, Kyotani T, Tomita A. Effect of Microstructural Changes on Gasification Reactivity of Coal Chars during Low Temperature Gasification. Energy and Fuels 2002; 16: 54-61.

Sheikh A. Modern application of gasification technologies: an overview. Paper presented at Power-Gen Europe. May 1995.

Shi Y, Xiao J, Quan S, Pan M, Zhang L. Fractal model for prediction of effective hydrogen diffusivity of gas diffusion layer in proton exchange membrane fuel cell. International Journal of Hydrogen Energy 2010; 35: 2863-2867.

Shirazi AS, Karimipour S, Gupta R. Numerical Simulation and Evaluation of Cavity Growth in In Situ Coal Gasification. Industrial and engineering chemistry research 2013; 52: 11712-11722.

Shufen L, Ruizheng S. Kinetic studies of a lignite char pressurized gasification with CO_2, H_2 and steam. Fuel 1994; 73: 413-416.

Shurtz RC, Fletcher TH. Coal Char-CO_2 Gasification Measurements and Modeling in a Pressurized Flat-Flame Burner. Energy and Fuels 2013; 27: 3022-3038.

Shurtz RC, Hogge JW, Fowers KC, Sorensen GS, Fletcher TH. Coal Swelling Model for Pressurized High Particle Heating Rate Pyrolysis Applications. Energy and Fuels 2012; 26: 3612-3627.

Silbermann R, Gomez A, Gates I, Mahinpey N. Kinetic Studies of a Novel CO_2 Gasification Method Using Coal from Deep Unmineable Seams. Industrial and engineering chemistry research 2013; 52: 14787-14797.

Sima-Ella E, Yuan G, Mays T. A simple kinetic analysis to determine the intrinsic reactivity of coal chars. Fuel 2005; 84: 1920-1925.

Singer SL, Ghoniem AF. An Adaptive Random Pore Model for Multimodal Pore Structure Evolution with Application to Char Gasification. Energy and Fuels 2011; 25:1423-1437.

Singh KN. Coal Bed Methane Potentiality – Case Studies from Umaria, Korba and Ib-Valley Coals, Son-Mahanadi Basin. Geological Society of India 2010; 76: 33-39.

Singh CPP, Saraf DN. Simulation of high-temperature water-gas shift reactors. Industrial and Engineering Chemistry Process Design and Development 1977; 16: 313-319.

Singh CPP, Saraf DN. Simulation of low-temperature water-gas shift reactor. Industrial and Engineering Chemistry Process Design and Development 1980; 19: 393-396.

Skodras G, Sakellaropoulos GP. Mineral matter effects in lignite gasification. Fuel Processing Technology 2002; 77-78: 151-158.

Souza-Santos MLD. Comprehensive modelling and simulation of fluidized bed boilers and gasifiers. Fuel 1989; 68: 1507-1521.

Spinal JF, Mondragon F, Truong TN. Thermodynamic evaluation of steam gasification mechanisms of carbonaceous materials. Carbon 2009; 47: 3010-3018.

Srinivas B, Amundson NR. A Single-Particle Char Gasification Model. AIChE Journal 1980; 26: 487-496.

Srivastava VK, Jalan RK. Predictions of Concentration in the Pyrolysis of Biomass Materials-I. Energy Conversion Management 1994; 35: 1031-1040.

Srivastava VK, Sushil, Jalan RK. Predictions of Concentration in the Pyrolysis of Biomass Material-II. Energy Conversion Management 1996; 37: 473-483.

Sun Q, Li W, Chen H, Li B. The CO_2-gasification and kinetics of Shenmu maceral chars with and without catalyst. Fuel 2004; 83: 1787-1793.

Takarada T, Tamai Y, Tomita A. Reactivities of 34 coals under steam gasification. Fuel 1985; 64: 1438-1442.

Takeya G. Studies of the structure of coal and hydrogenation process. Pure and applied chemistry 1978; 50: 1099-1115.

Tay HL, Kajitani S, Zhang S, Li CZ. Effects of gasifying agent on the evolution of char structure during the gasification of Victorian brown coal. Fuel 2013; 103:22-28.

Thiele EW, Haslam RT. Mechanism of the steam-carbon reactions. Industrial and Engineering Chemistry 1927; 19: 882-887.

Tomeczek J, Gil S. The kinetics of coal chars hydrogasification. Fuel Processing Technology 2010; 91: 1564-1568.

Tomita A. Reactivity of char –effect of coal rank-14 years later. Carbon 1991; 29: 753-755.

Tremel A, Spliethoff H. Gasification kinetics during entrained flow gasification – Part II: Intrinsic char reaction rate and surface area development. Fuel 2013; 107: 653-661.

Umeki K, Yamamoto K, Namioka T, Yoshikawa K. High temperature steam-only gasification of woody biomass. Applied Energy 2010; 87: 791-798.

Umemoto S, Kajitani S, Hara S. Modeling of coal char gasification in coexistence of CO_2 and H_2O considering sharing of active sites. Fuel 2013; 103: 14-21.

Vamvuka D, Troulinos S, Kastanaki E. The effect of mineral matter on the physical and chemical activation of low rank coal and biomass materials. Fuel 2006; 85: 1763-1771.

Velej JF, Chejne F, Valdes CF, Emery EJ, Londono CA. Co-gasification of Colombian coal and biomass in fluidized bed: An experimental study. Fuel 2009; 88: 424-430.

Vostrikov AA, Psarov SA, Dubov DY, Fedyaeva ON, Sokol MY. Kinetics of Coal Conversion in Supercritical Water. Energy and Fuels 2007**;** *21*: 2840-2845.

Wakao N, Smith JM. Diffusion and reaction in porous catalysts. Industrial and engineering chemistry fundamentals 1964; 3: 123-127.

Wall TF, Liu G, Wu H, Roberts DG, Benfell KE, Gupta S, Lucas JA, Harris DJ. The effects of pressure on coal reactions during pulverised coal combustion and gasification. Progress in Energy and Combustion Science 2002; 28: 405-433.

Warnecke R. Gasification of biomass: comparison of fixed bed and fluidized bed gasifier. Biomass and Bioenergy 2000; 18: 489-497.

Watanabe H, Otaka M. Numerical simulation of coal gasification in entrained flow coal gasifier. Fuel 2006; 85: 1935-1943.

Wells WF, Smoot LD. Relation between reactivity and structure for coals and chars. Fuel 1991; 70: 454-458.

Wen CY, Chaung TZ. Entrainment Coal Gasification Modeling. Industrial and engineering chemistry process design and development 1979; 18: 684-695.

Wen, C.Y. Noncatalytic Heterogeneous Solid-Fluid Reaction model. Industrial and engineering chemistry 1968; 60: 34-54.

Wornat MJ, Hurt RH, Davis KA, Yang NYC. Single-particle combustion of two biomass chars. Twenty-Sixth Symposium (International) on Combustion/The Combustion Institute 1996; 3075-3083.

Wu S, Gu J, Li L, Wu Y, Gao J. The reactivity and kinetics of Yanzhou coal chars from elevated pyrolysis temperatures during gasification in steam at 900-1200 ^{0}C. Process Safety and Environmental Protection 2006; 84: 420-428.

Xu Q, Pang S, Levi T. Reaction kinetics and producer gas compositions of steam gasification of coal and biomass blend chars, part 2: Mathematical modelling and model validation. Chemical Engineering Science 2011; 66: 2232-2240.

Yadav VK, Kumar V. Modelling Gasification of Single Coal Particle. 5th International and 41th National Conference on Fluid Mechanics and Fluid Power (FMFP), 12th -14th December 2014, IIT Kanpur (Accepted).

Yang H, Chen H, Ju F, Yan R, Zhang S. Influence of Pressure on Coal Pyrolysis and Char Gasification. Energy and Fuels 2007; 21: 3165-3170.

Yang H, Li S, Fletcher TH, Dong M. Simulation of the Swelling of High-Volatile Bituminous Coal during Pyrolysis. Energy Fuels 2014 (In press).

Yang RT, Duan RZ. Kinetics and mechanism of gas-carbon reactons: conformation of etch pits, hydrogen inhibition and anisotropy in reactivity. Carbon 1985; 23: 325-331.

Yang RT, Yang KL. Kinetics and mechanism of carbon-steam reaction on the monolayer and multilayer edges of graphite. Carbon 1985; 23: 537-547.

Yang Y, Watkinson AP. Gasification reactivity of some Western Canadian coals. Fuel 1994; 73: 1786-1791.

Ye DP, Agnew JB, Zhang DK. Gasification of a South Australian low-rank coal with carbon dioxide and steam: kinetics and reactivity studies. Fuel 1998; 77: 1209-1219.

Zajdlik R, Jelemensky L, Markos J, Remiarova B. Modelling of gasification of a Single Coal Char Particle. Chemical Papers 2001; 55: 364-368.

Zhang L, Huang J, Fang Y, Wang Y. Gasification Reactivity and Kinetics of Typical Chinese Anthracite Chars with Steam and CO_2. Energy and Fuels 2006; 20: 1201-1210.

Zhang Y, Hara S, Kajitani S, Ashizawa M. Modeling of catalytic gasification kinetics of coal char and carbon. Fuel 2010; 89: 152-157.

Zhao X, Zeng C, Mao Y, Li W, Peng Y, Wang T, Eiteneer B, Zamansky V, Fletcher TH. The Surface Characteristics and Reactivity of Residual Carbon in Coal Gasification Slag. Energy and Fuels 2010; 24: 91-94.

Zhu W, Song W, Lin W. Effect of the Coal Particle Size on Pyrolysis and Char Reactivity for Two Types of Coal and Demineralized Coal. Energy and Fuels 2008; 22: 2482-2487.

Zhuo Y, Messenbock R, Collot AG, Megaritis A, Paterson N, Dugwell DR, Kandiyoti R. Conversion of coal particles in pyrolysis and gasification: comparison of conversions in a pilot-scale gasifier and bench-scale test equipment. Fuel 2000; 79: 793-802.

Ziv EB, Kantorrovich II. Mutual effects of porosity and reactivity of char oxidation. Progress in Energy and Combustion Science 2001; 27: 667-697.

Zolin A, Jensen A, Pederses LS, Dam-Johansen K. A Comparison of Coal Char Reactivity Determined from Thermogravimetric and Laminar Flow Reactor Experiments. Energy and Fuels 1998; 12: 268-276.

Zygourakls K, Arri L, Amundson NR. Studies on the Gasification of a Single Char Particle. Industrial and engineering chemistry fundamentals 1982; 21: 1-12.